ISSN 1831-9424 (PDF)
ISSN 1018-5593 (Printed)

European Commission

Cognitive control systems in steel processing lines for minimised energy consumption and higher product quality

(Cognitive Control)

Research and Innovation

EUR 27317 EN

EUROPEAN COMMISSION
Directorate-General for Research and Innovation
Directorate D — Key Enabling Technologies
Unit D.4 — Coal and Steel

E-mail: rtd-steel-coal@ec.europa.eu
RTD-PUBLICATIONS@ec.europa.eu

Contact: RFCS Publications

European Commission
B-1049 Brussels

European Commission

Research Fund for Coal and Steel

Cognitive control systems in steel processing lines for minimised energy consumption and higher product quality

(Cognitive Control)

Andreas Wolf, Martina Thormann, Mohieddine Jelali
VDEh-Betriebsforschungsinstitut GmbH (BFI)
Sohnstraße 65, 40237 Düsseldorf

Björn Sjögren
Swera MEFOS AB (MEFOS)
Arontorpsvägen 1, SE-971 25 Luleå (Sweden)

Jürgen Bathelt, Peter Förster
ArcelorMittal Eisenhüttenstadt (AMEH)
Werkstraße 1, 15872 Eisenhüttenstadt (Germany)

Luis Felipe Recalde, Reza Katebi, Hong Yue
Industrial Control Centre (ICC)
University of Strathclyde
16 Richmond Street, GB-Glasgow G1 1XQ (UK)

Wolfram Gerlach
ThyssenKrupp Nirosta (TKN)
Oberschlesienstraße 16, 47807 Krefeld (Germany)

Grant Agreement RFSR-CT-2010-00037
1 July 2010 to 31 December 2013

Final Report

Directorate-General for Research and Innovation

2015 EUR 27317 EN

Europe Direct is a service to help you find answers to your questions about the European Union

Freephone number (*)**:**

00 800 6 7 8 9 10 11

(*) Certain mobile telephone operators do not allow access to 00 800 numbers or these calls may be billed.

More information on the European Union is available on the Internet (http://europa.eu).

Cataloguing data can be found at the end of this publication.

Luxembourg: Publications Office of the European Union, 2015

Print	ISBN 978-92-79-49482-6	ISSN 1018-5593	doi:10.2777/642342	KI-NA-27-317-EN-C
PDF	ISBN 978-92-79-49074-3	ISSN 1831-9424	doi:10.2777/90680	KI-NA-27-317-EN-N

Printed in Luxembourg

PRINTED ON WHITE CHLORINE-FREE PAPER

Contents

1 Final Summary

WP 1: Development of methods for continuous control performance assessment

Task 1.1: Analysis of existing control loops and identification of tuning parameters and data needs [ALL PARTNERS]

ICC and BFI focused on identifying common sources of poor performance in hot rolling mills, annealing and galvanizing processes. The identified root-causes were in this case process, transition or scheduling strategies, variable operating points, use of SISO controllers, sensor and actuator faults, model uncertainties and internal/external disturbances. AMEH was interested in assessing and improving the control systems in two processing plants: the gauge control system at the hot strip mill, including AGC, monitor control, mass flow control and looper control and the strip guiding controls in the annealing lines. TKN runs several annealing lines. After Analysing the potential of their furnaces, it was decided to choose the annealing furnace "KL3"; MEFOS chose the annealing furnace "KBR" at Outoumpu Aveta.

Task 1.2: Development and implementation of databases [AMEH, MEFOS, TKN]

From the chosen aggregates process data was selected for further performance analyses. Within these processes the strip speed was significantly influenced by acceleration and deceleration. This meant that strip-length samples were not equally distant in time. This was motivating performance evaluation in a length-based setting rather than in a time-based setting and also avoided the need to estimate any time delay, as the distance from actuator to sensor is constant in the length-based scenario. After these pre-processing steps, the data of each coil was analysed.

Task 1.3: Development offline test of automatic control-loop performance evaluation methods [ALL PARTNERS]

The results of Task 1.1 were used to choose appropriate Control Performance Assessment (CPA) methodologies in Task 1.3. Continuous offline methods were implemented by BFI and ICC for time-delay estimation, detection of nonlinearities and ANalysis Of VAriance (ANOVA) over Minimum Variance (MV)-CPA. New methodologies for controller only pre-assessment, monitoring of nonlinearities and systematic diagnosis were developed. The methods were tested on SISO systems and cold rolling mill data, hot rolling mills, annealing furnaces in cooperation with MEFOS, AMEH and TKN.

ICC provided new methods for controller pre-assessment. The pre-assessment was achieved by combining recursive closed-loop subspace identification with QR decomposition, wavelet decomposition for feature extraction and a Model Predictive Control (MPC) benchmark designed with the extracted deterministic features of the original data (or filtered data) from the wavelet decomposition. QR decomposition was used for process identification to avoid ill-conditioned problems on the algorithm due to none or poor persistent excitation. A new methodology for monitoring of nonlinearities was also developed for Task 1.3. The methodology used State-Dependent (SD) model identification to identify any existing nonlinearities and a Filtering and CORrelation (FCOR) scheme for Control Performance Monitoring (CPM)

For using the Harris index, steady-state data for the benchmarking of control loop performance was selected. In practical application, for instance, when analysing the thickness control of a hot strip mill, there are large amounts of measurement data to be analysed, containing also periods of steady and non-steady-states. It is quite a difficult task to separate time periods manually, hence methods were

introduced by BFI to separate the time spans automatically. The methods are based on the detection of steady and non-steady states parts of the measuring signal. Furthermore, a static energy index was introduced as the ratio between energy of the strip and the fuel. If this index excites a limit, there are hints to malfunction in the furnaces, demonstrated in Task 5.2. Besides the well-known Harris index, the idle index for detection of sluggish controller was introduced and the Visioli index added. The aim of the methodology is to evaluate an abrupt load disturbance response if the tuning of the adopted PI controller guarantees good load-disturbance rejection performance.

WP 2: Development of techniques for the automatic diagnosis of root causes of poor control performance

Task 2.1: Development of methods to determine the root causes of performance losses detected in the control loops [ICC, BFI]

The diagnosis algorithm developed here comprised the following steps:

- Pre-analysis of nonlinearity and dead-time estimation.
- Feedback controller assessment.
- Process and disturbance assessment.

For this task, BFI added an extra method for oscillation detection based on regularity of zero-crossings of the autocorrelation function (ACF) of the process data. In addition, similar techniques have been studied, called the decay ratio approach of the auto-covariance function. Furthermore, nonlinearity detection based surrogates analysis was added. Finally, BFI has presented methods to detect stiction as the root-cause of oscillation.

The methods implemented by ICC in Task 1.3 were combined into a decision tree approach to predict root-causes of poor performance. Each methodology was expressed as a metric. Metrics extracted from a nominal data set (or data with the best performance) were used as decision rules in the decision tree. The resulting decision tree was fed with new data and a possible root-cause is predicted.

Task 2.2: Synthesis of promising diagnose procedure to be applied to the specific loops considered [all]

A new CPM and diagnosis methodology was developed for Tasks 2.2 to tackle multivariable processes. The methodology combines recursive closed-loop subspace identification, MPC benchmark, wavelet decomposition, Kernel Principal Component Analysis (PCA) for faults monitoring and angle-classifiers for root-cause identification. The CPA benchmark was designed as in controller pre-assessment with the addition of the stochastic features to improve the MPC design. MPC benchmark was also chosen for its ability to assess input variability or input energy. Root-causes in data were monitored at several frequencies through the wavelet decomposition. Statistical metrics such as Hotteling's statistic (T^2) and Square Prediction Error (SPE) were used for monitoring in all the decomposed frequencies. Identification of root-causes was achieved by determining the angle between the Principal Components (PC's) of a detected abnormality in the data against known principal components from pre-identified root-causes. The identification was enhanced by applying other data features such as amplitude of the statistical metrics and PC's' worst directions.

This method was applied on a multivariable case study and on the data of the annealing furnace MEFOS partner provided. This has lead to further investigations of the control loops of the MEFOS partner, especially on the performance due to thickness jumps and analyses of model used within the control loop. Furthermore, this method was presented by MEFOS to supervise temperature measurement based on PCA analyses.

BFI, in discussion with its industrial partner AMEH and TKN, has provided a comprehensive diagnosis procedure for valve-controller loops, starting with oscillation detection: when the control loop

has been found to be oscillating, the most probable origin was assumed valve stiction. However, non-linearity had to be checked as a possible source of oscillation. A stiction detection method was then applied and its level estimated. It was tested with the simulation and diagnoses developed in the project.

Task 2.3: Development of the diagnosis of root-cause reporting systems[MEFOS, AMEH; ICC, TKN]

A structure of a performance monitoring and root-cause diagnosis reporting was proposed. It has been inspired by the structure used in the cpmPlus Loop Performance Manager of ABB, but extended by the new methods and features developed within this project.

WP 3: Development of methods for automatic tuning by generating optimal setup parameters and controller settings

Task 3.1: Development of strategies and methods for re-tuning controllers [ALL PARTNER]

The continuous annealing furnace which was investigated by Swerea MEFOS reheats steel strips of various steel grades, thicknesses and surface finish. Thicker strips require more time in the furnace, and the optimal reheating parameters were calculated by temperature prediction software that takes data from furnace instrumentation and operator input for factors including the furnace wall temperatures, the strip thickness and emissivity, fuel flow rates, etc. The model included the furnace geometry which is a fixed parameter. The dominant type of heat transfer at these high temperatures is radiative, so the reheating is particularly sensitive to the surface emissivity. One potential source of sub-optimal control loop performance was the interaction between the radiative heat transfer model in the strip temperature predictor and the strip emissivity data. The strip emissivity should have normally increased with increasing temperature, since an oxidized steel surface has a higher emissivity than a blank steel surface. There were also strips with oxidized surfaces where the change in emissivity of the surface through the furnace was not known.

The University of Strathclyde focused on the development of the following three methodologies: Supervisory MPC gain compensation, "one shot" gain compensation based on covariance control, and iterative gain compensation. The methodologies required estimation of the process dynamic matrix and noise matrix. The estimation was carried out using a recursive closed-loop subspace identification method based on process data only. The Control Performance Assessment (CPA) index was used to trigger the re-tuning process as well as the stopping mechanism. It wass expected that the re-tuning process starts after improper tuning of the controller which had been identified as the main source of poor performance by a diagnosing method.

The main innovation of the controller retuning methods developed by BFI wass that controller tuning is treated in the context of control performance monitoring (CPM). This implied control performance measures which are continuously monitored on a regular basis, i.e. during normal operation, and performance statistics used to schedule loop re-tuning and automatically determine the optimal controller parameters. Three methods have been developed by BFI: The first controller retuning is based on set-point data. The approach is to compare the achieved performance with that of a PI Control tuned with IMC rules based on first order model with time delay. Two performance indications were used, namely the settling time and integral of absolute error. The second method used identification to determine the close-loop servo transfer function and the disturbance impulse response to determine via optimisation the optimal parameter of the PI and PID Control. The third, control assessment based on relative damping index, fitted a second order plus time delay continuous model to the impulse response provided by the Harries Index method. The damping of the second order model provided suggestions on tuning the parameter of the controller.

Task 3.2: Working out decision masking concept and supervision procedures for automatic re-tuning [ALL PARTNERS]

A principal decision procedure for carrying out the right measures for improving the performance of a control system was provided. A continuous CPM system indicated whether the control performance has been acceptable, i.e. meets the required specification in terms of standard deviation or other measures, product quality, energy consumption or even safety. This level wass thus more related to the direct economical performance of the plant shown later in Task 5.2. When proceeding with the performance analysis, the current performance is compared to that of the selected benchmark, to find out whether the installed controller performed well under the current process condition.

Furthermore, strategies for variation of controller parameters for automatic re-tuning PI and PID controller were given. Iterative controller tuning required the specification of a proper step size for each controller parameter, usually given as percentage. Cautious adjustments to the controller parameters were necessary to guarantee closed-loop stability and performance improvement. There were many strategies for varying the controller settings in each iteration. Some of them are described in the following, including their strengths and weaknesses. Basically, a large step size helps to reduce the number of iterations required but may increase the risk to converge to controller parameters far from the optimum.

The simplest approach is to vary only the proportional gain K_P unless the existing controller is either too sluggish or too aggressive. In such cases, the integral time T_I can also be changed (but only one parameter at a time). Otherwise, the variation of K_p, should only lead on to a value near the optimum, and then a "fine tuning" could be done by slight variation of T_I. The simultaneous adjustment of the controller settings, i.e. decreasing K_p, and increasing T_I (and possibly decreasing T_D) when the controller is aggressive and vice versa in the case of a sluggish controller, is the fastest method to find the optimum tuning. However, this approach is not transparent in practice and should only be considered by well-qualified users. The third method is based on successive variation of the control parameter. In this approach, the proportional term is tuned first until the highest performance index value is reached. This is followed by tuning the integral time and possibly derivative time, which may lead to further improvement in Harries index η. Although this approach usually takes more iterations than the simultaneous strategy, it is highly recommended in practice because of its transparency.

Task 3.3: Procedure simulation of automatic re- tuning of the control loops, comparison of selected methods [ALL PARTNERS]

The University of Strathclyde compared its three developed methods with the Visioli's method. Four metrics were used to validate the improvement: controller performance assessment, idle index I_i, area index I_a and output index I_o. A simple SISO system with PI control was used as a benchmark. The results show the calculated controller parameters of the four methods. Note that supervisory method and covariance control method find the new controller parameters at the first iteration since they are "one-shot" solutions. In practice, the supervisory method sampled the process at a different sampling rate compared to the local controllers. The re-tuning procedure had consequently taken longer. The iterative methodologies took 4 and 3 iterations respectively. The modified Iterative Feedback Tuning (IFT) method took less than the Visioli method since the latter is based on small percentage variations of the controller parameters rather than an optimal recursion. It was important to take into account that the modified IFT method can take higher numbers of iteration according to the complexity of the process. In general no big differences among the performance of the method were found.

BFI used two benchmarks for testing the methods: one with time delay and one without. Both were controlled by PI control. The optimisation method reached the optimal control parameter directly. It was found out that the set-point based method needed two iterations and has been sensitive to the choice of the ARMAX model. The relative damping index method needed 3-5 iteration, but reached less performance in one case. Nevertheless, the relative damping index method was applied in Task 5.1 because it needs no external excitation.

WP 4: Implementation,, interface programming and on-site implementation of automatic control optimization techniques

Task 4.1: Development and test of the SCADA interface to the performance and fault monitoring software [ICC]

The University of Strathclyde ombined all the methodologies used and developed by the ICC into a MATLAB software tool. Supervisory Control And Data Acquisition (SCADA) functionality was added to the software tool through the Object linking and embedding Process Control (OPC) toolbox. OPC is a MATLAB toolbox developed to provide connectivity, directly from MATLAB and Simulink, between OPC clients running software applications and any OPC Data Access (DA) and Historical Data Access (HDA) compliant servers. The toolbox allows reading, writing and logging OPC data from devices such as distributed control systems, SCADA systems and programmable logic controllers that conform to the OPC Foundation DA standard

Task 4.2: Implementation of procedures adapt and verify performance assessment and automatic root-cause diagnosis results [ALL PARTNERS]

In this task several method tools were developed to implement performance assessment and root-cause diagnostics. BFI and TKN developed a simulation and diagnostic tool for annealing furnace KL3. It contains a simulation tool of the dynamic behaviour of the furnace and controller; a fault injection tool to simulate the reaction of the furnace and controller on faults in sensor and actuator; a diagnostic tool to analyse the performance and cause of possible degradation. Data from simulation or coming from the plant were analysed. The results are shown in Task 5.2. A similar tool has been adapted for the annealing line VZA2 at AMEH. MEFOS assisted AVESTA by setting up monitoring and diagnoses for the annealing furnace KBR.

Task 4.3: Implementation of continuous monitoring and automatic retuning decision making procedures [BFI, MEFOS, AMEH, TKN]

In simulation and diagnosis tools by BFI for the KL3 of TKN, a set-up optimisation tool was also integrated. Additionally, it provided a tool to optimize the set-point of the furnace controller. The set-point was optimized in such a way that the deviations from the desired strip temperature caused by thickness changes and strip speed changes were reduced. This lead to more homogeneous strip quality. In the tool for AMEH BFI some iterative controller re-tuning features were added, based on the relative damping index. The results have been described in Task 5.1. MEFOS assisted AVESTA by setting up monitoring and controller retuning based on MPC methods.

WP 5: Final testing and evaluation of developed tools and systems

Task 5.1: Methods and systems for demonstration at the galvanizing lines and linked pickling/cold rolling mill at the ArelorMittal Eisenhüttenstadt [AMEH, BFI]

In this task controller performance analysis, root-cause analysis of performance degradation and automatic re-tuning using the tools, provided by BFI, was demonstrated at the galvanizing line VZA2 of AMEH. First results showed that some controllers were switched off quite often by the operators. When analysing these controllers, insufficient performance was detected. A further analysis showed that the reason for degradation wass due to oscillation, but stiction as a cause for oscillation has been excluded.

After some further investigation by AMEH, it was found that the strip, which reaches a temperature of 300 C at the end of the RTHA zone, did not show any or at least slight oscillations. Still, if the strip reached only 180°C in this zone, the strip started to oscillate. Therefore, an additional temperature measurement and controller was installed. The strip temperature at the end of this zone was kept constant at 300°C and afterwards no oscillations have been observed any longer.

Iterative tuning was applied to one controller which showed insufficient performance but no oscillation. After two iterations, a significant performance increase was achieved.

Task 5.2: Methods and systems for demonstration at (stainless steel) bright annealing lines at ThyssenKrupp Nirosta [TKN, BFI]

In this task, the control performance and root-cause analysis of performance degradation using the tools developed in this project was demonstrated at the bright annealing line of TKN. First, the performance of the furnace was analyzed using MIMO methods provided by ICC.

Afterwards a root-cause analysis based on Furnace Simulation Diagnosis Tools was carried out. Offset of temperature measurement could be detected and lead to asymmetric load distribution in the furnace. Counter measures were implemented and tested. In the performance analyses, it was pointed out that the violation of T^2 at high scales could be related to sources of oscillation. To verify this assumption, the behaviour of the temperature control at changes in the thickness was investigated. This lead to improvement of the reaction of the furnace controller due to thickness changes, reducing costs significantly.

Task 5.3: Methods and systems for demonstration at annealing lines of MEFOS [MEFOS]

In this task, the control performance and root cause analysis of performance degradation using the tools developed in this project were demonstrated at the annealing lines of MEFOS. First the performance of the furnace was analysed. Then the root-cause of the performance degradation was carried out. Based on a number of temperature measurements using DATAPAQ and thermocouples attached to the strip, it was clearly detected that there is a deviation between the calculated and the measured temperature. By further analysing the oxygen level in the furnace, it was concluded that false air was leaking into the furnace. After calculating the energy balance of the furnace, it was detected that the gas radiation model for the oxyfuel combustion has not been elaborated correctly.

Task 5.4: Evaluation of final results and recommendations [ALL PARTNERS]

The analyses and tuning methods applied in this project had several effects on the investigated plant: the detection of sensor fault, in this case an offset on the temperature measurement, saves approx. 1.3GWH per year and yields to significant cost saving. Furthermore, the overall benefit of the measures applied in this project at TKN lead to a reduction of out-tolerance of grain size of about 150.000 €a year.

Generally, before applying performance analyses, root-cause analyses and re-tuning wass recommended: at first the verification of data had to be consistent, otherwise this could have lead to false interpretation of the later analysis steps. The first analysis checked whether the signal is “alive” and the second whether the analysed controller is really switched on or off. Then the data of interest was selected. In order to avoid unnecessary metrics calculations, the controller has been assessed to rule out improper tuning or inadequate control structure first. Improper tuning was considered the main cause of poor performance.

There is not a database of general root-causes in steel processing lines. Most of the methodologies for diagnosis are based on the identification of new data features against known data features. Even if the accuracy of a given methodology identifies new abnormal data features, they can not be linked to a known or new root-cause. Diagnosis for steel processing lines is at the stage where many destructive tests have to be carried out in order to identify possible root-causes of poor performance. It is important to keep in mind that some root-causes have shared effects. The identification of a given root-cause may need several tailored diagnosis methodologies or monitoring at different frequencies.

Control re-tuning has to be a task initiated manually. Although diagnosis mechanisms suggest that

re-tuning is needed, only the expertise of the plant personnel can dictate if that task is necessary. Iterative controller tuning should be carried out with caution.

2 Objectives of the project

The aim of the proposal was to create cognitive automation systems with the capabilities of automatic monitoring of control performance, self-detection and automatic diagnosis of faults (sensors, actuators, controller) and self-adaptation in control system environments to optimise the product quality and minimise energy consumption in steel lines (cold rolling mills, annealing, galvanising) during the whole life cycle. In details, the project objectives were:

- New technologies for continuous online performance assessment of complex setup and control systems in different steel processing lines were developed.
- Methods for automatic diagnosis of root-causes of poor control performance were developed.
- Economical criteria, particularly energy consumption were explicitly considered in the control performance metrics and monitoring and re-tuning algorithms.
- An integrated control data system, containing all information about performance, re-tuning actions and loop testing or maintenance advices were developed.
- Strategies and procedures for integrating the automatic control improvement into the automation systems and the maintenance practices for different finishing lines were developed.
- The developed methods were implemented and transformed into tailored software tools working automatically and continuously with the control data system.
- The supervised automatic control performance optimization methods and systems and the use of control data system were tested and demonstrated at different industrial facilities.

3 Description of activities and discussion

3.1 WP 1: Development of methods for continuous control performance assessment

The main objectives of this WP were:

- Detailed definition of requirements for the control systems to be monitored and tuned at the different target mills were carried out.
- Databases needed for the monitoring and tuning were provided
- Critical review of the control performance assessment technology in the steel processing area and fields was carried out.
- Different methods of control performance assessment were investigated and compared.
- New methods towards continuous and online control performance monitoring, explicitly considering energy consumption were developed.
- A set of rules for alert generation and the structure of the assessment reporting were worked out.
- Selected methods to data gathered from the different plants were applied .

3.1.1 Task 1.1: Analysis of existing control loops and identification of tuning parameters and data needs [ALL PARTNERS]

In the following, a short study of the control loops in steel processing lines is described first, with the aim of identifying sources of performance degradation and critical tuning parameters as well as assessing possible causes for poor loop performance. Then, an analysis of the industrial control systems to be evaluated and improved within the project is presented, (being deliverable D1.1).

There are various sources in a steel line that may degrade the performance of the processes and sub-processes, e.g.:

- *Type of processes*. Metal processing lines are generally divided into sub-processes. Each sub-process modifies the properties of the product. These changes cannot be tracked automatically.
- *Transition or scheduling strategies*. Every single piece of the final product depends on the customer-order specifications. Variations in product properties can be traced back to the starting point, consequently, delays of production, continuity and idle times must be scheduled.
- *Variable operating points*. The whole steel line is set-point-dependent. To obtain customer-order specifications, every sub-process uses individual setups [Pit11]. Models for setup variations are highly nonlinear and difficult to implement.
- *SISO controllers*. It has been reported that most of the sub-processes have poorly tuned SISO controllers with a half-life of about six months [Jel06b].
- *Other sources*. Common sources include sensor and actuator faults, model uncertainties and disturbances. A significant part of these uncertainties comes from inaccurate values of friction coefficients. Disturbances can be internal or external, for example, from roll eccentricity [Pit11].

3.1.1.1 Selection of target plants and first analysis at AMEH

AMEH was interested in assessing and improving the control systems in two processing plants:

1. Gauge control system at the hot strip mill, including AGC, monitor control, mass flow control and looper control.

2. Strip guiding controls in the annealing lines.

Figure 3.1 shows the structure of the gauge control at AMEH's hot strip mill. In figure 3.2 some variables from the control system are illustrated. It can be observed that the control performance was not satisfactory due to the possible root causes: oscillating loops, inaccuracies in the strip or time delay model or mutual interaction between some control loops. This control behaviour was thus analysed using the methods developed in Task 1.3 and the root-causes diagnosed by the techniques developed in Task 2.1.

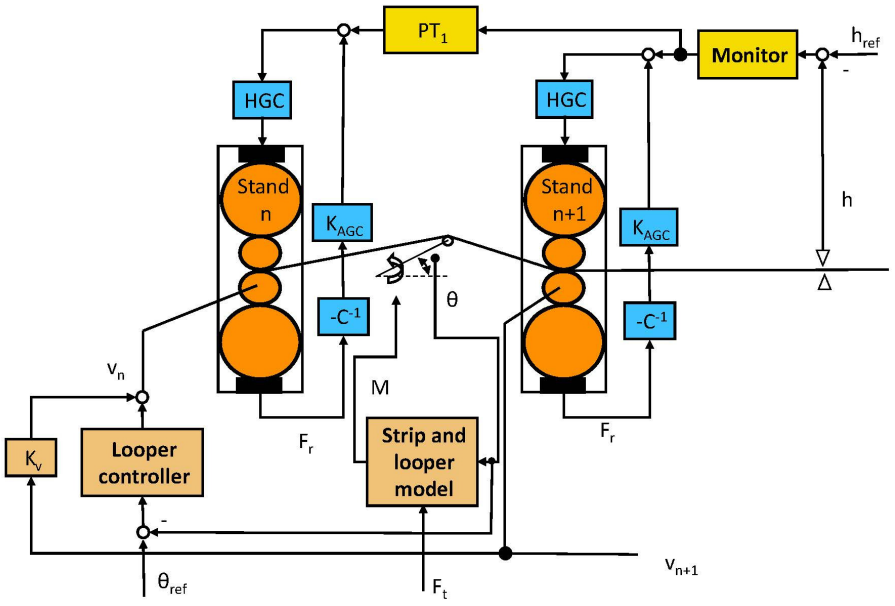

Figure 3.1: Structure of the gauge control at AMEH's hot strip mill

A first analysis of the current control structure showed that it had the configuration depicted in figure 3.3. The implemented structure looked like, but was no Smith predictor. This is not – at least from a theoretical viewpoint – the favorable structure, and thus may lead to performance problems. The modification of the control structure hence improved the quality of the strip thickness.

The second target application of the project at AMEH was a strip guiding control system in the annealing lines, since these are key control loops that affect the final strip quality and the productivity of the hot-dip galvanising lines.

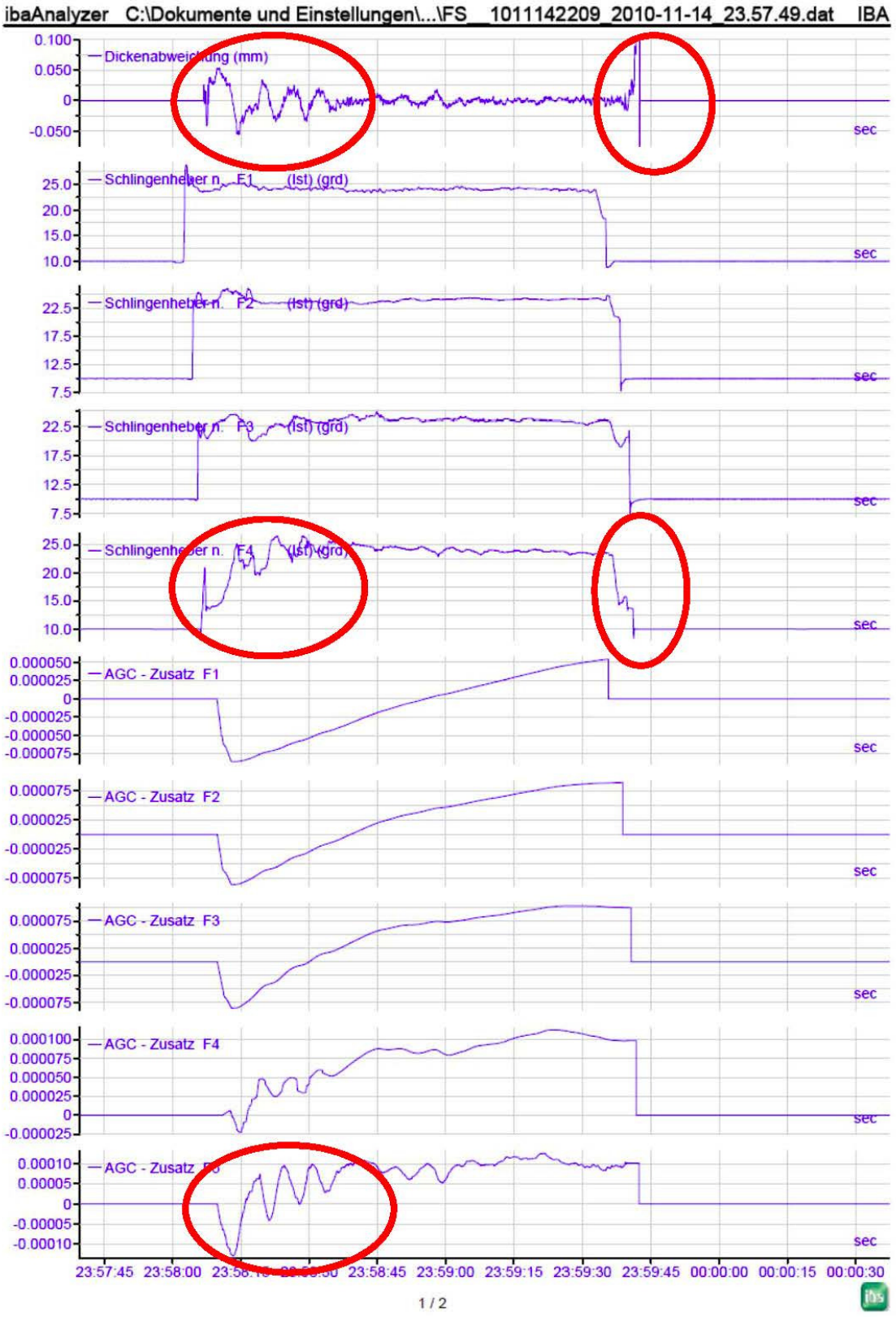

Figure 3.2: Signals from the gauge control

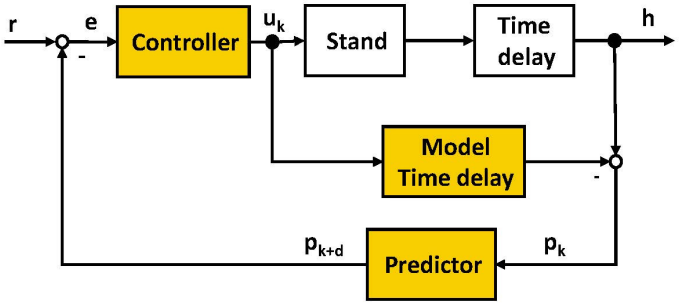

Figure 3.3: Basic control structure as currently implemented at the hot strip mill

3.1.1.2 Selection of target plants and first analysis at TKN

TKN possesses several annealing lines; their features are given in Table 3.1. The optimisation potential of the annealing lines within this project was analysed with the aim to choose the line with the biggest potential benefit. Finally, two annealing lines (KL 3 and GBL 3) were chosen for further elaboration.

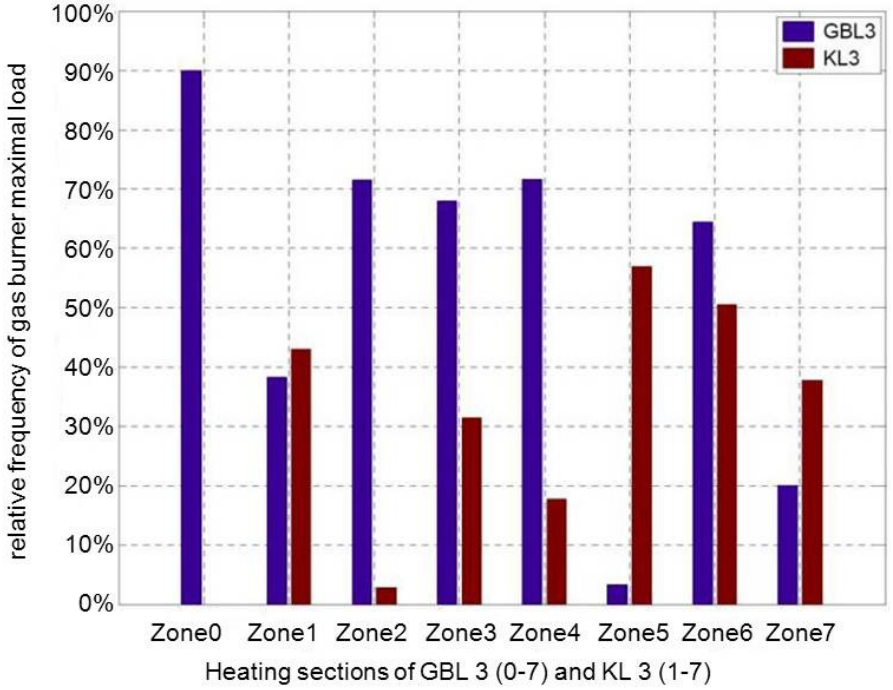

Figure 3.4: Maximum load comparison of annealing lines KL 3 and GBL 3

Table 3.1: Features of the analysed process lines at TKN

Process line	Remaining term	Last control system revamping	Docum. control system	Data in DB	Grain size measur.
WL 2	Ca. 4 years	before 1980	-	-	-
KL 2	Ca. 5 years	1999	available	-	-
GBL 3		2007	available	available	-
KL 3		2002 New construction, 2010 Tension control	available	available	available

Both lines had similar properties with respect to control structure, date of last revamping, setup model and documentation. For every approach of controller optimisation, it is necessary that the actuators are in the limitations as little as possible.

In Fig. 3.4, the relative frequencies of maximum loads of each heating zones were compared. The last zone of GBL 3 had a maximum load in 38% of production time in comparison to 20% of the KL 3's last zone. In total, KL 3 heating sections operated less often with maximal load. This allowed the controller more often to work as it was designed, and thus an optimal tuned/structured controller became more important. For this reason, KL 3 was chosen to be evaluated and improved within this project.

3.1.1.3 Selection of target plants and first analysis at MEFOS

Outokumpu Avesta was interested in improving the process control capability of their annealing line, KBR. The layout of the annealing furnace at Outokumpu Stainless, Avesta is shown in figure 3.5. The furnace consists of 2 parts divided into 6 zones; zone 1 and 2 are located in the first part and zones 3, 4, 5 and 6 are located in the second part. The steel strip travels across the zones via a support roll between the 2 furnace parts at the end of zone 2. There are a total of 35 burners, 25 thermocouples and 5 pyrometers are used to control the furnace and steel strip temperature. The furnace is 39 m long with an interior width of 4 m. Strips up to 2 m wide are annealed at temperatures of approx 1100°C and the strip thickness vary between 1.5 and 12.8 mm, both hot and cold rolled strips are treated. The maximum speed is set by the pickling station at 24 m/min. The mass flow is generally aimed at 80 tonnes/hour for cold rolled strips and 96 tonnes/hour for hot rolled strips. The cold rolled strips are generally more resistant to the heat transfer because of the lower emissivity of the relatively oxide free surface, necessitating a lower mass flow.

The coiled strips are welded together in sequence to create a continuous process. There is a strip buffer on the entry side so the process can be uninterrupted when welding the strips together. The strips are annealed in the annealing furnace and then quickly cooled with air and water to create the desired material properties.

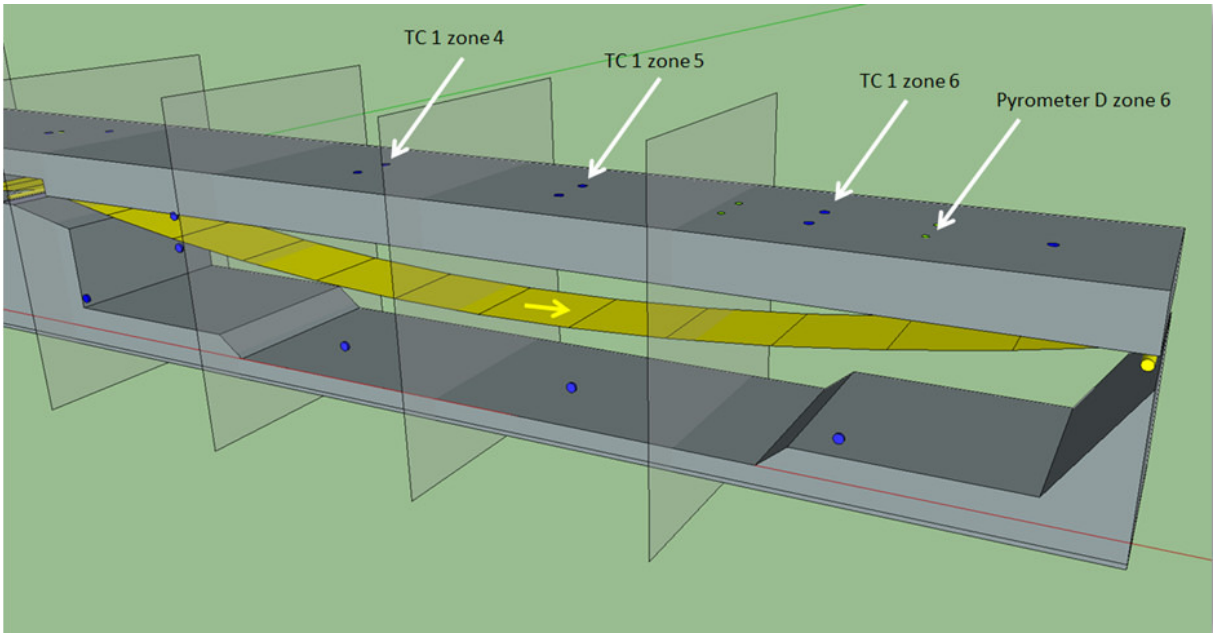

Figure 3.5: Location of the thermocouples and the pyrometer used in the following examples. Distance between thermocouples is around 5 m

The temperature in the furnace is predicted and controlled by DynaMIC, software, which is partly based on the Swerea MEFOS software STEELTEMP®. The prediction software has been developed by Prevas and it utilizes the incoming strip and furnace parameters to determine the strip temperature and how many and how much to fire the set of burners in each zone, each 0.5 m of the strip is calculated and the predictions are made zone per zone. The prediction software is supported by the furnace pyrometers that can also be used as controls alone, or partly, together with the calculations.

The continuous strip is made up of different strips with different thickness that are welded together earlier in the process. The cold rolled strips are separated by a 13 m long strip. Each end of the strip has a 6.5 m long holding strip used to hold and grip the strip during the cold rolling process. This 6.5 m strip

is chosen with similar thickness to the actual strip if possible but it is normally thicker, at about 4 mm. The ends are welded to each other to form a continuous strip resulting in a reoccurring 13 m section that will consequently be cooler than the actual, most often thinner, strip. The furnace is controlled only by the DynaMIC control software when the 13 m section passes the furnace as the pyrometers react heavily to the colder strip.

3.1.2 Task 1.2: Development and implementation of databases [AMEH, MEFOS, TKN]

The databases (being deliverable D1.2) required to acquire and store the signals necessary for the continuous control performance monitoring of the selected control loops were adapted or developed. Interfaces between the databases and the existing automation data buses were also established. Hardware required for the databases and to run the control loop performance evaluation and automatic re-tuning systems was installed at the plants and interfaced to the automation systems.

3.1.2.1 Databases established at hot strip mill of AMEH

All signals of the hot strip mill of AMEH that may be needed for control performance assessment were recorded over three months, consisting of approximately 14000 coils:

- Strip thickness / thickness deviation
- Strip width / width deviation
- Strip flatness coefficients
- Strip wedge
- Temperatures / temperature deviations (exit F1, exit F7, entry coiler)
- Rolling forces, torques
- Rolling speeds
- Looper angles, tensions
- Roll gap positions
- Work roll bending forces
- Shifting (CVC) positions
- AGC offsets
- Strip length
- Tilting positions

Because metal rolling is a batch process, where time between two coils or passes is in the range of minutes, control performance evaluation was usually carried out offline after completing the batches and coil by coil. Before the performance of the controller can be analyzed, the following pre-processing steps had to be carried out:

- Test on plausibility.
- Down-sampling.
- Converting time-dependent signals to length-dependent signals.

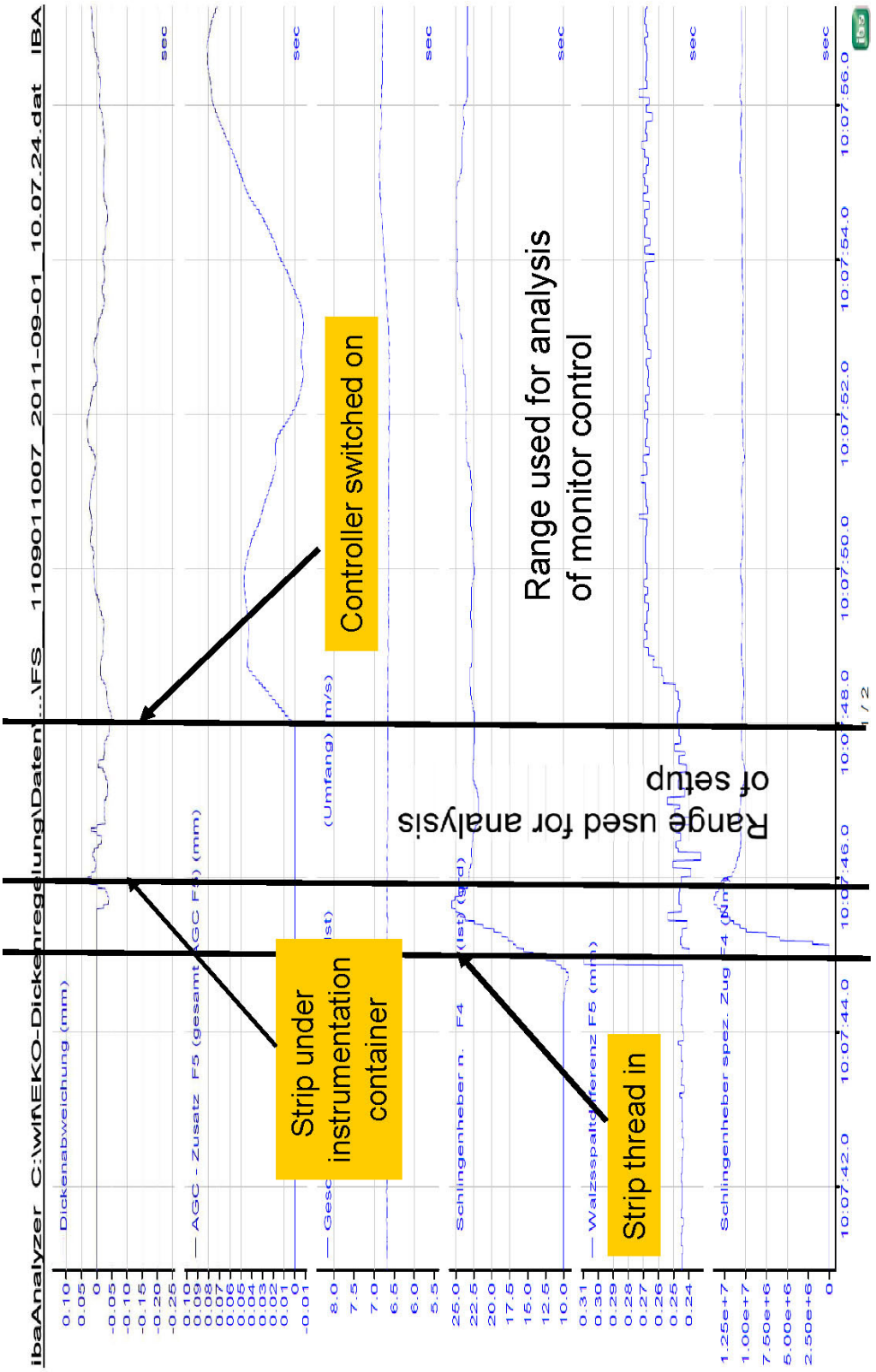

Figure 3.6: Pre-analysis of hot strip gauge control signals

In rolling mills, the strip speed is not continuously constant (due to acceleration, deceleration). This means that strip-length samples are not equally distant in time. This accounted for carrying out performance evaluation in a length-based setting rather than in a time-based setting, avoiding the need to estimate any time delay, as the distance from actuator to sensor is constant in the length-based scenario. Indeed, this is a simple and straightforward approach to calculate the performance indices for the whole rolling phase, including acceleration and deceleration. Note, however, that data was usually gathered in a time-based setting, and transformed into a length-based setting using the strip speed [Jel07].

After these pre-processing steps, the data of each coil was split up into ranges for the different rolling phases, e.g. setup, control-on, etc.; see Fig. 3.7. Then the performance of the thickness controller was analyzed. For the calculation of the Harris index, the thickness deviation data was taken; for the Visioli index, the manipulating variable (AGC offset) data was needed supplementary.

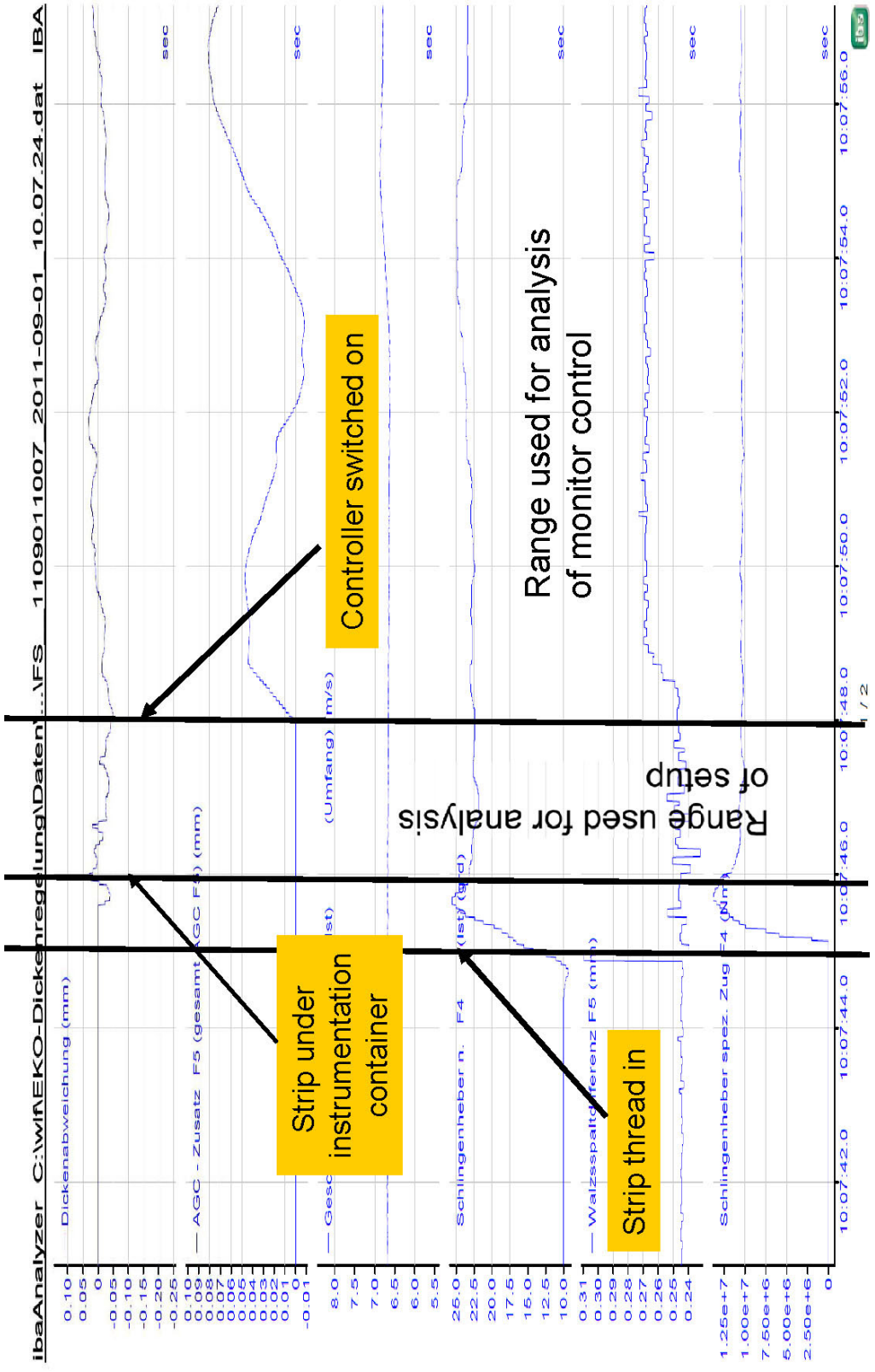

Figure 3.7: Pre-analysis of hot strip gauge control signals

3.1.2.2 Databases established at the galvanizing line of AMEH

All signals of the galvanizing line of AMEH that maybe needed for control performance assessment were recorded over three months:

- furnace temperature for each furnace zone
- strip temperature
- strip speed
- strip width
- strip thickness
- strip position for each furnace zone
- position of the steering for each furnace zone

The same pre-processing steps were carried out as for the hot strip mill data.

3.1.2.3 Databases established at the annealing lines of TKN

Data interfaces and acquisition systems were checked for the availability of process data required for automatic control performance monitoring. Data and parameter types and formats were agreed on during meetings and discussions with the plant personnel. Data was stored and transferred to BFI per remote access, so that analysis was possible when requested. Data from the annealing line KL3 was gathered over a period of some months and analyzed using the CPM routines developed in MATLAB. Figure 3.8 shows a typical example of data measured and analyzed within the project.

A first analysis revealed the importance of plausibility checks and the requirements for many coils were merged to have an appropriate length of data, suitable for performance analysis. Otherwise the data lengths would have been too short and the results unreliable, due to the sampling time of $T_s = 10$s as can be seen below.

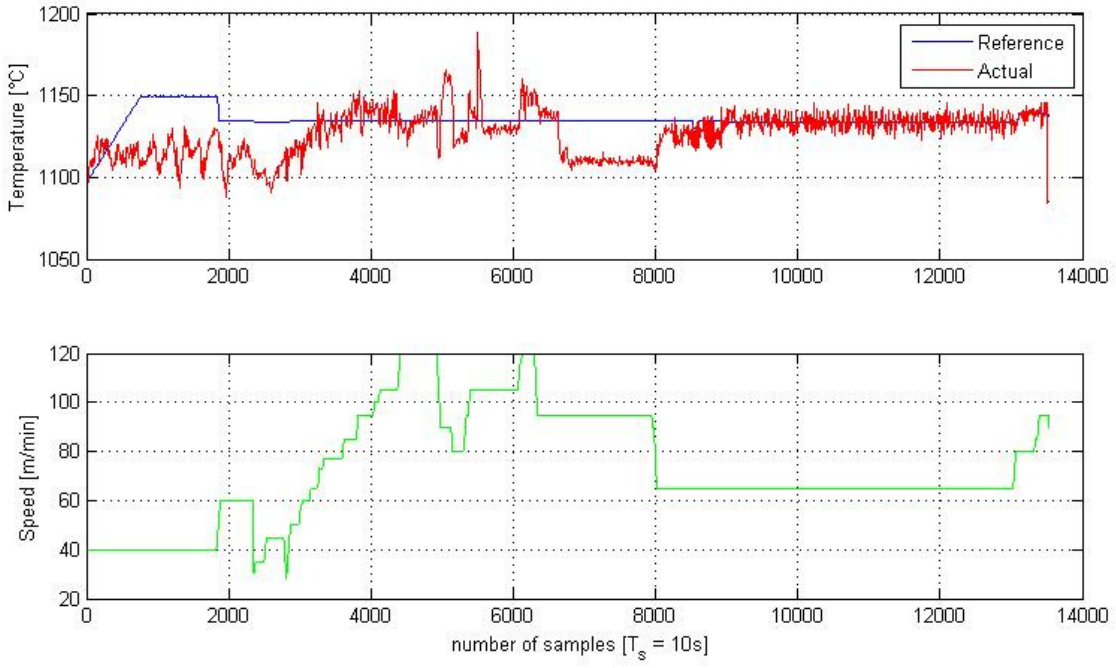

Figure 3.8: Example of time trends measured at the annealing line KL3 of TKN

3.1.2.4 Databases established at the annealing furnace of Outokumpu Stainless (MEFOS)

Data interfaces and acquisition systems were checked for the availability of process data required for automatic control performance monitoring. Data and parameter types and formats were agreed on during meetings and discussions with the plant personnel. Data was stored and transferred to MEFOS.

The data was collected from 17 consecutive strips in the annealing furnace. Sampling was done with a 10 s cycle time and the whole record was 7 hours and 26 minutes long. Of the strips that were annealed during this time the first 7 were hot rolled and the following 10 cold rolled.

12.8 mm was the initial strip thickness followed by thinner and thinner strips in steps of 0.1–2 mm down to 1.5 mm as the thinnest.

The large number of parameters and responses made the visualization of the data difficult. The following graphs thus only represent chosen parts. For example figure 3.9 displays the effect of the strip change, in this case from 1.5 up to 2 mm cold rolled strips. The change was registered at 06:32:50 and the first part of this new strip reached the zone 6 pyrometer at approximately 06:35:50, the cooler 13 m holding strip was clearly distinguishable because of the rapid drop in pyrometer temperature at 06:35:20.

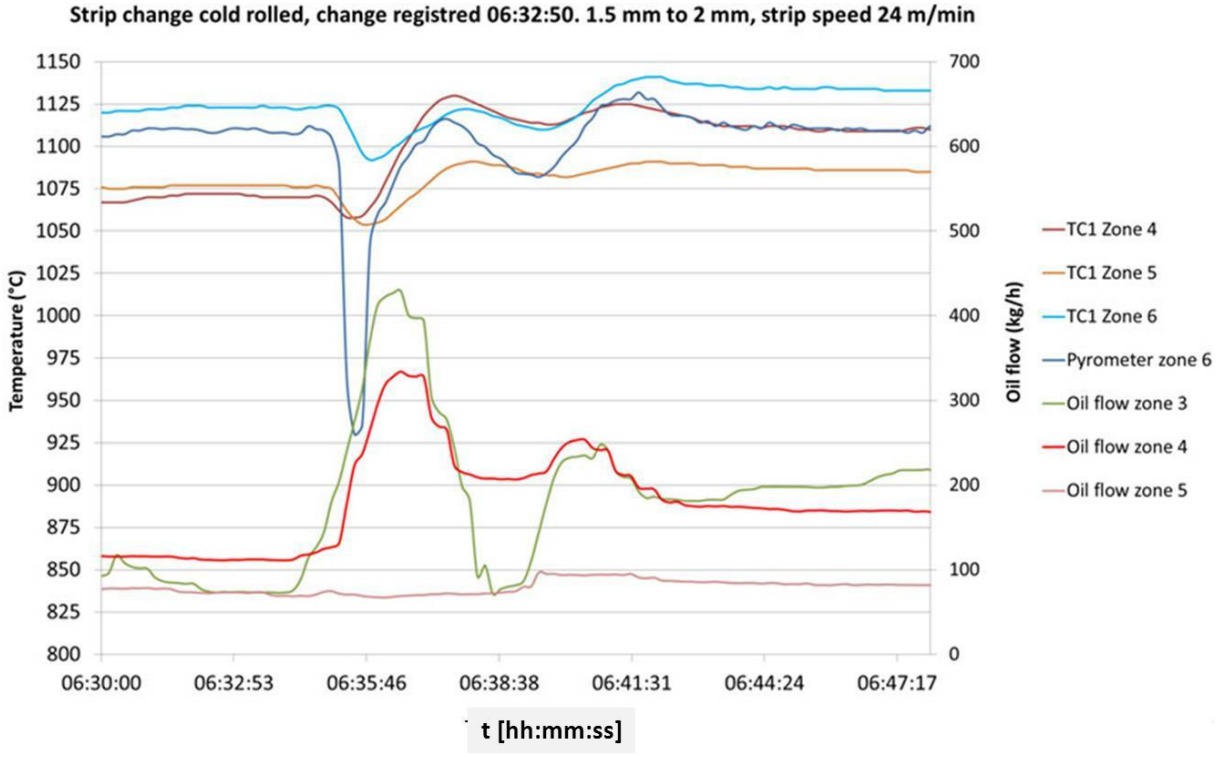

Figure 3.9: Strip change and resulting reaction from thermocouples in zone i (TC1 zone $i \in [4,5,7]$), pyrometers (Pyrometer zone 6) and burners (Oil flow zone $j \in [4,5,6]$)

3.1.3 Task 1.3: Development offline test of automatic control-loop performance evaluation methods [ALL PARTNERS]

Software tools (being deliverable D1.3) for automatic performance evaluation of control loops requires at least three steps:

1. Data pre-processing for control performance monitoring
2. Pre-analysis of the process to look for system nonlinearities, oscillations, variations in time delays, etc.
3. Calculation of adequate performance metrics.
4. Identification of sources of poor performance.

Without lack of detail, these four steps provide a comprehensive procedure to assess process performance as well as controller performance.

This task took longer than planned, because some extra ideas to detect sensor faults based on energy index for furnaces have been added. These ideas have been motivated by practical experiences at the annealing furnace of TKN.

3.1.3.1 Data pre-processing for control performance monitoring

For using the Harris index [Har89] one has to select steady-state data for the benchmarking of control loop performance. In practical application, for instance, when analysing the thickness control of a hot strip mill, there are large amounts of measurement data to be analysed, containing also periods of steady and non-steady-states. It is quite a difficult task to separate time periods manually, hence methods are introduced to separate the time spans automatically.

The methods are based on the detection of steady and non-steady states parts of the measuring signal.

Batch steady state detection. [Rhi95] published a steady-state index based on the ratio of the variance of the control error. In steady-state, the control error is an independent stochastic noise with mean value zero. The steady-state index R is defined as follows:

$$R = \frac{\sigma_{e1}^2}{\sigma_{e2}^2} \tag{3.1}$$

with the variance of the control error; see also (Figure 3.10):

$$\sigma_{e1}^2 = \frac{1}{2 \cdot (n-1)} \cdot \sum_{i=l}^{n} (e_{1,i})^2 \tag{3.2}$$

and variance of the difference between the current and last control error

$$e_{2,i} = e_{1,i} - e_{1,i-i} \tag{3.3}$$

$$\sigma_{e2}^2 = \frac{1}{2 \cdot (n-1)} \cdot \sum_{i=l}^{n} (e_{2,i})^2 \tag{3.4}$$

For a closed-loop control in steady-state the steady-state index R is nearly 1. If the control loop is non-steady-state, the value of R increases as shown in figure 3.11 for the thickness control. The drawback of steady-state index R is that the control error has to be stored for computation of the index.

Recursive steady state detection Coa [Cao95] published another variant of this steady-state index R. The steady-state index R_f uses the same deviations of the control error e1, e2 (Figure 3.10). [Cao95] additionally uses for R_f a filter to avoid storing past data of control error for calculating the variance.

$$R_f = \frac{\sigma_{e1,f,i}^2}{\sigma_{e2,f,i}^2} \tag{3.5}$$

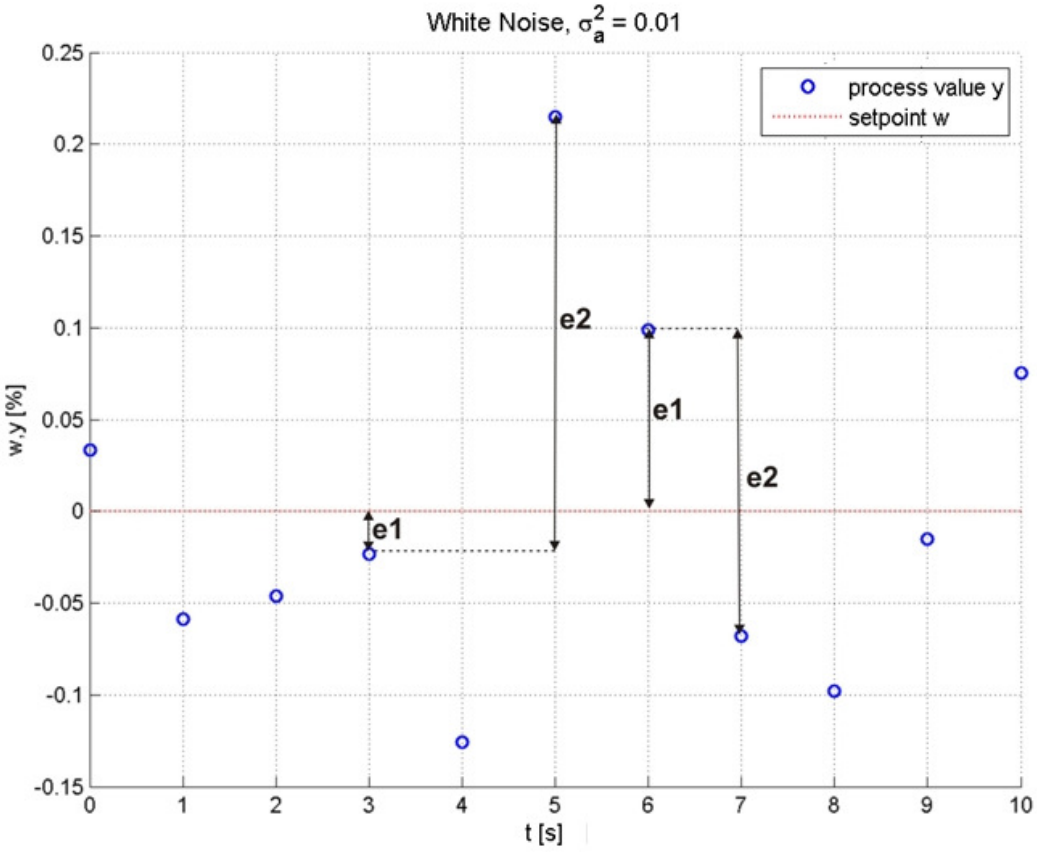

Figure 3.10: Control error

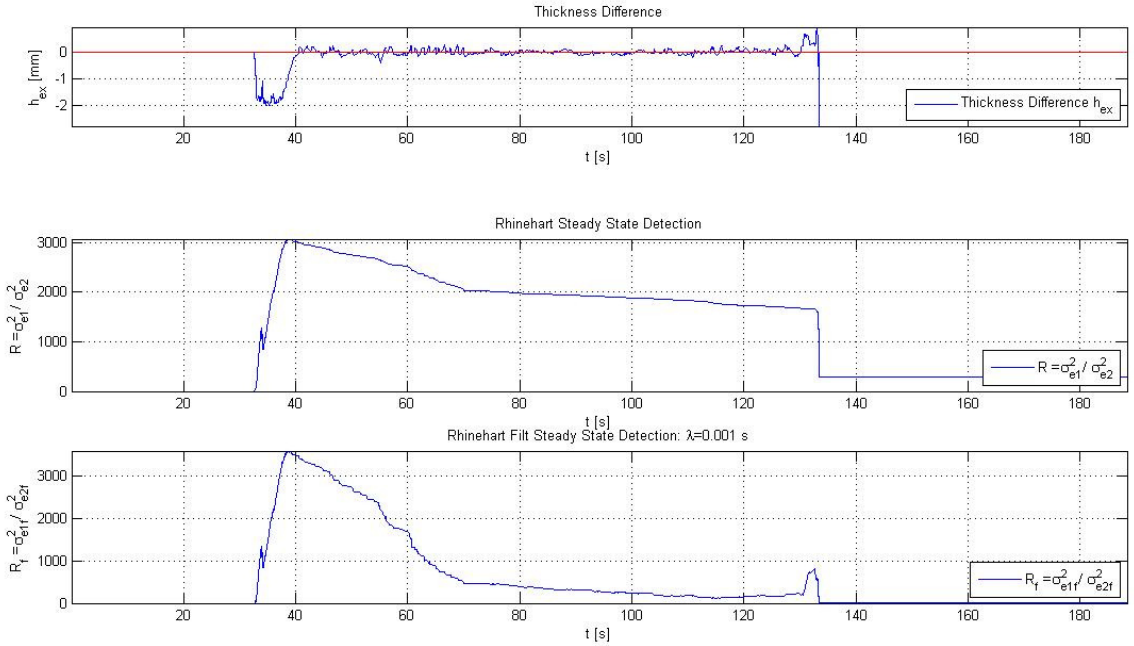

Figure 3.11: Steady-state detection

with filter for the variance of control error

$$\sigma_{e1,f,i}^2 = \lambda \cdot (e_{1,i})^2 + (1-\lambda) \cdot \sigma_{e1,f,i-l}^2 \tag{3.6}$$

and the difference of the control error

$$e_{2,i} = e_{1,i} - e_{1,i-i} \tag{3.7}$$

$$\sigma_{e2,f,i}^2 = \frac{\lambda}{2} \cdot (e_{2,i})^2 + (1-\lambda) \cdot \sigma_{e2,f,i-l}^2 \tag{3.8}$$

This method uses only the last stored ratio of R_f, so it also can be used for an on-line detection of steady state. This performance index R_f is also nearly 1 for a closed-loop control in steady-state.

Figure 3.11 shows the steady-state indices R and R_f (λ=0.001s) for the thickness control h_{ex}. As can be seen in the figure, the steady-state indices R and R_f increased to $R = 3074$ and $R_f = 3588$ at 40s. At the time of 130s they had the value of $R = 1735$ and $R_f = 804$. If the control is in steady-state, the indices R and R_f are close to 1. Hence, the event of start-up of thickness control was found at 40s and the switch off of the control at 130s. Therefore, the time span between 40s and 130s is taken for control performance monitoring data. Data compression altered these measures significantly.

3.1.3.2 Pre-analysis of the process

Detection of nonlinearities is carried out with the Choudhury's method [Cho04]. This is based on the presence of phase coupling in the output error signal. Phase coupling leads to higher order spectral features that can be detected in the bicoherence signal. Two indices are derived from the bicoherence, the Non-Gaussianity Index (NGI) and the Non-Linearity Index (NLI):

$$NGI := \overline{\hat{bic}^2} - \overline{bic^2_{crit}} \tag{3.9}$$

$$NLI := \left| \hat{bic}^2_{max} - \left(\overline{\hat{bic}^2} + 2\sigma_{\hat{bic}^2} \right) \right| \tag{3.10}$$

where $\hat{bic}^2$ is the estimated bicoherence, σ is the standard deviation of the bicoherence and the subscripts *crit* and *max* stand for critical and maximum values, respectively. Average bicoherence values ($\overline{bic^2}$) are used in both indices. The bicoherence is defined as follows:

$$bic^2(f_1, f_2) := \frac{|B(f_1, f_2)|^2}{E\{|Y(f_1)Y(f_2)|^2\} E\{|Y(f_1 + f_2)|^2\}} \tag{3.11}$$

$B(f_1, f_2)$ is the bispectrum at frequencies (f_1, f_2) and is given by:

$$B(f_1, f_2) := E\{Y(f_1)Y(f_2)Y(f_1 + f_2)\} \tag{3.12}$$

$Y(f_i)$ with $i = 1, 2$ are the Fourier transforms of the output data y_t at frequency f_i, and E is the expectation function. The process is Gaussian if $NGI \leq 0$ and linear if $NLI = 0$. We use threshold values i.e. $NGI < 0.001$ and $NLI < 0.01$ for analysis, under which the output signal can be assumed to be Gaussian and linear at a 95% confidence level [Cho04].

Oscillation analysis. For automatic detection of oscillations in control loops it is important to isolate possible sources of bad control performance, e.g. aggressive controller tuning or too high stiction in control valves. On the other hand, when an oscillation is present in the data, the performance (Harris) index values are not reliable, as discovered by Horch [Kad02a], particularly when the oscillation is caused by non-linearities. Therefore, oscillation detection should be included in a very early stage of a performance assessment procedure.

Detection and diagnosis of oscillatory behaviour in a production process is of importance because process variability has an impact on profit. Available methods to identify oscillations in process variables are discussed in detail in the recent overview by Karra et al. [Jel09a].

The method used here is that proposed in [Tho03] based on regularity of zero-crossings of the autocorrelation function (ACF) of the process data. The underlying idea is that a regular oscillation will cross the signal mean at regular intervals. Therefore, the intervals between zero-crossings of an oscillatory time trend can be exploited for offline detection of oscillations. The deviations of the intervals between the zero-crossings are compared to the mean interval length; a small deviation indicates an oscillation.

Instead of looking at the zero-crossings of the time trend, the zero-crossings of the ACF are used, since using ACF for oscillation detection significantly reduces the impact of noise.On that account, the pattern of zero-crossings of the ACF reveals the presence of an oscillation more clearly than the zero-crossings of the time trend. By looking at the regularity of the period, an oscillation can be detected.

Regularity is assessed by the use of a statistic, r, termed the regularity factor. It derives from the sequence of ratios between adjacent intervals Δt_i at which deviations cross the threshold. Thus the mean period of the oscillation T_p can be determined from

$$\bar{T}_\mathrm{p} = 2\frac{\sum_{i=1}^{n}\Delta t_i}{n} = \frac{2}{n}\sum_{i=1}^{n}(t_i - t_{i-1}) \tag{3.13}$$

and the dimensionless *regularity factor*, r is [Tho03]

$$r = \frac{1}{3}\frac{\bar{T}_\mathrm{p}}{\sigma_{T_\mathrm{p}}}, \tag{3.14}$$

where σ_{T_p} is the standard deviation of T_p. An oscillation is considered to be regular with a well-defined period if r is greater than unity. That is why the *regularity factor r* can be regarded as an *oscillation index*.

Determination of time delay. Priori knowledge of time delays is required for estimating the minimum achievable variance. Its estimation also provides insights into other aspects of the process such as the need of high performance dead-time controllers [Hor00] or as suggested in [Cho09], the lack of properly tuned derivative terms in the controller for time-delay compensation.

There are several methods for time delay estimation [Lyn96, Bjo03]. Perhaps the most common and reliable method, as suggested in [Jel06a], is the correlation-based method. Correlation methods are widely used to determine the delay between two signals. The method consiss of computing the cross-correlation function [Kna76]:

$$R_{x_1,x_2}(\tau) = E\{x_1(k)\,x_2(k-\tau)\} \tag{3.15}$$

where E denotes expectation, x_1, x_2 can be process input and output variables, respectively. Time delay estimation from routine operating data requires either external excitations or abrupt changes in the control signals [Jel06a]. These changes can also be produced by smooth nonlinearities or perturbations. For this reason it is recommended to pre-filter the signals to avoid estimation errors.

3.1.3.3 Pre-assessment of processes via energy based index's

Monitoring of static energy index for annealing furnaces. The static energy [And08] is defined as the ratio between energy of the strip and the fuel

$$\eta_\mathrm{energy} = \frac{E_\mathrm{steel}}{E_\mathrm{fuel}} = \frac{E_\mathrm{steel}\Delta t}{E_\mathrm{fuel}\Delta t} = \frac{P_\mathrm{steel}}{P_\mathrm{fuel}} \tag{3.16}$$

Thermal power in the strip

$$P_\mathrm{steel} = \dot{m}_\mathrm{steel} c_p T_\mathrm{steel} \tag{3.17}$$

with mass fow of the steel

$$\dot{m}_\mathrm{steel} = d \cdot w \cdot v \tag{3.18}$$

where d is the strip thickness, w the width and v the strip speed and the thermal power

$$P_\mathrm{fuel} = H_\mathrm{fuel} \cdot m_\mathrm{fuel} \tag{3.19}$$

where H_fuel is heat value of the fuel and $\cdot$ is the mass flow of the fuel. This is percentage of fuel energy transferred to the steel feedstock. For this to be 100%, all the fuel energy would need to be transferred to the steel, and energy losses (structural and exhaust gas) equal zero. A furnace efficiency of 50% (based on the gross CV) could be expected for a well designed and operated reheating furnace. In batch, and heat treatment furnaces it will be lower [And08].

For monitoring the following procedure is suggested.

$$\kappa_{energy} = \begin{cases} 1 & \text{if} \left| \eta_{energy,ref} - \eta_{energy} \right| \leq \Delta_{energy} \\ 0 & \text{if} \left| \eta_{energy,ref} - \eta_{energy} \right| > \Delta_{energy} \end{cases} \tag{3.20}$$

First record the data with reference to the situation and calculate reference energy index $\eta_{energy,ref}$. Second calculate the form current data the energy index η_{enery} and compare it with the reference index η_{energy}. If the difference exceed the limit Δ_{energy} it could give hints to mail function in values or leakages. Some results are shown in Task 5.2

3.1.3.4 Pre-assessment of controller performance via disturbance filtering

A method for pre-assessment of controller performance using disturbance filtering and a model-based MPC method are presented. The assessment of the existing controller is achieved by filtering the effect of disturbances using Multiscale Principal Component Analysis (MsPCA). Using filtered data, controlled inputs and setpoints, a model of the process is established through closed-loop subspace modelling and is consequently used to design the MPC controller. A model-based performance metric is then designed.

A method for pre-assessment of controller performance using disturbance filtering and a model-based MPC method are presented. The assessment of the existing controller is achieved by filtering out the effect of disturbances using MsPCA. Using filtered data, controlled inputs and setpoints, a model of the process is established through closed-loop subspace modelling and is consequently used to design the MPC controller. A model-based performance metric is then designed.

Assuming that the process variance can be expressed as a sum of terms that represent every possible root-cause of poor performance as follows:

$$\begin{aligned} var\{y_t\} = \quad & var\{y_t\}_b + var\{y_t\}_p + var\{y_t\}_c + var\{y_t\}_d + var\{y_t\}_{osc} + var\{y_t\}_{nonl} \\ & + var\{y_t\}_{c.m.} + var\{y_t\}_{s.e.} \end{aligned} \tag{3.21}$$

where the variance inflation of the output (y_t) is due to: delays (b), process dynamics (p), controllers (c), disturbances (d), oscillations (osc) internal or external, nonlinearities (nonl), component malfunctions (c.m.) and shared effects (s.e.) respectively. Tailored diagnosis methodologies have been developed to tackle these root-causes individually [Hua03] and diagnosis methods for controllers are scarce and have only been developed for MPC [Tia11].

When nonlinearities are present, the above representation can be incorrect because the superposition principle does not hold, but for variance quantification purposes, it is still valid. In (3.21), the terms corresponding to oscillations and nonlinearities should be pre-assessed to specify if a linear performance metric can be used. Delays also affect the feedback invariant terms and constitute an inner process constraint.

Traditionally, variance inflation due to poor control was considered the main cause of poor performance, but no metric for its quantification has been proposed. Re-arranging equation (3.21) as follows:

$$var\{y_t\} - var\{y_t\}_c = var\{y_t\}_r \tag{3.22}$$

with: $var\{y_t\}_r = var\{y_t\}_p + var\{y_t\}_d + var\{y_t\}_{c.m.} + var\{y_t\}_{s.e.}$ It can be seen that the residual variance $var\{y_t\}_r$ depends on any other sources except the controller. If the value of $var\{y_t\}_r$ is insignificant, diagnosis can be avoided. Notice that variance inflation due to delays, nonlinearities and oscillations are deleted, since they have been pre-assessed. A similar approach to quantify the effects of non-linearities can also be developed. The metric by itself does not indicate the significance of the residual variance inflation. Therefore a measurable control improvement or profit analysis should be given to judge if diagnosis is necessary.

The performance metric is formulated as the ratio of the determinants of the variance-covariance matrices of the actual process inputs and outputs with their optimal counterparts [McN03]. The output variability is given by:

$$\eta_y^F = \frac{det\left\{R_{Y_f^o}\right\}}{det\left\{R_{Y_f}\right\}} \tag{3.23}$$

whereas the input energy index is given by:

$$\eta_u^F = \frac{det\left\{R_{U_f^o}\right\}}{det\left\{R_{U_f}\right\}} \tag{3.24}$$

F stands for filtered, Y_f and U_f are output and input future (f) sequences. The index varies $0 < \eta < 1$ showing good performance when it is close to 1 or vice versa. The covariances ($R_{U_f^o}$ and $R_{Y_f^o}$) come from the optimal input and output data sequences provided from the solution of the cost function used to design the MPC controller. The cost function is given by:

$$J_{min} = \min_{U_f} \left\{\hat{Y}_f^T \hat{Y}_f + U_f^T R U_f\right\} \tag{3.25}$$

$\hat{Y}$ is the identified output data using closed-loop subspace identification with QR-decomposition and filtered using MsPCA.

MsPCA is a combination of Principal Component Analysis (PCA) and wavelet decomposition. Wavelet decomposition can be achieved as a filtering procedure. The signal is projected onto a matrix W containing a scaling-function low pass filter coefficients H_L at the coarsest range (L) and wavelet high pass filter coefficients J_i corresponding to range $i = 1,2,...,L$. The transformation matrix W is given by:

$$W = \begin{bmatrix} H_L & J_L & J_{L-1} & \cdots & J_i & \cdots & J_1 \end{bmatrix}^T \tag{3.26}$$

The range is selected to provide maximum separation between the stochastic and the deterministic components of the signal. A heuristic maximum range is given as $L = log_2(n)$ [Bak97], with n as the minimum size of the output data $\vec{y}$.
The data $\vec{y} = [y_t, y_{t+1}, \cdots, y_{t+n}]$ is decomposed into $L+1$ ranges as follows:

$$\vec{y}W = Z \tag{3.27}$$

with $Z = \left\{z_L^H, z_i^J\right\}$, $i = (1,2,...,L)$. PCA is applied on each scale. PCA divides the data z_i into two significant patterns: linear tendencies of the model $\hat{z}_i$ and model uncertainties $\tilde{z}_i$ so that:

$$z_i = \hat{z}_i + \tilde{z}_i \tag{3.28}$$

and

$$\hat{z}_i = \hat{T}_i \hat{P}_i^T J_i \tag{3.29}$$

$\hat{z}_i$ is the filtered data. $\hat{T}$ and $\hat{P}$ are the Principal Components (PC's) loadings and PC's scores respectively. For MsPCA, the PC's loadings obtained by PCA of $\vec{y}$ and $\vec{y}W$ are identical, whereas the PC's scores of $\vec{y}W$ are the wavelet transform of the scores of $\vec{y}$ [Bak97].
The filtered data $\vec{y}$ can thus be reconstructed from $\hat{Z} = \left\{\hat{z}_L^H, \hat{z}_i^J\right\}$ as follows:

$$\hat{\vec{y}} = \hat{Z}W^T \tag{3.30}$$

since $WW^T = I$.

Simulation Study The approach procedure was condensed into the following steps:

1. Apply MSPCA on the data $\vec{y}$ to obtain the de-noised output $\hat{\vec{y}}$.
2. Use $\hat{y}_t$ together with u_t and y_{sp} to obtain the process model using recursive subspace identification with QR decomposition.
3. Design a MPC using the estimated model from the previous step
4. Calculate the input and output covariance matrices $R_{U_f^o}$, $R_{Y_f^o}$ from the MPC control system.
5. Calculate input and output covariance matrices from the original system
6. Calculate the output variability index η_y^f and energy index η_u^f.

7. Repeat steps 3 - 6 using the original data.
8. Calculate the residual performance index η_y^r

For simulation, the following SISO system was considered:

$$G_p(s) = \frac{1}{10s+1}e^{-5s} \tag{3.31}$$

The process was controlled by the following PI controller:

$$K_{PI}(s) = 0.9 + \frac{1}{5s} \tag{3.32}$$

A source of noise was present $w \sim N(0, 0.1)$. The simulation has run for 6000 samples. At time $t = 3000$ a load disturbance change has been made. The MPC-based performance metric were also calculated

Table 3.2: Controller pre-assessment

	Time delay [s]		Nonlinearities [-]		
original	4.83		-3.47		
	Performance Indexes				Residual Index
	$\eta_y[-]$	$\eta_u[-]$	$\eta_y^f[-]$	$\eta_u^f[-]$	$\eta_y^r[\%]$
original	0.5717		0.625		9.32
re-tuned	0.7538	0 6870	0.823	0 7115	9.18

for comparison purposes. Time delay estimation and detection of nonlinearities are calculated using the cross-correlation method [Kna76], and Choudhury's method [Cho08], respectively. These results are presented in table 3.2. A negative value of NLI satisfied the threshold ($NLI < 0.01$) given by the Choudhury's method for a system to be linear. The value of the CPA metric pointed out a poor performing process. To de-noise the output signal, MsPCA was used with $L = 5$.

Table 3.2 shows the performance index of the original output data η_y, the performance index of the filtered output data η_y^f and the percentage of the residual performance index. The results showed that poor tuning accounted for more than 90% of the overall variance. The value of η_y was smaller than that of η_y^f because the residual variance reduces the overall performance index. The user decided whether it is convenient to re-tune the controller or not.

The MPC controller benchmark was used to re-tune the original controller. The resulting PI controller coefficients were: $K_p = 1.8$ and $T_i = 10.21$. The new performance indices after controller re-tuning are presented in table 3.2. Performance indices were higher but still not close to 1 since a PI controller cannot provide a better performance. Input variability was also reduced as shown in the table.

It is important to mention that the residual index was not affected by the controller re-tuning. Compensation of the residual variance required either a new controller design for disturbance rejection or a new control structure with feedforward compensation.

3.1.3.5 Procedure for control performance assessment and diagnosis based on minimum variance metric

A sequential method for control performance assessment and diagnosis using classification tree to predict possible root-causes of poor performance was set up. Process pre-assessment (nonlinearities detection, delays estimation and controller pre-assessment) was carried out before a Minimum Variance (MV)-CPA metric was calculated to provide a comprehensive assessment.

Controller pre-assessment Pre-assessment approaches have been presented previously and used in this section as part of the process pre-assessment.

To diagnose the root-causes for poor controller performance, the following indexes were defined to quantify the percentage of improvement by feedback (fb) control re-tuning:

$$I_y^{fb} = \frac{R_{\hat{Y}}^{fb} - R_{\hat{Y}^o}^{fb}}{R_{\hat{Y}}^{fb}} \times 100; \quad I_u^{fb} = \frac{R_{\hat{U}}^{fb} - R_{\hat{U}^o}^{fb}}{R_{\hat{U}}^{fb}} \times 100\% \tag{3.33}$$

Whereas, the covariances ($R_{U_f^o}$ and $R_{Y_f^o}$) come from the optimal input and output data sequences provided from the solution of the cost function, Eq.(3.25), used to design the MPC controller. When measured disturbances are available, the percentage of improvement from feedforward control can be calculated. If this percentage is insignificant, inadequate control structure should be considered as the root-cause of poor performance.

Control performance assessment and ANOVA CPA is implemented as minimum variance metric as follows:

$$\eta_y = \frac{\sigma_{mv}^2}{\sigma_y^2} \tag{3.34}$$

where σ_{mv}^2 is the variance achieved under minimum variance (MV) control and σ_y^2 is the plant output variance.

ANOVA decomposes the plant output variance into delay-independent terms called feedback invariant (fbi) and feedback/feedforward invariant (fbi/ffi). Additional terms affected by the implemented controllers are feedback-invariant/feedforward-dependent (fbi/ffd), feedback dependent (fbd) and feedback/feedforward dependent (fbd/ffd). The decomposed output variance is therefore given by:

$$\begin{aligned} \sigma_y^2 &= \sigma_{mv}^2 + S_{fbd}\left(b, G_w^0, G_p, G_c^{fb}\right)\sigma_{w_t^0}^2 + S_{fbi/ffd}\left(b, G_w^1, G_p, G_c^{ff}\right)\sigma_{w_t^1}^2 \\ &\quad + S_{fbd/ffd}\left(b, l, G_w^1, G_p, G_c^{fb}, G_c^{ff}\right)\sigma_{w_t^1}^2 \end{aligned} \tag{3.35}$$

$$\sigma_{mv}^2 = S_{fbi}\left(b, G_w^0\right)\sigma_{w_t^0}^2 + S_{fbi/ffi}\left(b, l, G_w^1\right)\sigma_{w_t^1}^2 \tag{3.36}$$

$S_{fbi}, S_{fbd}, S_{fbi/ffi}, S_{fbi/ffd}$ and $S_{fbd/ffd}$ are residuals estimates. Each term in (3.35) is calculated individually. Time series models of G_w^0 and G_w^1 are identified and truncated to obtain the residual estimates.

Industrial case study A model was established for a three-stand two-high rolling mill. A multi-loop architecture was implemented to control the process using a combination of PID and other controllers. Thickness, mass flow and speed control were implemented in every stage. Thickness of the last stand was analysed and time delay at the thickness sensor was monitored. Controllers were assumed to be properly tuned. Roll eccentricity was added at every stand to increase disturbances in simulation. The strip thickness was reduced from $15mm$ to $5mm$.

The output strip thickness of the third stand is presented in figure 3.12. The simulation length was 350s. A set-point change in strip thickness from $4mm$ to $5mm$ was introduced at $t = 280s$ in stand 3. Similar set-point changes were carried out in stand 1 ($15mm - 4.6mm$) at $t = 100s$; and stand 2 ($15mm - 4.3mm$) at $t = 190s$. The changes in set-points in stands 1 and 2 were reflected in the strip thickness at stand 3 due to the mass conservation principle. Operating data was collected and analysed in every stand. CPA was only applied to the last stand. Roll eccentricity was changed to test the decision tree under disturbance. When roll eccentricity has been increased, the output strip thickness became oscillatory after $t = 220s$. On account of this the simulations were presented up to time $t = 220s$. The output strip thickness with reduced eccentricity is given in figure 3.13 whereas the output strip thickness in stand 3 with increased eccentricity is presented in figure 3.14.

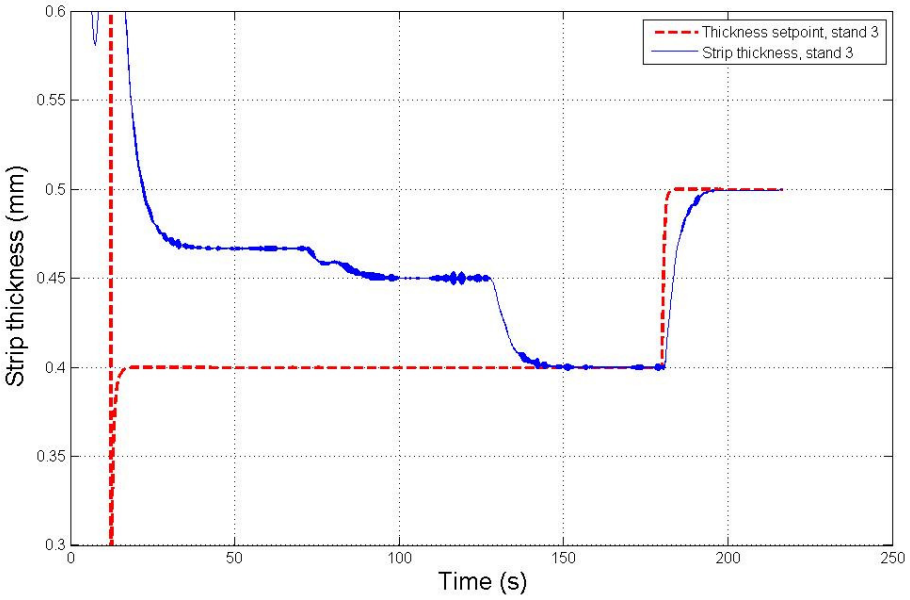

Figure 3.12: Output strip thickness at stand 3 with the nominal model

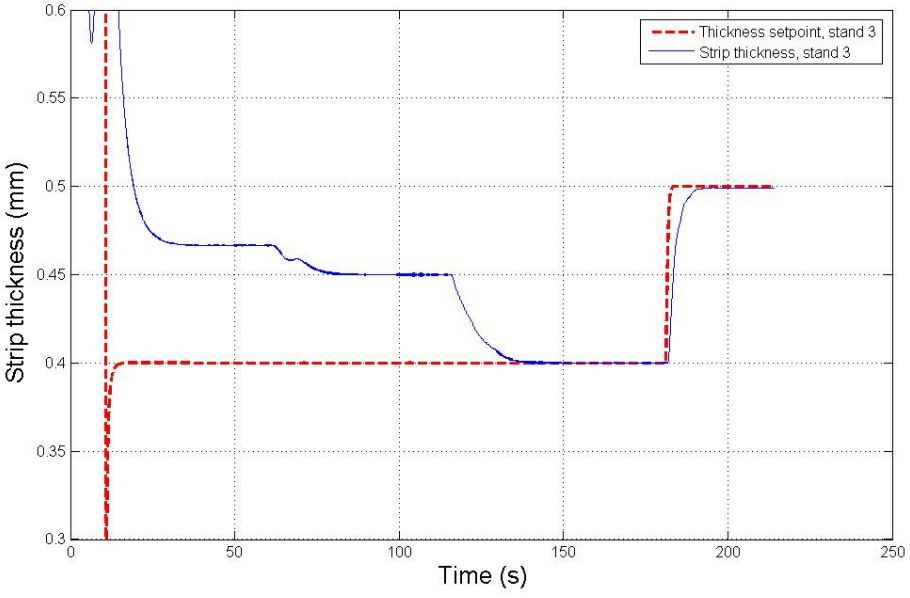

Figure 3.13: Output thickness at stand 3 for the model with reduced eccentricity

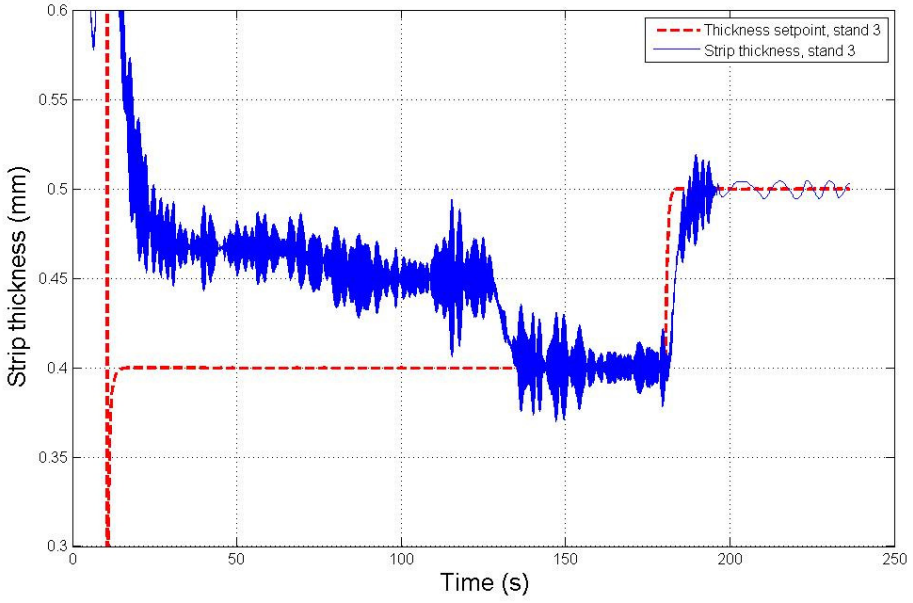

Figure 3.14: Output thickness at stand 3 for the model with increased eccentricity

Results of assessment and diagnosis of the three cases are presented in table 3.3.

Table 3.3: Complete assessment of output thickness in stand 3: nominal (N), reduced (R) and increased (I) eccentricity models

	Nonlinearities detection		Delay estimation	
	NGI [-]	NLI [-]	b [s]	$\hat{b}$ [s]
N	0.41	1.23	1.03	1.04
R	4.15	-7.73	1.03	1.27
I	0.49	0.10	1.03	0.98

Profit Control Analysis					
	$var(u)$ [%]	$var(y)$ [mm]	η^F_{y+u} [-]	I^{fb}_u[%]	I^{fb}_y[%]
N	0.25	0.62	1.54	0	38.31
R	0.25	0.51	1.27	0	49
I	0.32	0.51	1.28	0	48.66

Control Performance Assessment		
	η_y (linear) [-]	η^{nonl}_y (nonlinear) [-]
N	0.80	0.79
R	0.81	
I	0.83	0.69

The results suggested nonlinearities on models nominal and increased eccentricity. Controller pre-assessment was calculated with a cumulative index (η^F_{y+u}) which is only the sum of the output index and the energy index ($\eta^F_{y+u} = \eta_y + \eta_u$) and is used to ease the hypothesis test since the diagnosis depends only on the percentages of improvement indices. In these three cases the percentage of control improvement was relatively high.

3.1.3.6 Procedure for control performance assessment and diagnosis based idle and visiol index

Idle index for detection of sluggish control The idle index, provided by BFI, was introduced by Hägglund [Hag95] to assess the time for a loop needed to recover from a stepwise load disturbance.

The idle index (I_i) is defined as (figure 3.15)

$$I_{\mathrm{i}} = \frac{t_{\mathrm{pos}} - t_{\mathrm{neg}}}{t_{\mathrm{pos}} + t_{\mathrm{neg}}} \tag{3.37}$$

for loops with a positive gain, and

$$I_{\mathrm{i}} = \frac{-t_{\mathrm{pos}} + t_{\mathrm{neg}}}{t_{\mathrm{pos}} + t_{\mathrm{neg}}} \tag{3.38}$$

for loops with a negative gain. The idle index describes the relation between times of positive and negative correlation between the control signal and the process output increments, Δu and Δy, respectively.

To form the index, the time periods when the correlations between the signal increments are positive and negative, respectively, are calculated first. The following quantities are updated at every sampling instant

$$\begin{aligned} t_{\mathrm{pos}} &= \begin{cases} t_{\mathrm{pos}} + T_{\mathrm{s}} & \text{if } \Delta u \Delta y > 0 \\ t_{\mathrm{pos}} & \text{if } \Delta u \Delta y \leq 0 \end{cases} \\ t_{\mathrm{neg}} &= \begin{cases} t_{\mathrm{neg}} + T_{\mathrm{s}} & \text{if } \Delta u \Delta y < 0 \\ t_{\mathrm{neg}} & \text{if } \Delta u \Delta y \geq 0 \end{cases} \end{aligned} \tag{3.39}$$

where T_{s} is the sampling time.

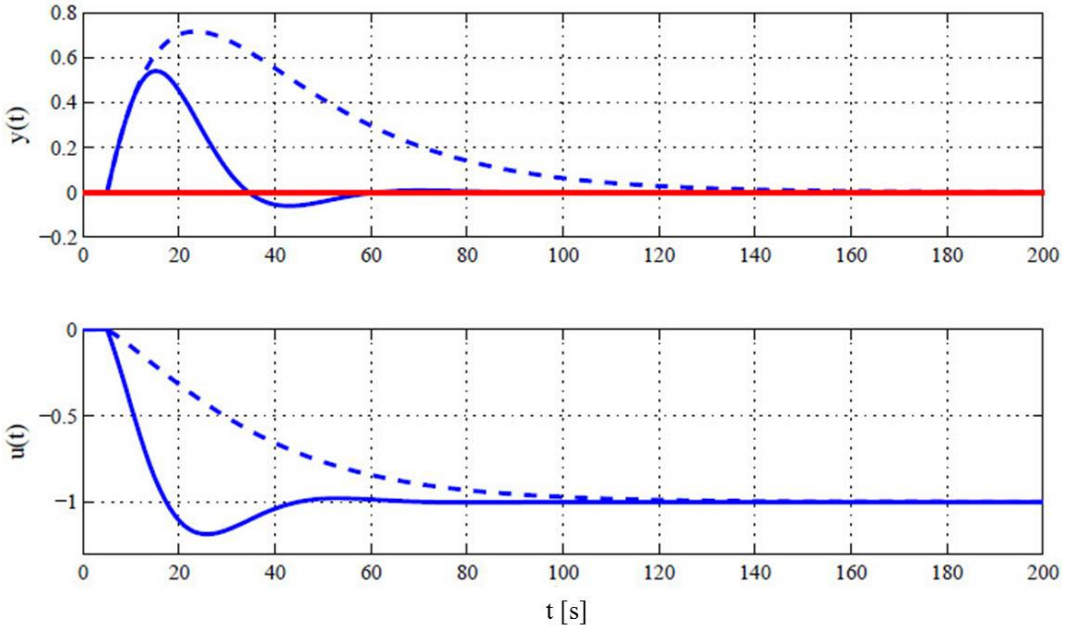

Figure 3.15: Good (solid) and sluggish (dash) control of load disturbances

I_{i} is bounded in the interval $[-1, 1]$. A positive value of I_{i} close to 1 means that the control is sluggish. Values close to 0 indicate that the controller tuning is reasonably good. Negative values of I_{i} close to -1 may imply well-tuned control, but can also be obtained for oscillatory control as well.

Visioli index for controller-tuning assessment The aim of the methodology proposed by Visioli [Vis05] is to verify, by evaluating an abrupt load disturbance response, if the tuning of the adopted PI controller guarantees good load-disturbance rejection performance. The performance index proposed is called the *area index* (*AI*) and is based on the control signal $u(t)$ that compensates for a step load disturbance occurring on the process. The value of the area index then decides whether it can be deduced if the control loop is too oscillatory.

The area index is calculated as the ratio between the maximal value of the determined areas (Figure 3.16) and the sum of them, excluding the area A_0, *i.e.* the area between the time instant, in which the step load disturbance occurs and the first time instant at which $u(t)$ attains u_0. Formally, the area index is defined as:

$$I_{\mathrm{a}} := \begin{cases} 1 & \text{if } N < 3 \\ \frac{\max(A_1,\ldots,A_{N-2})}{\sum_{i=1}^{N-1} A_i} & \text{elsewhere} \end{cases} \tag{3.40}$$

$$A_i = \int_{t_i}^{t_{i+1}} |u(t) - u_0| \mathrm{d}t \qquad i = 0, 1, \ldots, N-1, \tag{3.41}$$

where u_0 denotes the new steady-state value achieved by the control signal after the transient load disturbance response, t_0 the time instant in which the step load disturbance occurs, t_1, ..., t_{N-1} the subsequent time instants and t_N the time instant in which the transient response ends and the manipulated variable attains its steady-state value u_0. From a practical point of view, the value of t_N can be selected as the minimum time after that $u(t)$ remains within a p% (*e.g.* 1%) range of u_0.

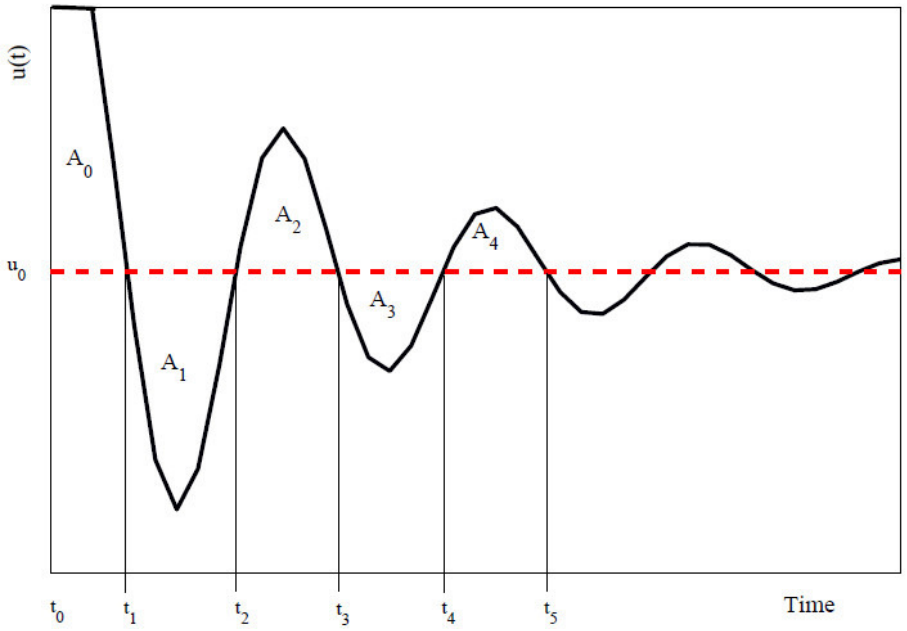

Figure 3.16: Significant parameters for determining the area index

The area index can be combined with other indices to assess the performance of PI controllers. Based on the results obtained, the rules presented in Table 3.4 have been devised by Visioli [Vis05] to assess the tuning of the PI settings. The value of the area index is considered to be low if it is less than 0.35, medium if it is $0.35 < I_\mathrm{a} < 0.7$ and high if it is greater than 0.7. The value of the idle index is considered to be low if it is less than -0.6, medium if it is $-0.6 < I_\mathrm{i} < 0$ and high if it is greater than zero.

From Eq. 3.41, it can be deduced that the value of the area index is always in the interval (0, 1]. It has been concluded that the more the value of AI approaches zero, the more the control loop is oscillatory, whilst the more the value of AI approaches unity the more the control loop is sluggish. Therefore, a well-tuned controller gives a medium value of AI.

Table 3.4: Visioli's performance-assessment rules for PI controllers

	$I_\mathrm{i} < -0.6$ (low)	$I_\mathrm{i} \in [-0.6,\ 0]$ (medium)	$I_\mathrm{i} > 0$ (high)
$I_\mathrm{a} > 0.7$ (high)	K_c too low	K_c too low, T_I too low	K_c too low, T_I too high
$I_\mathrm{a} \in [0.35,\ 0.7]$ (medium)	**K_c ok, T_I ok**	K_c too low, T_I too low	-
$I_\mathrm{a} < 0.35$ (low)	K_c too high and/or T_I too low	T_I too high	T_I too high

Application to hot strip mill gauge control at AMEH The performance of AMEH's HSM gauge control was analyzed using the data gathered during the production in Sept.–Nov. 2011. Figure 3.17 shows the calculated values of the Harris index and their distributions for the production data from

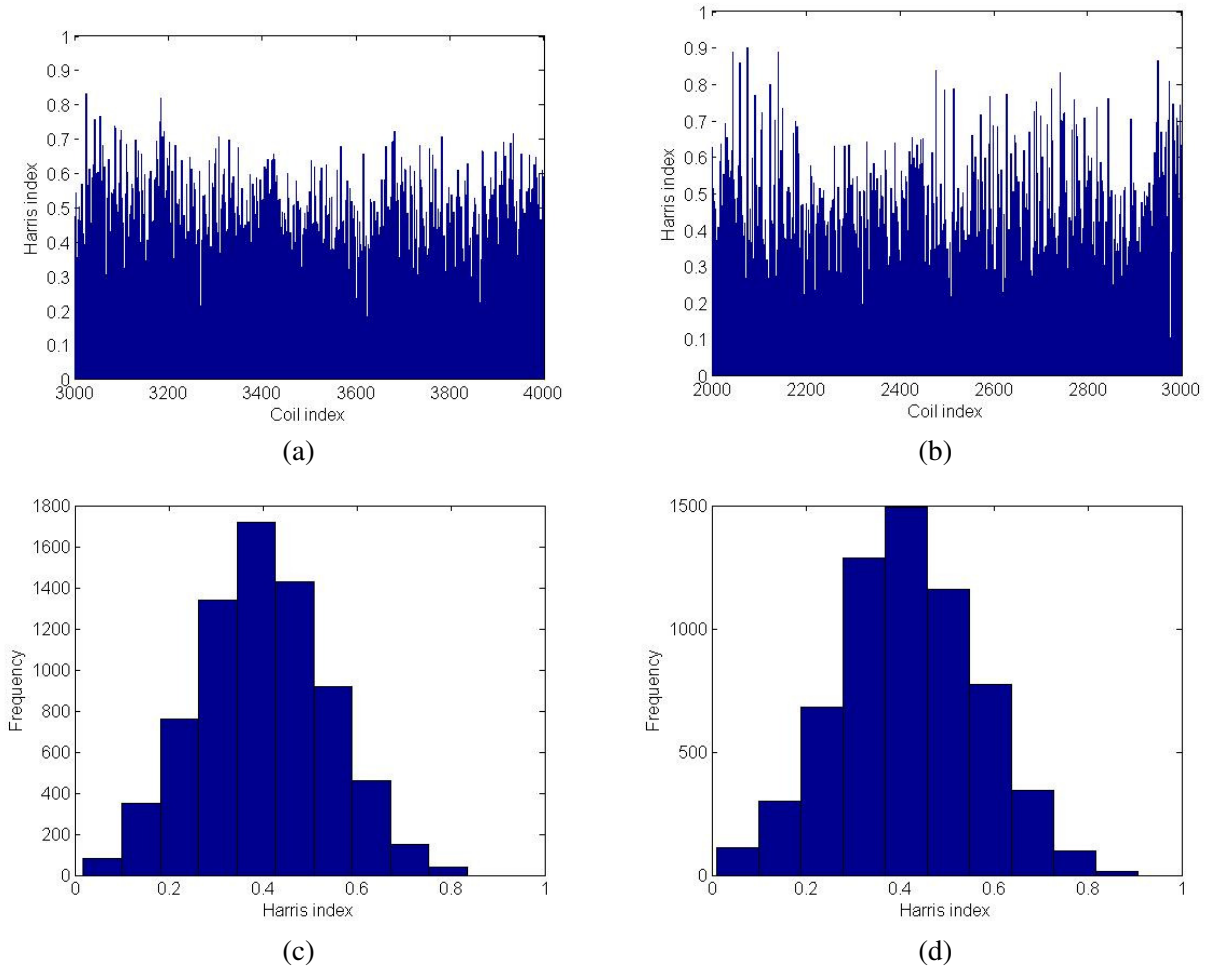

Figure 3.17: Harris index values and their distributions for (a, c) Sept.–Oct. and (b, d) Oct.–Nov. production

two periods. The mean Harris index lied around 0.4, i.e. the overall performance of the gauge control system was considered as fair, but there has been a clear potential for improvement.

In figure 3.18, the oscillation detection results were illustrated in terms of the oscillation index. Although the index is below the threshold (i.e. $r < 1$) for the majority of coils, a part of the strips showed an oscillatory behaviour. This had to be further investigated and diagnosed in Task 2.1.

To study the individual effects of disturbances and controller parts on the output variance, the ANOVA method was applied to each coil's data. The result of this analysis is shown in Table 3.5. It can be concluded that (1) speed and entry thickness feedforward controls did not lead to performance improvement, so that no alterations were needed here; (2) the output variance was substantially reduced by retuning the feedback control part.

To get possible hints on how the gauge control system compensated possible disturbances, the performance was analyzed using the Visioli index. The results in Figs. 3.19 and 3.20 show that the monitor thickness controller seemed to be weakly tuned, so that its retuning was recommended in terms of at least lower integration time constant T_I. This was confirmed by observations/experience of the plant personnel, who stated that the controllers were tuned very conservatively which may produce sluggish control behaviour.

Application to temperature control at TKN's annealing line At TKN's annealing line KL3, the strip temperature is controlled by a PI controller in the last zone, with feedforward control of speed, strip thickness and width. In other zones, temperatures are in open-loop control with subordinated furnace room temperature controls; see figure 3.21.

Data was analyzed in terms of performance (Harris) index and oscillation index by BFI. The results in figure 3.22 show that the overall performance was not satisfactory and thus had to be improved. Oscillations were not an issue, as can be concluded from figure 3.23. Some typical examples are

Table 3.5: Average index values of AMEH's HSM gauge control performance

Analysis period/ Number of coils	PI	PI_FF speed F4	PI_FF speed F5	PI_FF thickness F4	PI_FF looper angle F4
Sept.- Oct. 7236	0.40	0.95	0.96	0.95	0.81
Oct.-Nov. 6900	0.45	0.95	0.95	0.90	0.85

Assessment	PI
High	0.7–1.0
OK	0.4–0.7
Poor	0–0.4

PI: Performance index for feedback control
PI_FF: Performance index for feedforward control

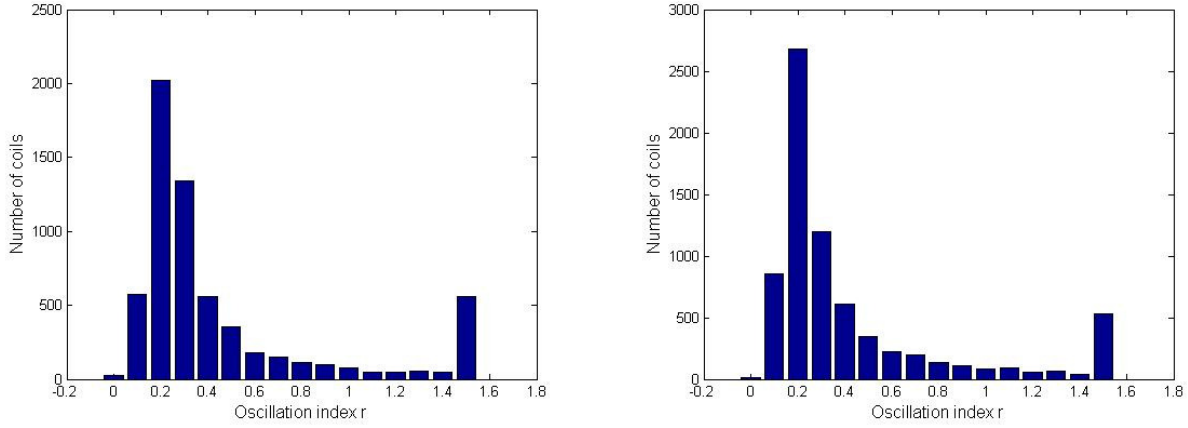

Figure 3.18: Histograms of oscillation index values for (a) Sept.–Oct. and (b) Oct.–Nov. production

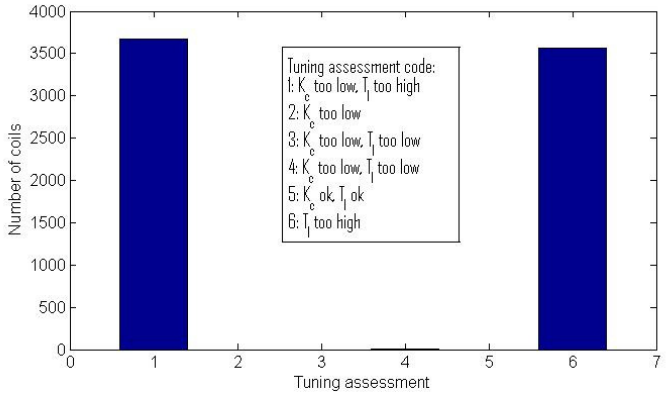

Figure 3.19: Controller tuning assessment using Visioli's index for Sept.–Oct.

described in more details in subsequent sections.

The first example showed good control performance; see figure 3.24. In this case, the set-point and actual values were close to each other, and the Harris index value $\eta = 0.82$ and the impulse response do clearly confirm the high performance. Similar results were achieved and similar conclusions can be stated for the example in figure 3.25. Here, a small control error remained, so that the Harris-index values was lower ($\eta = 0.72$), but the control performance still satisfying.

Now an example with bad performance follows, as can be seen in figure 3.26. The actual temperature values did not follow the changing set-points. A big control-error offset remained, as can be perfectly

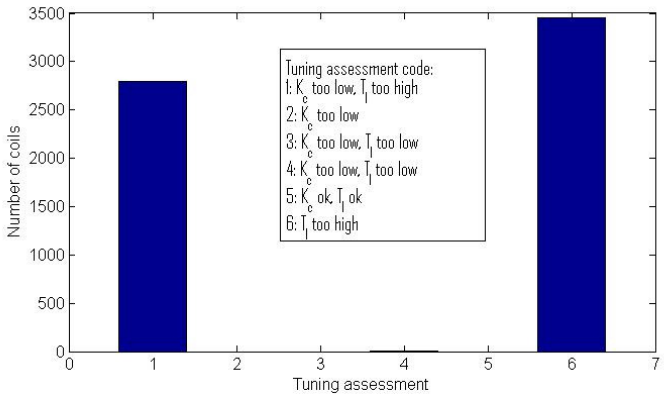

Figure 3.20: Controller tuning assessment using Visioli's index for Oct.–Nov.

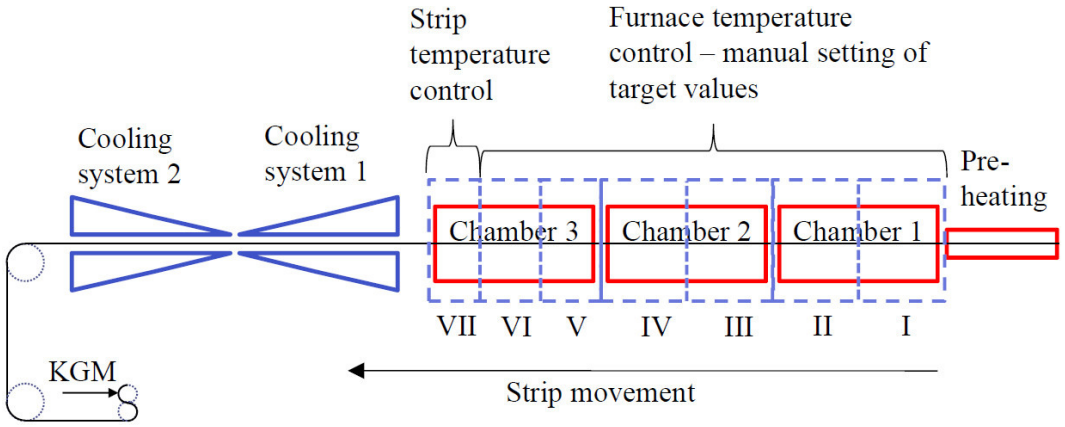

Figure 3.21: Schematic demonstration of the continuous annealing furnace KL3

seen in the impulse response never achieving zero. The root-cause may be that the actuating variable has often been operated at the limit (i.e. $u = 100\%$). The performance index had a value $\eta = 0.1$, indicating very low performance.

For the last example shown in figure 3.27, the same conclusions were drawn. The results strongly revealed the effect of actuator limitation. This problem had to be solved, e.g. by redistribution of control actions over the different furnace zones.

Furthermore, the ANOVA method was used for the process data, considering that the speed and the strip width and thickness were measured variables. The first results revealed that the performance cannot be improved by feedforward control of the measured disturbances.

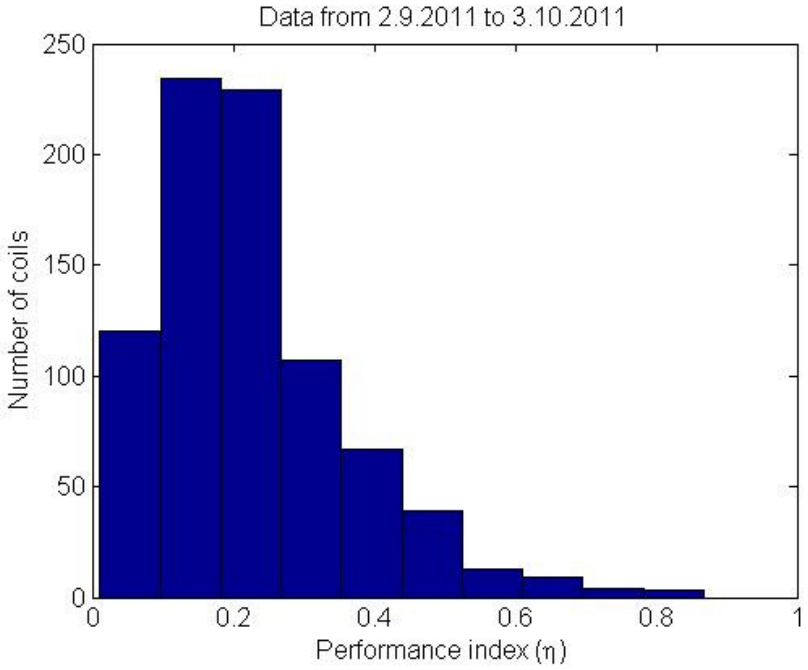

Figure 3.22: Histogram of the Harris index values calculated from temperature control data

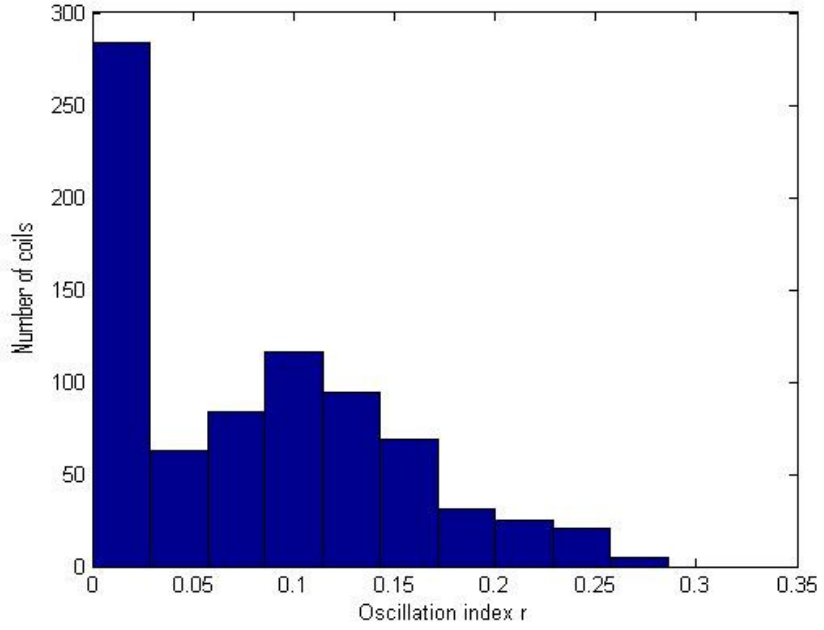

Figure 3.23: Histogram of the oscillation index values calculated from temperature control data

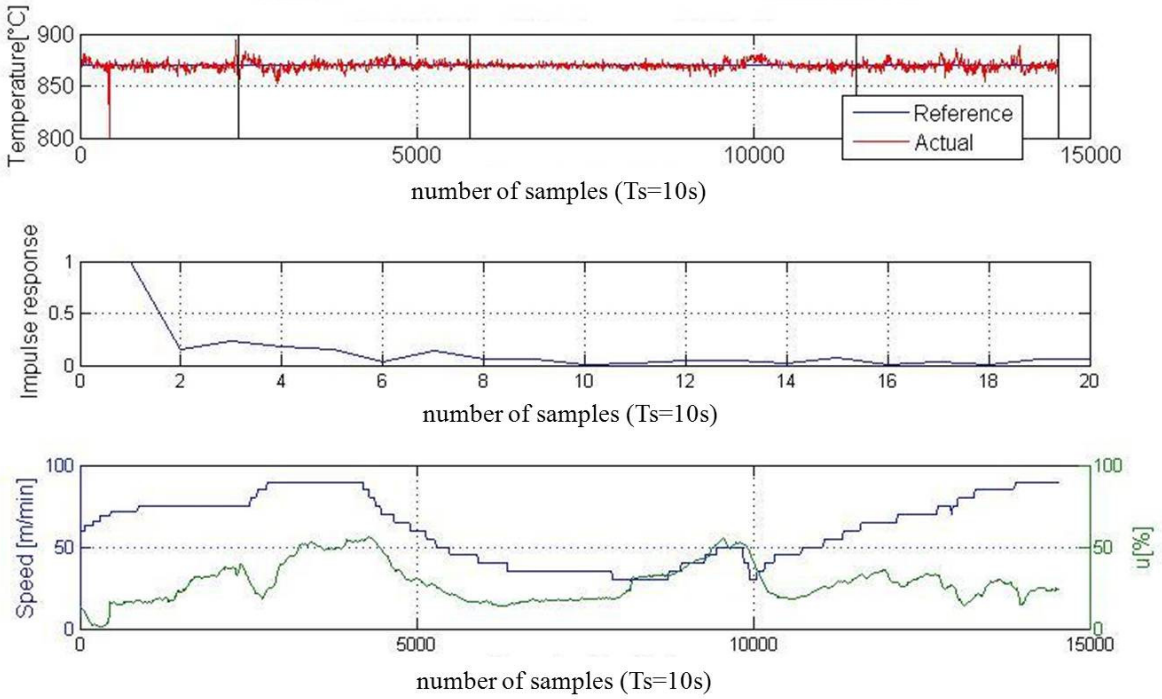

Figure 3.24: Measured data and calculated impulse response for coil no. 111727-111133, Harries Index $\eta = 0.82$

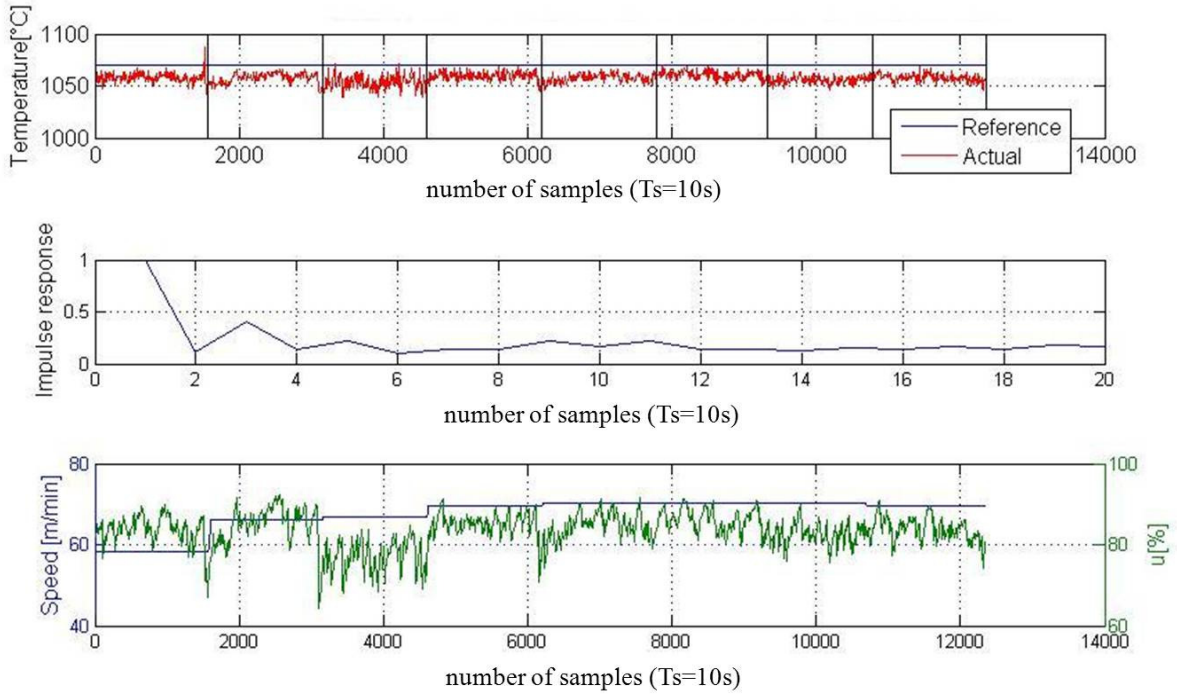

Figure 3.25: Measured data and calculated impulse response for coil no. 111844-111851, Harries Index $\eta = 0.72$

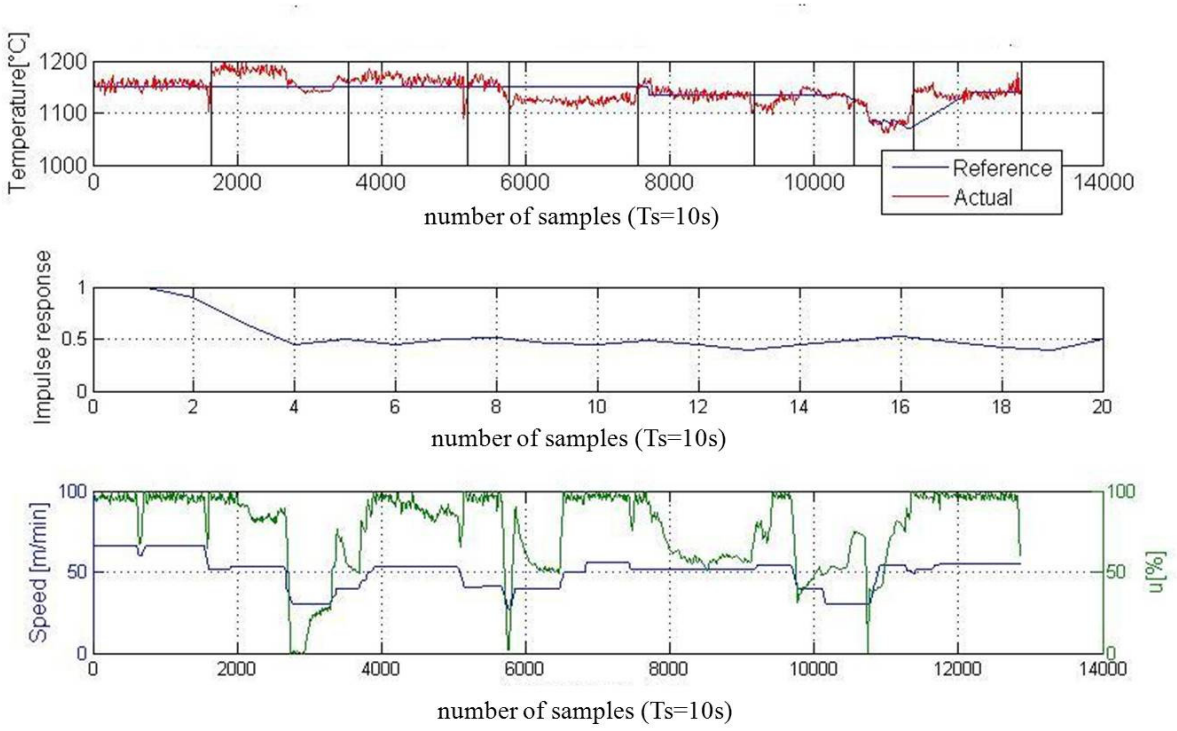

Figure 3.26: Measured data and calculated impulse response for coil no. 111157-111165, Harries Index $\eta = 0.10$

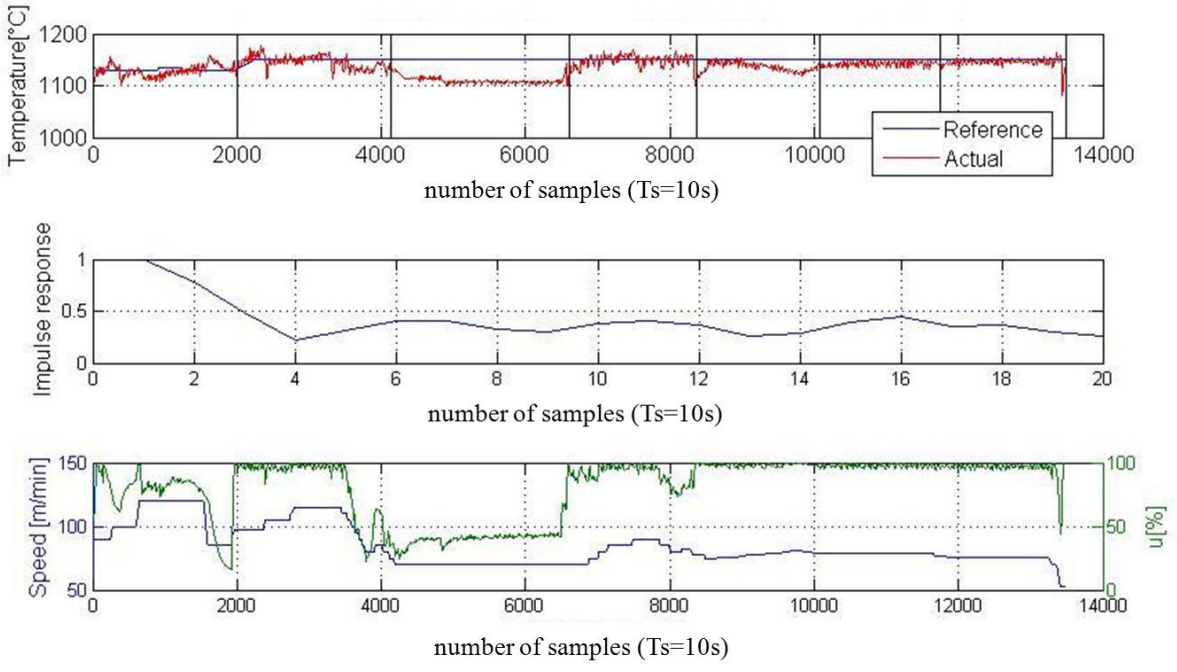

Figure 3.27: Measured data and calculated impulse response for coil no. 111127-111133, Harries Index $\eta = 0.11$

3.1.3.7 Control performance monitoring of nonlinear processes

A computationally cheap method was developed by ICC to monitor and quantify the effects of nonlinearities on the process output performance. The nonlinear performance index was calculated using and estimating an state-dependent model of the nonlinear process. The quantification of existing nonlinearities was achieved by comparing the nonlinear index to a minimum variance performance metric.

The identification of the state-dependent model was achieved using a weighted Kalman filter as follows:

$$\hat{\theta}_{t+1} = F_{t-1}\hat{\theta}_t + K_t\left[y_t - H_t\hat{\theta}_t\right] \tag{3.42}$$

$$\hat{y_t} = H_t^T\hat{\theta}_t \tag{3.43}$$

where K_t is the Kalman filter gain given by:

$$K_t = F_t P_t H_t^T\left[H_t P_t H_t^T + \Sigma_a\right]^{-1} \tag{3.44}$$

and P_t is the state covariance:

$$P_{t|t} = \tau F_t P_t F_t^T + \Sigma_e \tag{3.45}$$

with τ forgetting factor and error covariance prediction as follows:

$$P_{t+1|t} = \tau F_t P_t F_t^T + \Sigma_e - K_t\left[H_t P_t H_t^T + \Sigma_a\right]K_t^T \tag{3.46}$$

The above Kalman filter is applied to the following state space model formulated from observational data:

$$\theta_t = F_{t-1}\theta_{t-1} + V_t \tag{3.47}$$

$$y_t = H_t^T\theta_t + a_t \tag{3.48}$$

where $a_t \sim N(0,\Sigma_a)$, $V_t \sim N(0,\Sigma_v)$ and

$$\begin{aligned}\theta_t = \quad & \big(\mu_{t-1},\varphi_{t-1},\cdots,\varphi_{t-k_y},\psi_{t-1},\cdots,\psi_{t-k_u}, \\ & \zeta_{t-1},\cdots,\zeta_{t-k_\xi},\gamma_{t-1},\cdots,\gamma_{t-k_a},\alpha_{t-1},\cdots, \\ & \alpha_{t-k_y},\beta_{t-1},\cdots,\beta_{t-k_u},\delta_{t-1},\cdots,\delta_{t-k_\xi}, \\ & \eta_{t-1},\cdots,\eta_{t-k_a}\big)\end{aligned} \tag{3.49}$$

$$\begin{aligned}H_k = \quad & \big(1\cdots -y_{t-1},\cdots,-y_{t-k_y}\cdots u_{t-1-d},\cdots,u_{t-k_u-d}\cdots \\ & \xi_{t-1},\cdots,\xi_{t-k_\xi}\vdots a_{t-1},\cdots,a_{t-k_a}\cdots\mu_{t-1},\cdots, \\ & \mu_{t-k_y}\cdots 0,\cdots,0\big)\end{aligned} \tag{3.50}$$

$$F_{t-1} = \left(\begin{array}{c|ccc} I & \Delta x_{t-1}^T & & \\ & & \Delta x_{t-1}^T & \\ & & & \Delta x_{t-1}^T \\ \hline 0 & \multicolumn{3}{c}{I} \end{array}\right) \tag{3.51}$$

$$V_t = \left(0,\cdots,0\vdots v_t,\cdots,v_t\right) \tag{3.52}$$

with state vector $x_{t-1} = \left[y_{t-1}^*, u_{t-d}^*, a_{t_0}, \xi_{t_0}\right]$ and the coefficients of θ_t are linear functions of the state vector.

The performanc+e monitoring metric is calculated using the FCOR algorithm as follows:

$$\eta_y = \frac{r_{y,a}^2(0)+r_{y,a}^2(1)+r_{y,a}^2(2)+\cdots+r_{y,a}^2(d-1)}{\sigma_y^2\sigma_a^2} \tag{3.53}$$

with:

$$r_{y,a}(i) := E\left[y_t a_{t-i}\right],\ (i = 0,1,...,d-1) \tag{3.54}$$

The FCOR algorithm requires the estimation of a_t using a whitening filter. The Formulated Kalman filter can be formulated as a *restricted complexity whitening filter* using the *innovations sequence* $\omega_t = y_t - \hat{y_t}$. From (3.48), ω_t resembles a_t.

Results of the non-linear performance monitoring

The resulting algorithm is tested with the three-stand two-high rolling mill and a real oxyfuel furnace

Results for the rolling mill For the rolling mill, monitoring was implemented in the last stand. The metric is shown in figure 3.28. The performance index presented an increasing reduction as the roll eccentricity increased.

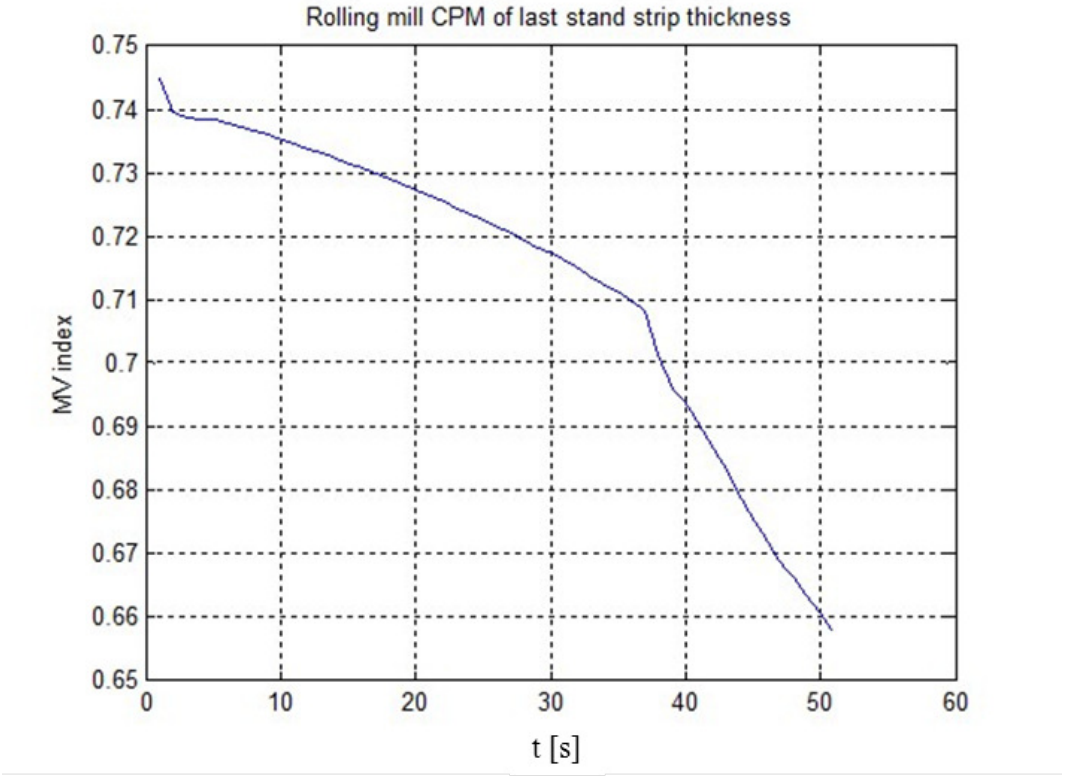

Figure 3.28: MV performance index for strip thickness of last stand of the rolling mill

Performance analysis of the annealing line of MEFOS by ICC The furnace consists of 2 parts divided into 6 zones, zone 1 and 2 are located in the first part and zones 3, 4, 5 and 6 are located in the second part. The steel strip travels across the zones via a support roll between the 2 furnace parts at the end of zone 2. This data originates from the second part is where this data comes from.

A total of 35 burners, 25 thermocouples and 5 pyrometers are used to control the furnace and steel strip temperature. The furnace is 39 meters long with an interior width of 4 meters. Strips up to 2 meters wide are annealed at temperatures at around $1100°C$ and the strip thickness varies between 1.5 and $12.8mm$, both hot and cold rolled strips are treated. The maximum speed is $24m/min$. The cold rolled strips are generally more resistant to the heat transfer because of the lower emissivity of the relatively oxide free surface. This necessitates a lower mass flow.

The furnace control system utilizes the incoming strip and furnace parameters to determine the strip temperature and how many and how much to fire the set of burners in each zone, each $0.5m$ of the strip is calculated and the predictions are made zone by zone. The prediction software is supported by the furnace pyrometers that can also be used as controls alone, or partly together with the calculations.

The firing of the burners is controlled as follows: if more than 50% firing is needed on the firing burners, one additional burner is fired. If less than 25% of firing is needed, one of the burners is turned off. Less than 25% firing in a burner leads to low efficiency and incomplete combustion of the fuel.

The continuous strip is made up of different strips with different thickness that are welded together earlier in the process. The cold rolled strips in the continuous line are separated by 2 joined $6.5m$ long strips. Each end of the individual strips has a $6.5m$ long holding strip that is used to hold and grip the individual strips during their cold rolling. This $6.5m$ strip is chosen with similar thickness to the initial hot rolled strip. The strip is cold rolled with a reduction of at least 50% but the holding strip is not.

The holding strip will thus remain at the initial thickness of more than 200% of the resulting cold rolled strip. The ends are welded to each other to form the continuous strip resulting in a reoccurring 13 meter section thicker and consequently cooler than the actual strip, this can clearly be seen as sudden dips in temperature of the pyrometers in zone 5 and 6.

Thermocouple 3 in zone 6 has been considered for CPM. There was no real set-point data, but it was suggested that the temperature had to be kept at $1100°C$. An approached set-point data was used during the analysis. The thermocouples from zone 6 is depicted in figure 3.29. The performance index of the zone can be seen in figure 3.30. From time ($t = 0$ min) to ($t = 400$ min), the performance index was relatively high. Oscillations appear since the time delay was calculated at every recursion. The drop in the index after ($t = 400$ min) was due to the sudden drop of the temperature values. Abrupt variation of the assessed variables caused abrupt changes in the calculation of the correlation. After ($t = 800$ min) the temperature values dropped considerably compared with the assumed constant set-points. The results were improved with a priori knowledge of the real set-point values.

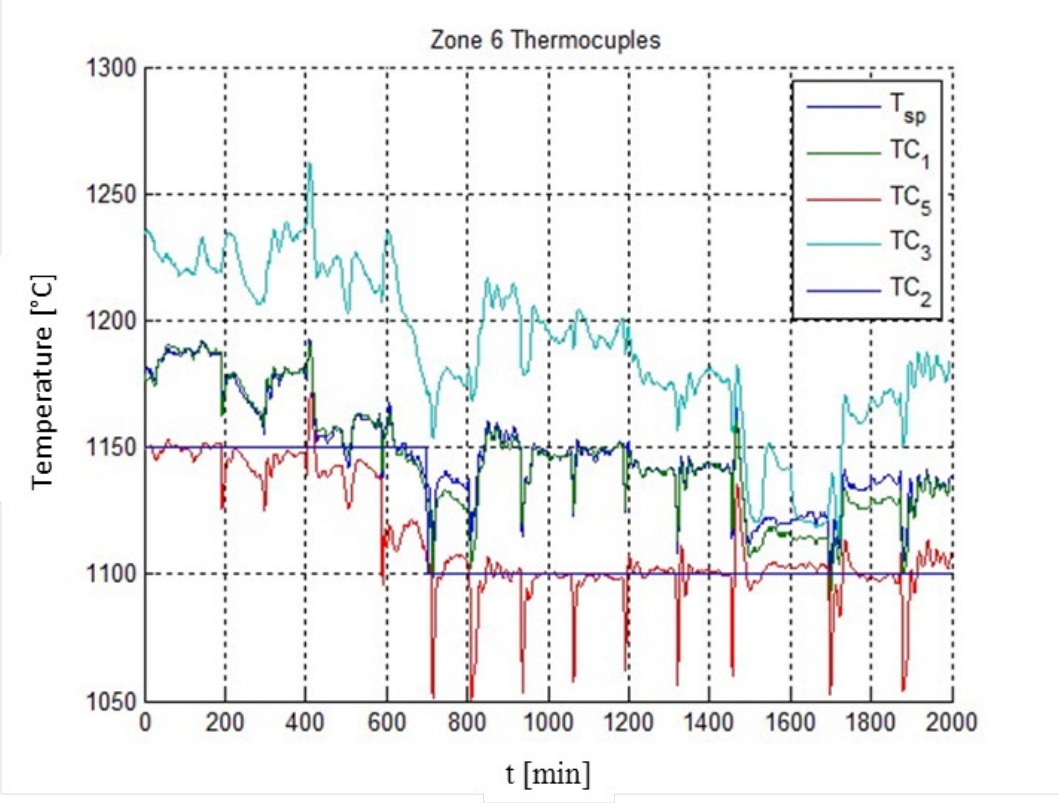

Figure 3.29: Furnace, Zone 6, thermocouples temperature values

Further analyses of the oxyfuel furnace by MEFOS Based on the performance assessment by ICC further analyses of the oxyfuel furnace was carried out by MEFOS. On that account several cases have been analysed:

Case 1: Figure 3.31 displays the effect of the strip change from 1.5 up to 2 mm cold rolled strips. The change was registered at 06:32:50 and the first part of this new strip reached the zone 6 pyrometer at approximately 06:35:50; the cooler 13 m holding strip was clearly distinguishable because of the rapid drop in pyrometer temperature at 06:35:20.

The increase in strip thickness from 1.5 to 2 mm necessitated a slight increase in oil flow. The oil flow in both zone 3 and 4 reacted heavily to the thickness change which caused a 30°C temperature variation cycle with a duration of approximately 6 min / 150 m.

Case 2: The variations in annealing temperature exemplified in case 1 were reoccurring throughout the set of the 10 cold rolled strips. The variations during the first 200-300 m of the strips are shown in figure 3.32. Note that the graphs represent the processed strips only and not the 13 m holding strip.

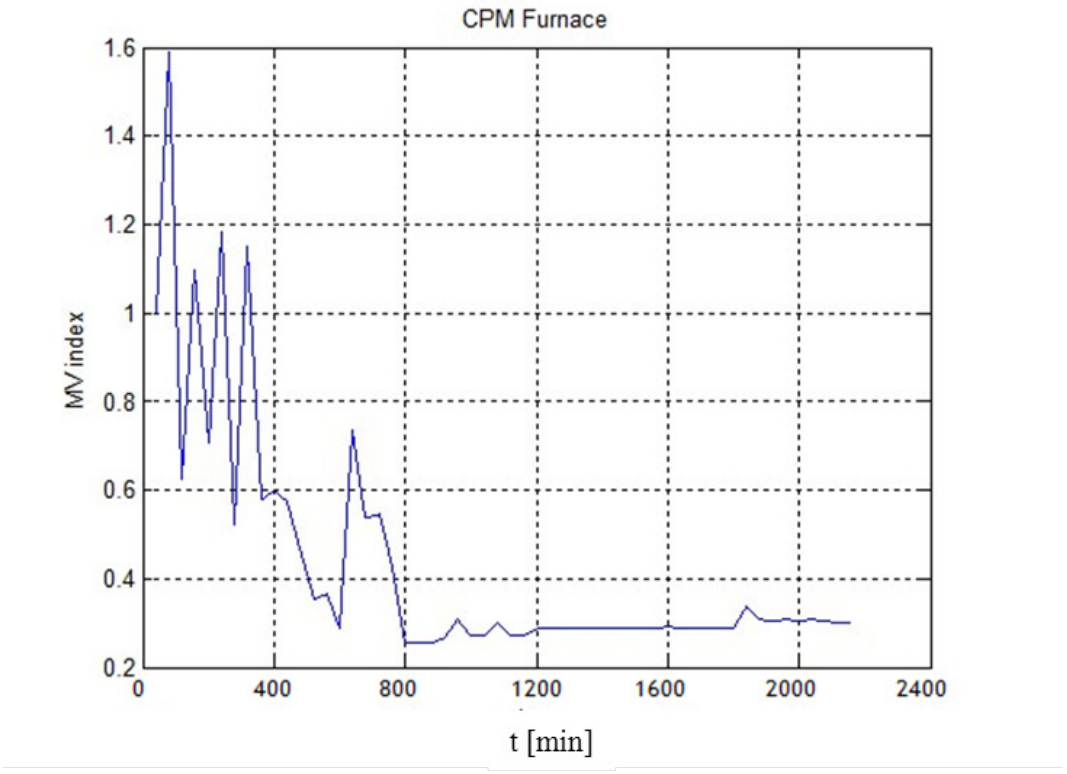

Figure 3.30: MV performance index for thermocouple 3 from furnace zone 6

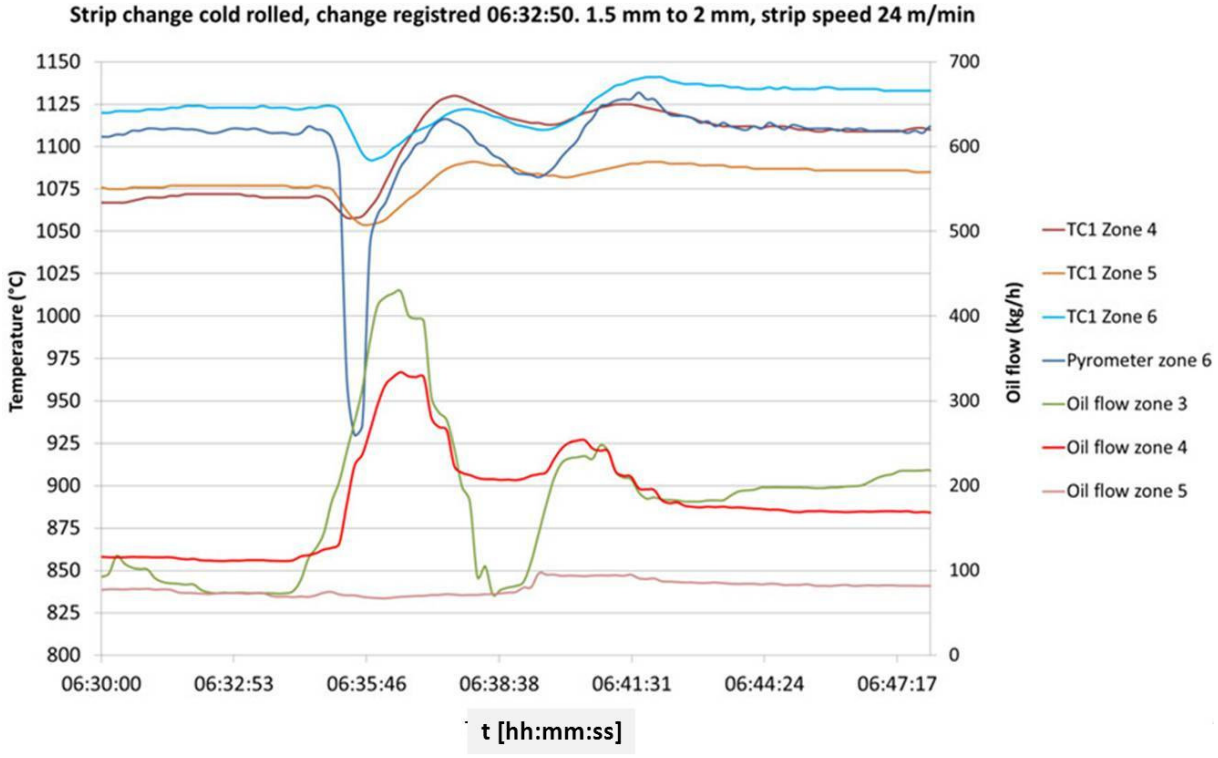

Figure 3.31: Strip change and resulting reaction from thermocouples (TC), pyrometers and burners

The variations were particularly large in the first 100 m, where the furnace control had to deal with the entry of a new strip and the exit of a strip with a different thickness. The 13 m holding strip has presumably made it even more difficult to directly find the optimal burner firing schedule. Nevertheless, after these initial control problems, the temperatures showed very little variations.

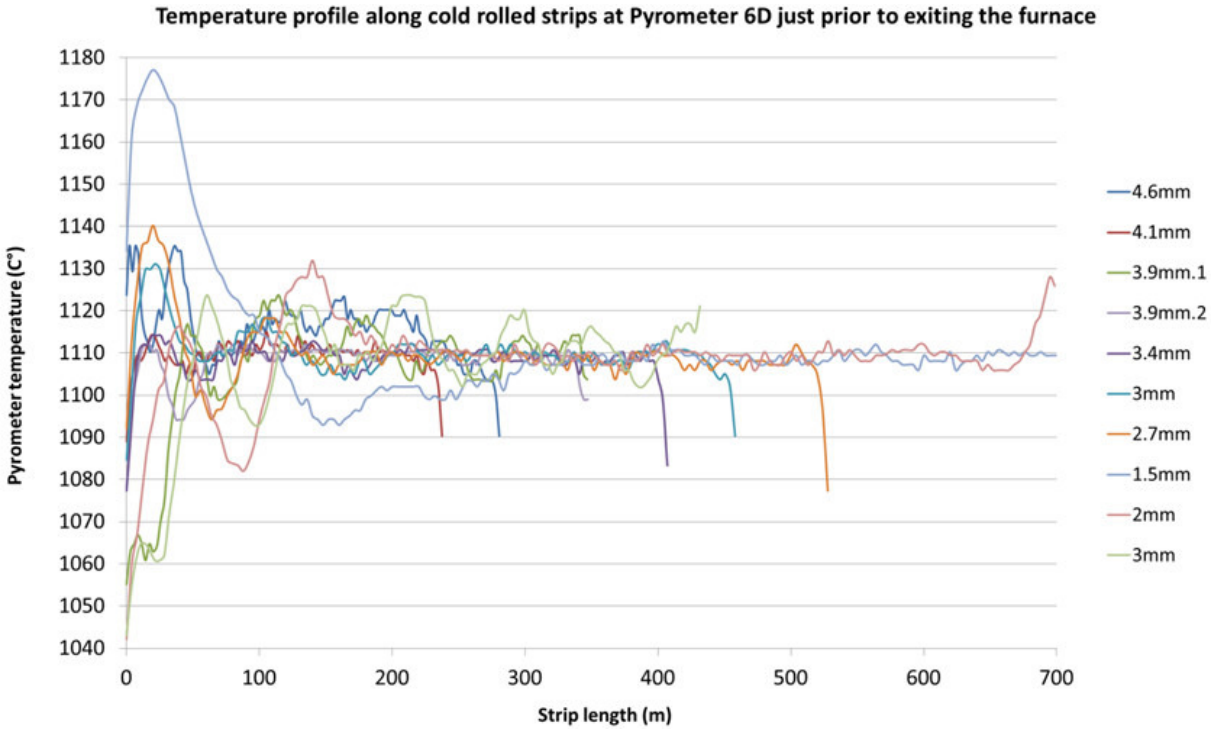

Figure 3.32: Temperature distribution over the length of the various cold rolled strips

Case 3: Two subsequently annealed cold rolled strips were of equal thickness; in this case 3.9 mm. The temperature distribution along the length of the 2 strips together with the average fuel consumption during their annealing is shown in figure 3.33.

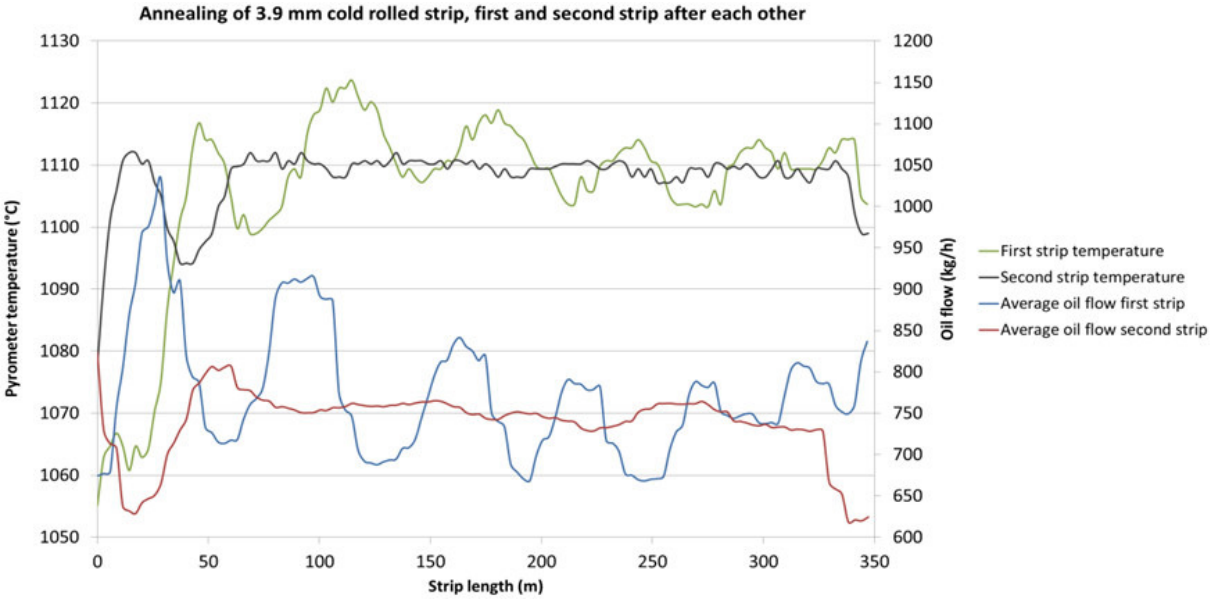

Figure 3.33: Temperature distribution over the length of the 2 3.9 mm strips and average fuel consumption during the annealing sequence. Temperatures are measured by Pyrometer 6D in zone 6

The first 3.9 mm strip never found an equilibrium temperature. The 15°C and 150 kg/h variations were ongoing throughout the annealing of this strip. The second strip however did rapidly found a steady temperature and fuel consumption. Aside from the temperature variations in the first strip the fuel consumption was also on average 5% higher than the second strip.

Figure 3.34 shows the number of burners firing during the passage of the two 3.9 mm strips. The band change occured at 04:29:00 and it is obvious how the number of firing burners in zone 3 were varying between 9 and 5.

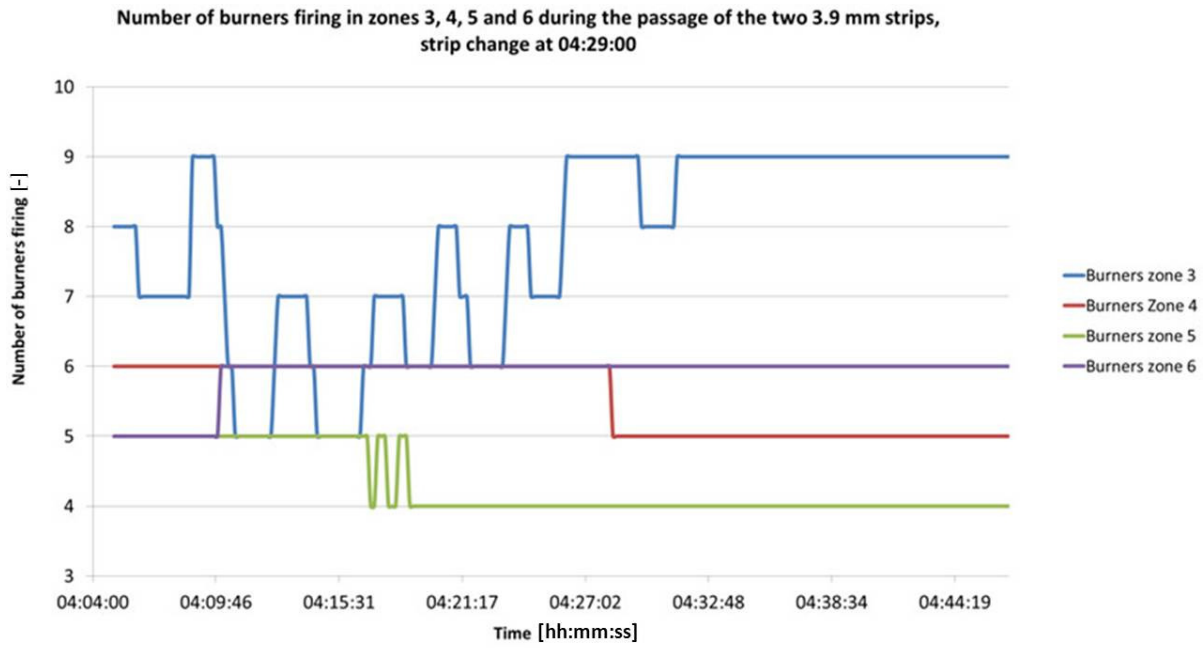

Figure 3.34: Number of burners firing during the passage of the two 3.9 mm strips

Case 4: The strip change was clearly an obstacle in finding a stable furnace and strip temperature. Figure 3.35 demonstrates the pyrometer 6D temperature and the total oil flow in zones 3-6. The strip mass flow was kept nearly stable even though the strip thickness changes from 4.1 to 3.9 to 3.4 to 3 and finally to 2.7. The 4.1 mm strip was 2.05 m and the rest 1.89 meters wide. The dip in mass flow during each strip change was the result of a too low strip speed for the first meters of the thinner sectioned strip. The mass flow is thus slightly lower but as the band accelerates, the mass flow reached the previous level. Even though the mass flow was not the sole parameter in terms of oil flow, it has been still interesting to note its variations. The average oil flow seemed to be reasonably stable throughout the 6 strip series. However, such large variations in oil flow, particularly during strip changes, should not have needed such a dramatic change.

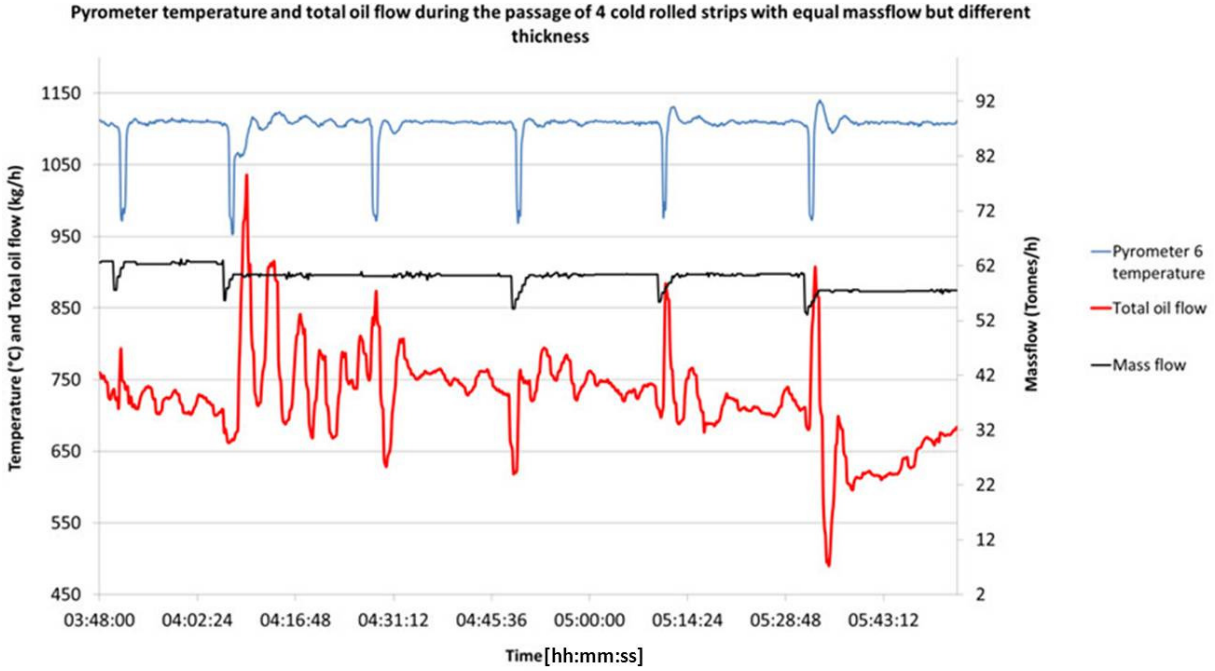

Figure 3.35: Pyrometer temperature and total oil flow during the passage of 4 cold rolled strips

Analysis of the collected data showed that the logistics of their annealing demanded an improved model to cope with the variations in speed and material thickness. Illogical variations in oil flows were

found throughout the investigated process data series. One of the reasons for this was the strip change that has been taking place nearly every 20 min. This interfered with the furnace stability and caused the burners to fire in a non-optimal fashion. The uneven oil flow resulted in uneven strip temperature shown by the pyrometers in zone 6. The temperature differences were in the order of 20–80°C in the first 200 m of each strip. The differences increased with decreasing strip thickness.

The actual negative effects of the temperature variations were difficult to establish since they depended on the final fabrication and use of the strip. The variations however affected the microstructure and properties of the strip to some extent and therefore have been considered. An annealing temperature that is too low, can, for example lead to incomplete recrystallization of the material. A limit-exceeding temperature leads to high ferrite levels in duplex stainless steel.

The above discussion can be concluded as follows:

- Illogical variations in oil flow caused variations in the strip temperature and occasional unnecessary oil consumption.
- Large variations in oil flow and strip temperature throughout the strip passage were seen on 3 out of the 10 cold rolled strips.
- Temperature variations were occasionally large, especially for thinner strips. This might have affected the material microstructure and properties, e.g. recrystallization.

3.2 WP 2: Development of techniques for the automatic diagnosis of root causes of poor control performance

The main objectives of this WP were:

- A Critical review of condition monitoring and fault diagnosis technology with emphasis on control systems and their components (sensors, actuators, models, controllers) was carried out.
- Critical faults and their occurrence mechanisms in the control loops were identified and classified.
- Tailored root-cause diagnosis strategies/methods for the considered faults, combining different analysis methods, to generate symptom/diagnosis/action tables were developed.
- Diagnosis software and reporting system concepts was created and the proposed methods were validated.

3.2.1 Task 2.1: Development of methods to determine the root causes of performance losses detected in the control loops [ICC, BFI]

. Root-cause or causal analysis is a challenging task in CPA and its synthesis has been rarely addressed [Hua03]. Poor performance can be caused by improper or inadequate controller tuning and lack of maintenance, inappropriate control structure, poor or missing feedforward compensation, equipment malfunction or poor design, and specially due to distributed oscillations [Hub11]. Some of the most promising methodologies are: diagnosis of the variance decomposition [Des93], diagnosis tree analysis (also called hypothesis tree) of the variance decomposition [Che05], statistical diagnosis of root-cause directions [Tia11, Yu,08], rule-based flow chart diagnosis of nonlinearities [Cho08], Bayesian synthesis of monitoring systems for root-cause probabilistic diagnosis [Hua03], and distributed oscillations diagnosis [Bon06, Tho07, Bau07, Bau08]. The later is specifically developed for industrial applications with thousands of control loops such as in the petrochemical industries.

Whatever the methodology, the diagnosis procedure is based on comparisons between the actual variance and the last lowest variance [Che05, Tia11, Hua03, Kad02a]. Furthermore a diagnosis algorithm requires the following steps:

1. Pre-analysis of nonlinearities and dead-time estimation.
2. Feedback controller assessment.
3. Process and disturbances assessment.

Detection of oscillations is implicitly considered within the pre-analysis of nonlinearities or is implemented as a separate monitoring system [Jel06a, Hua03].

In this task Software tools (being deliverable D2.1) for automatic performance evaluation of control loops have been developed and methods are presented for

- oscillation detection in control loops (BFI);
- non-linearity detection in control loops and (BFI);
- root-cause analysis of oscillations (BFI);
- PCA-based methods for root-cause detection in control loop (ICC).

3.2.1.1 Oscillation detection

In addition, Thornhill's method for oscillation detection based on regularity of zero-crossings of the autocorrelation function (ACF) of the process data, BFI has studied another similar technique, called the decay ratio approach of the auto-covariance function, and proposed by Miao and Seborg [Mia99].

This technique is based on the analysis of the auto-covariance function of normal operating data of the controlled variable or the control error. The approach utilises the decay ratio R_{acf} of the auto-covariance function, which provides a measure of oscillation in the time trend. Figure 3.36 illustrates the definition of R_{acf}, described by the equation

$$R_{\text{acf}} = \frac{a}{b}, \tag{3.55}$$

where a is the distance from the first maximum to the straight line connecting the first two minima, and b is the distance from the first minimum to the straight line that connects the zero-lag auto-covariance coefficient and the first maximum.

As the decay ratio of the auto-covariance function is directly related to the decay ratio of the signal itself, it is a convenient oscillation index. A value R_{acf} smaller than 0.5, corresponding to a decay ratio in the time domain smaller than 0.35, may be considered as acceptable for many control problems. On the other hand, if $R_{\text{acf}} \geq 0.5$, then the signal is considered to exhibit an excessive degree of oscillation. Therefore, R_{acf} can be used to detect excessive oscillations in control loops according to the following simple procedure:

1. Calculate the auto-covariance function of the measured y or e and determine the ratio R_{acf} (Equation 3.55). In the cases where there are less than two minima, set the index value to zero.

2. If R_{acf} is greater than a specified threshold, say 0.5, it is concluded that the considered signal is excessively oscillatory. The selection of the threshold is somewhat subjective and application-dependent.

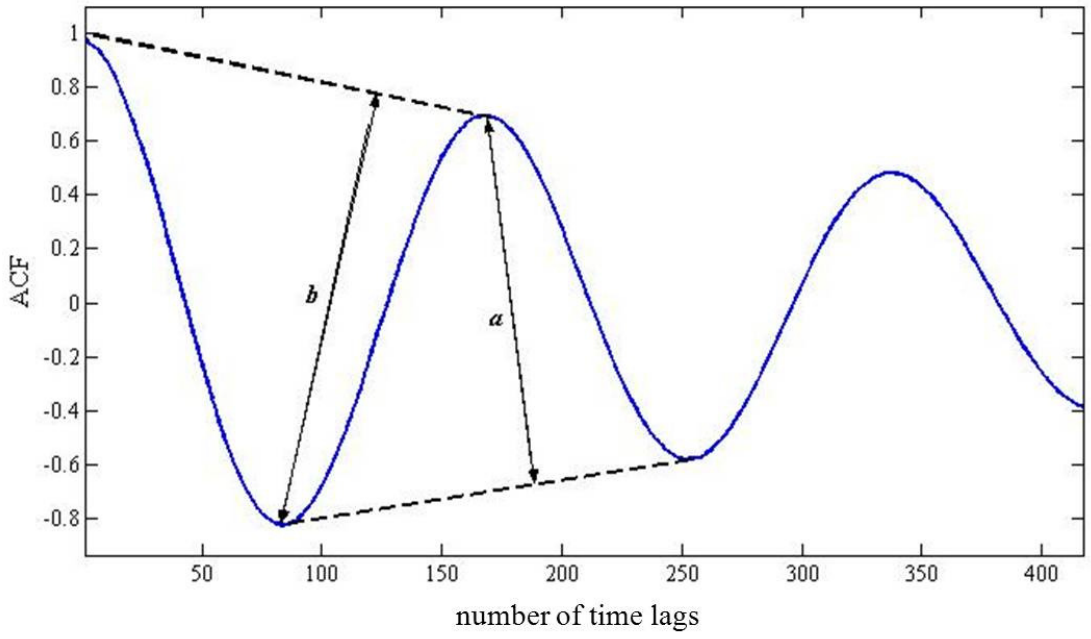

Figure 3.36: Determination of the decay ratio of the auto-covariance function

Both oscillation methods have been applied to selected data from hot-strip gauge control at AMEH shown in Figure 3.37. It can be clearly observed that oscillation appears at the first part of the strip and then disappears as the speed is decreased by the operator. The results of the oscillation detection based on regularity of zero-crossings of the ACF for the first and second part of the data are illustrated in Figure 3.38 and Figure 3.39, respectively. The analysis gives the regularity indices of $r = 7.5 > 1.0$, correctly indicating the presence of oscillation, and $r = 0.6 < 1.0$, indicating no oscillation. Now, applying the decay ratio approach leads to decay ratios $R_{\text{acf}} = 0.65 > 0.5$ and $R_{\text{acf}} = 0.40 < 0.5$ for the first and second part of the data, respectively. Thus this method also gives the right indications.

3.2.1.2 Non-linearity detection

In addition Choudhury's method for detection of loop non-linearity based on higher-order statistics, BFI has examined a different technique based surrogates analysis, as proposed by Thornhill [Tho05].

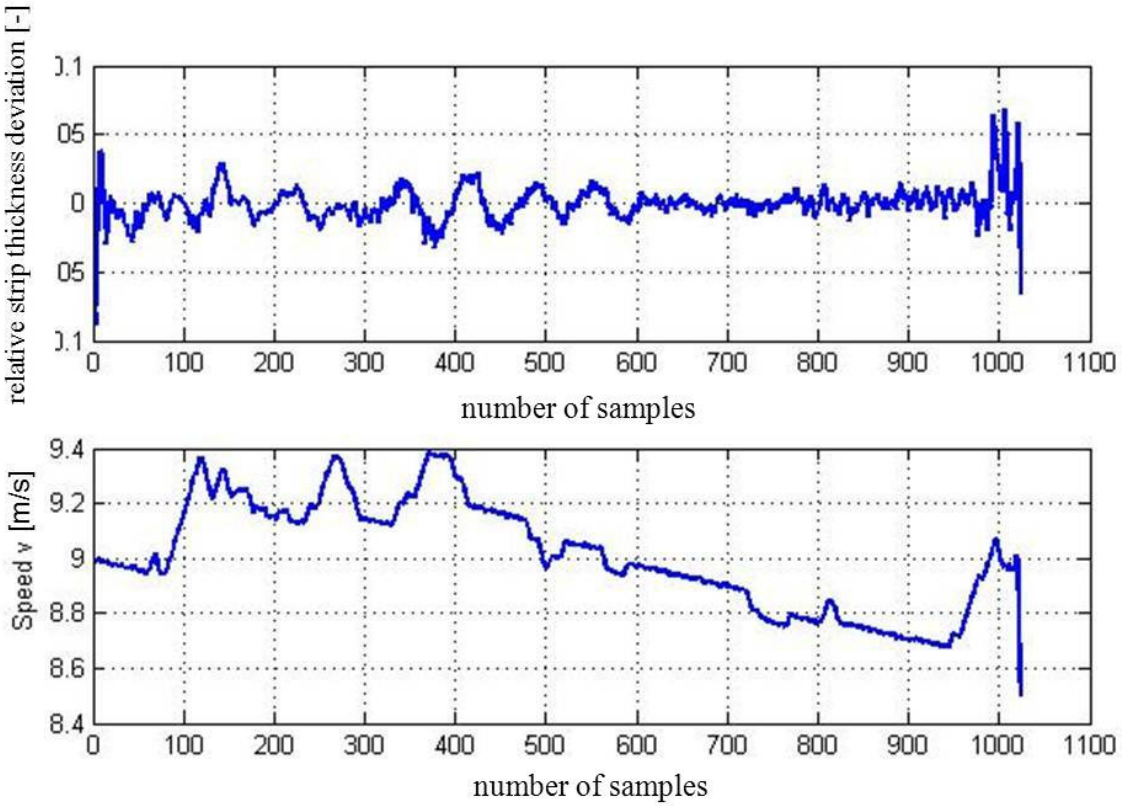

Figure 3.37: Data from gauge control at AMEH's hot-strip mill

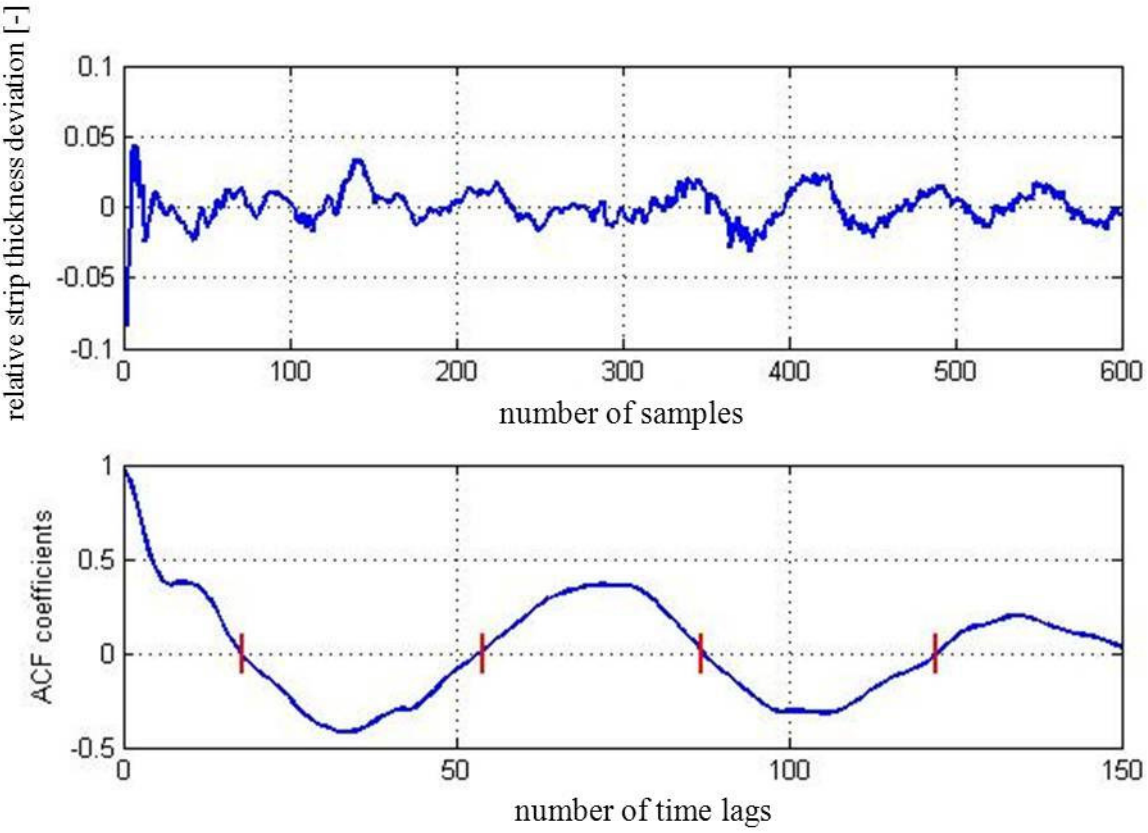

Figure 3.38: Results of oscillation-detection analysis for the first part of data

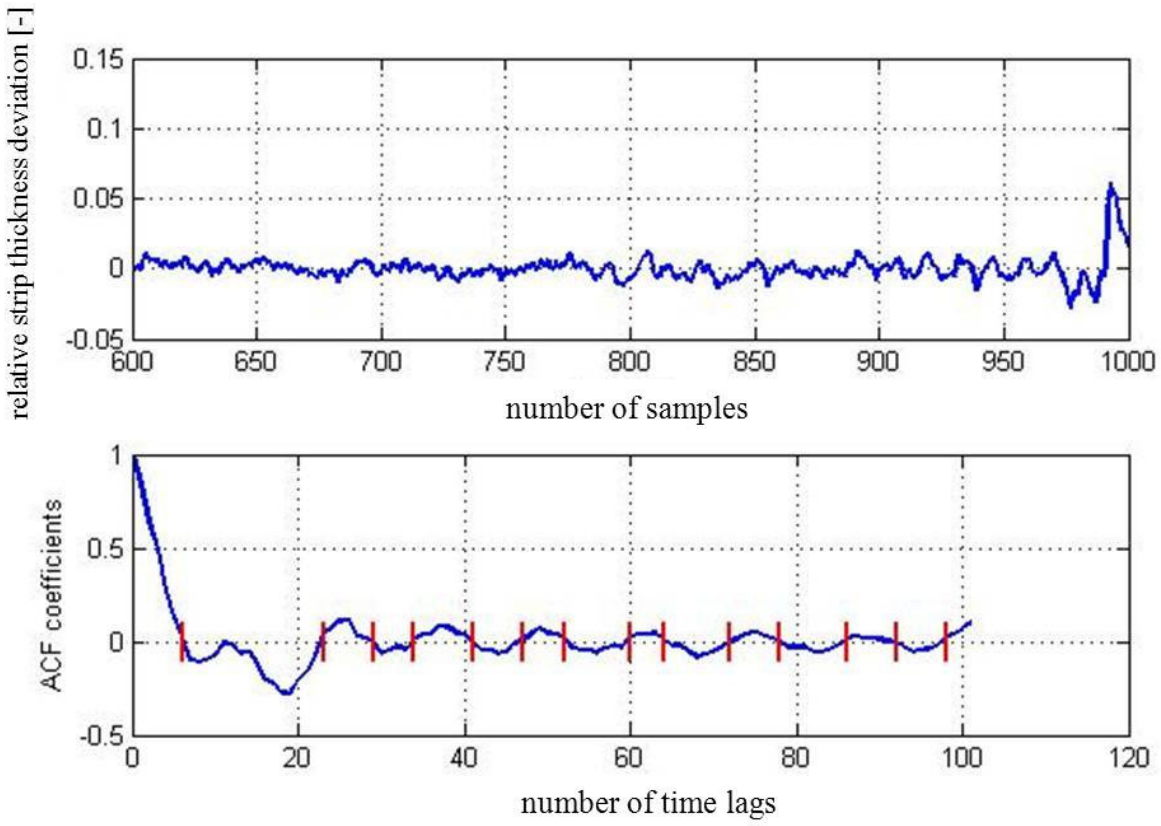

Figure 3.39: Results of oscillation-detection analysis for the second part of data

The basic assumption of this method is that a data set (mathematically a time series) with phase coupling (as symptom of non-linearity) has more regular pattern and, hence, is more predictable than a surrogate having the same power spectrum but with randomised phases. For this purpose, a (non-)predictability index is required to decide whether dynamic non-linearities are present in the data or not. Figure 3.40 shows an example that visualises a surrogate for a given data set: it can be observed that the original data set is more predictable than its surrogates, thus implying the presence of non-linearity in the control loop.

A statistic based on a three-sigma test has been formulated using nonlinear predictability as [Tho05]

$$NPI = \frac{\bar{\Gamma}_{\text{surr}} - \Gamma_{\text{test}}}{3\sigma_{\text{surr}}}, \tag{3.56}$$

where Γ_{test} is the mean squared prediction error of the test data, $\bar{\Gamma}_{\text{surr}}$ the mean or the reference distribution, and σ_{surr} its standard deviation. This nonlinearity test can be interpreted as follows:

- If $NPI > 1$, then non-linearity is inferred in the data. The higher NPI, the more nonlinear is the underlying process.
- If $NPI \leq 1$, the process is considered to be linear.
- Negative values in the range $-1 \leq NPI < 0$ are not statistically significant and arise from the stochastic nature of the test.
- Results giving $NPI < -1$ do not arise at all, because the surrogate sequences, which have no phase coherence are always less predictable than nonlinear time series with phase coherence.

A detailed mathematical description of this method will not be included here, but can be found in [Tho05]. A comparison with Choudhury's method is found in [Jel09b] (Chapter 13).

The application of Thornhill's non-linearity-detection method to the end-matched data set in Figure 3.38 (i.e. samples 90–600) yields the non-predictability index value $NPI = 0.36$, clearly indicating no non-linearity (and thus no stiction) in the control loop. The root cause for this oscillation should be linear, such as aggressive controller tuning or other process disturbances.

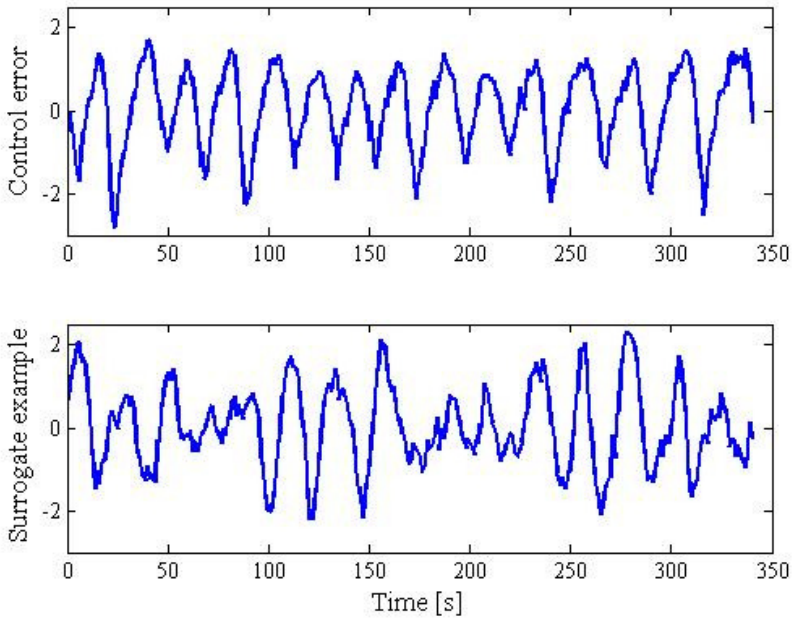

Figure 3.40: Example of a time trend and its surrogate data

3.2.1.3 Valve stiction detection

Control valves are the most commonly used actuators or final control elements in the process industries. They are mechanical devices subject to wear and tear with respect to time. Therefore, valves may develop serious problems and should be regularly maintained. Surveys indicate that about 20–30% of all control loops oscillate due to valve problems caused by valve non-linearities, such as stiction, hysteresis, dead-band or dead-zone. It is well-known that valve stiction in control loops causes oscillations in a form of periodic finite-amplitude instabilities, known as *limit cycles*. Stiction in control valves is thought to occur due to seal degradation, lubricant depletion, inclusion of foreign matter, activation at metal sliding surfaces at high temperatures and/or tight packing around the stem. This phenomenon increases variability in product quality, accelerates equipment wear, or leads to control system instability.

Stiction can be best explained by the input–output behaviour of a sticky valve illustrated in figure 3.41. Without stiction, the valve would move along the dash-dotted line crossing the origin: any amount of OP adjustment would result in the same amount of manipulated variable (MV) change. Nevertheless, for a sticky valve, static and kinetic/dynamic friction components have to be taken into account. The input–output behaviour then consists of four components deadband, stickband, slip jump and the moving phase, and is characterised by the three phases [Ros07]:

1. **Sticking.** MV is constant with time, as the valve is stuck by the presence of the static friction force F_s (deadband plus stickband). Valve deadband is due to the presence of Coulomb friction F_c, a constant friction that acts in the opposite direction to the velocity.

2. **Jump.** MV changes abruptly, as the active force F_a unblocks the valve.

3. **Motion.** MV varies gradually; F_a is opposed only by the dynamic friction force F_d.

There several methods to detect stiction in control loops by only using OP and PV signals; the MV signal is usually not available. An extensive survey and comparative study can be found in [Jel09b] (Chapter 13). The method selected here is based on curve fitting technique, proposed by He et al. [He 07].

The basic principle of this method is to perform a fitting of PV, OP, or SP−PV data, to detect the typical signature of stiction and distinguish it from other causes like aggressive tuning or external disturbances. More specifically, the controller output or process variable are fitted piece-wise (every *significant half cycle*) to both triangular and sinusoidal curve segments (figure 3.42) using a least-squares method. If the fit for the triangular wave is better, then stiction is concluded; otherwise no stiction occurs.

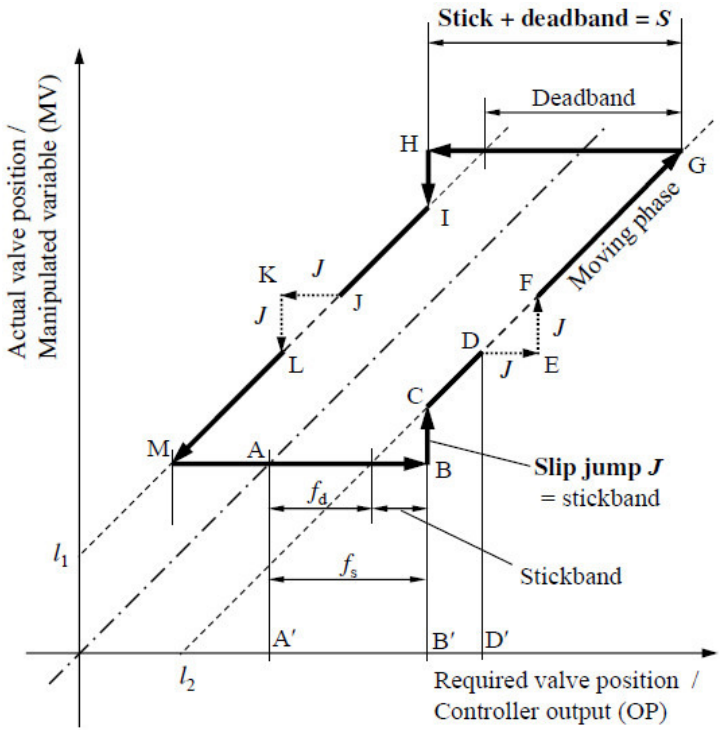

Figure 3.41: Relation between controller output and valve position under valve stiction [Cho05c, Kan04]

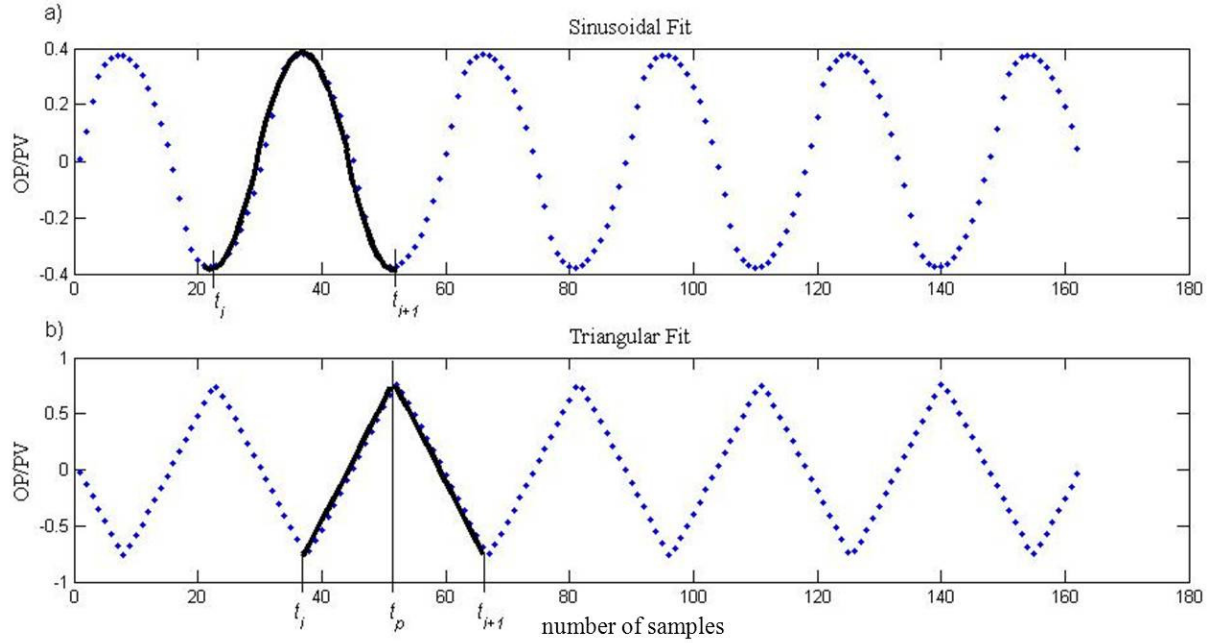

Figure 3.42: Schematic of the curve fittings: sinusoidal fitting (upper subplot); (b) triangular fitting (lower subplot)

By comparing the error between real and fitted data, the accuracy of approximation is evaluated by obtaining the overall mean squared error for sinusoidal fitting MSE_{sin} and the overall mean squared error for triangular fitting MSE_{tri}. A stiction index is then computed as

$$\eta_{\text{stic}} = \frac{MSE_{\text{sin}}}{MSE_{\text{sin}} + MSE_{\text{tri}}}, \tag{3.57}$$

The procedure for stiction detection based on this index can be summarised as follows:

1. Check if the loop is oscillating and determine the zero crossings and the oscillation period (Use, for instance, Thornhill's or Miao's method).

2. Fit a sinusoidal wave and a triangular wave to the measurements of controller output for a self-regulating process or to the measurements of process variable for an integrating process as well as possible; compute the stiction index using Equation 3.57.

3. Take decision according to:

$$\begin{aligned} \eta_{\text{stic}} \geq 0.6 &\Rightarrow \text{Stiction}, \\ 0.4 < \eta_{\text{stic}} < 0.6 &\Rightarrow \text{No decision}, \\ \eta_{\text{stic}} \leq 0.4 &\Rightarrow \text{No stiction}. \end{aligned} \tag{3.58}$$

3.2.1.4 Sequential diagnosis using a classification tree

Performance diagnosis can be achieved as a comparison between the actual variance residual given by (3.35) and the lowest variance residuals [Che05, Tia11, Hua03, Kad02a]. A decrease in control performance triggers the first hypothesis test. To verify the accuracy of the index value, nonlinearities and time-delay variations have to be tested. Controller pre-assessment is the next hypothesis test. Indices for controller improvement (profit analysis) may reveal poor control tuning and inadequate control structure. The remaining sources of performance degradation are poor or missing feedforward compensation, process and disturbance variations and possible model mismatch. Hypothesis tests based on each component of ANOVA can identify these remaining sources [Che05].

The resulting hypothesis tests can be arranged into a tree-like graph and form a decision tree. To form the tree, define each root-cause as a class, each index value and ANOVA components of the lowest known variance as a set of thresholds for the hypothesis tests and each new index, and variance values as tree inputs. It is possible to classify each new tree input within a given class by growing a binary tree. Each internal node in the tree is a decision-making unit that applies a hypothesis test to the inputs. Following the outcome of the test, the tree inputs go to the next sub-branch. The tree inputs will eventually reach an internal node that corresponds to a specific class or root-cause. The sequential combination of process pre-assessment indices and ANOVA components described in Task 1.3, Section 3.1.3.5 provides the decision tree as shown in figure 3.43.

Industrial case study Following the industrial case study presented in section 3.1.3.5, the nominal model is used to generate the decision tree presented in figure 3.43.

The results of ANOVA and diagnosis are presented in Table 3.6. Minimum Variance CPA was used for ANOVA. Since model nominal and increased eccentricity showed non-linearities, a nonlinear CPA index was calculated. This index was lower than the linear one. Once the model with reduced eccentricity had been calculated, it was seen that its indexes values are better than the nominal model. Therefore, the first recommendation of the diagnosis tree was to make this model nominal. The diagnosis tree was re-designed and the nominal and increased eccentricity models were compared to it. The results showed that in both cases the root-cause was change in process and disturbance as expected due to the change in roll eccentricity for simulation purposes.

3.2.1.5 Angle-classifier diagnosis

Tian [Tia11] developed a statistical method for monitoring and diagnosis of predictive controllers. The underlying principle consists of extracting eigenvectors from the actual dataset and comparing them

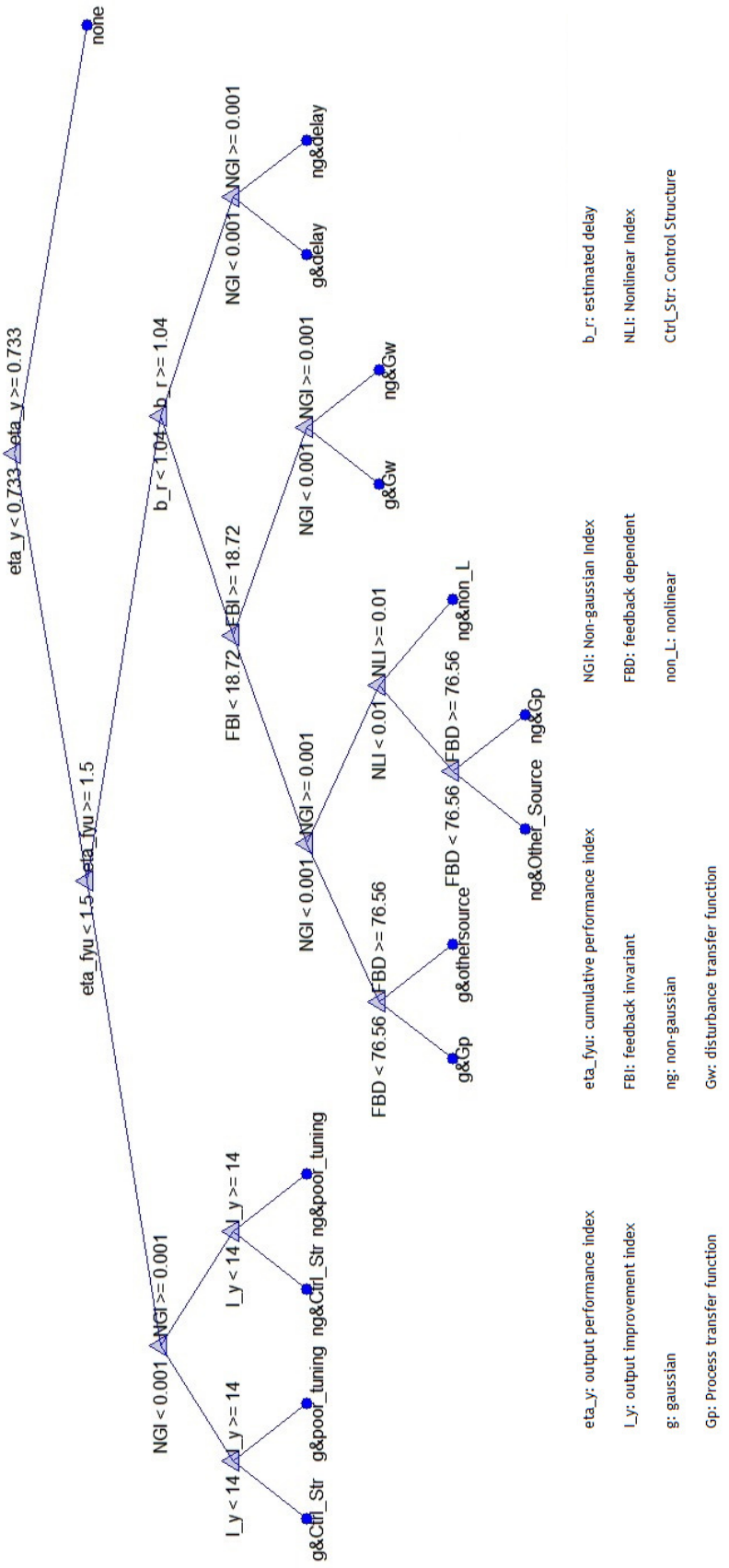

Figure 3.43: Hypothesis tree design using Matlab classification tree function

Table 3.6: Complete assessment of output thickness in stand 3: nominal (N), reduced (R) and increased (I) eccentricity models

ANOVA						
	mv	variance inflation due to:			linear	nonlinear
		fb	*ff*	*ff*/*fb*	η_y	η_y^{nonl}
N	17.73	71.56			0.80	0.79
R	21.57	93.02			0.81	
I	46.39	228.75			0.83	0.69

DIAGNOSIS		
	ROOT-CAUSE	RECOMMENDATION
N	change in process and disturbance	
R	performance improved	use as nominal
I	change in process and disturbance	

with pre-calculated eigenvectors from possible abnormal data (data from poor performing processes). Eigenvectors that represent abnormal data are called classifiers. The causes of performance deterioration can be expressed as a set of classifiers $\{C_i\}_{i=1}^{g}$ with $i = 1,2,...,g$, possible causes. g is the total number of known causes. Each classifier C_i defines a subspace V_i that is represented by its feature eigenvector φ_i in such a way that for a given subspace V_{act} compared against the set of subspaces $\{V_i\}_{i=1}^{g}$, its feature eigenvector φ_{act} forms the minimum angle to the most likely possible classifier C_i with eigenvector φ_i. The angle is calculated as follows:

$$\theta_{act,i} = cos^{-1}\left(\frac{\varphi_{act}^T \varphi_i}{\|\varphi_{act}\|\|\varphi_i\|}\right) \tag{11}$$

where $\|.\|$ denotes the vector norm, and the minimum angle $\theta_{act,i}$ is:

$$\theta_{act}^{*} = \min_{1\leq i\leq g} \theta_{act,i} \tag{12}$$

$\theta_{act,i}$ varies from 0°C to 90°C as shown in figure 3.44. The above method requires the extraction of

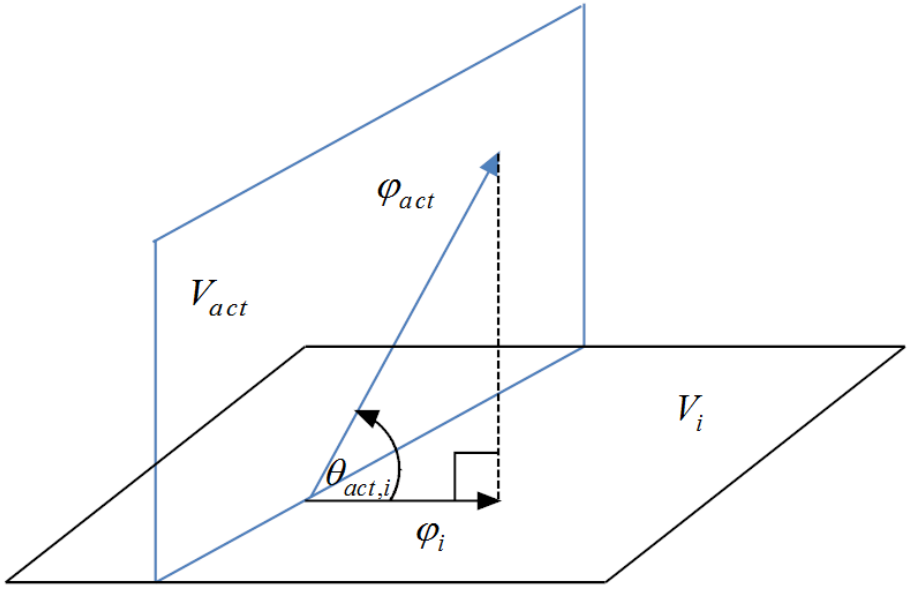

Figure 3.44: Eigenvector angles [Tia11]

the eigenvectors from the operational data, which is achieved using ordinary PCA. The PC's loadings obtained by PCA from Y are identical to the ones obtained by MsPCA from WY [Bak97]. Consequently the eigenvectors extracted using MsPCA contain the features of the original data and can be directly used for the eigenvector-angle approach .

Industrial case study Consider again the rolling mill, now the roll force was assessed. The roll force, its wavelet transformation and the extracted error can be seen in figure 3.45. The procedure for

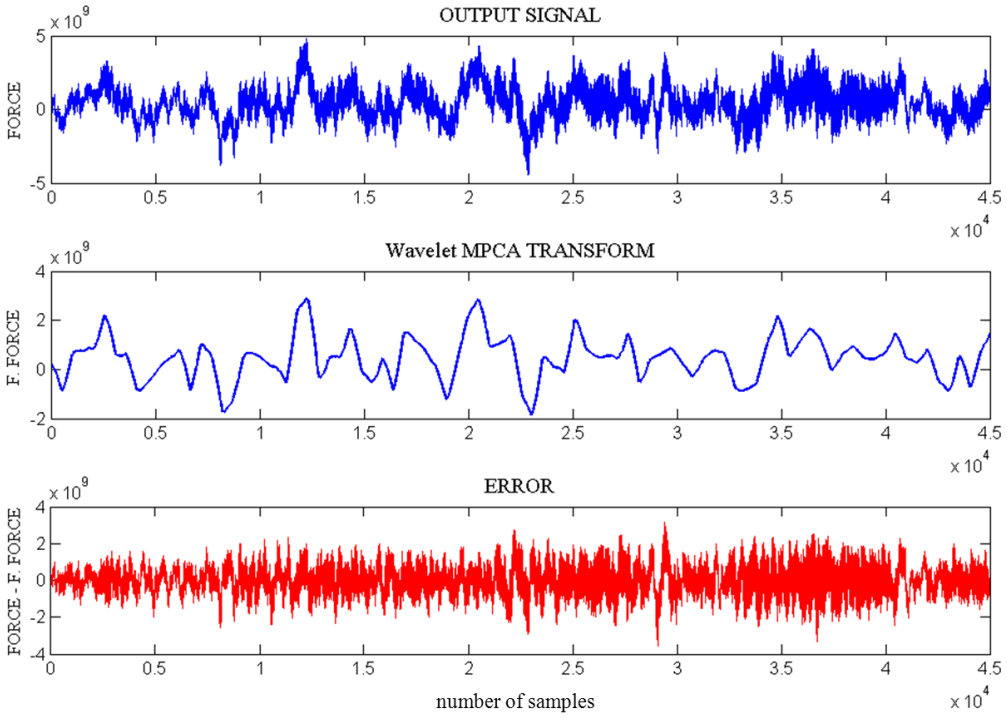

Figure 3.45: Force output signal, filtered signal and extracted error

assessment and diagnosis was condensed into steps as follows:

1. Form the data matrix from historical operating data.

2. Apply MsPCA to the data matrix to compute the wavelet decomposition, covariance matrix of wavelet coefficients for each scale with a given threshold, and PCA loadings and scores of the wavelet coefficients.

3. Calculate an optimal PID controller from estimated data or, if the process model is available, design an optimal PID controller and calculate the process variance.

4. Use the original data matrix and the reconstructed data (from the wavelet decomposition) to obtain the process error (or the stochastic feature) and calculate a cost function.

5. If the PID-like performance index shows poor performance (i.e. $I_{PID} < 0.6$ chosen empirically. This index magnitude is similar to $I_{MV} < 0.5$ when comparing both benchmarks), run the angle-classifier algorithm with the stored PC's loadings and the existing set of classifiers $\{C_i\}_{i=1}^{g}$

6. Find the minimum angle θ_{act}^{*} that points out to the most likely root-cause.

Three cases were diagnosed: excessive integral action (PID fast response), missing derivative action (PI well-tuned) and sensor faults. The indexes for these three scenarios can be seen in figure 3.46.

The results of the angle-classifier algorithm can be seen in table 3.6. Case 1 (PID fast response) presented an angle value closed to 0° at the PID fast class as expected. Similar results are found for case 2. On the other side, case 3 (sensor fault) could not be accurately related to any of the existing under-performing controllers classifiers which means that the low performance index is not due to the controller but due to other type of sources. The smallest angle for this case corresponded to PI fast which suggested that, whatever the cause was (in this case due to sensor fault) has made the process oscillate.

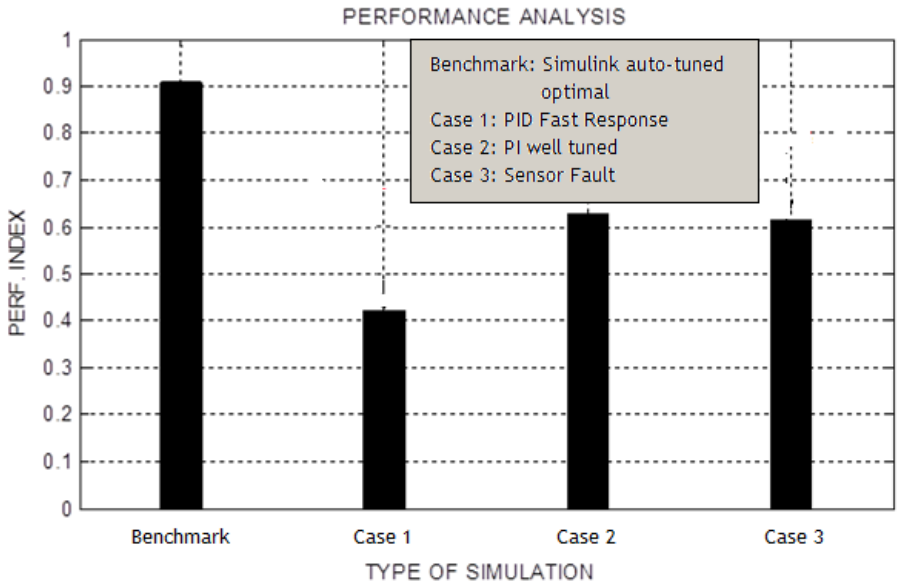

Figure 3.46: Indices of the root-causes to be diagnosed

Table 3.7: Angle-classifier diagnosis

	PID slow	PID opt	PID fast	PI slow	PI opt	PI fast
Case 1	62.82	57.79	0.00012	7.12	24.62	43.59
Case 2	67.94	20.57	62.37	62.31	0.030	57.22
Case 3	38.94	28.57	62.37	62.31	78.22	27.22

3.2.2 Task 2.2: Synthesis of promising diagnose procedure to be applied to the specific loops considered[all]

The main results of this task are were:

- CPM software tool (ICC)
- Diagnosis analysis for annealing furnaces with slicing strips (MEFOS)
- Supervision of thermocouples in furnace (MEFOS)
- Diagnosis procedure for value-controlled loop's (BFI/TKN/AMEH)

3.2.2.1 CPM software tool

The University of Strathclyde has worked on a new method for synthesis of Control Performance Assessment, monitoring, detection and identification of root-causes, being deliverable D2.1. The chosen method was based on Adaptive Multiscale Principal Component Analysis and Model Predictive Control. Multiscale Principal Component Analysis (MSPCA) is used to decompose the data set into scales that represent data features at different frequencies. Multiple frequency ranges can detect an extended spectrum of root-causes when threshold boundaries in data mean and covariance are violated. The solution of MSPCA is done using the Kernel approach to allow the detection of non-linearities. A MPC-CPA index is determined using the extracted deterministic features of the data. The benchmark design is enhanced with the use of the stochastic data features as if noise measurements were available.

This design approach provides a better performance assessment. The development of the approach has taken longer than planned, but could be finished within the project. The reasons for the delay have

been some numerical instability in the optimisation methods. This also caused a delay in task 2.3, but the task could be also finished in the project.

The approach is described in figure 3.47. Using the transformation matrix defined in Task 1.3, the data set Y_t is decomposed into $L+1$ scales as follows:

$$(Y_{n,j} \bullet W_i) = \left[\begin{array}{cc} cA_{L,j} & cD_{i,j} \end{array} \right] \tag{3.59}$$

where the operation carried out is the Dot product ($\bullet$), $j = 1,2,...,m$. $cA_{L,j}$ and $cD_{i,j}$ are the approximation and detail coefficients at each variable. The reconstruction of the data set at each scale is therefore given by:

$$Z_L^H = (cA_L \bullet H_L) \tag{3.60}$$

$$Z_i^J = (cD_i \bullet J_i) \tag{3.61}$$

Z_L^H represents the approximated data set, Z_i^J $(i = 1,2,...,L)$ represents stochastic features spread over all the observations according to its power spectrum [Bak97], with Z_L^J being the data set at the finest scale or the deterministic feature. The extracted data sets can be used for MPC controller design (using only the stochastic and deterministic features) or for monitoring (using all the scales).

The MPC benchmark is designed as in Controller pre-assessment with a slight modification on the index. Since the determinant is the product of all eigenvalues, the index is writen as follows:

$$\eta_z = \frac{\prod_{j=1}^{m} \lambda_j^{Z_L^{J,o}}}{\prod_{j=1}^{m} \lambda_j^{Z_L^H}} \tag{3.62}$$

Furthermore, it is possible to find a direction in the data along which the worst sub-optimality occurs [Qin07]. Given a direction p, $\| p \| = 1$, the projection of the process output data and their optimal counterparts onto this direction is given by:

$$\Pi_p \left(Z_L^H\right) = \frac{p^T Z_{L,f}^H p}{p^T p} = p^T Z_{L,f}^H \tag{3.63}$$

$$\Pi_p \left(Z_L^{J,o}\right) = \frac{p^T Z_{L,f}^{J,o} p}{p^T p} = p^T Z_{L,f}^{J,o} \tag{3.64}$$

The direction p along which the largest variance ratio occurs is:

$$p = \arg\max \frac{var\left\{\Pi_p \left(Z_L^J\right)\right\}}{var\left\{\Pi_p \left(Z_L^o\right)\right\}} = \arg\max \frac{p^T R_{Z_{L,f}^H} p}{p^T R_{Z_{L,f}^{J,o}} p} \tag{3.65}$$

The maximization of p is the direction of critical performance improvement.

Kernel Principal Component Analysis The objective of kernel PCA is to extract principal components ($PC's$) from a data set which may or may not contain nonlinearities [Sch96]. To do so, the computation of the covariance matrix $R_{Z_i^J}$ which is originally carried out in the real numbers space ($\Re^m$), now has to be carried out in a $feature$ space (F) where operations among nonlinearly related variables can be expressed as a dot product. The transformation of the data (Z_i^J) to space F corresponds to an image of the data ($\phi\left(Z_i^J\right)$) and is achieved by using nonlinear functions called Kernels.

PCA diagonalizes the covariance matrix $R_{Z_i^J} = \frac{1}{n}\sum_{i=1}^{n} \phi\left(Z_{i,m}^J\right)^T \phi\left(z_{i,m}^J\right)$ and its solution is given by the following eigenvalue problem:

$$\lambda V = R_{Z_i^J} V \tag{3.66}$$

with $\lambda \geq 0$ eigenvalues and V eigenvectors. Since $R_{Z_i^J} V = \frac{1}{n}\sum_{k=1}^{n} \left(\phi\left(Z_{i,k}^J\right) V\right) \phi\left(Z_{i,k}^J\right)$, all the solutions of V must lie within the span of $\phi\left(Z_{i,k}^J\right), ..., \phi\left(Z_{i,n}^J\right)$, then:

$$\lambda\left(\phi\left(z_i\right) \bullet V\right) = \left(\phi\left(z_i\right) \bullet R_{Z_i^J} V\right) \tag{3.67}$$

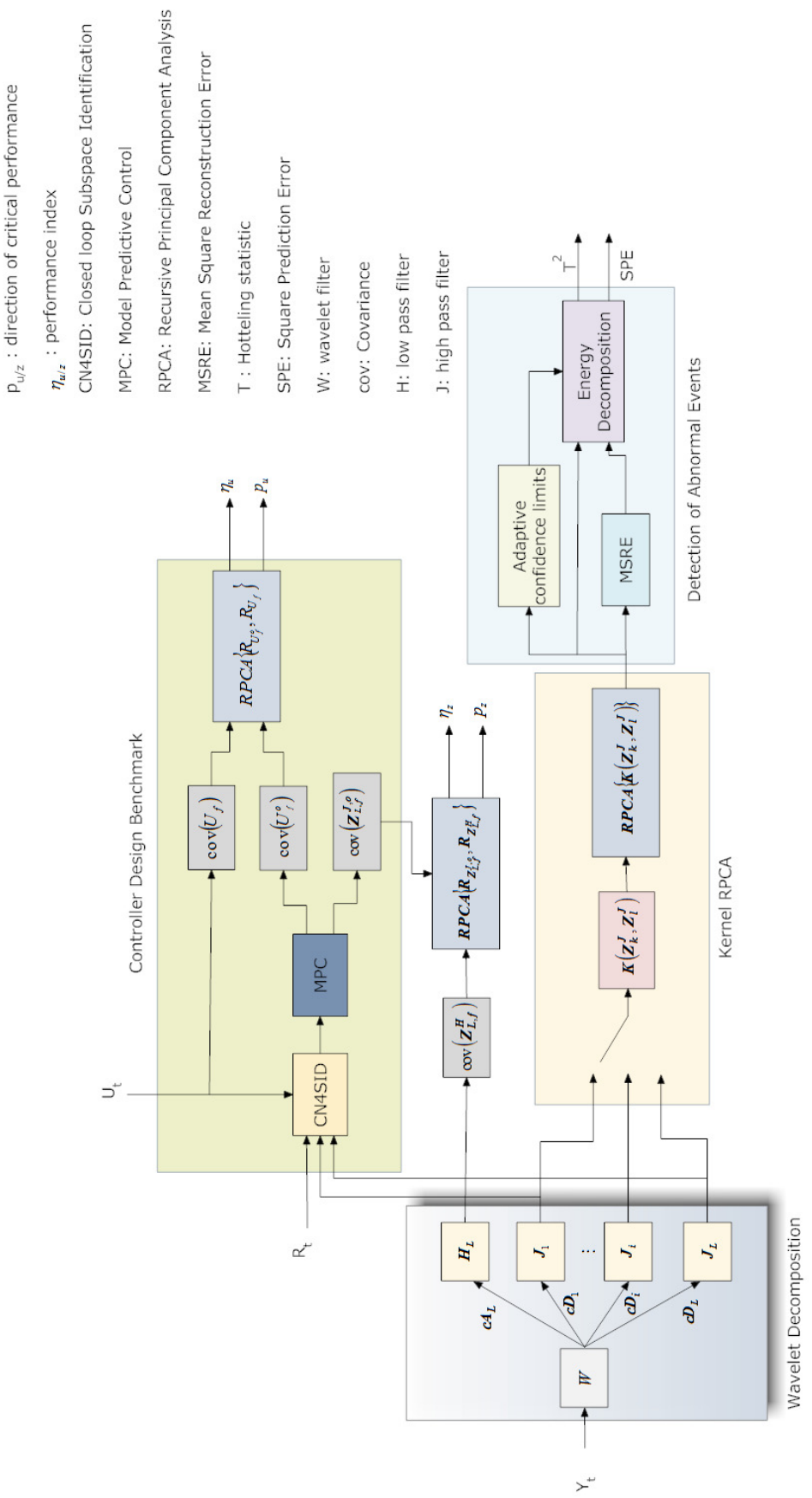

Figure 3.47: Methodology for Control Performance Monitoring and Diagnosis based on Adaptive MsKPCA

and consequently, there exist coefficients a_k, $(k = 1,2,...,n)$ such that:

$$V = \sum_{k=1}^{n} \alpha_k \phi\left(Z_{i,k}^J\right) \tag{3.68}$$

Rewriting (3.67) and defining a $n \times n$ matrix $K(Z_{i,k}^J, Z_{i,l}^J) := \left(\phi\left(Z_{i,k}^J\right) \bullet \phi\left(Z_{i,l}^J\right)\right)$, $(l = 1,...,n)$ then:

$$\lambda KA = K^2 A \tag{3.69}$$

with $A = [\alpha_1,...,\alpha_n]^T$ and since K is symmetric with a set of eigenvectors that span the whole space, then:

$$n\lambda A = KA \tag{3.70}$$

The problem is reduced to the diagonalization of the kernel K. In order to keep the normality constraint of the eigenvectors, it is necessary to normalize the coefficients α_i in F such as $1 = \lambda A \bullet A$.

The extraction of $PC's$ is possible by using a new data set or test point Z with an image $\phi(Z)$ in F as follows:

$$t_h := \left(V^h \bullet \phi(Z)\right) = \sum_{k=1}^{n} \alpha_k^h K\left(Z_{i,k}^J, Z\right) \tag{3.71}$$

where $h = 1,...,H$ and H is the number of $PC's$.

Kernels which have been successfully implemented are polynomial kernels, radial basis function kernels and sigmoid kernels [Sch96]. Radial Basis Function (RBF) kernels can maintain $K(Z_{i,k}^J, Z_{i,l}^J)$ constant. This property allows the implementation of optimal reconstruction methods and thus they will be used in this paper. The radial basis function kernel is given by:

$$K(Z_{i,k}^J, Z_{i,l}^J) = exp\left(-\frac{\| Z_{i,k}^J - Z_{i,l}^J \|^2}{2\sigma^2}\right) \tag{3.72}$$

Detection and optimal reconstruction of data In kernel PCA, the reconstruction of original patterns is no longer possible since the vector V in F does no longer have a pre-image in $\Re^n$. It is, however possible, to find a vector w in $\Re^n$ which maps to a vector that optimally approximates V [Dun98], [Dun96], [Tak02], [Cho05b]. This method reconstructs the original data without the effects of noise or abnormal features [Cho05b].

Determination of number of $PC's$ To reconstruct a ϕ-image of an input data set Z_i^J from its projections t_h, onto the first PC's in F, it is necessary to define a projection operator as follows:

$$\Pi_h\left(\phi\left(Z_i^J\right)\right) = \sum_{h=1}^{H} t_h V^h \tag{3.73}$$

If H is large enough, $\Pi_h\left(\phi\left(Z_i^J\right)\right) = \phi\left(Z_{i,k}^J\right)$, otherwise: 1) $\sum_{k=1}^{n} \| \Pi_h\left(\phi\left(Z_i^J\right)\right) - \phi\left(Z_{i,k}^J\right) \|^2$ will be minimal and; 2) the retained variance is maximal among all projections onto the orthogonal directions of F [Mik99].

In order to deal with outliers, the projection has to be modified introducing a "certainty" of data $\tilde{Z}(t) = B(t)Z + (I - B(t))w(t-1)$, as follows:

$$t_k(t) = \sum_{k=1}^{n} \alpha_k^h K\left(Z_{i,k}^J, \tilde{Z}(t)\right) \tag{3.74}$$

For $t > 0$, $I \in \Re^{m \times m}$, $B(t) \in \Re^{m \times m}$ $B(t) = diag(\beta_1(t),...,\beta_m(t))$. Each $\beta_j(t)$ denotes "certainty" of $Z_{n,j}^J$ $(j = 1,...,m)$. The estimation of the certainty is given by the difference between $Z_{n,j}^J$ and $w_j(t-1)$ as follows:

$$\beta_j(t) = exp\left(-\frac{\left(Z_{n,j}^J - w_j(t-1)\right)^2}{2\delta_j^2}\right) \tag{3.75}$$

δ_j is the standard deviation of the difference and is given by [Tak02]:

$$\delta_j = 1.4826\left(1+\frac{5}{n-1}\right)\underset{k}{\text{med}}\sqrt{\varepsilon_{kj}^2} \tag{3.76}$$

ε_{kj}^2 is the difference between the j-th component and the k-th training data. Since the reconstruction must be carried out in the input space rather than in F, it is necessary to use the vector w such that:

$$\Pi_h\left(\phi\left(Z_i^J\right)\right) = \phi\left(w\right) \tag{3.77}$$

When $\Pi_h\left(\phi\left(Z_i^J\right)\right)$ has no pre-image w, it can be approximated by minimizing:

$$\Omega\left(w\right) = \| \phi\left(w\right) - \Pi_h\left(\phi\left(Z_i^J\right)\right) \|^2 \tag{3.78}$$

and considering that RBF kernels $K\left(w,w\right) = const.$, (3.78) can be expressed as:

$$\begin{aligned}\Omega\left(w\right) &= \left(\phi\left(w\right)\bullet\Pi_h\left(\phi\left(Z_i^J\right)\right)\right)+\Omega \\ &= \sum_{k=1}^{n}\gamma_k\left(t\right)K\left(w,Z_{i,k}^J\right)+\Omega\end{aligned} \tag{3.79}$$

where Ω are the terms that do not contain w and:

$$\gamma_k\left(t\right) = \sum_{h=1}^{H} t_h\left(t\right)\alpha_i^h \tag{3.80}$$

To find the extremum, a gradient with respect to w has to make $\nabla_w\Omega\left(w\right)=0$:

$$w\left(t\right) = \frac{\sum_{k=1}^{n}\gamma_k\left(t\right)K\left(Z_{i,k}^J,\tilde{Z}\left(t\right)\right)Z_{i,k}^J}{\sum_{k=1}^{n}\gamma_k\left(t\right)K\left(Z_{i,k}^J,\tilde{Z}\left(t\right)\right)} \tag{3.81}$$

Detection of root-causes of poor performance The results of the Kernel PCA and its data optimal reconstruction are not the end product of the methodology, instead a more intuitive result of the relations among variables is presented as monitoring statistics that quantify the change in variable correlation. Root-causes of poor performance can be characterized by these changes. Variable correlations are usually quantified using statistics such as *SPE* and T^2-statistic. In fault detection, *SPE* is mostly used because it is a direct measurement of the correlation breakdown. T^2-statistic on the other side, quantifies the inflation of the variance of the $PC's$ subspace. Due to the broad spectrum of possible root-causes, both statistics are used for monitoring.

These statistics in feature space can be obtained using energy decomposition [Cho05a]. Assuming that the observations follow a Gaussian distribution in the feature space, the energy of the observations is given by:

$$\mu\left(Z_i^J\right) = \phi\left(Z_i^J\right)^T\tilde{R}_{Z_i^J}^{-1}\phi\left(Z_i^J\right) \tag{3.82}$$

where $\tilde{R}_{Z_i^J}$ is the regularized covariance matrix and is calculated as follows:

$$\tilde{R}_{Z_i^J} = V\Lambda V^T + \lambda_\perp\left(I-VV^T\right) \tag{3.83}$$

Λ is a diagonal matrix of the $PC's$ and $\lambda_\perp$ is a constant value which replaces all the zero and near-zero eigenvalues of $\tilde{R}_{Z_i^J}$. The energy μ can therefore be decomposed into two parts as follows:

$$\mu\left(Z_i^J\right) = \quad T^2+\lambda_\perp^{-1}SPE \tag{3.84}$$

Real time applications require recursive determination of the confidence limits [Li 00]. Since the covariance matrix is unknown in the feature space, the statistics may not conform to a generalized χ^2 distribution [Cho05b]. Alternatively, it is possible to calculate the $100\left(1-\alpha\right)\%$ limit by means of a F-distribution as follows:

$$T_{lim}^2 = \frac{H\left(n-1\right)}{n-H}F\left(H,n-1;\alpha\right) \tag{3.85}$$

where $F(H, n-1; \alpha)$ is the F-distribution with degrees of freedom H and $n-1$ and level of significance α.

$$SPE_{lim} = \theta_1 \left\{ \frac{C_\alpha \sqrt{2\theta_2 p_0^2}}{\theta_1} + 1 + \frac{\theta_2 h_0 (h_0 - 1)}{\theta_1^2} \right\} \tag{3.86}$$

with:

$$\theta_m = \sum_{j=l+1}^{m} \lambda_j^m \; m = 1,2,3 \tag{3.87}$$

$$h_0 = 1 - \frac{2\theta_1 \theta_3}{3\theta_2^2} \tag{3.88}$$

and C_α is the normal deviate that cutting off an area of α upper tail if h_0 is positive or lower tail if h_0 is negative.

Identification of abnormal events Faults identification is carried out based on the identification of which variable or combination of variables are responsible for the statistics thresholds violations [Cho05a].

The method is based on the fact that the partial derivative of a function with respect to a specific dimension can indicate the relative importance of the corresponding variable on that function.

Since the statistics depend upon the kernel function, it is possible to define the contributions of each variable on the statistics. By using the gradient of the kernel function, the absolute value of the partial derivative represents the amount of influence of the variable on the function. The two contributions are as follows:

$$C_{T^2,i} = \left| \frac{\partial T^2}{\partial v_i} \right| \tag{3.89}$$

$$C_{SPE,i} = \left| \frac{\partial SPE}{\partial v_i} \right| \tag{3.90}$$

where $C_{T^2,i}$ is the contribution of the i-th variable on T^2-statistic and $C_{SPE,i}$ is the contribution of the i-th variable on SPE. The absolute value can also be used to indirectly account for the magnitude of the abnormal event, in this case onto a particular statistic.

The final methodology can be combined with the diagnosis methods previously derived depending on the application.

Case studies The method was tested against a multivariable case study and the strip temperature data at the Swerea MEFOS annealing process. Since the method is mathematically complex, its implementation was summarised in the following steps:

1: Set $k = 0$ and the initial data set $X_{k+1}^0 = \begin{bmatrix} X_k^0 \\ X_{n_k+1}^0 \end{bmatrix}$

2: Set $L = log_2(n)$ and perform the adaptive wavelet decomposition of the data set and retrieve Z_i^J $(i = 1,2,...,L)$

3: Set the future and past outputs (Z_L^J), inputs, set-points and extracted disturbances (Z_1^J) data sequences and identify the process and noise model using the subspace identification method based on recursive least squares with QR decomposition.

- Retrieve the models and calculate the performance index η_z and the energy index η_u.
- Retrieve the directions p of worst sub-optimality.

4: Perform kernel PCA on each Z_i^J $(i = 1,2,...,L)$ and retrieve the PC's from each scale.

5: Calculate the T^2 and SPE statistics on each scale and check for confidence limits violations.

- Calculate the contributions of individual variables on T^2 and SPE

6: Set $k \leftarrow k+1$, update X^0_{k+1}.

7: Go to step 2 and repeat the procedure.

X^0_k is the k-th data block necessary to perform batch wavelet decomposition [Li 00] as well as subspace identification [Kad02b]. X^0_{k+1} is calculated when the next block of data $X^0_{n_k+1}$ is available.
In order to make the algorithms recursive, X^0_k is chosen to be the minimum data block to perform wavelet decomposition and $X^0_{n_k+1}$ can be a one-sample vector of the outputs. The minimum data block depends on the number of scales L and has been chosen as $2L$.

Multivariable case study: The study corresponded to the following multivariable plant:

$$G_p = \begin{bmatrix} \frac{z^{-1}}{1-0.4z^{-1}} & \frac{z^{-2}}{1-0.1z^{-1}} \\ \frac{0.3z^{-1}}{1-0.1z^{-1}} & \frac{z^{-2}}{1-0.8z^{-1}} \end{bmatrix} \tag{3.91}$$

$$G_d = \begin{bmatrix} \frac{1}{1-0.5z^{-1}} & \frac{-0.6}{1-0.5z^{-1}} \\ \frac{0.5}{1-0.5z^{-1}} & \frac{1}{1-0.5z^{-1}} \end{bmatrix} \tag{3.92}$$

with disturbance variance $\sigma = 0.0016I$ and sampling time $t_s = 1$s. [Yua08]. The controllers for the process were specified as:

$$G_{c_j} = K_{p_j}\left(1 + \frac{t_s}{\tau_{i_j}(1-z^{-1})}\right) \tag{3.93}$$

$j = 1,2$, parameters $K_{p_1} = 0.24$ and $\tau_{i_1} = 1.60$ for the first loop; and $K_{p_2} = 0.04$ and $\tau_{i_2} = 2.67$ for the second loop.

The performance of the control system was then assessed under the following situations: original plant, variance change ($t = 500$ s on output y_2 and runs for 300 s), external oscillations ($t = 1000$ s on output y_1 and runs for 300s), equipment failure (this case actuator fault) ($t = 1500$ s on output y_2 and runs for 300 s), stiction ($t = 2000$ s on output y_1 and runs for 300 s), sensor fault ($t = 2500$ s on output y_2 and runs for 300 s), process change ($t = 3000$ s on output y_1 and runs for 300 s), equipment degradation ($t = 3500$ s on output y_2 and runs for 5 0s) and improper control tuning ($t = 4000$ s on output y_1 and runs for 300 s). It was expected that each situation presents a particular behaviour at one or more scales.

Equipment malfunctions such as sensor and actuator faults, and other equipment wear or failure were usually considered as a separated problem [Jel06b]. Their effects were treated within FDI and therefore considered in our approach.

For improper control tuning the gain K_{p_1} was done 4.4 times higher. On the other side, the change in process dynamics was:

$$G_p = \begin{bmatrix} \frac{z^{-1}}{1-0.4z^{-1}} & \frac{16z^{-2}}{1-0.1z^{-1}} \\ \frac{0.3z^{-1}}{1-0.1z^{-1}} & \frac{z^{-2}}{1-0.8z^{-1}} \end{bmatrix} \tag{3.94}$$

Figure 3.48 shows the impact of previously described situations on the outputs of the multivariable plant

Table 3.8 comprises the obtained results. Three scales were used. It was expected that deterministic changes such as plant change or equipment problems appear at scale 1 whereas root-causes related to high frequency noise would appear at the highest scale. Each root-cause may produce some change in the statistics at all scales, however not all the thresholds are violated. Table 3.8 represents a set of possible characteristic behaviour of individual root-causes.

The simulation results are presented in detail in figure 3.49 - 3.57. The figures show the onset of the situation at $t = 0s$ until $t = 180s$. Figure 3.49 shows that no threshold (green line) is violated due to exiting disturbance, when the plant is fault free. This was important to validate to exclude false arm caused by noise in the measurement. After a change of dynamics in the plant, one threshold of the

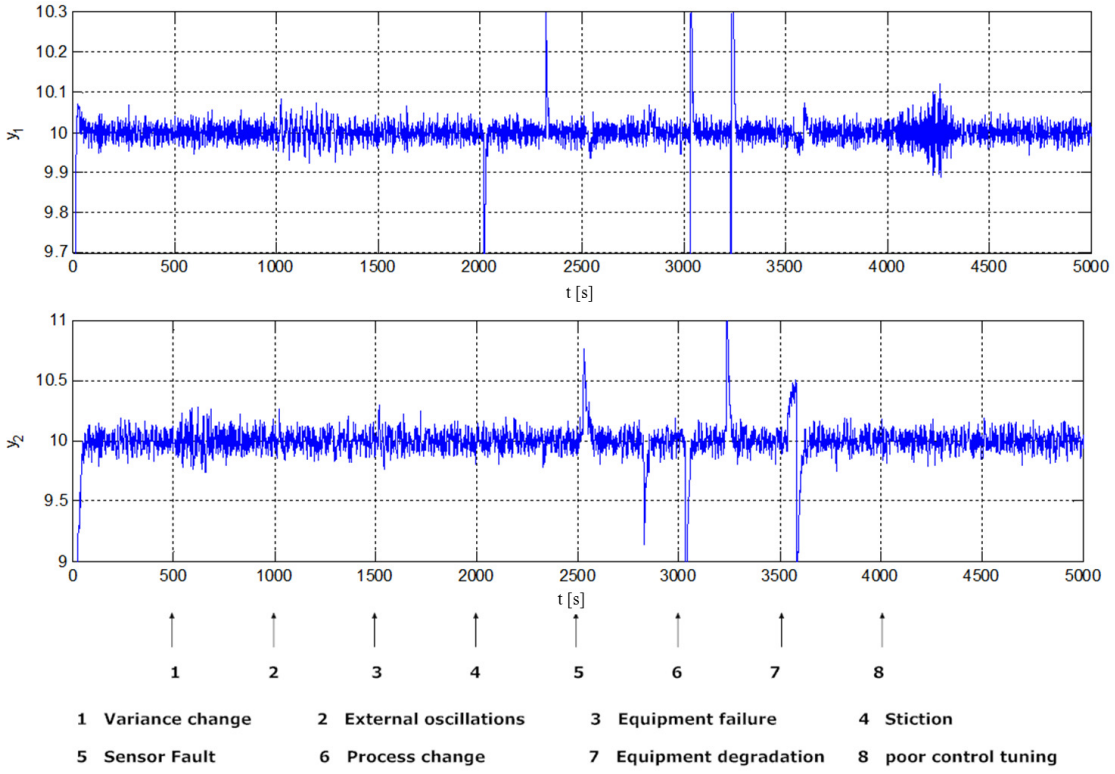

Figure 3.48: System outputs under several root-causes

Table 3.8: Summary of detection of root-causes

Root-cause	Scale	Statistic	Behaviour
original plant (figure 3.49)	1	non detected	no thresholds violation due to existing disturbance
plant change (figure 3.50)	1	SPE	continuous increase beyond threshold
external oscillations (figure 3.51)	3	T^2	oscillatory threshold violation
equipment degradation (3.52)	1	SPE	constant threshold violation
equipment failure (e.g actuator fault) (figure 3.53)	1	SPE	peak beyond threshold at failure time
sensor fault (figure 3.54)	1	SPE	smooth peak beyond threshold
disturbance change (figure 3.56)	2	SPE	random small peaks beyond threshold
nonlinearities (figure 3.55)	3	SPE	oscillatory threshold violation
poor tuning (figure3.57)	1-2	non detected	slight variation of the statistics but no threshold violation

statistic is violated 20 seconds after onset of the fault as illustrated in Figure 3.50. In the case of external oscillation added to the output of the plant the threshold of T2 (scale 3) statistics is violated periodically, because high frequency components appear in this scale. Equipment degradation (e.g. slow decrease of the measurement system gain) is shown by a constant threshold violation as seen in figure 3.52. This effect is similar to the effect of change in process dynamics. In this case, it is unable to distinguish between both. The impact of the equipment's failure in form of sensor and actuator failures (e.g sudden change of the sensor and actuator gain) is shown in figure 3.53 and 3.54. Actuator and sensor failures have both shown peaks, exceeding the threshold in the T2 statistic of scale 1. The peak of the actuator fault has been sharper than the one of the sensor, but it has been difficult to distinguish between actuator and sensor faults. Stiction (e.g nonlinearity) has been clearly detectable in the violation of the threshold

of SPE statistic in scale 3. Furthermore, if the disturbance G_d on the output has been changed, this has been detected by random small peaks, exceeding the threshold of SPE statistic's in scale 3. Still, improper controller tuning (increasing the gain K_{p1} 4.4 times) has not been detectable as can be seen in figure 3.57.

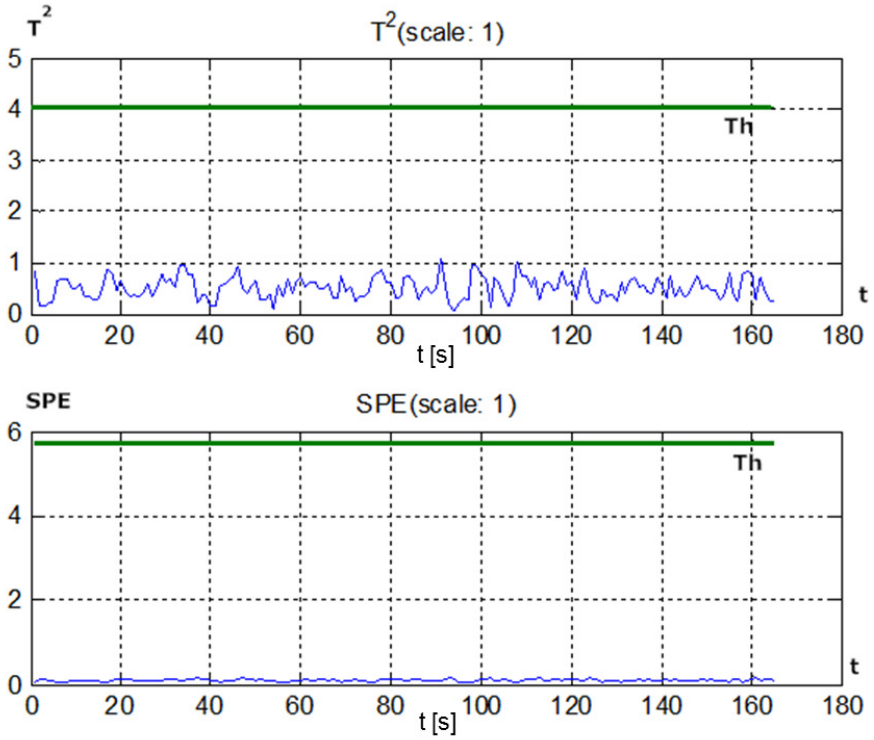

Figure 3.49: Detection statistics for the original system

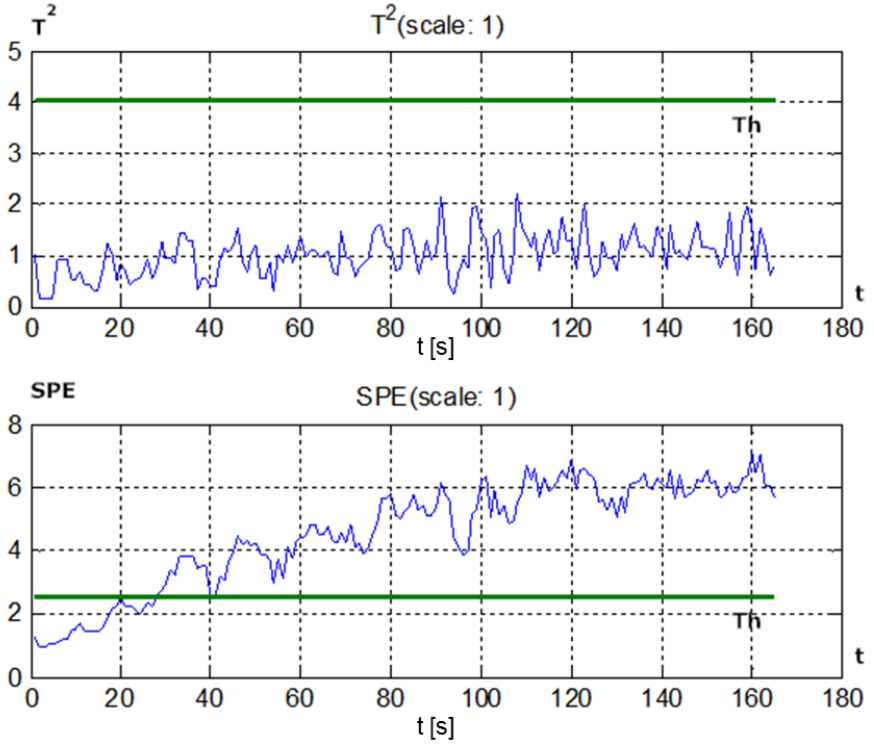

Figure 3.50: Statistics for system after change in dynamics

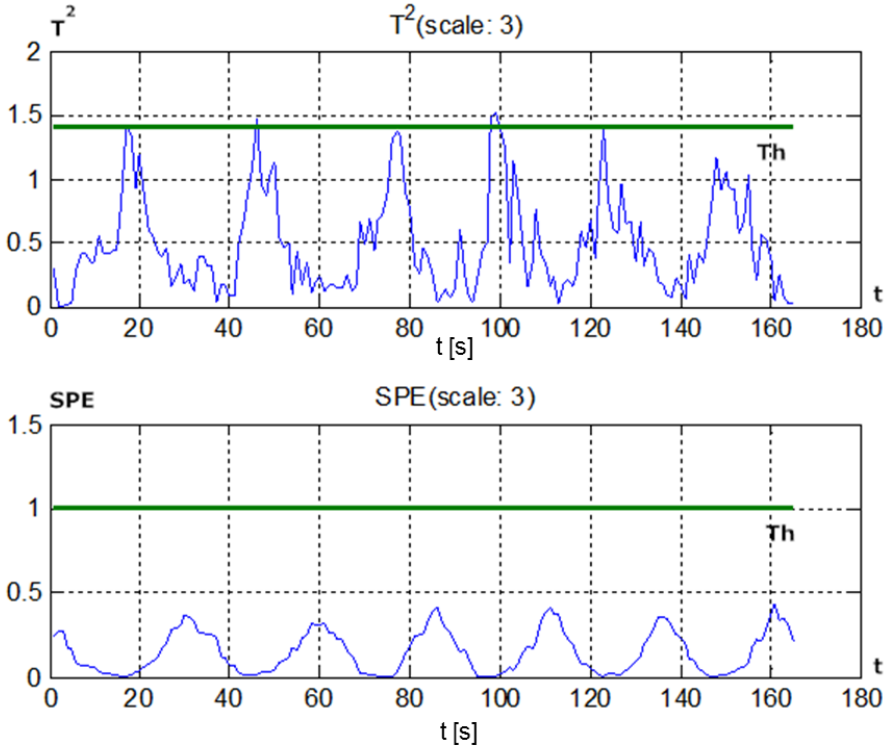

Figure 3.51: Statistics for system external oscillations

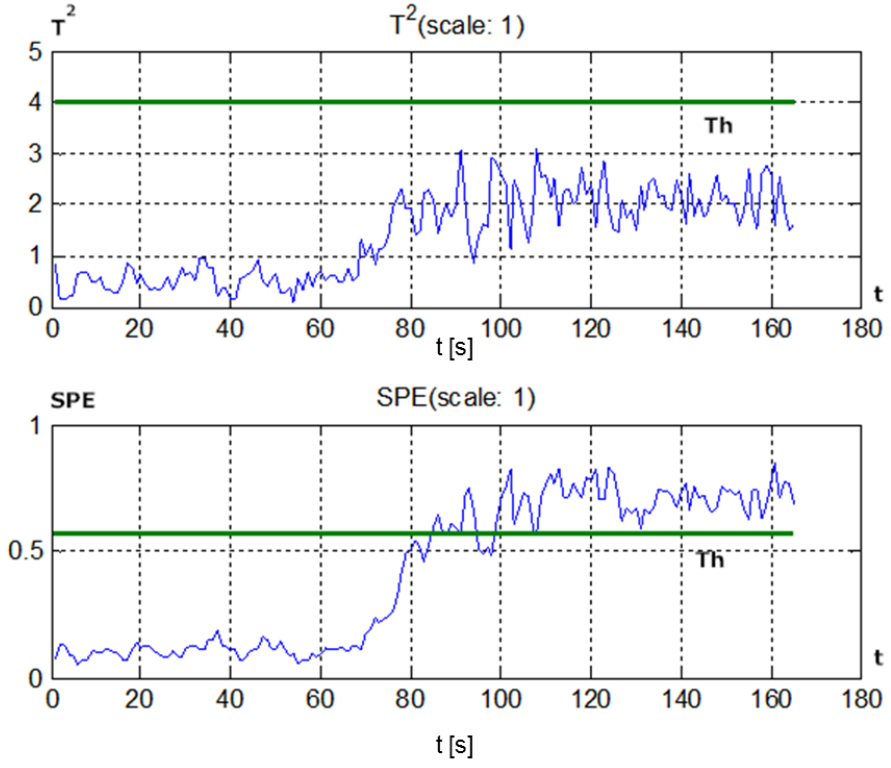

Figure 3.52: Statistics for system with equipment degradation

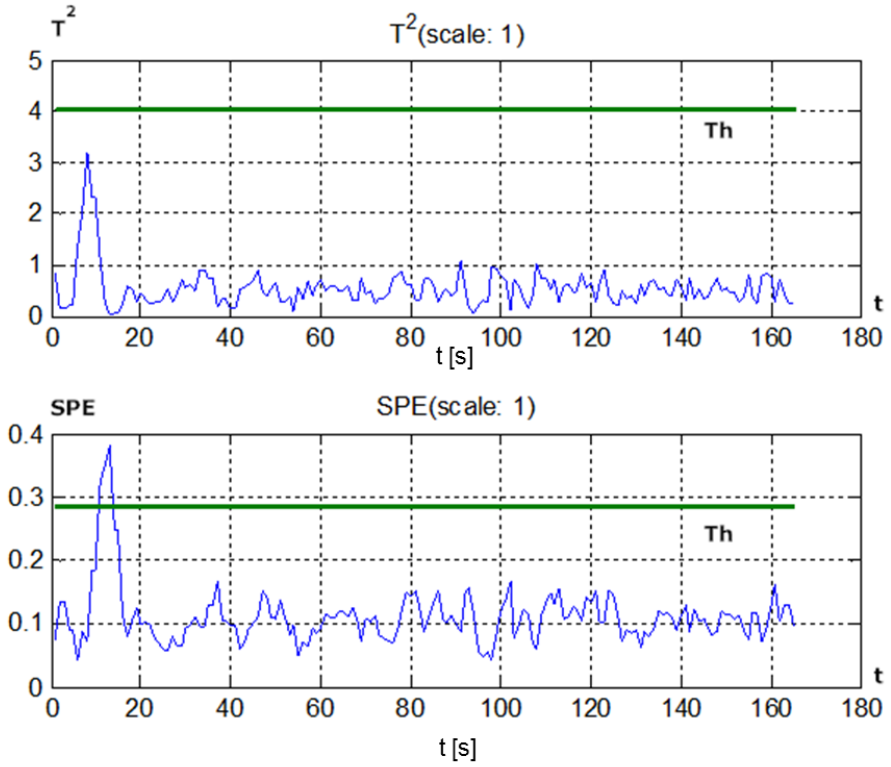

Figure 3.53: Statistics for system with equipment failure

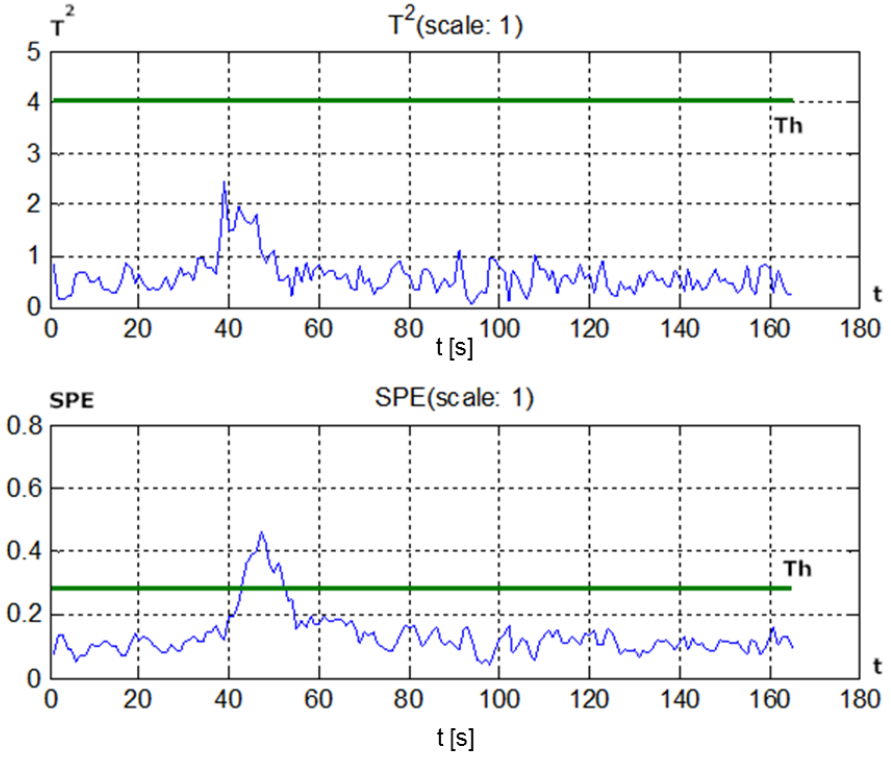

Figure 3.54: Statistics for system with sensor faults

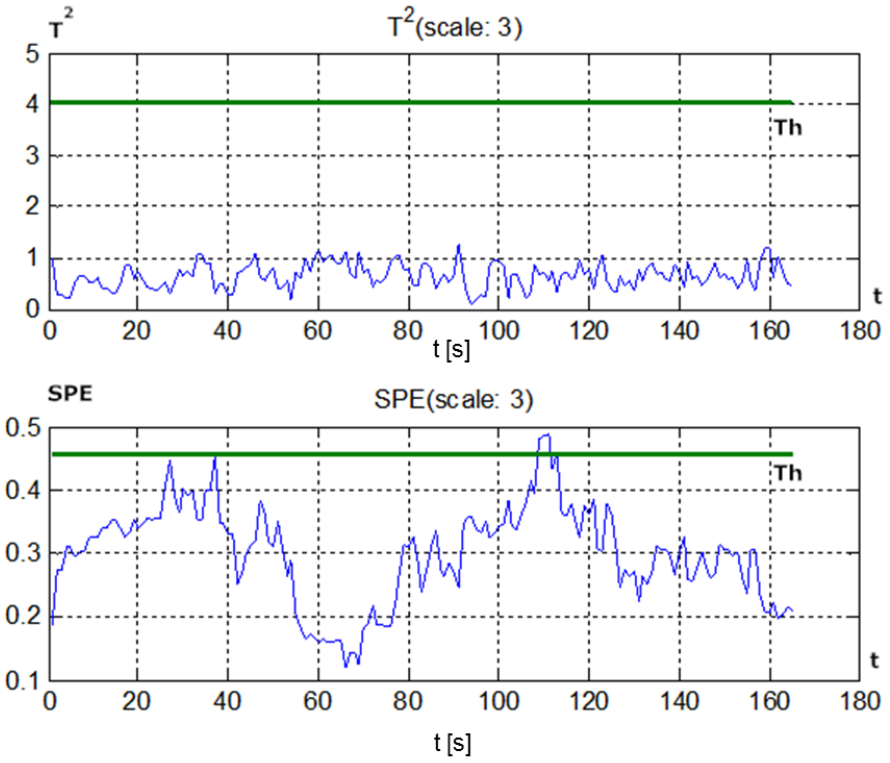

Figure 3.55: Statistics for system with weak stiction

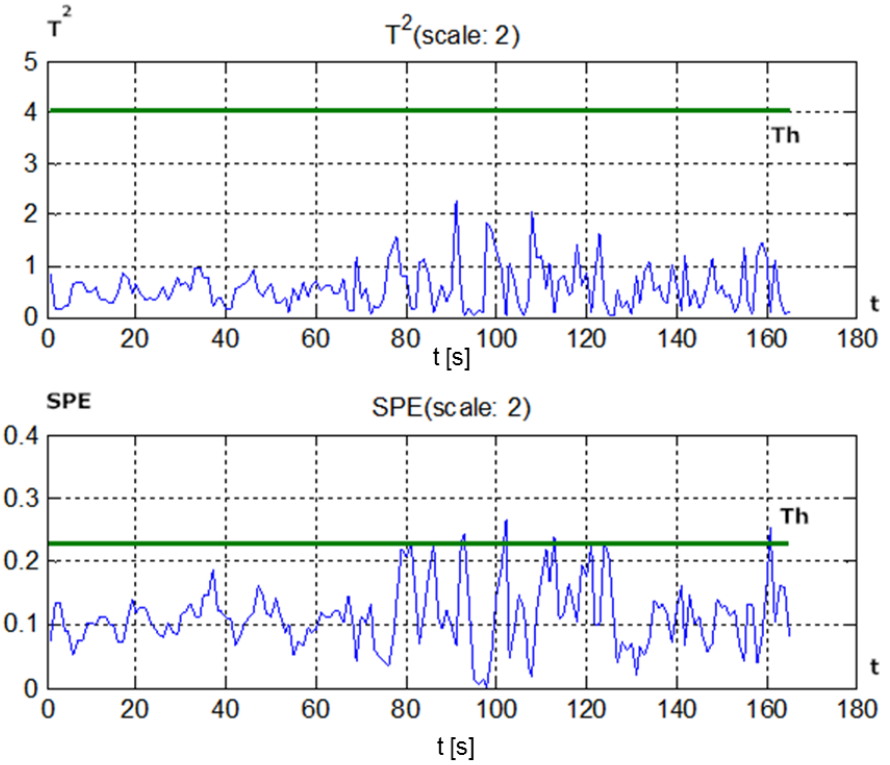

Figure 3.56: Statistics for system with disturbance change

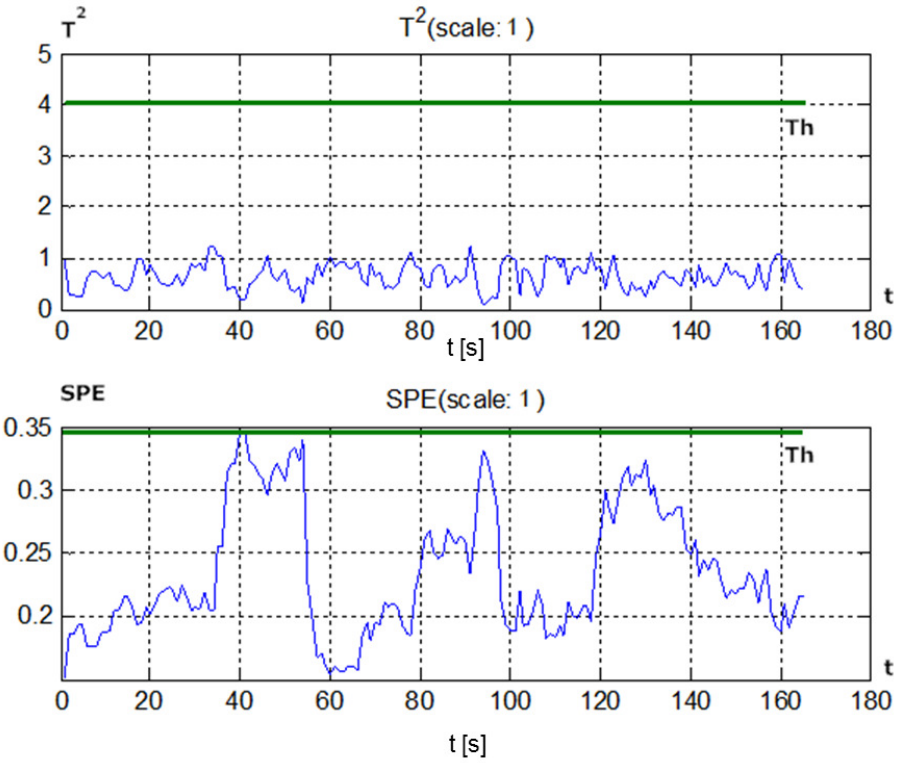

Figure 3.57: Statistics for system with controller poor tuning

The strip temperature data at the Swerea MEFOS annealing process: The annealing process consists of 6 zones. Each zones provides a different temperature to the strip. For analysis purposes, setpoint data, wall temperatures and strip temperatures have been used. The temperature of the strip is measured at the end of each zone except zone 1 and 2 where calculated values are present in the dataset. The dataset corresponds to 40 consecutive strips of varying thickness, width and steel grade welded together through holding strips. Setpoints are changed depending on both thickness and material quality, also causing changes in strip speed. The data presents a considerable drift to the setpoints for zones 1 and 2 and abrupt peaks from $t = 5000$ s to $t = 9000$ s. The operation was stopped at about $t = 9400$ s due to line closing down. During the analysis, some discrepancy was expected in the detection stage because these data drifts and abrupt changes increased the number of PC's. The temperature of the strip at each zone is given in figure 3.58 and its analysis is given in figure 3.59. Initially, there was a threshold violation on T^2 corresponding to a setpoint change. After time 4000 s, the abrupt peaks at each setpoint change appeared at scale 3. From the results of Table 3.8, a violation of T^2 statistics at scale 3 can be inferred as external sources of high frequency distortion. The amplitude of the peaks varied and so the presence of oscillatory sources was unlikely. No further diagnosis was made since the data was not reliable and the patterns from the case studies were not corroborated with real data.

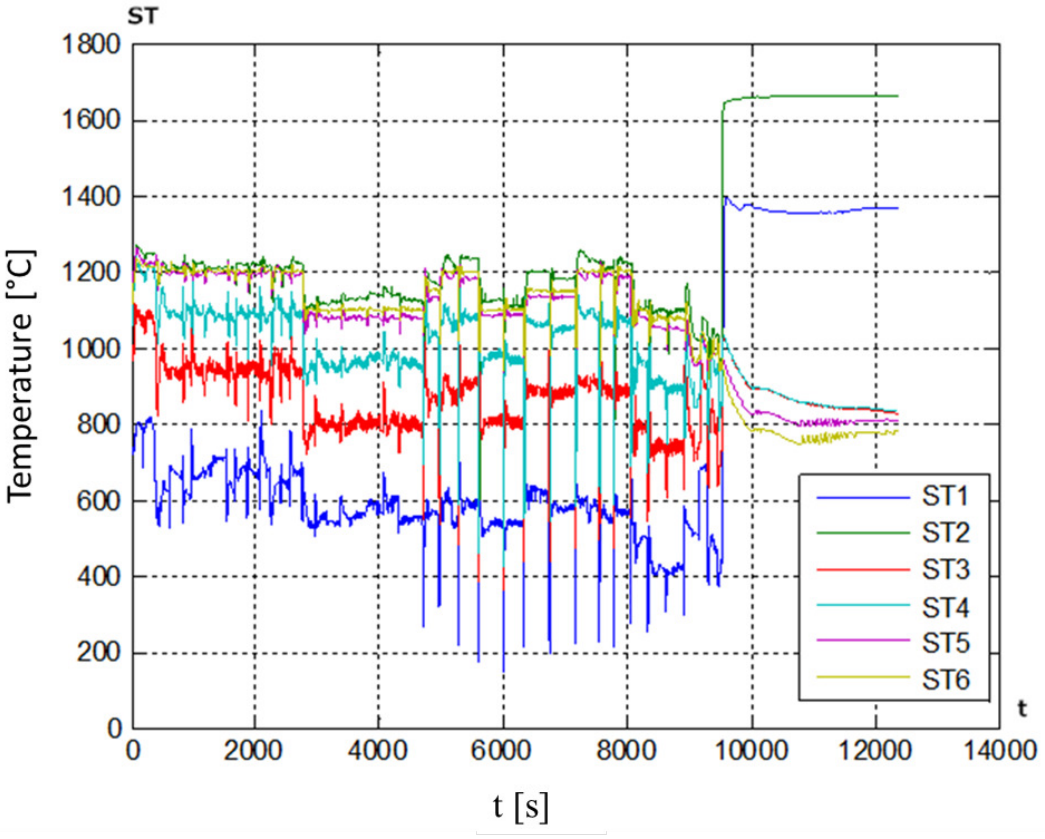

Figure 3.58: Strip temperature at annealing process (Swerea MEFOS data)

3.2.2.2 Further analyses by MEFOS of existing control loops reaction to splicing strips inspired by the results of ICC

In the annealing furnace strip and strip thickness were connected with the help of a splicing strip. The splicing strip disturbed in the temperature uniformity, since it could have had differing thickness and emissivity. The response of the temperature controller was examined after the passage of a splicing strip as e.g. in figure 3.61. The controller quickly returned the strip temperature to the set-point temperature, indicating a well-tuned system during the passage of the first splicing strip. There was a larger change in the strip thickness for the second splicing strip in the figure below, and the response was not as smooth.

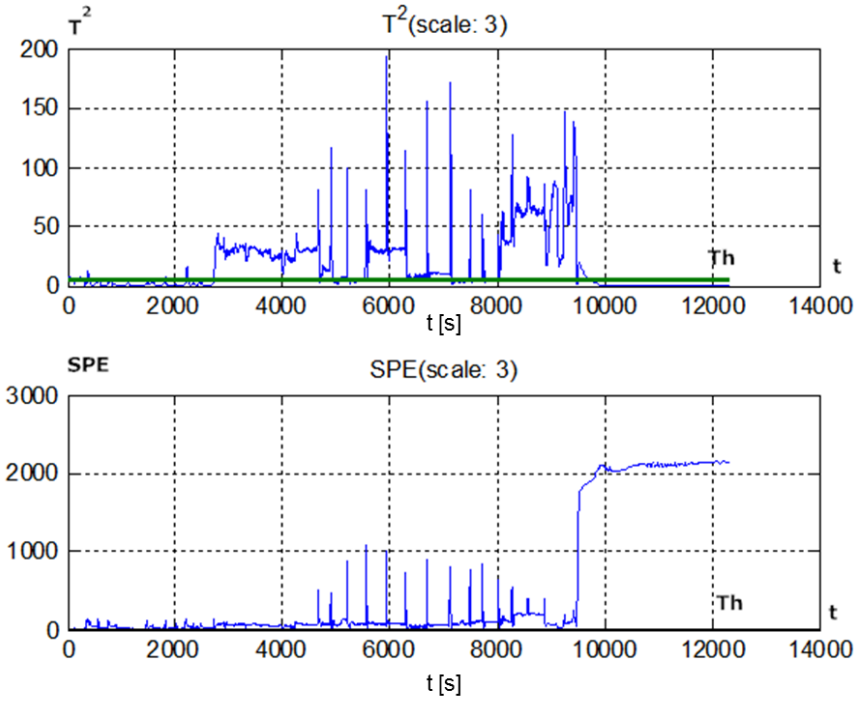

Figure 3.59: Statistics for strip temperature at annealing process

Note that the temperature deviation of the process during the passage of the splicing strip has not been critical, since the splicing strips were reused and not included in the final product to the customer. This also made the analysis of the control data more difficult, since temperature deviations during the passage of the splicing strips did not contribute to a lower final product quality. Ways to improve the temperature uniformity even with the use of splicing strips was a goal of this project. One possibility was to tailor the properties of the splicing strips (i.e., splicing strip emissivity, width and thickness), so there is less temperature disturbance.

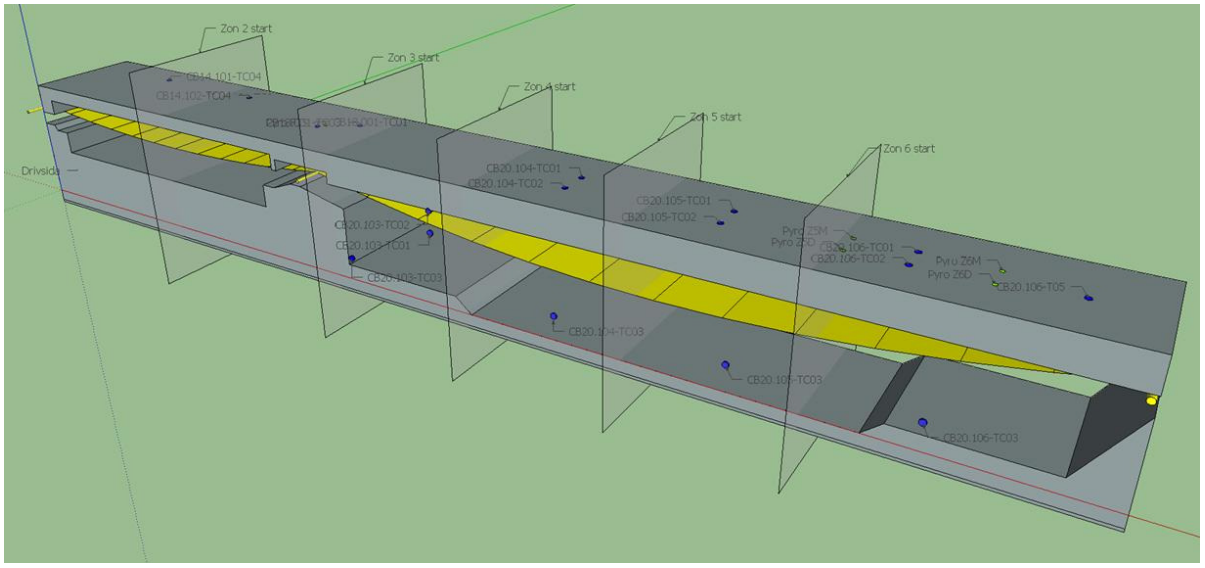

Figure 3.60: A model of the annealing furnace showing the temperature measurement positions

Test with scanning pyrometer. Different observations were made regarding process problems that seem to be of another nature then temperature control. One of the reoccurring problems in the line was varying unflatness of the strips. That is usually an indication of uneven temperatures across the strip width so its origin could derive from bad temperature control laterally. For this purpose a scanning pyrometer was obtained to determine the variations in temperature across the strip width.

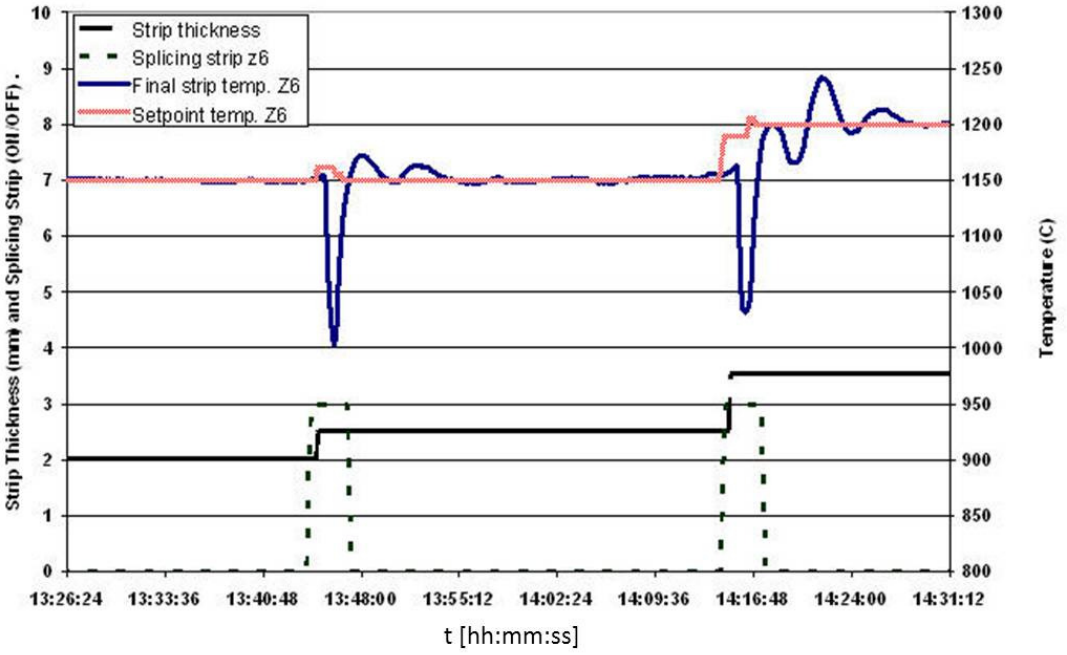

Figure 3.61: Response of the pressure controller due to disturbance caused by change of strip thickness (splicing strip and next strip)

A first test was made and it showed variations both across and from side to side, see figure 3.62. The reason for such anomalies can be caused by a number of different reasons. One could have its origin in strip tracking, i.e. how well the strip is centred in the furnace. If the strip moves over to one side, the burners on that side will be more efficient and will give the strip a tilted temperature profile. Another reason could be a bad calibration of the burners, side to side that will have the same result. A tilted temperature profile will also make double pyrometers show different temperatures since their field of view is separated on the strip. Unfortunately, it has not been able to make any further tests due to the breakdown of the scanning pyrometer. The pyrometer was returned to the manufacturer for repair and there has been a problem getting it fixed due to shortage of special components, according to the manufacturer. When the pyrometer finally was returned and put in use it broke down once more with an additional long waiting period for the repair. The scanning pyrometer was not used after that in this project.

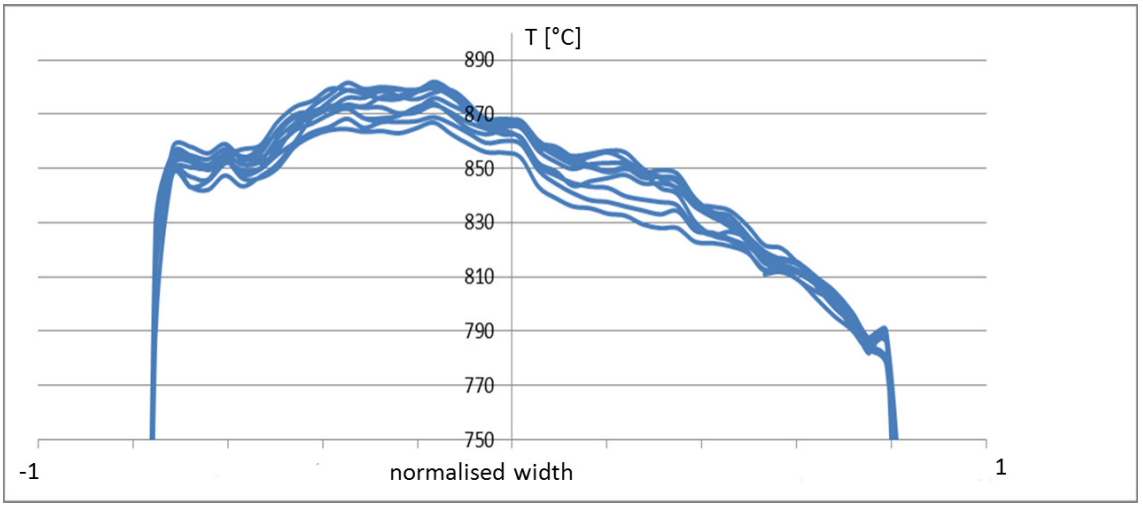

Figure 3.62: Scanning pyrometer on finished strip

Mapping the actual strip temperatures in the furnace. When trying to obtain the correct emission factor for the strip during the annealing process one needs to know the temperature evolution of the strip during processing. Determining the actual temperatures of the strip moving through the furnace was a main problem. Tests were made with a radio transmitting temperature logger. However, the radio signal was severely shielded by the furnace, even if the logger itself can withstand the temperatures in the furnace it was not possible to transmit the signal with a satisfying result. Due to these problems, a logger was designed to be put on the strip and travel through the furnace, logging up to 6 thermocouples was obtained. A dummy was produced with the same weight and size as the real logger and tests were made to determine how to attach the logger to the strip and to verify that the logger would fit through the furnace. A preliminary test with DataPaq logger with one thermocouple was performed. Figure 3.63 shows a test with one thermocouple connected to the DataPaq, going into the furnace. The responsible manager of the annealing line additionally supported the tests by applying an internship for the conduction and evaluation. Several of the measurements were from the report made by the intern Linda Johannesson.[Joh]

Figure 3.63: Test with one thermocouple connected to the DataPaq, going into the furnace

In figure 3.64 the logged temperature of the strip compared to the set-points of the different furnace zones is depicted. The finishing temperature was almost always corresponding exactly to the calculated temperature. That can be explained by the fact that it was possible to calibrate or adjust the calculation to whatever measured points available. This also explained why the theoretical and the measured temperatures almost always corresponded where the strip entered furnace two at approx. 14-16 m, at he location of an adequate temperature measurement. It was observed that when the furnace was accelerating or decelerating the results of the calculations were detereorating.

It was obvious that the final set-point, Z6, correlated well with the finishing temperature of the strip, while the other set-points were difficult to pin point exactly to the heating curve. A few test with multiple thermocouples showed that it was practically impossible to attach more than one thermocouple without stopping or slowing down the line. Stopping and then starting the line is costly since the quality of both, the strip that is in the furnace during the stop and the strip that goes through the furnace after the stop may get properties out of tolerance band when the speed is varying, see figure 3.65.

3.2.2.3 Supervision of thermocouples in furnace

In the following a supervision method for thermocouples is described by MEFOS. Thermocouples in a furnace are subject to two types of deterioration, slow drift or breaking. It is essential that it is immediately detected when a thermocouple breaks, but more necessary to detect when a thermocouple

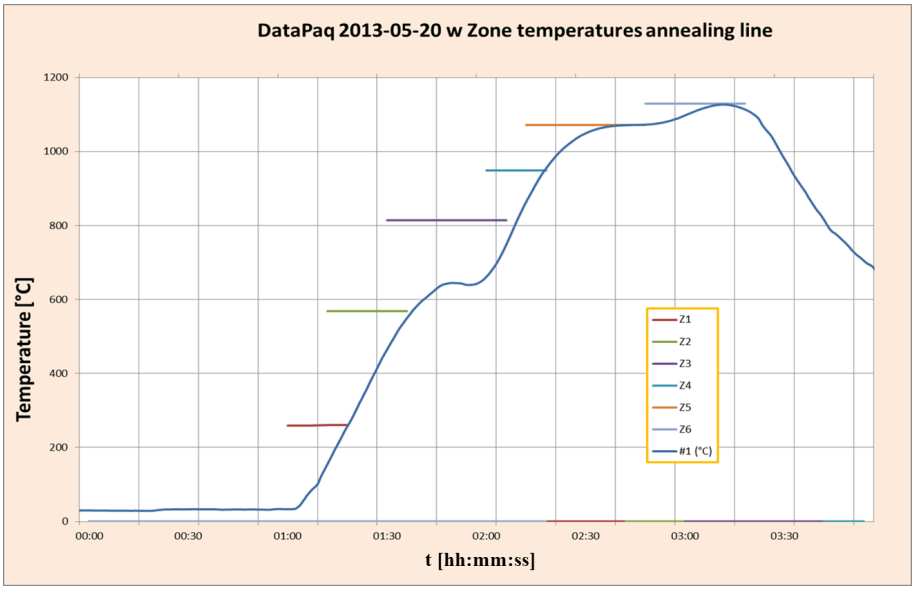

Figure 3.64: : Strip temperature from temp logger and set-points for strip temp in each zone.

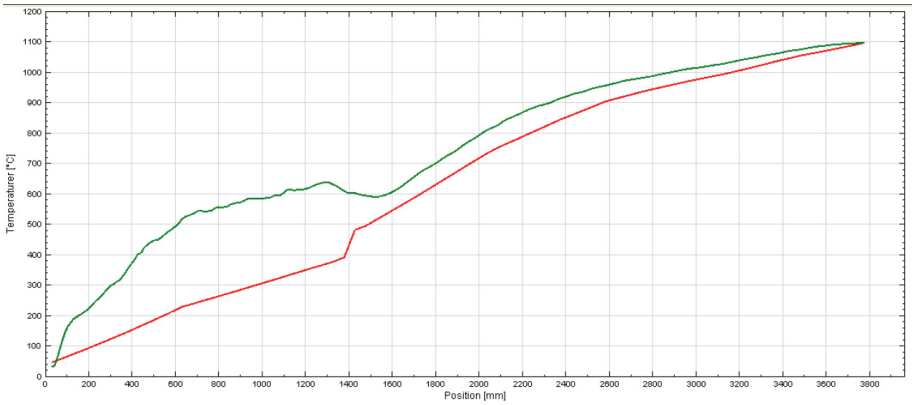

Figure 3.65: Strip ID 63589485 Strip temperature through the furnace measured (green) and the calculated (red) [Start time 12:12, Width: 2058mm, Thickness: 8.1mm, Speed 12.2 m/min. Measuring pos:120 m (total length 137 m), Surface:1D (bright)]

starts to drift, and when it must be replaced. It is also necessary to confirm that the replacement element is mounted correctly and that it shows the same temperature as the thermocouple that was replaced. To be able to do this, thermocouple data was collected over a long period of time, at least three or four months. A model was created from normal process control data where signals that clearly deviate from nominal behavior is deleted. The data was then divided into two parts, data for training and data for verification. A PCA-model (Principal Component Analysis) was created from training data, with a model setup for each thermocouple. A number of setups were created depending on production variables. To analyse and check the sensors, the PCA-models used among other things the fact that a correctly tuned model will have a normally distributed error. Q-statistics, i.e. square sum model errors, were used and also CUMSUM, a cumulative sum of model errors was used. CUMSUM sums up the model errors and sends an alarm when it gets out of the allowed window, i.e. too high or too negative. CUMSUM will also give a good estimation of when the error occurred.

3.2.2.4 Comprehensive diagnosis procedure for valve-controlled loops

The diagnosis procedure proposed by BFI for valve-controlled control loops combined techniques already described before (Tasks 1.2 and 2.1) and is shown in Figure 3.66. It started with oscillation detection: when the control loop was found to be oscillating, the most probable origin was assumed to be valve stiction. However, non-linearity had to be checked as a possible source of oscillation.

A stiction detection method was then applied and its level estimated. If stiction has been detected and had a significant level, then a gain-change test was performed before the costs of downtime and

maintenance could be justified. This is based on the fact that changes in oscillation frequency due to variation in controller gain helped to confirm the presence of stiction in the loop. This method was a simple alternative test that was applied online without significant disruption of the plant production before applying an invasive stiction detection method.

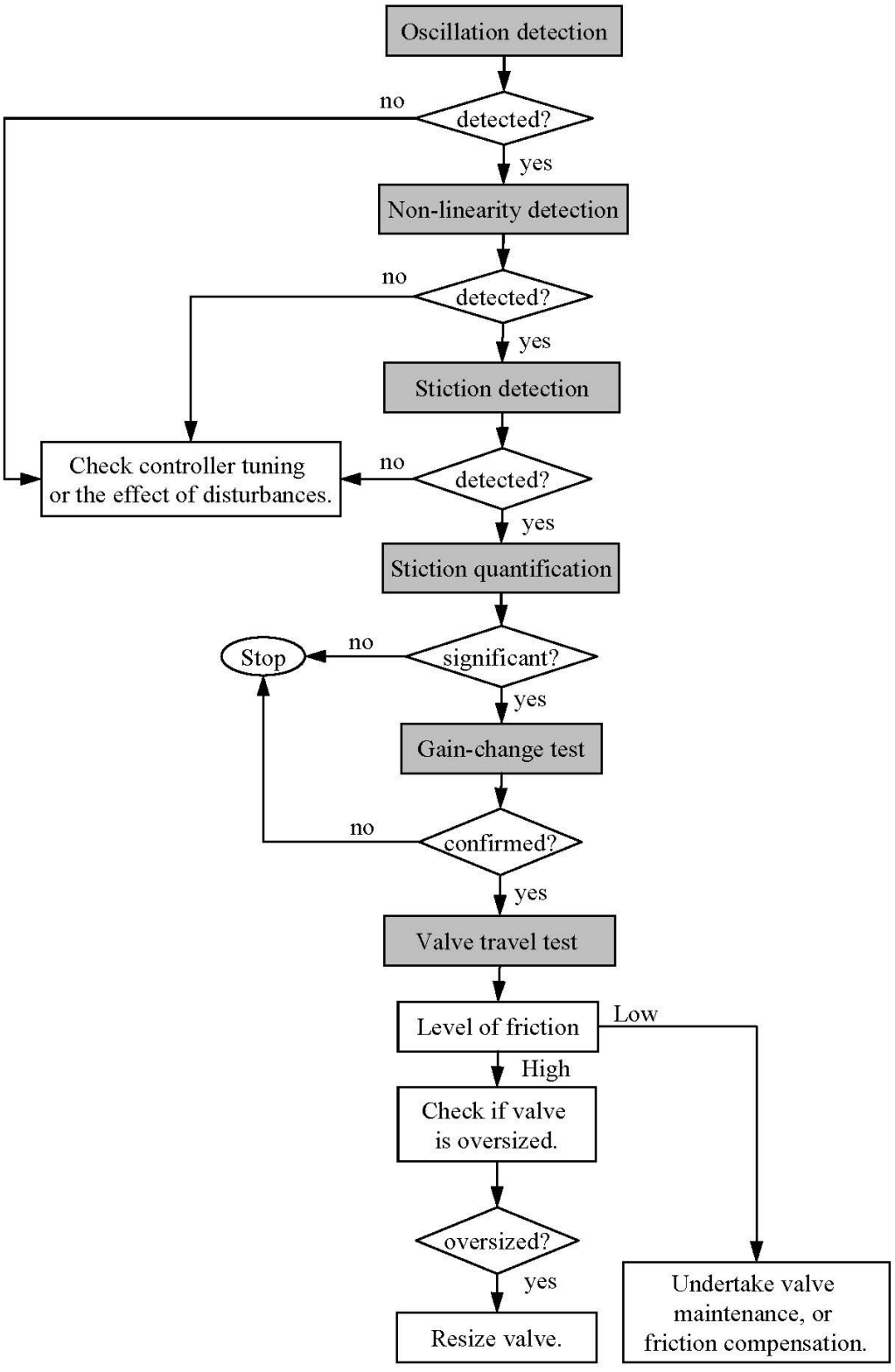

Figure 3.66: Diagnosis procedure to discover the cause of oscillations and recommended actions to eliminate them

When stiction was confirmed, valve travel test were carried out, preferably with the valve in service. This test was done following the traditional procedure given by Gerry and Ruel [Ger01]:

1. Put the controller in manual with the output near the normal operating range.
2. Change the controller output by 5 to 10% to overcome the hysteresis on the loop. If the process

variable does not move from this change, repeat it until the process variable moves.

3. Wait for the process variable to settle.

4. Make a small change in the controller output, say about 0.2%, in the same direction as the last step. Wait for the same amount of time as the previous step to see if the process variable moves.

5. Repeat Step 4 until the process variable moves, i.e. until the stiction band is overcome.

If the level of friction had been high, the best solution was to undertake valve maintenance. If the valve had been oversized, the suggestion was to resize it. Otherwise, the impact of friction will stay high and thus improvement in the control performance will not be possible. The negative effects of stiction were not totally eliminated without repairing the valve. In cases where valve repairing has not been possible, due to, e.g. economic reasons, increasing the proportional gain and disabling integral action in the positioning controller, or even use a stiction compensation technique were probable solutions.

A critical stage of the proposed procedure was distinguished between different possible root causes of oscillations in the control loop. These were aggressive controller tuning, external disturbance, or valve nonlinearity, particularly stiction. For this purpose, the novel technique for detection and estimation of valve stiction in control loops from normal closed-loop operating data, proposed by Jelali and Karra [Jel10], was used. This method is based on a two-stage identification algorithm, where the control system is represented by a Hammerstein model including a two-parameter stiction model, e.g. that of Kano [Kan04], and a linear model for describing the remaining part of the plant/process; see figure 3.67.

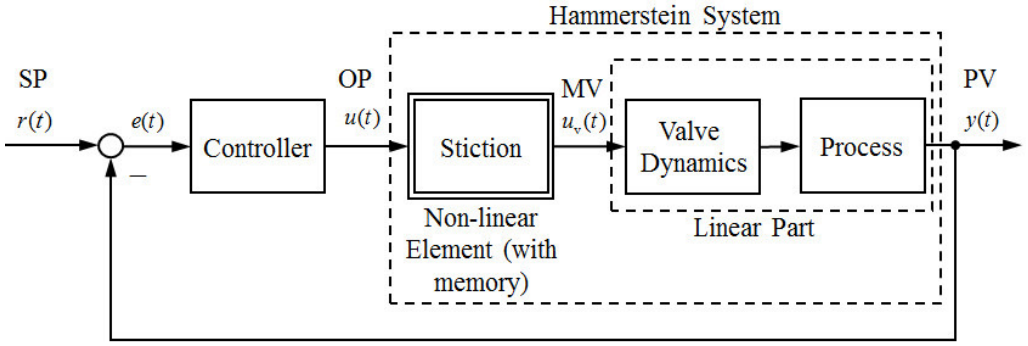

Figure 3.67: Process-control loop with valve stiction within an identification framework

The two-stage identification technique is illustrated in figure 3.68. This consists of the following features:

- A two-parameter stiction model $\mathrm{NL}_{\mathrm{stic}}(J,S)$, where S is the deadband plus stickband and J slip jump; see Figure 3.41 that shows the input–output behaviour of a sticky valve.

- The linear dynamics is represented through simple, i.e. a low-order, model $G_{\mathrm{lp}}(\tau,\theta)$, where τ is the process time delay and θ the parameter vector to be estimated by a least-squares (LS) or prediction-error (PE) identification method.

- A global search technique, such as pattern search or genetic algorithms, is used to estimate the non-linear (stiction) model parameters (J and S), subordinated with a LS or PE identification of the linear model parameters.

For a more detailed mathematical description of this procedure, one should refer to the corresponding references [Jel08, Jel10].

The complete oscillation detection and diagnosis procedure is shown in Figure 3.69 and can be summarised as follows:

1. Detect the presence of oscillations; see Task 2.1.

2. Detect the presence of stiction; see Task 2.1.

3. Identify a Hammerstein model and quantify stiction; see figure 3.68.

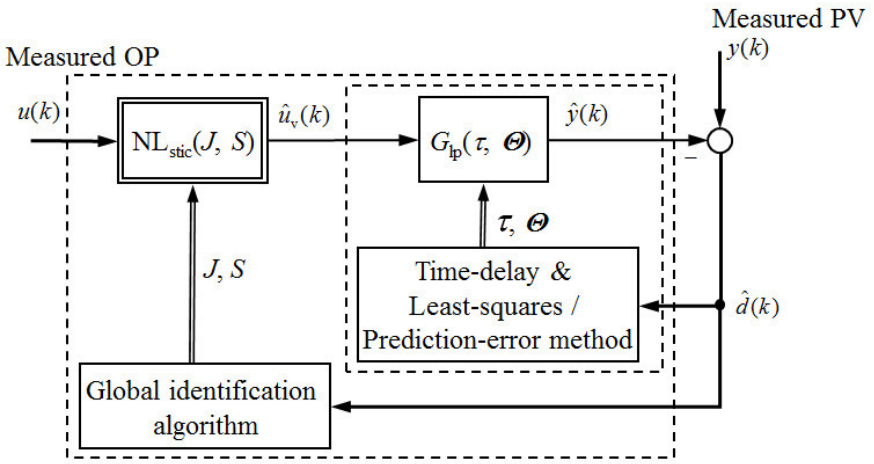

Figure 3.68: Two-stage identification of the system parameters

4. Use the identified Hammerstein model to estimate the PV trend $\hat{y}(k)$. The signal $\hat{d}(k) = y(k) - \hat{y}(k)$ gives an estimate of the external disturbances. If $\hat{d}(k)$ is oscillatory, which can be quantified by an oscillation index, the oscillation is due to external disturbances.

5. Estimate the controller model (when not known) based on measured data SP–PV and OP, e.g. using the arx function from MATLAB identification toolbox. Calculate the controller parameters depending on the controller type and representation.

6. Use the identified linear model and the (estimated) controller to simulate the closed loop without stiction. Apply, for instance, step changes on the loop and assess the controller, e.g. using the Harris index; see Task 1.3. If the assessment indicates oscillatory/aggressive behaviour, aggressive controller tuning contributes to the loop oscillation.

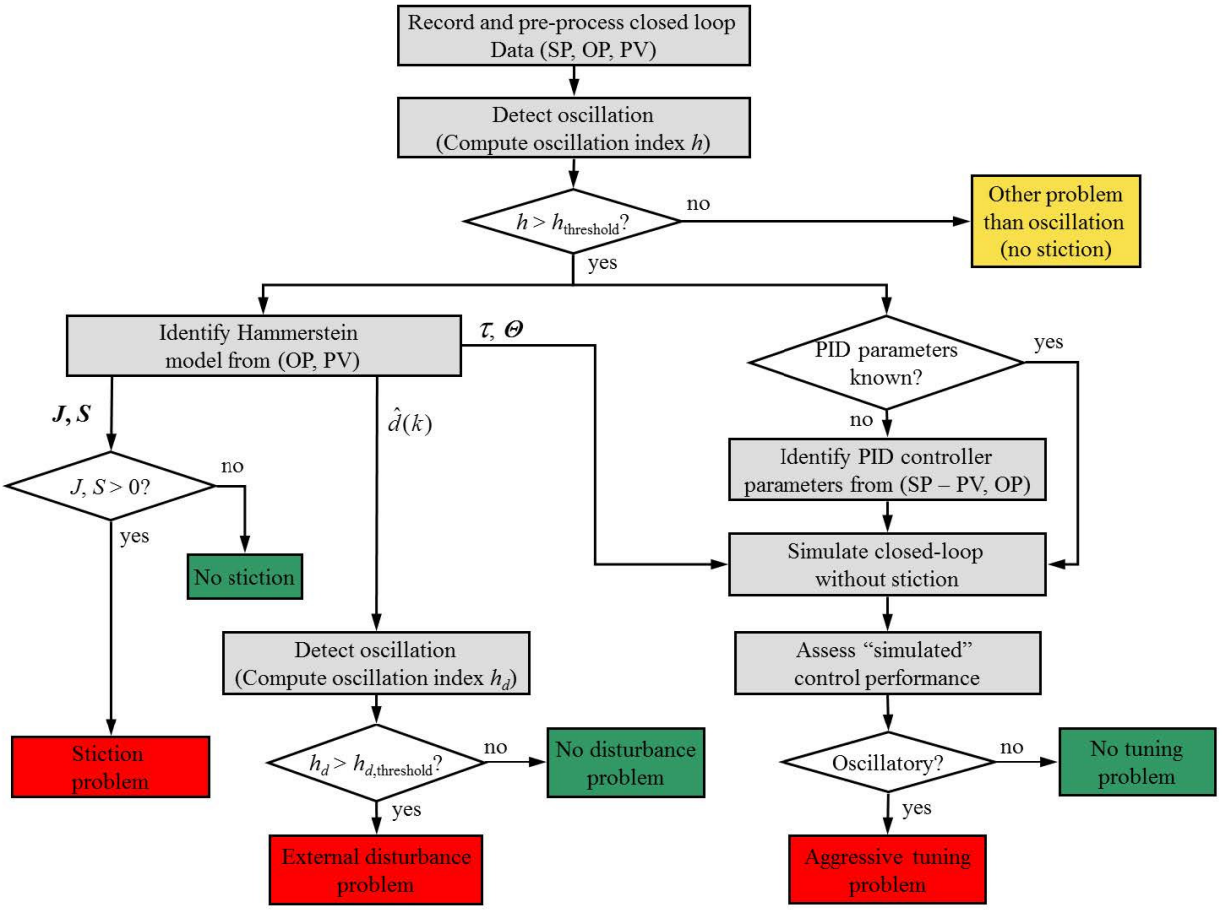

Figure 3.69: Flow chart of the oscillation detection and diagnosis procedure

3.2.3 Task 2.3: Developement of the diagnosis of root cause reporting systems[MEFOS, AMEH; ICC, TKN]

In figure 3.70 a suggested structure of a performance monitoring and root-cause diagnosis reporting system is shown, being deliverable D2.2. This has been inspired by the structure used in the cpmPlus Loop Performance Manager of ABB, but extended by the new methods and features developed within this project (shown in red-filled blocks). The green rounded rectangles represent the operations performed by the reporting system. The automatic controller tuning required interaction with plant personnel, who elaborated the results of CPM, initiated auto-tuning and confirmed its results and actions.

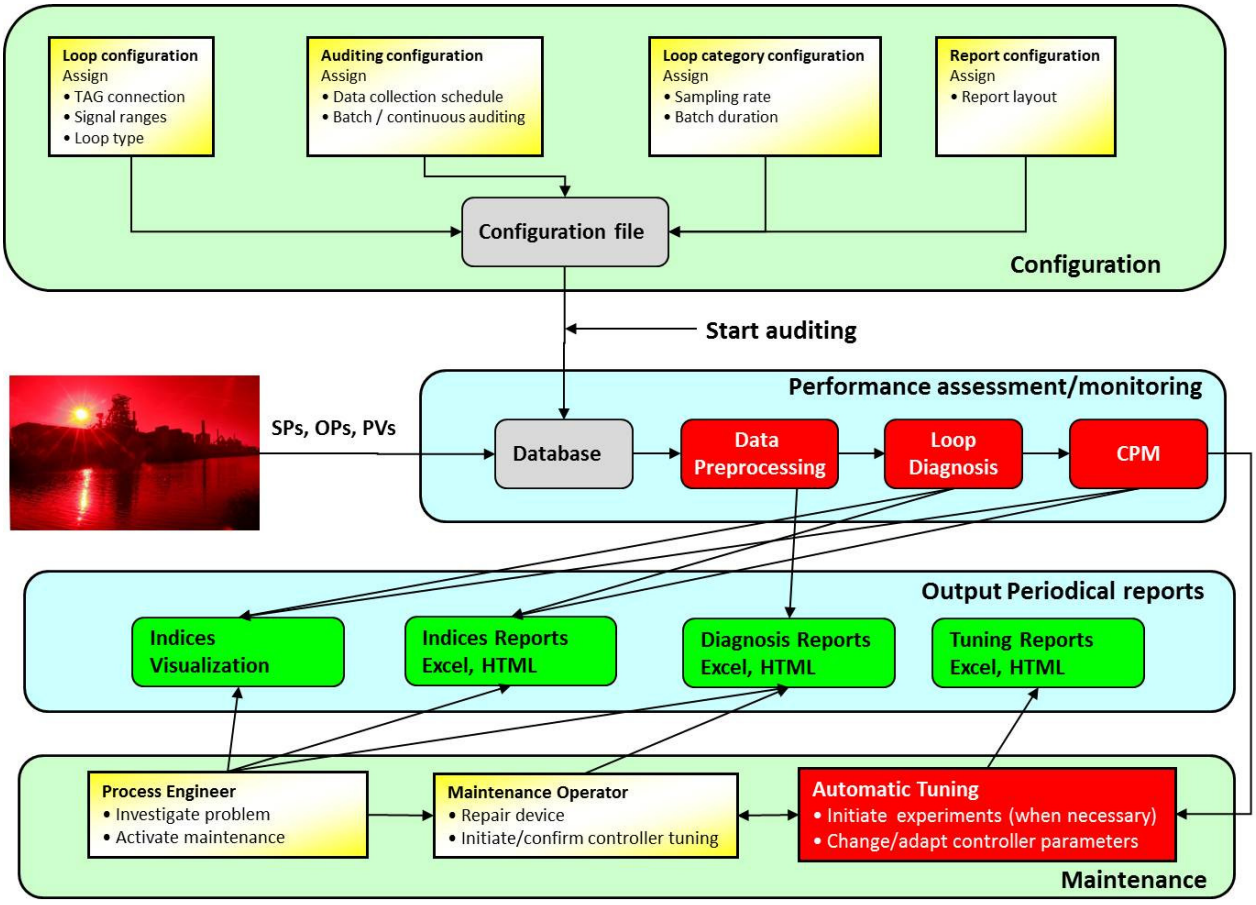

Figure 3.70: Structure of the performance monitoring, diagnosis and reporting system

The plant engineers also had to configure auditing: tags connections, signals ranges, loop types, to schedule the data collection, to set the report layout. After configuration, it was possible to switch to auditing. From this point, the root cause reporting system was performing everything automatically in the background of the process. The system acquired for every loop: data for setpoints (SP), controller outputs (OP) and process variables (PV). Additionally, other plant and strip data was necessary and provided to the monitoring and tuning system to get specific and synchronised results.

At the end of every batch data collection system calculated performance indices from these signals and stored the indices in the database. Periodically (weekly or monthly) or on-demand, the system generated reports. There were 4 types of output: reports of indices, reports of diagnosis, visualization reports and tuning reports.

The maintenance technicians (probably not too much expert in control theory) just looked at the "‘Diagnoses Reports"’, where they found the bad performing loops and easy suggestions on where the problem is located. The process engineers (having more knowledge in control theory) also looked at the "‘Indices Reports", where the exact picture of the process status can be depicted. They have been able to plot the indices trend to see the loop’s recent history, and naturally they also looked at the maintenance reports used by their maintenance operators.

In figure 3.100 an application of the structure for annealing furnaces is illustrated. In this specific case, the performance of the furnace room temperature control at different zones was analysed, and

assessment results based on the Harris index and modified variants of it are given. figure 3.101 indicates some more detailed results: the disturbance impulse response and the prediction horizon plot, which give indications on how fast disturbances are compensated and on the time delay value (i.e. prediction horizon) that should be selected for computing the extended Harris index; see the lower part of Figure 3.101.

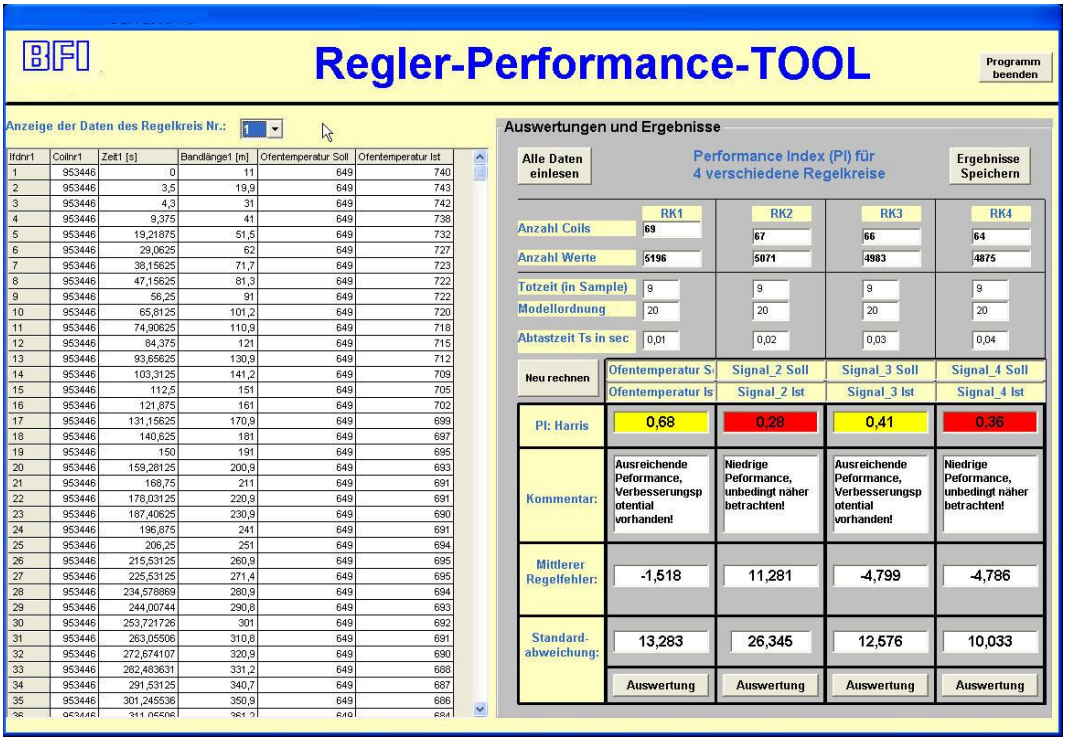

Figure 3.71: Layout of the control performance tool

Figure 3.72: Results of the performance tool

3.3 WP 3: Development of methods for automatic tuning by generating optimal setup parameters and controller settings

The main objectives of this WP were:

- The controller auto-tuning technology used in steel processing was reviewed.
- New methods for automatic generation of optimal setup parameters and optimal controller settings were developed.
- Simulation software for pre-assessment of re-tuning were developed.
- Methods were compared and it was decided on the best ones for controller re-tuning.
- Supervision mechanism for the proper interaction of the assessment, diagnosis and components were developed.

3.3.1 Task 3.1: Development of strategies and methods for re-tuning controllers [ALL PARTNER]

Methods and strategies and software for automatic re-tuning of the control loops (being deliverable D3.1) were developed for:

- Multivariate analysis of furnace control systems (MEFOS)
- Optimization-based controller retuning (ICC)
- Iterative controller retuing based on CPM (BFI/TKN/AMEH)
- Controller retuing based on routine and set-poit response data (BFI/TKN/AMEH)

3.3.1.1 Multivariate analysis of furnace control system

The continuous annealing furnace investigated by Swerea MEFOS reheats steel strips of various steel grades, thicknesses and surface finish. Thicker strips require more time in the furnace, and the optimal reheating parameters are calculated by temperature prediction software that takes data from furnace instrumentation and operator input for factors including the furnace wall temperatures, the strip thickness and emissivity, fuel flow rates, etc. The model includes the furnace geometry which is a fixed parameter. The dominant type of heat transfer at these high temperatures is radiative, so the reheating is particularly sensitive to the surface emissivities. One potential source of sub-optimal control loop performance is the interaction between the radiative heat transfer model in the strip temperature predictor and the strip emissivity data. The strip emissivity should normally increase with increased temperature, since an oxidized steel surface has a higher emissivity than a blank steel surface. There are also strips with oxidized surfaces where the change in emissivity of the surface through the furnace is not well known.

A multivariate analysis was made of selected factors from the furnace control system data for most of one day using SIMCA P+ investigating the effect of selected factors including the zone temperatures, strip thickness and strip emissivity. The model had 10954 data points with an $R^2 and Q^2$ of 0.93 with a plot of the predicted temperatures given in figure 3.73. The predicted temperatures were closer to the measured one at higher than at lower temperatures, which can be due to factors such as the passage of the splicing strips, and changing the furnace temperatures for reheating various types of steel strips.

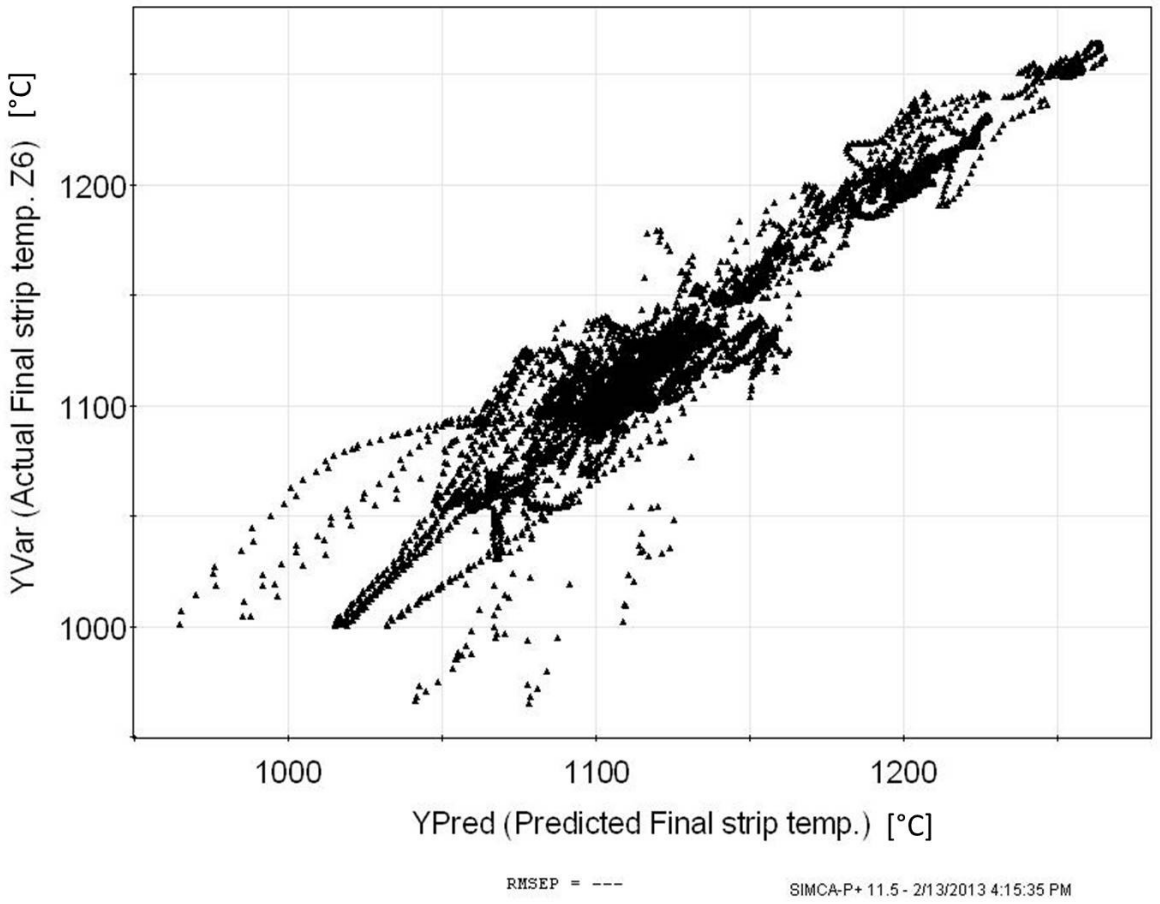

Figure 3.73: Data showing the scatter in the temperature predictions

Figures 3.74 and 3.76 below show the model coefficients and the variable importance. The small error bars on the factors indicate the small error in the model when using a confidence level of 95%. A higher final zone temperature (Z5 and Z6) and a higher oil flow rate gave a strong positive correlation with the final measured strip temperature as expected. A thicker strip and a splicing strip gave a negative correlation which can also be expected, since there is normally a strong drop in strip temperature during the passage of a splicing strip. The negative correlation for the strip emissivity and the final strip temperature could indicate sub-optimal performance for the radiation heat transfer model in the furnace control system, since oxidation of the strip normally increases the strip emissivity.

A plot of predicted strip temperatures and the actual strip temperatures are given as a function of time in Figure 3.77. The model was able to follow slow and broad temperature swings better than fast and sharp temperature swings characteristic of the passage of splicing strips. Sometimes the model had a period when it predicted temperature cycles well, but for other periods the temperatures can be too low or too high. This could indicate that other factors should be included in the model or that there are strips for which the emissivity data and radiation model could be improved.

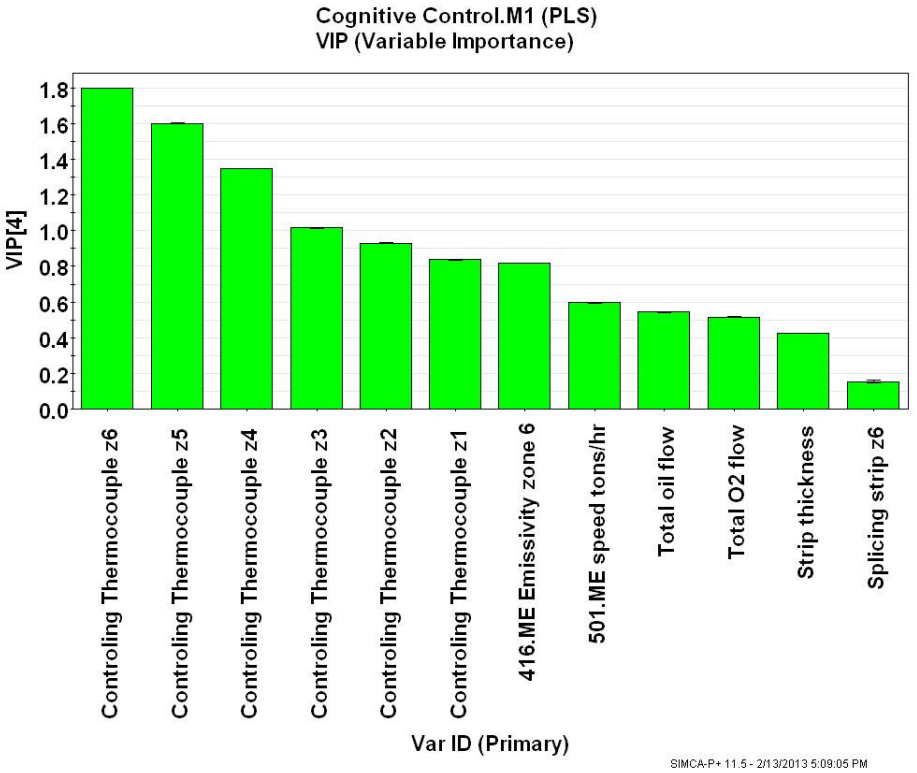

Figure 3.74: Plot of variable importance for the final strip temperature prediction model

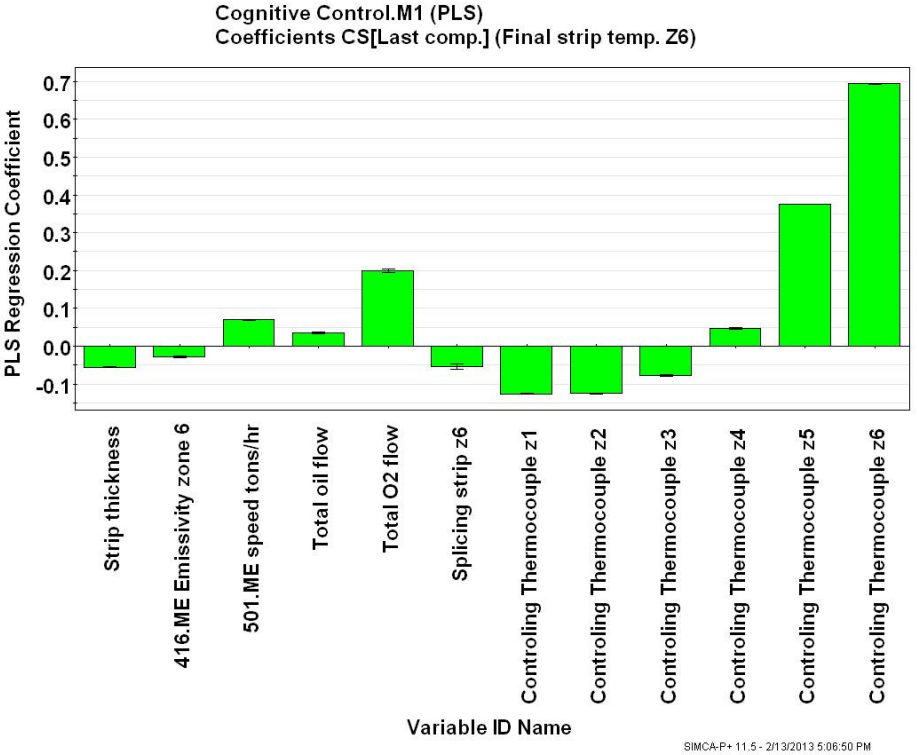

Figure 3.75: Plot of model coefficients for the final strip temperature prediction model

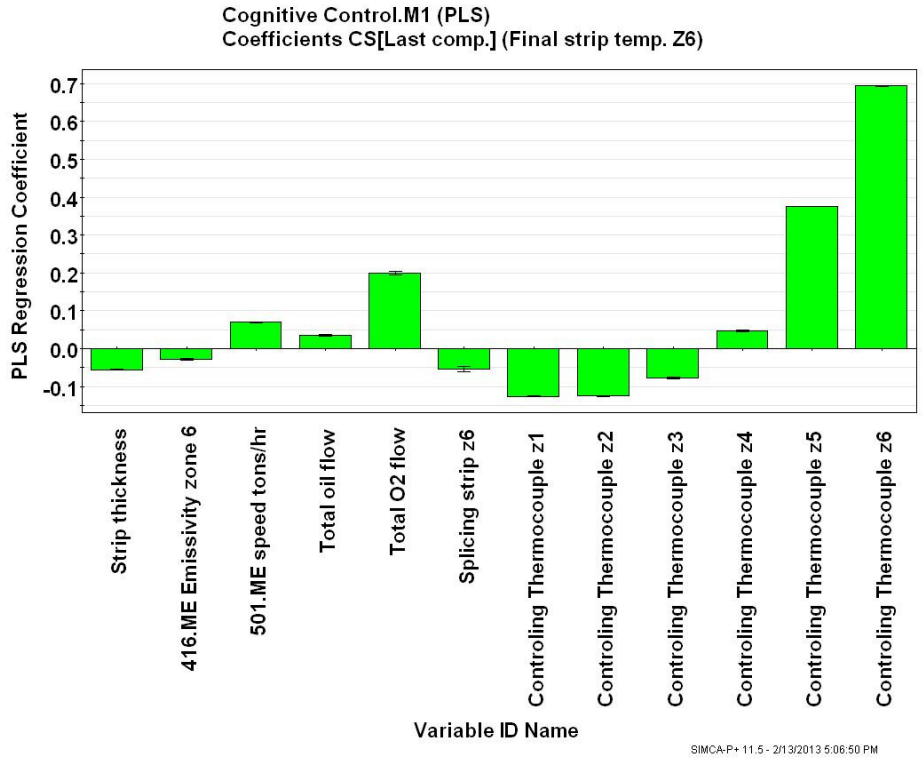

Figure 3.76: Plot of model coefficients for the final strip temperature prediction model

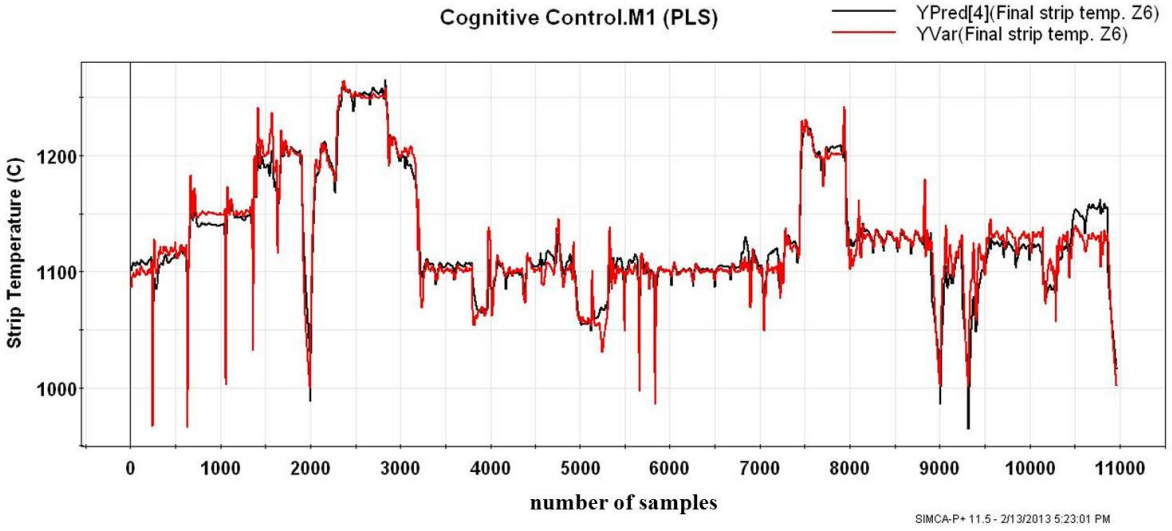

Figure 3.77: Time series of the predicted temperatures

3.3.1.2 Optimisation-based controller retuning

The University of Strathclyde focused on the development of the following three methodologies: Supervisory MPC gain compensation, "One shot" gain compensation based on covariance control, and iterative gain compensation. The methodologies require estimation of the process dynamic matrix and noise matrix. The estimation was carried out using a recursive closed-loop subspace identification method based on process data only. The Control Performance Assessment (CPA) index was used to trigger the re-tuning process as well as the stopping mechanism. It was expected that the re-tuning process started after improper tuning of the controller which had been identified as the main source of poor performance by a diagnosing method.

Supervisory MPC gain compensation Once the critical loop has been identified and poor tuning of the controllerhas been diagnosed, a corrective measure can be implemented. The main control level is used to handle constrains that basic controllers cannot handle. In some cases disturbances are also difficult to handle in lower levels and require the formulation of local setpoint optimization [Tat10]. For setpoint optimization, the real-time optimization level can be divided into plant-wide optimization and local set-point optimisation. The latter can be combined with the main control level (usually containing an MPC) for optimization synthesis [Tat10]. The formulation of the optimisation problem is given as follows:

$$J_k = \min_{\triangle u_k, u^{ss}, y^{ss}} \left\{ \sum_{i=1}^{N} \|y^{ss} - y_{k+i|k}\|^2 + \lambda \sum_{i=0}^{N_u-1} \|\triangle u_{k+i|k}\|^2 + \alpha \left(c_u^T u^{ss} - c_y^T y^{ss} \right) \right\} \tag{3.95}$$

$s.t.$

$$u_{min} \leq u_{k-1} + \textstyle\sum_{j=0}^{i} \triangle u_{k+j|k} \leq u_{max} \tag{3.96}$$

$$-\triangle u_{max} \leq \triangle u_{k+i|k} \leq \triangle u_{max} \tag{3.97}$$

$$y_{min} \leq M_i \triangle u_k + y^0_{k+i|k} \leq y_{max} \tag{3.98}$$

$$u_{min} \leq u^{ss} \leq u_{max} \tag{3.99}$$

$$y_{min} \leq y^{ss} \leq y_{max} \tag{3.100}$$

$$y^{ss} = F\left(u_{k-1}, e\right) + H_k \left(u^{ss} - u_{k-1}\right) \tag{3.101}$$

$$y_k = GK \triangle u_k + y^0_k \tag{3.102}$$

$$\triangle u_k = K \left(y^{ss} - y^0_k \right) \tag{3.103}$$

y^{ss} and u^{ss} are the steady state set-point values calculated in the real-time level, N and N_u are the prediction and control horizons, λ is a weighting factor for the controlled inputs, c_u and c_y are pricing factors related to process economic considerations, α is a setpoint weighting coefficient. Equations (3.96)-(3.100) are inputs, outputs and setpoint constraints. Equation (3.101) is a nonlinear model of the steady state output set-point given by a comprehensive steady state process model ($F\left(u_{k-1}, e\right)$) that depends on disturbances (e) and steady state set-point input and a gain matrix H_k to represent the forced trajectory or the trajectory only depending on $\triangle u^{ss}$. Equation (3.102) is the system output given by the superposition of the forced response and the free response respectively. K is a matrix of local controllers and y^0_k is the free output trajectory. The control structure is shown in figure 3.78.

For each control loop, a PID controller is given by:

$$K_{PID,ii}\left(q, \gamma\right) = \gamma^T C\left(q\right) \tag{3.104}$$

with

$$\gamma = \begin{bmatrix} k_{P,ii} & k_{I,ii} & k_{D,ii} \end{bmatrix} \tag{3.105}$$

$$C\left(z\right) = \begin{bmatrix} 1 & q^{-1} & q^{-2} \end{bmatrix} \tag{3.106}$$

$K_{PID,ii}$ is the controller of the i-th diagonal element of K. The optimization problem can be very complex. Each control loop should be optimized individually to decrease computational burden. Identification of the trouble loop is necessary before any re-tuning procedure.

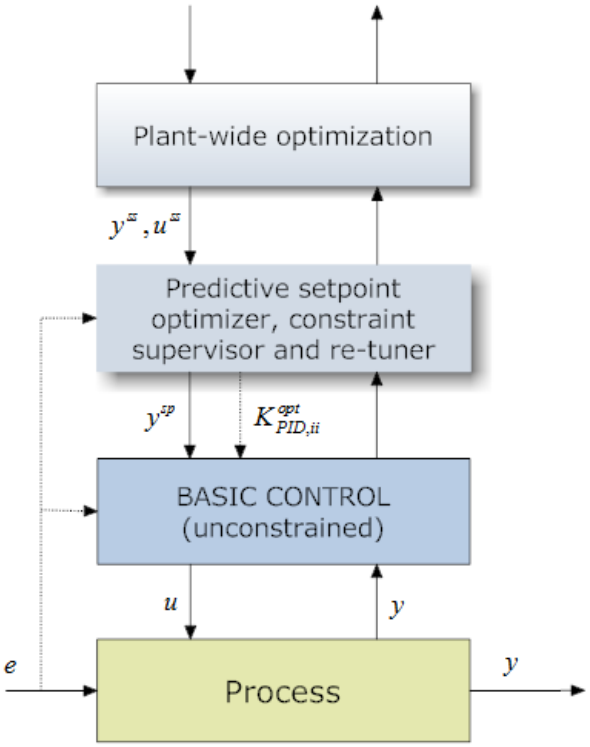

Figure 3.78: Supervisory control structure with setpoint optimization

"One shot" gain compensation based on Covariance Control One way to calculate the compensation gain results from covariance control design. Covariance control solves the following control problem: suppose that a state covariance satisfying a certain closed-loop performance is given, there are controllers allowing assigning that desired covariance [Ske98]. Covariance control offers a "one shot" algebraic solution for control re-tuning provided that the optimal system covariance is given.

The method uses the MPC benchmark already calculated for CPA. The calculation of an optimal gain that achieves the desired covariance given by the benchmark is the solution to a linear algebra problem. For a system in state space form as follows:

$$x^p_{k+1} = A_p x^p_k + B_p u_k + K_k e_k \tag{3.107}$$
$$y_k = C_p x^p_k + D_p u_k + e_k \tag{3.108}$$
$$E\{e_k\} = 0 \tag{3.109}$$
$$E\left\{x^p_k e^T_l\right\} = 0 \tag{3.110}$$
$$E\left\{e_k e^T_l\right\} = E\delta_{kl};\ k > l;\ E > 0 \tag{3.111}$$

where $x^p_k \in \Re^{n_p}$, $u_k \in \Re^{n_u}$, $y_k \in \Re^{n_y}$ and e_k are the plant states, input signals, output signals and innovation sequence respectively. A, B, C and D are matrices of compatible dimensions where (A,K) and (A,B) are controllable and stabilizable since a controller has been previously implemented. K is the Kalman gain. The state space model of the controller (possibly PID control) is given by:

$$x^c_{k+1} = A_c x^c_k + B_c y_k \tag{3.112}$$
$$u_k = C_c x^c_k + D_c y_k \tag{3.113}$$

with $x^c_k \in \Re^{n_c}$ controller states. Combining equations (3.107) and (3.112) in matrix form:

$$x_{k+1} = (A + BGC)\, x_k + (D + BGK)\, e_k \tag{3.114}$$

$$x_k = \begin{bmatrix} x^p_k \\ x^c_k \end{bmatrix};\ A = \begin{bmatrix} A_p & 0 \\ 0 & 0 \end{bmatrix};\ B = \begin{bmatrix} B_p & 0 \\ 0 & I \end{bmatrix};\ C = \begin{bmatrix} C_p & 0 \\ 0 & I \end{bmatrix} \tag{3.115}$$

$$D = \begin{bmatrix} D_p \\ 0 \end{bmatrix};\ K = \begin{bmatrix} K_k \\ 0 \end{bmatrix};\ G = \begin{bmatrix} D_c & C_c \\ B_c & A_c \end{bmatrix} \tag{3.116}$$

Defining the state covariance $X := E\left\{x_k x_l^T\right\}$ and assuming that the disturbance variance remains constant, then:

$$X_{k+1} = (A+BGC)X_k(A+BGC)^T + (D+BGK)E_0(D+BGK)^T + X_0 \tag{3.117}$$

By assuming that $E_0 = I$ and $X_0 = 0$, the steady-state value of X becomes:

$$X := \lim_{\substack{k\longrightarrow\infty \\ l\longrightarrow 0}} E\left\{x_k x_l^T\right\} \tag{3.118}$$

$$X = (A+BGC)X(A+BGC)^T + (D+BGK)(D+BGK)^T \tag{3.119}$$

Completing the squares on equation (3.119):

$$\left(BG+AXC^TR^{-1}\right)R\left(BG+AXC^TR^{-1}\right)^T = Q \tag{3.120}$$

with:

$$Q = X - AXA^T - DD^T + AXC^TR^{-1}CXA^T \tag{3.121}$$

$$R = CXC^T + KK^T;\ DK^T = 0 \tag{3.122}$$

There exists a controller G which assigns X as an optimal covariance state that satisfies the following conditions:

i)

$$Q > 0 \tag{3.123}$$

ii)

$$\left(I-B^{\dagger}B\right)\left(Q - AXM^TR^{-1}MXA^T\right)\left(I-B^{\dagger}B\right) = 0 \tag{3.124}$$

iii)

$$\left(I-B^{\dagger}B\right) = 0 \tag{3.125}$$

In order to calculate G lets assume the existence of a matrix $L \in \Re^{(n_p+n_c)\times n_u}$ such that $Q = LL^*$, then:

$$\left(BG+AXC^TR^{-1}\right)R^{1/2} = LU \tag{3.126}$$

with $UU^* = I$. The controller G is given by:

$$G = B^{\dagger}\left(LUR^{-1/2} - AXC^TR^{-1}\right) + \left(I-B^{\dagger}B\right)Z_f \tag{3.127}$$

where Z_f is arbitrary and:

$$U := V_L\begin{bmatrix} I & 0 \\ 0 & U_f \end{bmatrix}V_R^T \tag{3.128}$$

$$\left(I-B^{\dagger}B\right)L = U_L\begin{bmatrix} \sigma_L & 0 \\ 0 & 0 \end{bmatrix}V_L^T \tag{3.129}$$

$$\left(I-B^{\dagger}B\right)AXC^TR^{-1/2} = U_L\begin{bmatrix} \sigma_L & 0 \\ 0 & 0 \end{bmatrix}V_R^T \tag{3.130}$$

SVD stands for Singular Value Decomposition. In order to provide further minimization of the control effort, U_f has to be chosen such as:

$$U_f := U_1U_2^T \tag{3.131}$$

$$\phi_2 R\theta_2^T = U_1\Lambda U_2^T \tag{3.132}$$

$$\begin{bmatrix} \theta_1 & \theta_2 \end{bmatrix} := I_1B^{\dagger}LV_L \tag{3.133}$$

$$\begin{bmatrix} \phi_1 & \phi_2 \end{bmatrix} := I_1B^{\dagger}AXM^TV_R \tag{3.134}$$

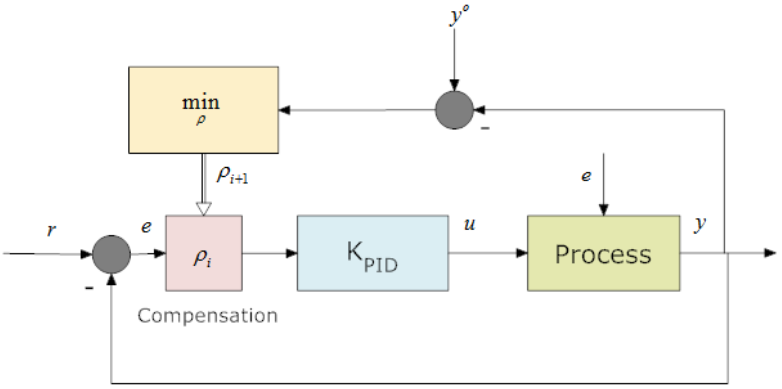

Figure 3.79: Modified Iterative Feedback re-tuning scheme

and $I_1 = \begin{bmatrix} I & 0 \end{bmatrix}$. When the actual controller is known, G can be split into the new compensation gain G_n and the actual controller gain G_a such that $G = G_n G_a$ and the compensation gain will be given by:

$$G_n = B^{\dagger}\left(LUR^{-1/2} - AXC^T R^{-1}\right) G_a^{\dagger} + \left(I - B^{\dagger}B\right) Z_f \tag{3.135}$$

provided condition ii) holds. The procedure to calculate G is condensed in the following steps:

1: Retrieve X from MPC benchmark

2: Calculate R and Q

- Factorize $Q = LL^*$

3: Use SVD to retrieve V_R and V_L from equations (3.130) and (3.129)

4: Calculate equations (3.134) and (3.133)

5: Use SVD to retrieve U_1 and U_2 from equation (3.132)

5: Calculate U_f, U and G using equations (3.131), (3.128) and (3.135)

Iterative Gain Compensation An optimal iterative approach can be formulated as an iterative feedback tuning approach. The method tracks the error between the original output and the output given by a performance metric benchmark (i.e. the output given by an MPC benchmark). The method scheme can be seen in figure (3.79):

And the problem formulation is described as follows:
Find an optimal gain compensation from the minimization of a criterion function with respect to the controller parameters given by:

$$\rho^* = \min_{\rho} J(\rho) \tag{3.136}$$
$$s.t.$$
$$J(\rho) = \frac{1}{2N} E\left\{\sum_{i=1}^{N} e_{y_i(\rho)}^2\right\} \tag{3.137}$$

From figure 3.79, $y(\rho)$ is given by:

$$y(\rho) = \frac{\rho K_{PID} G_0}{I + \rho K_{PID} G_0} r_t + \frac{I}{I + \rho K_{PID} G_0} e_t \tag{3.138}$$
$$= T_0(\rho) r_t + S_0(\rho) e_t \tag{3.139}$$

The criterion function is therefore:

$$J(\rho) = \frac{1}{2N}\left\{\sum_{i=1}^{N} \left(y_i^o - T_0(\rho) r_i\right)^2\right\} \tag{3.140}$$

Its minimization is given as follows:

$$0 = \frac{\partial J(\rho)}{\partial \rho} = \frac{1}{N}\left\{\sum_{i=1}^{N} e_{y_i(\rho)} \frac{\partial y(\rho)}{\partial \rho}\right\} \tag{3.141}$$

and

$$\frac{\partial y(\rho)}{\partial \rho} = \frac{1}{\rho}\left[T_0(\rho) r_t - T_0(\rho)^2 r_t - T_0(\rho) S_0(\rho) e_t\right] \tag{3.142}$$

Using equation (3.139) into (3.142), $\frac{\partial y(\rho)}{\partial \rho}$ will be:

$$\frac{\partial y(\rho)}{\partial \rho} = \frac{T_0(\rho)}{\rho}(r_t - y_t) \tag{3.143}$$

The gradient from equation (3.143) requires the input of $(r_t - y_t)$ in the process. Once the gradient is computed the following algorithm is obtained [Hja98]:

$$\rho_{i+1} = \rho_i - \mu_i R^{-1} \frac{\partial J(\rho)}{\partial \rho} \tag{3.144}$$

where R can be chosen as the identity matrix and μ as a harmonic series [Eck10]:

$$\mu_i = \frac{\mu_1}{i};\ i > 1 \tag{3.145}$$

The signal $(r_t - y_t)$ is used until $\rho_{i+1} = \rho_i$. Iterative methodologies are invasive and can take a long time to find the right controller parameter values.

3.3.1.3 Iterative controller retuning based on CPM

The main innovation of the controller retuning methods developed here by BFI was that controller tuning is treated in the context of control performance monitoring (CPM). This implies control performance measures are *continuously monitored* on a regular basis, i.e. during normal operation, and performance statistics used to schedule loop re-tuning and automatically determine the optimal controller parameters; see figure 3.80. For CPM, the methods developed in the task will be used. The main goal is to find controller settings that maximise the control performance index, for instance the Harris index or other quantities characterising the best achievable controller performance.

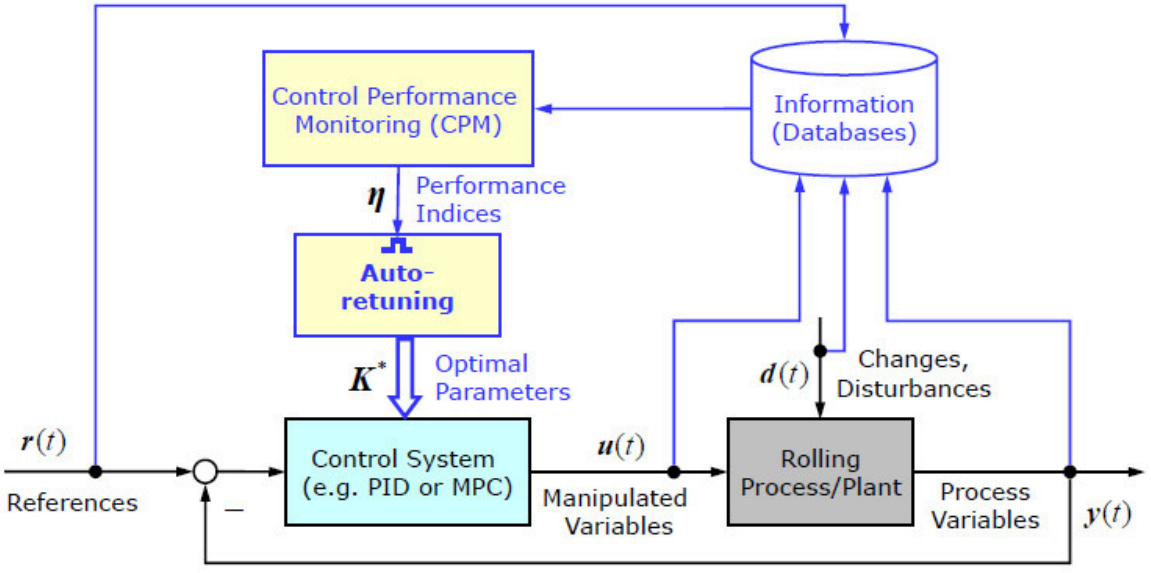

Figure 3.80: Basic principle of CPM-based controller re-tuning

Although the decision for re-tuning will be automatically taken, based on the performance indices determined in the controller assessment stage and logic included, it is recommended for safety reasons

that the user should always confirm the need for the re-tuning action and inspect the new controller parameters proposed by the retuning module. Also it is very important to track the changes in the control system parameters. For this purpose, decision-making procedures will be subject of task 4.3.

A new generation of techniques for controller tuning that has been (theoretically) introduced by Jelali [Jel07] is called *iterative controller tuning*. This method is completely non-invasive and will be explored further for automatic controller retuning in rolling automation systems.

The basic principle of this CPM-based tuning is that is carried out directly on the control loop by carefully and systematically changing controller parameters, using *routine data only*, thereby eliminating the model-identification step altogether. The controller settings are determined from iterative tuning on the *closed loop*, following the basic procedure (figure 3.81):

1. Collection and pre-processing of normal operating data;
2. Computation of the actual performance indices;
3. Comparison with benchmark/desired values;
4. Decision whether the performance is optimal/sufficient; if so, then break the procedure; or else, change the controller parameters, apply them on the process, then go to step 1 and repeat the procedure.

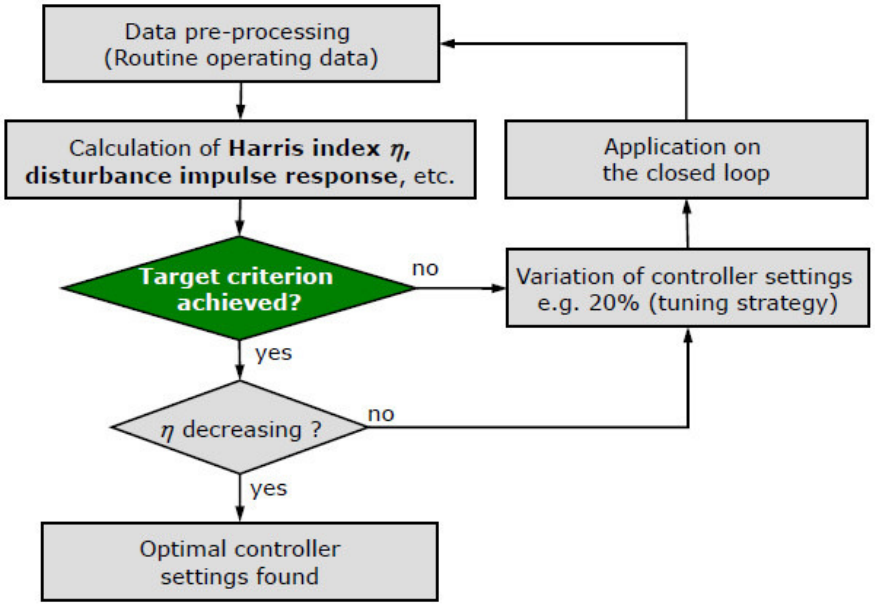

Figure 3.81: Basic procedure of iterative controller tuning

The objective is to iteratively improve the present controller settings until, e.g., the best PID-achievable performance is attained. To control the progress of the iteration, the Harris index, for instance, can be used as a measure of control loop performance improvement and the closed-loop disturbance impulse response (IR) curve as a diagnostic tool. The IR trace is generated as a by-product of the Harris-index computation. Appropriate characteristics of the IR, such as the offset, undershoot and number of oscillations, are used to control the progress of the iteration towards finding the optimal controller parameters.

In rolling automation, Step 4 of the procedure can be done, e.g., from pass to pass, coil to coil, or as long-term controller adaptation. Thereby, it is important to classify and schedule the controller parameters depending on strip/plant properties. In practice, control performance drifts will be clearly observed/detected after significant changes in entry strip properties, disturbance spectrum, set poins, or plant components.

Impulse response (IR) features. To use the right features for controlling the progress of the retuning procedure is very decisive to avoid taking a long time to arrive at PI-achievable performance. For this purpose, the following measures are introduced:

- The retuning procedure is simplified by only considering the three main categories of the IR plot for sluggish, optimally tuned and aggressive controllers, as shown in Figure 3.82.
- Suitable measures (*offset*, *undershoot* and *number of oscillations*) are used to characterize the IR response and thus avoid the visual inspection to classify the controller behaviour.
- Pattern recognition/matching techniques, such as self-organising maps, are investigated for the automatic classification of the controller behaviour.

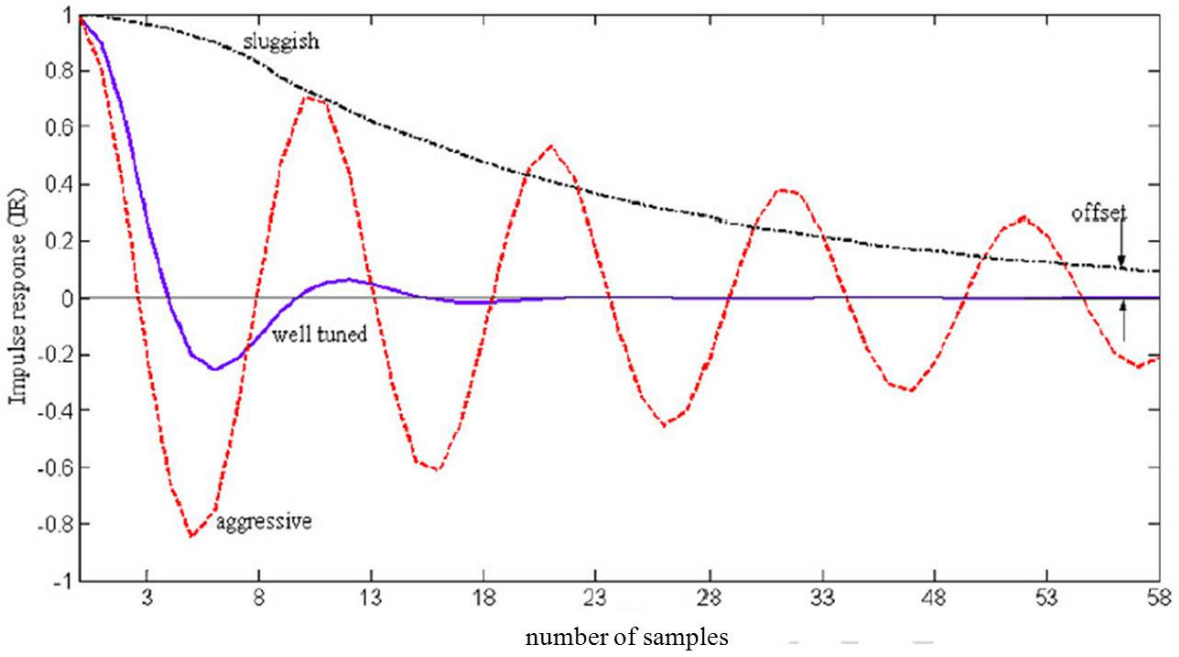

Figure 3.82: Impulse-response plots for sluggish, optimally tuned and aggressive controllers

The IR plot is compared with the three (or more) signature patterns in figure 3.82. The IR plot computed from routine data will fit in with one of the following basic possibilities;

- **Case A.** If the plot is similar to the pattern of detuned controller, then the existing controller is under-tuned and needs to be made aggressive to attain PI achievable performance;
- **Case B.** If the plot resembles the pattern of an optimally tuned controller , then the existing controller may be performing near the PI achievable performance. The Harris index will be very close to 1, and one may not wish to tune the controller any further. To confirm this, one should make the controller aggressive and check for the improvement in η. However, it depends on the application at hand and on the desired performance, i.e., which IR pattern is specified as optimal.
- **Case C.** If the plot is similar to the pattern of an aggressively tuned controller, then the existing controller is aggressively tuned and needs to be detuned to attain PI achievable performance.

Characteristics are introduced for determining the signature pattern (out of the three signature patterns) that best matches the estimated IR trajectory. One option is to calculate the IR characteristics *offset*, *undershoot* and *number of oscillations*, and use them for pattern matching. An other option is to apply the so-called *impulse-response area index* (*IRAI*), defined as [Jel13]

$$I_{\text{ai}} := \begin{cases} 1 & \text{for } n < 3 \\ \frac{\max(A_1,\ldots,A_{n-2})}{\sum_{i=1}^{n-1} A_i} & \text{elsewhere} \end{cases} \tag{3.146}$$

A_i stands for the area over or under the zero line of the IR curve (see Figure 3.83):

$$A_i = \int_{t_i}^{t_{i+1}} |g(t)|\,\mathrm{d}t\,, \qquad i = 0,1,\ldots,n-1. \tag{3.147}$$

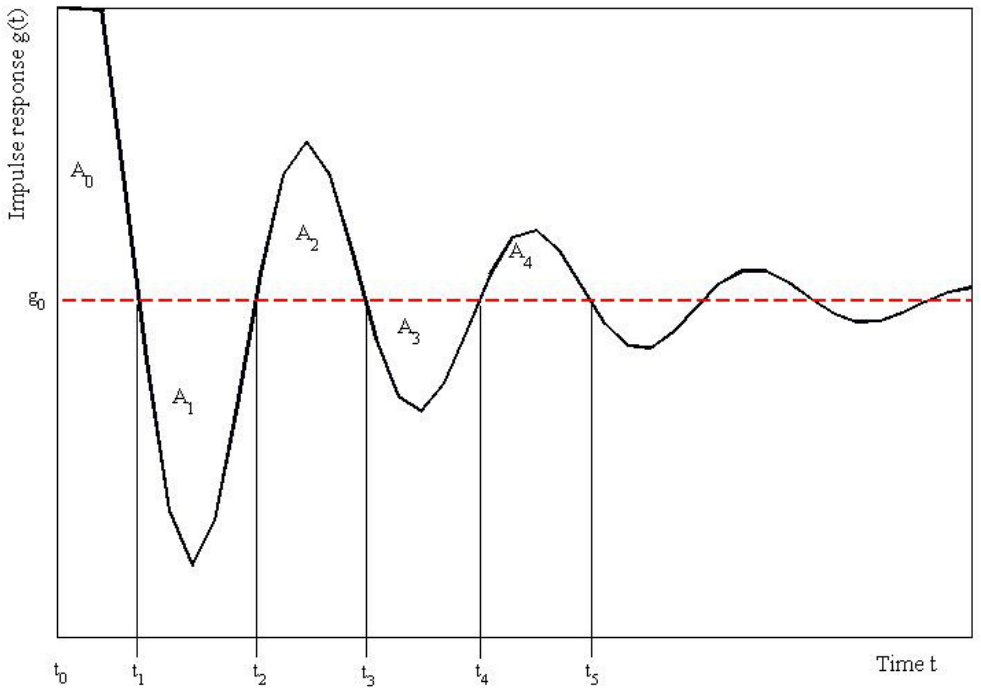

Figure 3.83: Significant parameters for determining the impulse-response area index

Typical controller retuning procedures. The procedure in Figure 3.84 starts by using a routine operating data set to determine the IR, the Harris index (η) and the impulse-response area index (I_{ai}). If the I_{ai} value lies in the target region, the controller parameters are slightly changed. It is then checked whether η is decreasing: if yes, the tuning is terminated, and the optimal controller settings are found. In the cases where the target region is not attained or the Harris index is not decreasing, the controller parameters are changed according to the selected variation strategy, the current controller settings (ensuring a stable closed loop) are applied on the process, and a new operating data set is recorded. The same aforementioned steps are repeated. The controller settings are systematically changed and applied to the closed loop until the IR area index I_{ai} is within the range [0.3, 0.7] *and* the Harris index value η attains a satisfactory value, which should be close to the optimal (PID-achievable) performance.

Instead of using the I_{AI} as an indicator of optimal performance, different alternative criteria or techniques can be used. For instance, pattern-recognition methods allow to detect the corresponding performance behaviour and deliver an indication in which direction the controller parameters should be changed.

The retuning procedure in conjunction with pattern recognition starts by using a routine operating data set to determine the IR and the Harris index (η). Pattern recognition is run to detect the template IR shape giving the minimal dissimilarity measure to the test IR shape. If the IR shape for well-tuned control is detected, i.e. a specified minimum distance to the well-tuned pattern is achieved, the controller parameters are slightly changed. It is then checked whether η is decreasing: if yes, the tuning is terminated and the optimal controller settings are found. In the cases where the target region is not attained or the Harris index is not decreasing, the controller parameters are changed according to the selected variation strategy, the current controller settings (ensuring a stable closed loop) are applied to the process, and a new operating data set is recorded. The same aforementioned steps are repeated until a minimal distance to the IR pattern for a well-tuned controller (to be specified) is achieved.

Kohonen feature maps have been implemented here and trained using simulation data. The learning pattern have been chosen in such away that the pattern cover the whole range of impulse responses. The data have been labeled by a control expert. As an illustrative example, the IR test patterns are considered shown in figure 3.85. The results of the pattern detection procedure are illustrated in figure 3.86. It can be observed clearly that the algorithm detects the pattern template correctly (figure 3.82) for each test data set. The data set no. 2 has been classified as aggressive, the data sets 1, 3 and 4 as well tuned, and the data sets 5 and 6 as sluggish. Recall that SOMs involve minimising a (Euclidean) distance measure

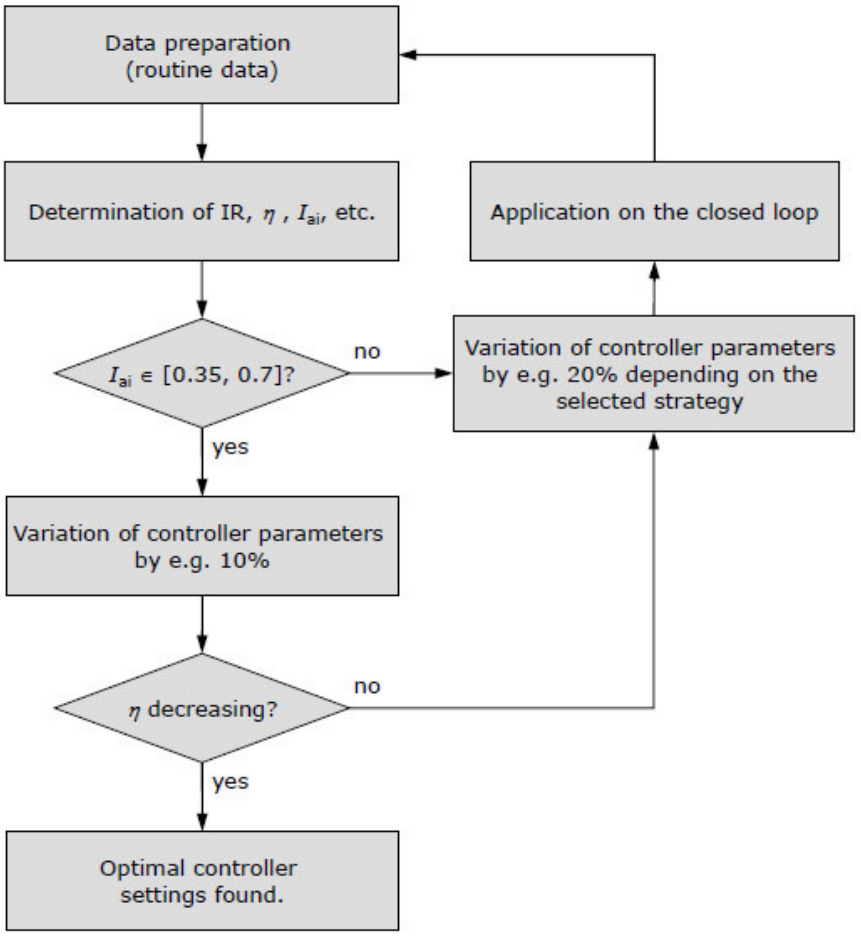

Figure 3.84: Flow chart of iterative controller assessment and tuning based on routine data and the impulse-response area index

to the prototypes.

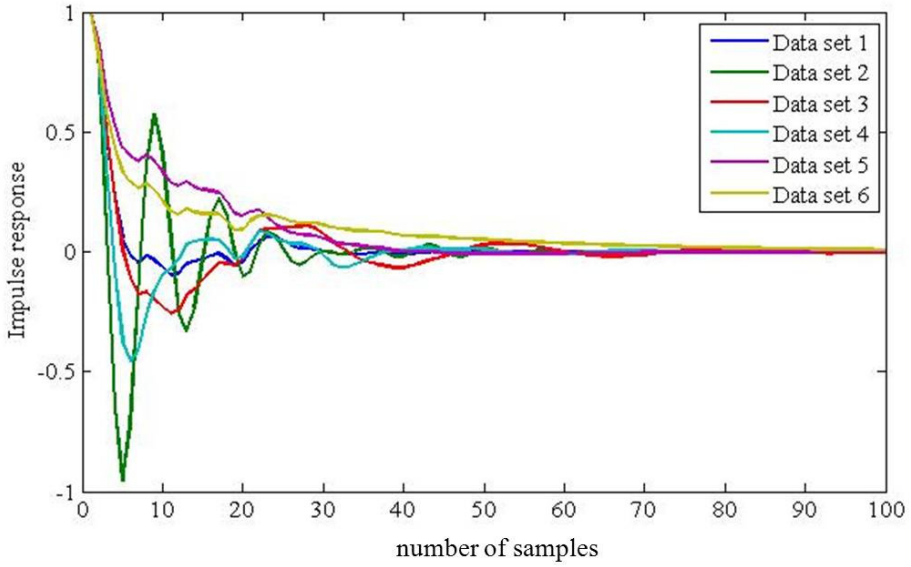

Figure 3.85: Test data sets for the Kohonen feature maps

3.3.1.4 Controller retuning based on routine and set-point response data

In many rolling processes or situations, set-point changes are naturally introduced. In such cases, the (closed-loop) data can be perfectly used to assess the control performance, identify a process model and retune the control system. The followig procedure is proposed to establish the best-achievable

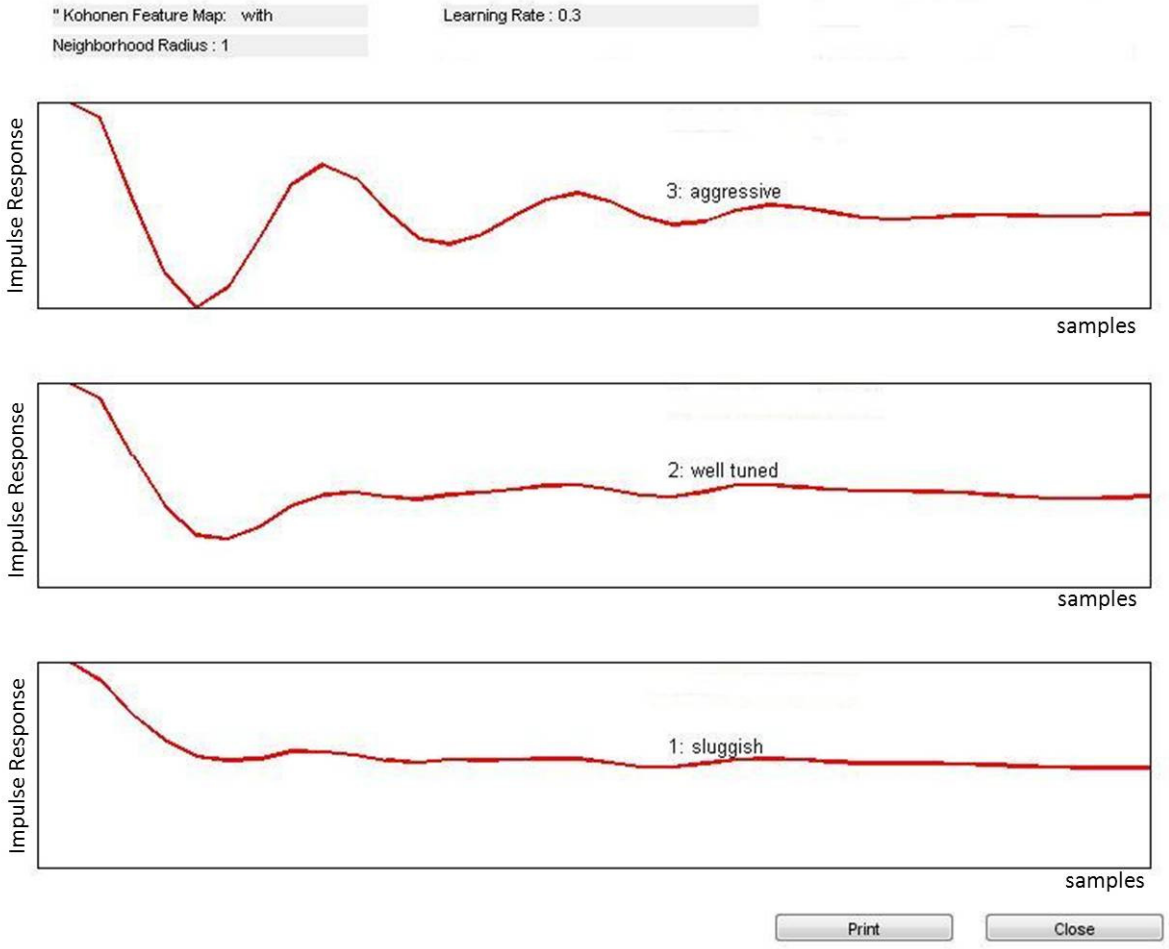

Figure 3.86: Results of pattern detection using Kohonen feature maps for the test data in Figure 3.82, Kohonen feature map was trained with Neighorhood Raidius =1 and Learning Rate =0.3

performance:

1. Assess the control performance using the method suggested by Swanda and Seborg [Swa99].
2. Obtain the process model using closed-loop data (with set-point changes).
3. Use an optimisation-based method with the identified process model to calculate the PID-achievable performance.

Controller assessment based on set-point response data. Performance indices are based on set-point data in [Swa99] to characterise the performance of PID-type feedback control loops. Index values are determined to indicate the transition point from satisfactory control to unsatisfactory control.

The rationale of Swanda and Seborg's approach is to compare the achieved performance with that of a PI controller tuned with the IMC (internal model control) rule based on a FOPTD process model:

$$G(s) = \frac{K_\mathrm{p} \mathrm{e}^{-T_\mathrm{a} s}}{Ts+1}, \tag{3.148}$$

where K_p is the static process gain, T_a the apparent time delay, and T is the (apparent) time constant or lag. The term "apparent" is used to emphasise that the parameters are approximate. T_a is a simple mean to characterise the net time delay, right-half-plane zeros and system order. In this context, two important performance indications, namely, the normalised versions of the settling time T_set (figure 3.87) and the IAE (integral of absolute error) are considered:

$$T^*_\mathrm{set} = \frac{T_\mathrm{set}}{T_\mathrm{a}}, \tag{3.149}$$

$$IAE_{\mathrm{d}} = \frac{IAE}{|\Delta r| T_{\mathrm{a}}}, \tag{3.150}$$

where Δr is the size of the set-point step-change. Both criteria are related to each other by [Swa99]:

$$IAE_{\mathrm{d}} \approx \frac{T^*_{\mathrm{set}}}{2.30} + 0.565 \qquad \text{for} \quad T^*_{\mathrm{set}} \geq 3.30. \tag{3.151}$$

Under this condition (Equation 3.151), the corresponding gain margin A_{m} and phase margin φ_{m} can also be expressed as functions of T^*_{set} by

$$A_{\mathrm{m}} = \frac{\pi}{2} IAE_{\mathrm{d}} = \frac{\pi}{2} \left(\frac{T^*_{\mathrm{set}}}{2.30} + 0.565 \right), \tag{3.152}$$

$$\varphi_{\mathrm{m}} = \frac{\pi}{2} - \frac{1}{IAE_{\mathrm{d}}} = \frac{\pi}{2} - \frac{1}{\frac{T^*_{\mathrm{set}}}{2.30} + 0.565}. \tag{3.153}$$

These relationships have been derived by fitting the parameters to the analytical solutions for different models controlled by an IMC-PI controller and for a settling time defined at $y = 0.9\Delta r$. Swanda and Seborg [Swa99] claimed, they are accurate enough and applicable to other process models. Given T^*_{set}, eqations 3.152 and 3.153 can be used to throw light on the performance and robustness of the control system. These equations clearly indicate that if T^*_{set} is large, then gain and phase margins are large, leading to better robustness at the cost of poorer performance.

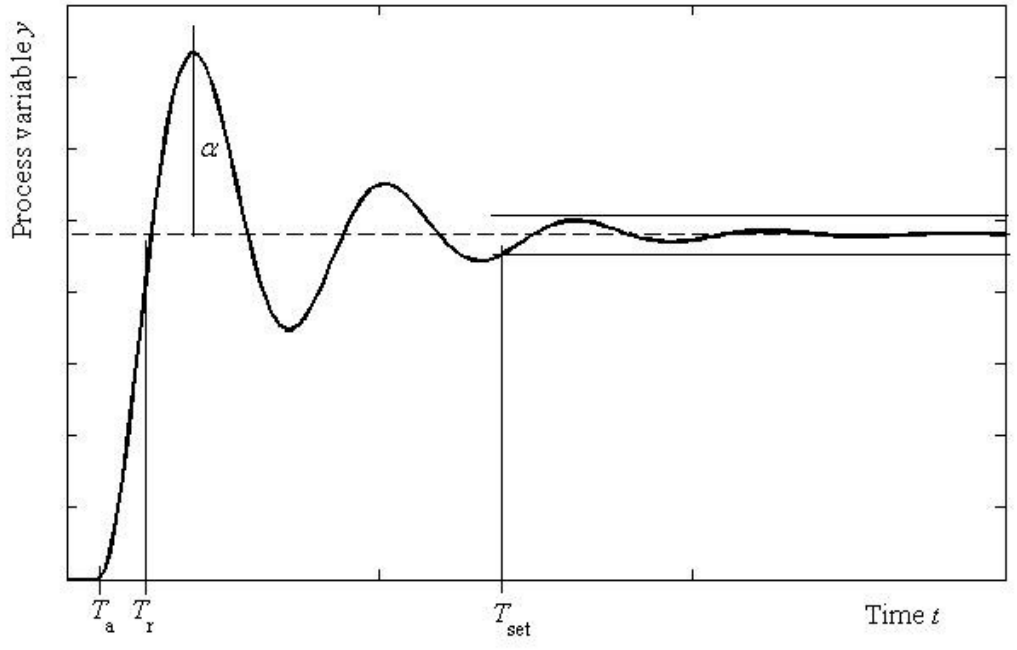

Figure 3.87: Set-point response features

To quantify how far a PI controller is of best achievable performance and to identify poorly performing control loops, different performance classes are defined, as given in Table 3.9. For a particular class, both conditions in Table 3.9 should be met. However, this definition can be relaxed to a single bound depending on the particular performance requirements.

The assessment procedure can be summarised as follows:

1. Obtain a closed-loop data set with set-point change (step-wise).
2. Identify the values of apparent time delay T_{a}, settling time T_{set} and overshoot α from collected process output data.

3. Calculate the normalised settling time T^*_{set} value.

4. Use Table 3.9 to assess the control performance.

5. Calculate the corresponding values of gain margin A_{m} and phase margin φ_{m} (Eqs. 3.152 and 3.153, respectively) and assess the performance-robustness trade-off.

Table 3.9: Swanda and Seborg's performance classes for PI control

Class	Dimensionless settling time T^*_{set}	Overshoot α [%]
High performance	$T^*_{\text{set}} \leq 4.6$	–
Fair/Acceptable performance	$4.6 < T^*_{\text{set}} \leq 13.3$	–
Excessively sluggish	$T^*_{\text{set}} > 13.3$	≤ 10
Aggressive/Oscillatory	$T^*_{\text{set}} > 13.3$	> 10

Optimisation based on set-point responses. For this purpose, system identification can be employed to determine the closed-loop servo transfer function, which takes the form of an ARMAX model. The well-known closed-loop relationship (see figure 3.88)

$$y(k) = \frac{G_{\text{c}}G_{\text{p}}}{1+G_{\text{c}}G_{\text{p}}}r(k) + \frac{G_\varepsilon}{1+G_{\text{c}}G_{\text{p}}}\varepsilon(k) \;=: G_r r(k) + H_\varepsilon \varepsilon(k). \tag{3.154}$$

gives

$$G_{\text{p}} = \frac{G_r}{(1-G_r)G_{\text{c}}} \qquad G_\varepsilon = \frac{H_\varepsilon}{(1-G_r)}. \tag{3.155}$$

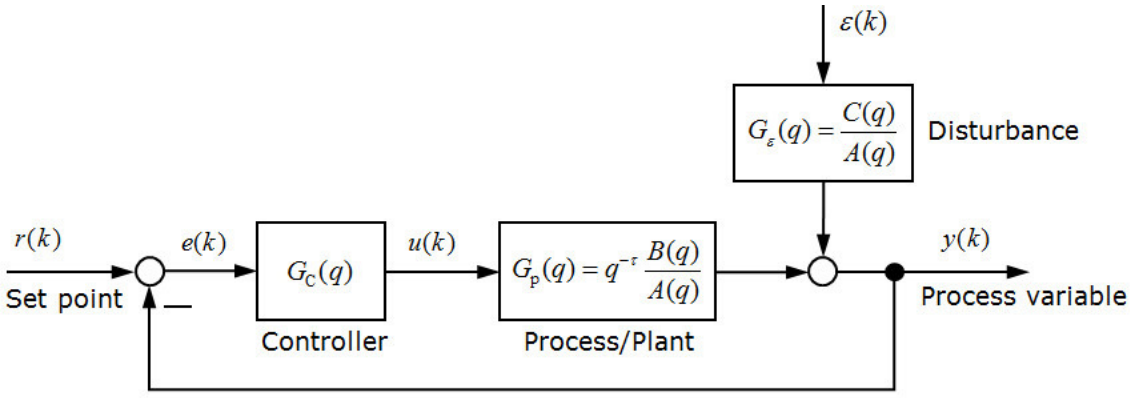

Figure 3.88: Feedback control system structure

Assuming the time-invariant process (G_{p}) and noise dynamics (G_ε), the optimal closed-loop disturbance impulse response $\tilde{G}^*_\varepsilon$ can be given as

$$\tilde{G}^*_\varepsilon = \frac{G_\varepsilon}{1+G^*_{\text{c}}G_{\text{p}}} = \frac{H_\varepsilon}{1+G_r\left(\frac{G^*_{\text{c}}}{G_{\text{c}}}-1\right)}, \tag{3.156}$$

where G^*_{c} is the optimal controller to be determined. Equation 3.156 implies that, with the knowledge of the current closed-loop disturbance impulse response (H_ε), the closed-loop servo transfer function (G_r) and the controller G^*_{c}, it is possible to estimate the closed-loop disturbance impulse response $\tilde{G}^*_\varepsilon$ for any given controller G^*_{c}. Specifically, to determine the optimal PI controller G^*_{c} (parameters K^*_{c} and T^*_{I}), the objective function to be minimised is

$$K^*_{\text{PID}} = \min_{K_{\text{PID}}}(1-\eta)^2, \qquad \eta = \frac{\sigma^2_{\text{PID}}}{\sigma^2_y} = \frac{\sum_{i=0}^{\infty} h^2_{\tilde{G}_\varepsilon}\sigma^2_\varepsilon}{\sigma^2_y}. \tag{3.157}$$

This equivalently maximises the Harris index value η. Again, for instance, the fminsearch/fmincon function from the MATLAB Optimization Toolbox can be employed to obtain the optimal controller parameters. Recall that noise variance σ_ε^2 is estimated as the prediction error from ARMAX fitting to the data with the set-point change.

In practice, the controller (setting) is often not known. In this case, the controller model can be estimated based on measured data (i.e. control error and controller output data), e.g. using the arx function from MATLAB Identification Toolbox. The controller parameters are then calculate depending on the assumed controller type and representation.

To summarise, the optimal PID controller settings can be computed—at least theoretically—using only one set of closed-loop data with set-point change, without the need of directly estimating the open-loop process or noise models. The obtained controller parameters will, however, be applied to the process to determine the closed-loop transfer functions. Therefore, it is important to use plant data that contain typical disturbances expected to affect the process. Our experience from many simulations showed that it is sometimes necessary to repeat the estimation step once again to ensure convergence to the optimal controller settings. Note that two separate sets of routine operating data are needed to calculate values of the Harris index before and after controller re-tuning.

Controller assessment based on Relative Damping Index An approach to automate the IR analysis is to fit a second-order-plus-time-delay (SOFTD) continuous model

$$G_{IR}(s) = \frac{K_{IR}e^{-T_{d,IR}s}}{T_{0,IR}^2 s^2 + 2T_{0,IR}D_{IR}s + 1} \tag{3.158}$$

to the impulse coefficients. The model estimation can be easily carried out, e.g. using the fminsearch function of the MATLAB Optimization Toolbox. The estimated parameters, the time delay $T_{d,IR}$ the damping factor D_{IR} provide measures of the disturbance rejection performance. $T_{d,IR}$ indicates how fast the disturbance is rejected by the controller. D_{IR} is related to its aggressiveness: if D_{IR} is greater than unity, the controller behaviour is over-damped; a value smaller than unity indicates that controller behaviour is under-damped with tendency to oscillate.

To get a relative measure of performance, the (Impulse response) relative damping index (RDI) is defined as

$$RDI = \frac{D_{IR} - D_{IR,aggressive}}{D_{IR,sluggish} - D_{IR}} \tag{3.159}$$

where D_{IR} is the damping factor of the fitted model, $D_{IR,aggressive}$ the limit of aggressive controller behaviour, and $D_{IR,sluggish}$ the limit of the sluggish controller behaviour. The performance limits sould be selected according to desired performace specification, typically $D_{IR,aggressive} = 0.3$ and $D_{IR,sluggish} = 0.6$. Note that a similar performance index has been recently introduced by Howard and Cooper, [How08, How10], but in relation with the auto-correlation function. The RDI can be interpreted as follows:

- If $RDI \geq 0$ i.e. $D_{IR,aggressive} \leq D_{IR} \leq D_{IR,sluggish}$, the control performance is good.
- If $-1 \leq RDI \leq 0$, i.e. $D_{IR} < D_{IR,aggressive}$ the control behaviour is aggressive.
- If $RDI < -1$, i.e. $D_{IR} > D_{IR,sluggish}$ the control behaviour is sluggish.

Based on the RDI, a new straightforward strategy for optimal controller re-tuning is proposed, as shown in figure 3.89. The procedure starts with using a routine operating data set to determine the impulse response (IR) and the Harris index η. The IR pattern is fitted to a second order model with time delay to compute the damping factor D_{IR} and the RDI. As long as $RDI < -1$ or the Harris index is not decreasing, the controller parameters are changed according to the selected variation strategy, the current controller settings (ensuring a stable closed loop) are applied to the process, and a new operating data set is recorded. This method is intuitive and can be completely automated. Simultaneously, the user can specify the target performance region by selecting the corresponding limits $D_{IR,aggressive}$ and $D_{IR,sluggish}$. For stricter performance requirements,$D_{IR,aggressive}$ has to be increased, and $D_{IR,sluggish}$ decreased.

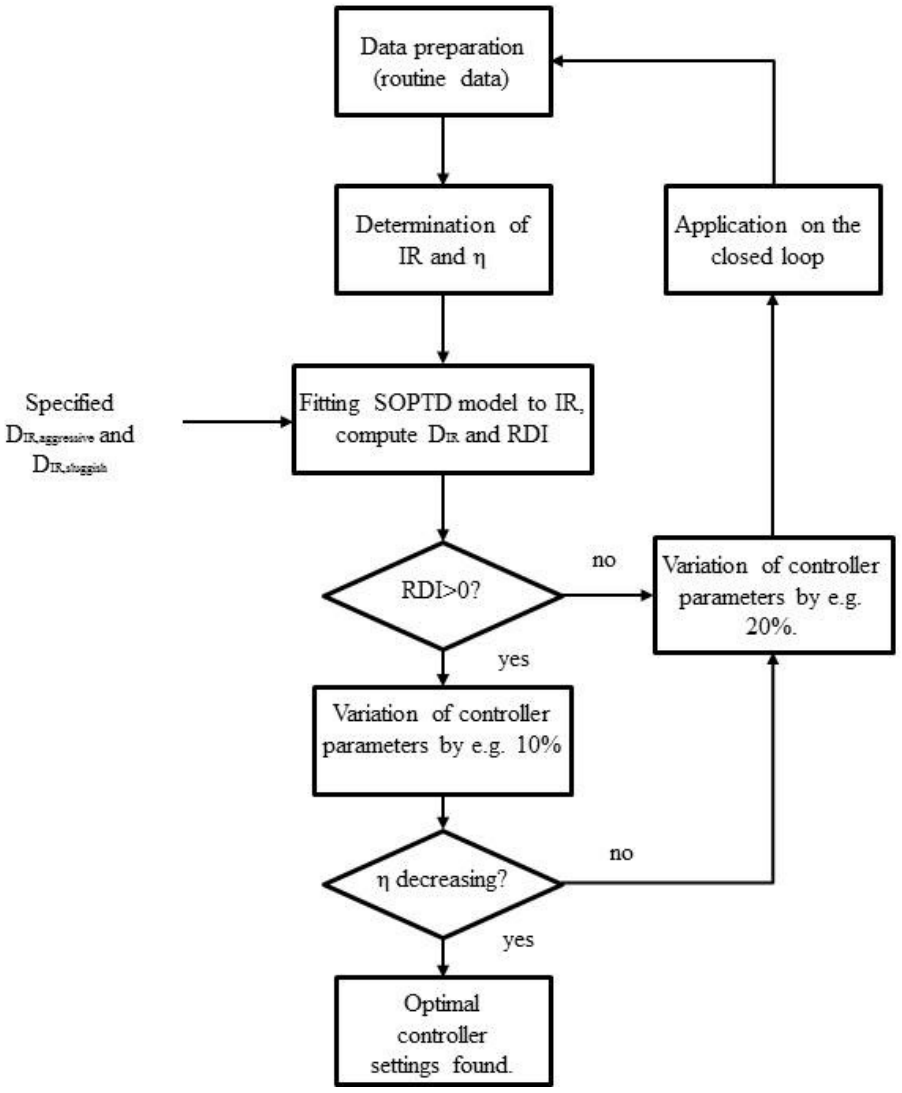

Figure 3.89: Flow chart of the iterative controller assessment and tuning based on the relative damping index

Potential application and benefits. Control systems that can be assessed and retuned by this new combined assessment and tuning method may lead to significant reduction of wasted strip length, and thus to clear commercial and environmental benefits; see figure 3.90 as illustration of the effect of this strategy.

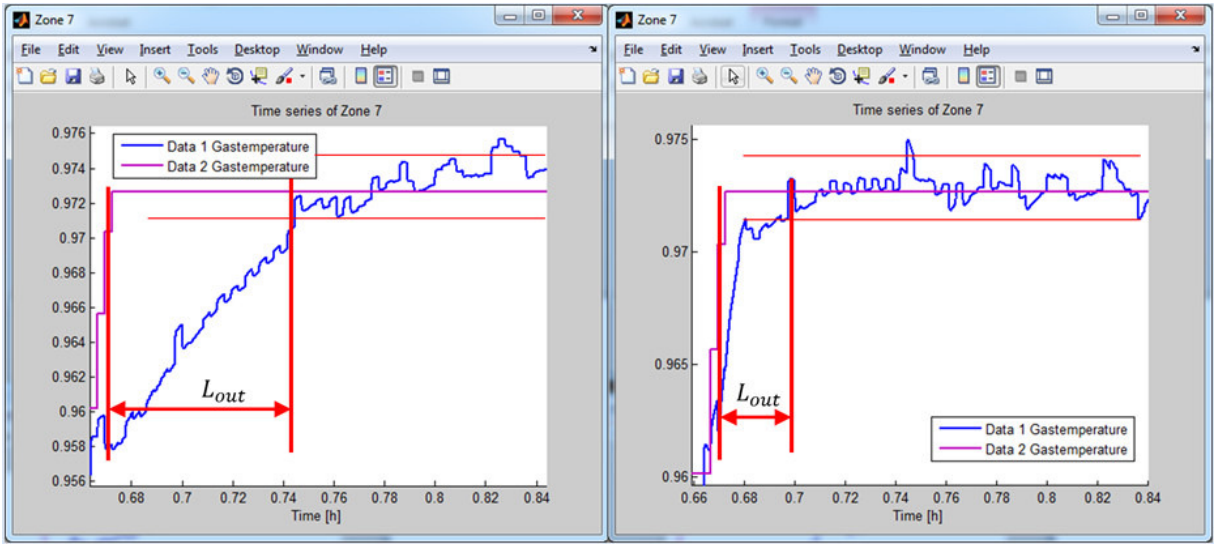

Figure 3.90: Potential effect of set-point optimization of temperature control in TKN's annealing line KL3

3.3.2 Task 3.2: Working out decision masking concept and supervision procedures for automatic re-tuning [ALL PARTNERS]

The main results of this task were:

- Concept and Software for decision making regarding convenience of re-tuning the control loops or not were developed, being deliverable D3.2 and D3.3:
  - General decision procedure for performance improvement developed in discussions between ICC,BFI and MEFOS
  - Strategies for variation of Controller parameter for PI and PID developed in discussion between BFI, AMEH and TKN

3.3.2.1 Development of decision procedure for performance improvement with differentiation between PID and MPC

A principal decision procedure, partly adopted form [Hug99], for carrying out the right measures for improving the performance of a control system is illustrated in figure 3.91 A continuous CPM system indicates whether the control performance is acceptable, i.e. meets the required specification in terms of standard deviation or other measures, product quality, energy consumption or even safety. This level is thus more related to the direct economical performance of the plant shown later in Task 5.2. When proceeding with the performance analysis, the current performance is compared to that of the selected benchmark, to find out whether the installed controller is performing well under the current process condition, using the techniques of WP1 of this report.

3.3.2.2 Strategies for variation of controller parameters for automatic re-tuning PI and PID controller

Iterative controller tuning requires the specification of a proper step size for each controller parameter, usually given as percentage. Cautious adjustments to the controller parameters are necessary to guarantee closed-loop stability and performance improvement. There are many strategies for varying the controller settings in each iteration. Some of them are described in the following, including their strengths and weaknesses. Basically, a large step size helps reduce the number of iterations re- quired but may increase the risk to converge to controller parameters far from optimum.

Variation of proportional gain alone and fine tuning of integral time The simplest approach is to vary only the proportional gain (K_p) unless the existing controller is either too sluggish or too aggressive. In such cases, the integral time (T_I) can also be changed (but only one parameter at a time). Otherwise, the variation of K_p, should only lead one to a value near the optimum, and then a "fine tuning" could be done by slight variation of T_I. Results from many simulations showed that an initial change of 20 % in K_p, or T_I in each iteration is reasonable to improve the controller without destabilizing the loop. If the resulting change in the performance index q is not significant, then the controller gain or integral time can be gradually increased up to 50 % in the subsequent iterations [Gor05]. However, this suggest that the current η value is not far from the optimum. It should be clear that the number of iterations required for finding the optimum depends directly on the step size.

Practically, some integral action is always desired in industrial environment for offset free set-point tracking and rejection of step-type disturbances. Hence, there should be at least moderate integral action in the final controller suggested, though this could come with a marginal drop in Harries index η.

Moreover,Goradia [Gor05] pointed out that the performance index takes an unimodal locus. Once the proper direction to improve the controller performance is determined, i.e. to make the controller aggressive or detuned, it can be proceeded iteratively in that direction as long as η continues to increase. After reaching the peak, *eta* starts to decrease even though moving in the same direction. The peak value of the Harries index η is the PI-achievable performance.

Simultaneous Variation The simultaneous adjustment of the controller settings, i.e. decreasing K_p, and increasing T_I (and possibly decreasing TD) when the controller is aggressive and vice versa in the case of a sluggish controller, is the fastest method to find the optimum tuning. However, this approach is not transparent in practice and should only be considered by well-qualified users.

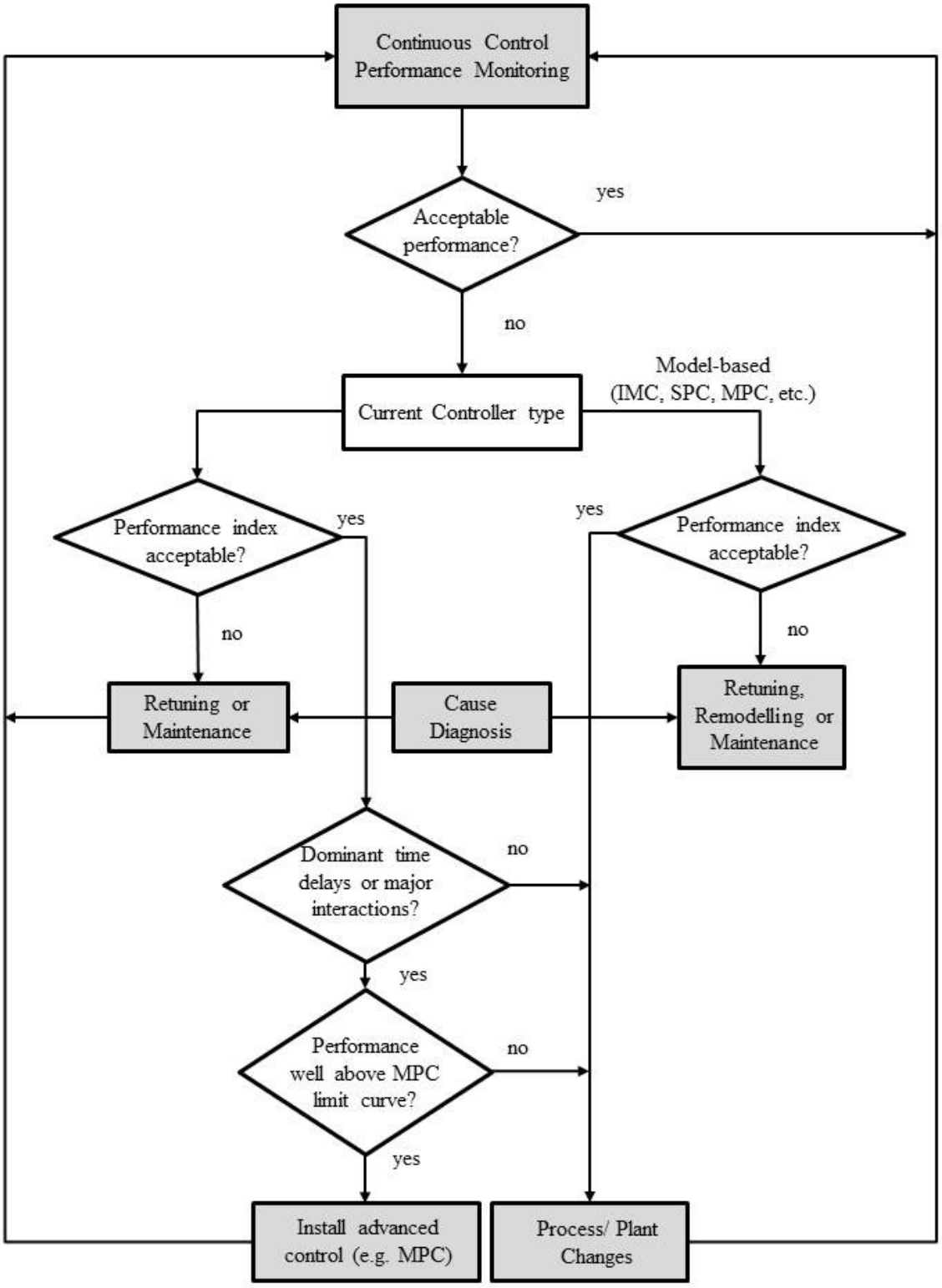

Figure 3.91: Decision procesdure for performance improvement with differentiation between PID and MPC

Successive Variation In this approach, the proportional term is tuned first until the highest performance index value is reached. This is followed by tuning the integral time and possibly derivative time, which may lead to further improvement in Harries index η. The three cases of controller tuning in this strategy are as follows:

1. If the estimated impulse response (IR) is similar to the sluggish IR-profile,(see figure 3.92), increase the proportional gain K_C, until the highest η has been reached. Then, check the impulse response. If the controller is still sluggish (aggresssive), decrease (increase) T_I until the highest η is obtained.

2. If the estimated impulse is close to the optimal impulse response profile, the controller is approaching optimal performance and doses not need to be tuned too much. Slight tuning of the parameters of about 10% is sufficient to obtain the maximum performance index, i.e. to make sure that the maximum η has been crossed.

3. If the estimated impulse response is similar to the aggressive impulse response profile, decrease K_C until the highest η has been reached. Then, check, the impulse used to determine the optimal controller settings against the signature impulse response plots. If the impulse response plot is sluggish (aggressive), decrease (increase) T_i until the highest performance index is obtained.

This approach is highly recommended in practice owing to its transparency. Although it usually takes more iterations than the simultaneous strategy. In this context it should be carefully considered when the controller has low proportional gain and high integral action, resulting in a show oscillatory closed-loop disturbance impulse response. This might be misunderstood as aggressive controller tuning unless other careful observations are made. Besides undershoot and number of oscillations, one should also look at the time when first "zero crossing" of the IR occurs. If it is very long compared to the process delay (which is assumed to be known), it is suggested that the oscillations may be due to a less aggressive controller regulating an integrating or lag dominant process. Hence, one should try to decrease the controller integral action to the minimum required (to reject the low-frequency disturbance) as a first step and then compare its IR to the standard patterns (figure 3.92. This will eliminate the possibility of confusing the oscillatory impulse response due to higher integral action with that really aggressive tuning.

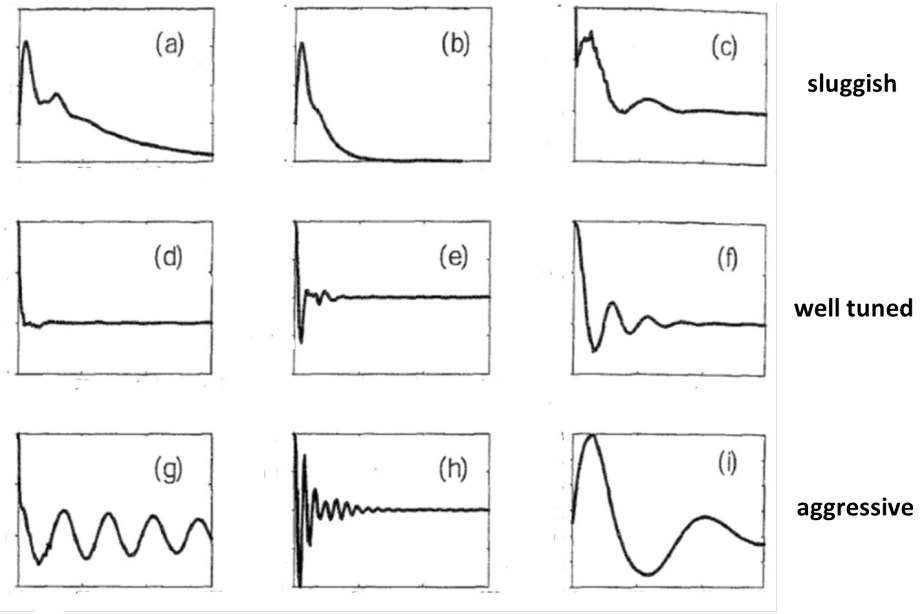

Figure 3.92: Standard nine signature patterns of the disturbance response for controllers: (a) extremely detuned; (b) detuned; (c) slightly detuned; (d) optimally tuned; (e) optimally tuned; (f) optimal tuned; (g) extremely aggressive; (h) aggressive / very oscillatory; (i) midldly aggressive [Gor05]

Constraints and loop stability In the context of parameter optimization considered here for controller tuning, it is decisive to carefully formulate the optimisation task. This is because even not correctly formulated problems can be "solved". Therefore,when using optimisation, it is essential:

- To carefully formulate the criterion to be minimized,
- To include all relevant constraints (in terms of stability arid robustness),
- To be aware of the several pitfalls of optimization, such as the existence of the local minima,
- To realize that the computation burden may be excessive.

If a system model is available, e.g. from the commissioning stage, or can be estimated from system identification, it is always advisable to simulate the closed loop and ensure that each controller parameter combination produces a stable system. For this purpose, the poles of the controlled system have to be checked: if they are found to be unstable, i.e. outside the unit circle (for time-discrete systems), the corresponding parameter combination must be removed.

3.3.3 Task 3.3: Procedure simulation of automatic re- tuning of the control loops, comparison of selected methods [ALL PARTNERS]

3.3.3.1 Simulation studies by the University of Strathclyde in discussion with MEFOS

The University of Strathclyde compared the three developed methods with the Visioli's method. Four metrics were used to validate the improvement: controller performance assessment, idle index I_i, area index I_a and output index I_o. The first one has already been defined in Task 1.3, whereas empirical rules for the other indexes have been proposed by Hagglund and Visioli [Hag95], [Vis05]. These rules are presented in Table 3.10:

Table 3.10: PI tuning rules for performance assessment (Visioli's performance rules)

	$I_i < -0.6$ (low)	$-0.6 \leq I_i \leq 0$ (medium)	$I_i > 0$ (high)
$I_a > 0.7$ (high) medium	increase K_c	increase K_c increase T_i	increase K_c decrease T_i
$0.35 \leq I_a \leq 0.7$	K_c **ok,** T_i **ok**	increase K_c decrease T_i	increase K_c decrease T_i
$I_a < 0.35$ (low)	decrease K_c $I_o < 0.35$: decrease T_i	decrease T_i	decrease T_i

Simulation and comparison results A simple SISO system presented in [Jel07] was used. The system was controlled by a PI control. System and control transfer functions were given in equations (3.160) and (3.161) respectively as follows:

$$G_p(s) = \frac{1}{10s+1} e^{-5s} \tag{3.160}$$

$$K_{PI}(s) = 0.9 + \frac{1}{5s} \tag{3.161}$$

with process noise source $e \sim N(0, 0.1)$. The simulation is run for 6000 samples. At time $t = 3000$ a load disturbance change was made. The load change was used as reference for control re-tuning. A recursive MPC-based metric was calculated. The output performance and energy index during the load disturbance are shown in figure 3.93. The metrics were filtered to avoid unnecessary re-tuning due to distortions. At $t = 3000$, both metrics showed a settle magnitude reduction. This reduction lasted until the implemented PI controller reached steady state value. The metrics also showed some values bigger than 1. These peaks appeared because the implemented controller had an under damped response. The output variance decreased due to negative values of the process output signal. The mean value of the output performance metric was $\eta_y = 0.5717$.

Using the control re-tuning rules given in Table 3.10, the calculated values of I_i and I_a suggested that the values of K_c and T_i should be increased. Furthermore,only a low controller performance index value suggests that process noise was not the source of poor performance and improper control tuning can be inferred.

Assuming that a diagnosis method has verified that the source of poor performance was improper tuning, the application of the methods presented in Task 3.1 gave the following values of the controller parameters presented in Table 3.11.

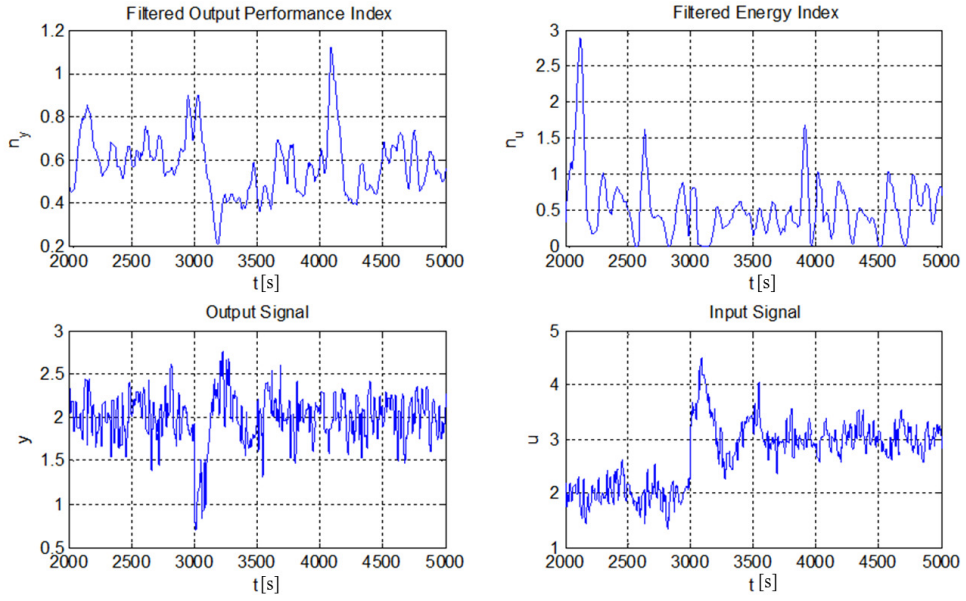

Figure 3.93: Filtered output performance and energy metrics

Table 3.11: Control re-tuning results

	iteration No.	K_c	T_i	I_a	I_i	η_y^c	$\overline{\eta_y}$
actual control	0	0.9	5	0.674	-0.307	0.625	0.5717
Supervisory gain compensation	1	**1.81**	**9.72**	**0.51**	**-0.63**	**0.812**	0.8045
Cov. Control compensation	1	**1.8**	**10.21**	**0.48**	**-0.63**	**0.823**	**0.8063**
Visioli's method	1	1.09	5.48	0.65	-0.43	0.663	
	2	1.33	6.79	0.65	-0.52	0.698	
	3	1.58	7.13	0.57	-0.59	0.781	
	4	**1.83**	**7.54**	**0.5**	**-0.67**	**0.783**	0.7985
modified IFT method	1	1.39	7.28	0.6	-0.47	0.695	
	2	1.53	9.78	0.54	-0.52	0.751	
	3	**1.85**	**10.26**	**0.53**	**-0.66**	**0.816**	0.8034

The results show the calculated controller parameters of the four methods. Note that supervisory method and covariance control method found the new controller parameters at the first iteration since they are "one-shot" solutions. In practice, the supervisory method sampled the process at a different sampling rate compared to the local controllers. The re-tuning procedure can consequently take longer time. The iterative methodologies took 4 and 3 iterations respectively. The modified IFT method took less than the Visioli method since the latter is based on small percentage variations of the controller parameters rather than an optimal recursion. It is important to take into account that the modified IFT method can take higher numbers of iteration according to the complexity of the process. The resulting output performance metrics for all the methods are presented in figure 3.94. The mean values of the output performance metrics are also shown in Table 3.11. No big differences among the performance metrics were detected. The covariance control method seemed to perform better. Visiolis' method showed the lower metric value but the variation was not significant. An average performance metric value of $\eta_y = 0.8032$ was considerably good. A further improvement might be achieved by replacing the PI controller with a PID controller. The re-tuned output is shown in figure 3.95.

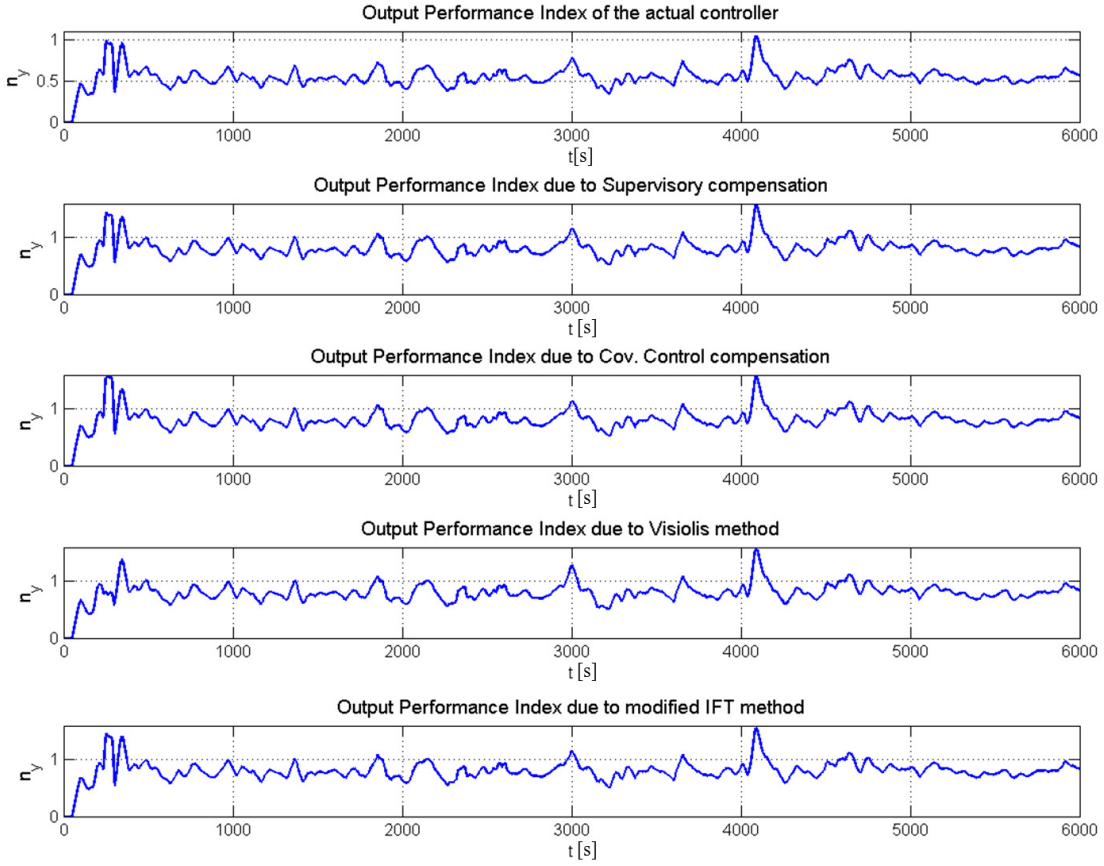

Figure 3.94: Filtered output performance metrics comparisson

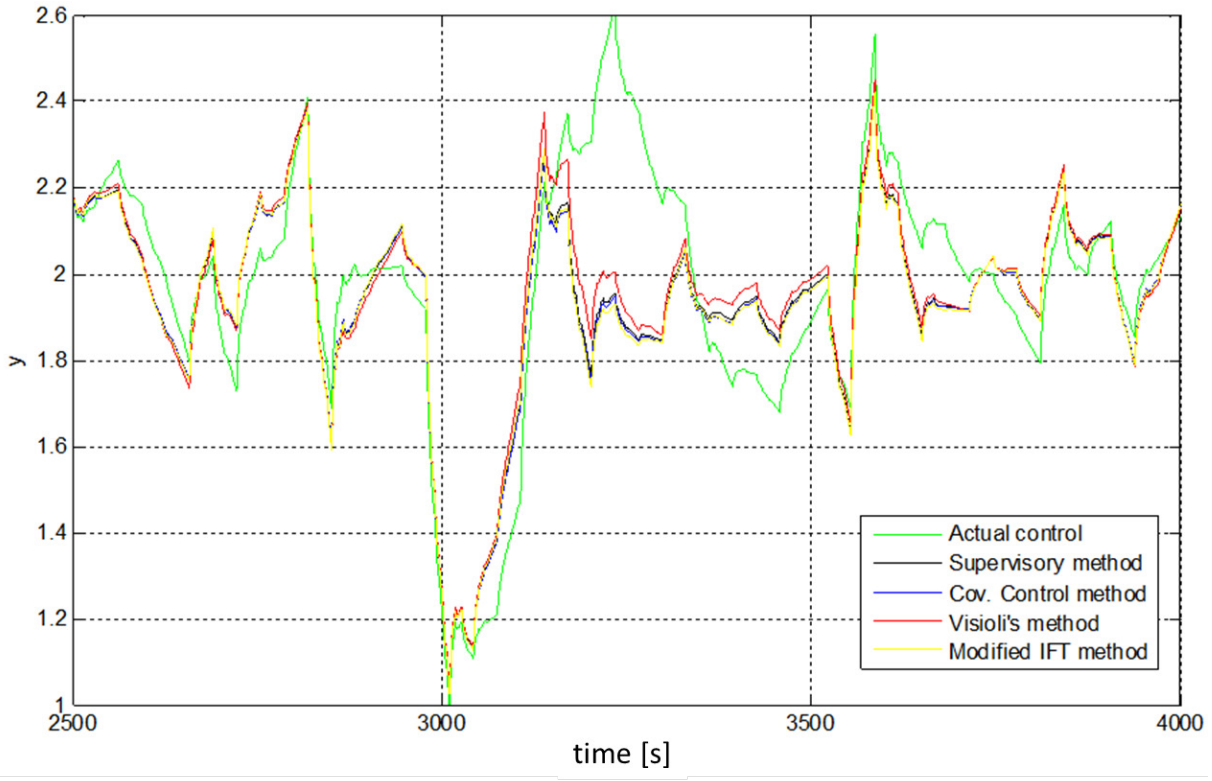

Figure 3.95: Re-tuned output comparison

3.3.3.2 Simulation studies by BFI in cooperation with TKN and AMEH

Table 3.12 provides a summary of the required parameters for the CPM-based controller tuning method presented by BFI.

Table 3.12: Comparrison of the CPM-based controller -tuning methods

No.	Method	Required data and models/parameters
1	Parameter optimization based on complete knowledge of process models	• Knowledge of the process and routine operating data for the estimation the disturbance model. • Data form active experiments on the open system for identification of the process model and routine operating data for the estimation the disturbance models.
2	Parameter optimization based on routine and set-point response data	• Time delay and • Data for the identification of ARMAX model of the closed loop
3	Iterative tuning based on impulse response assessment	• Time delay and • Routine operating data for the estimation the disturbance model(incl. impulse response)

Inspecting this table reveals the following points:

- Iterative tuning based on impulse response assessment is the most appealing strategy in practice, as it is completely non-invasive and necessitates a minimum of process knowledge.
- If set-point changes occur during normal process operation, parameter optimization based on routine and set- point response data is simple and effective
- If step -wise/abrupt changing load disturbance act on the process and these changes can be detected properly, iterative tuning based on load disturbance changes may be useful.
- Parameter optimization based on complete knowledge of the process models is the most involved tuning technique and will not be the first choice in practice, unless accurate models are available or can be estimated from routine operating data or with a minimum of experiments on the closed loop.

In the following the results of two examples are presented that have often been used in literature as benchmarks for controller tuning methods. The tables below contain the optimal control settings $\mathbf{K}_{\mathbf{PI}}^{*}$ achieved, the corresponding value of the performance index η^{*} and the number of iterations N_{Iter} required for the iterative techniques.

Example I A delay-free process described by

$$y(k) = \frac{q^{-1}}{1-0.8q^{-1}}u(k) + \frac{10.2q^{-1}}{1-q^{-1}}\varepsilon(k) \tag{3.162}$$

and a PI controller is considered. The disturbance noise has the variance $\sigma_{\varepsilon}^{2} = 0.01$. In this case, a PI controller may achieve the minimum variance. Indeed, the results given in this example show

Table 3.13: Tuning results for axample 1 (Initial parameters: $K_c = 0.14; T_I = 7.0 \Longrightarrow \eta_0 = 0.33$

Methods	$\mathbf{K}^*_{\mathbf{PI}} = [K_c^*; T_I^*]$	η^*	N_{iter}(Variation steps)
1	$[0.79; 5.00]$	0.98	-
2	$[0.80; 5.30]$	0.99	2
3	$[0.78; 4.1]$	0.50	5 $(\Delta K_C = 20\%, \Delta T_I = 10\%)$

that MVC performance is attained. All methods yield (nearly) optimal (stochastic) performance and parameter settings in the neighborhood of the optimal ones (given by method no.1); see table 3.13 It was found that method no. 2 may be sensitive to the choice of the ARMAX model parameters. The results in table 3.13 were obtained based on the identification of an ARMAX(3,2,2,1) model, and two iteration were needed. However, this is not generally the case.

Example II Now a process with time delay and affected by nonstationary disturbances (σ_ε^2) was considered:

$$y(k) = \frac{0.1q^{-5}}{1-0.8q^{-1}}u(k) + \frac{1}{(1-0.6q^{-1})(1-0.3q^{-1})(1-q^{-1})}\varepsilon(k) \tag{3.163}$$

In this case , a PI controller has no chance to attain MVC performance. The results in table 3.14 confirm that 50% of the minimum varianace can be maximally archieved, $\eta = 0.05$. Method no. 3

Table 3.14: Tuning results for Example 2 (Initial parameters: $K_c = 1.6; T_I = 15.0 \Longrightarrow \eta_0 = 0.37$

Methods	$\mathbf{K}^*_{\mathbf{PI}} = [K_c^*; T_I^*]$	η^*	N_{iter}(Variation steps)
1	$[2.57; 10.25]$	0.50	-
2	$[2.61; 9.77]$	0.50	-
3	$[2.3; 9, 60]$	0.50	3 $(\Delta K_C = 20\%, \Delta T_I = 20\%)$

is not suitable for such scenarios. This case typically shows that MVC-based benchmarking may not be the right (i.g. realistic) benchmarking option for PID-controlled loops. Rather the optimal PID controller itself should be taken as benchmark. Considering this, even the initial controller used does not have poor perfomance. Note that a predictive controller (compensating the time delay) is able to reduce the variance further, so that a re-design of the controller would pay off.

3.4 WP 4: Implementation„ interface programming and on-site implementation of automatic control optimization techniques

The main objectives of this WP were:

- Control data needed by the staff for online supervision and long-term optimization use were reviewed.
- The supervision methods and decision making procedures for monitoring (assessment and automatic diagnosis) and automatic re-tuning were implemented.
- Online software was created.
- Suitable user friendly and safe human interfaces (HMIs) for the accessing plant personnel were designed.
- HMIs were implemented and tested.
- All software components were integrated and tested online.

3.4.1 Task 4.1: Development and test of the SCADA interface to the performance and fault monitoring software [ICC]

The University of Strathclyde combined all the methodologies used and developed by the ICC into a MATLAB software tool. Supervisory Control And Data Acquisition (SCADA) functionality was added to the software tool through the Object linking and embedding Process Control (OPC) toolbox, being deliverable D4.2.

OPC is a MATLAB toolbox developed to provide connectivity, directly from MATLAB and Simulink, between OPC clients running software applications and any OPC Data Access (DA) and Historical Data Access (HDA) compliant servers. The toolbox allows reading, writing and logging OPC data from devices such as distributed control systems, SCADA systems and programmable logic controllers that conform the OPC Foundation DA standard [Mat11]. Figure 3.96 shows a monitoring tool using OPC.

The OPC toolbox provides data access client capabilities from within MATLAB. In order to use the functionalities of the toolbox access to an OPC server that supports DA Specification version 2.05 is needed Before accessing any server in a network,the workstation and possibly the OPC server host computer might also nee to be prepared in order to use the OPC toolbox. The preparation to use the OPC toolbox can be found on the MATLAB toolbox help.

OPC simulation servers are a free utility to help test and troubleshoot OPC applications and connections. Vendors such as Matrikon and Iconics offer free test tools to provide the client with a simulated environment so that in the event of a problem, no real process data is lost. Available software can be found in [Mat] and [iCO]. The tools are easy to use, the application simply have to be downloaded and installed them in the OPC client.

Figure 3.96: Object linking and embedding Process Control(OPC) connectivity

3.4.2 Task 4.2: Implementation of procedures adapt and verify performance assessment and automatic root-cause diagnosis results [ALL PARTNERS]

In the following the implementation of procedures adapted and verified performance assessment and automatic root-cause diagnosis by all partners.

Tool for TKN BFI together with TKN in discussion with ICC developed a simulation and diagnostic tool for the KL3, being deliverable D4.3 and D4.4. The layout of the tool is shown in figure 3.97.

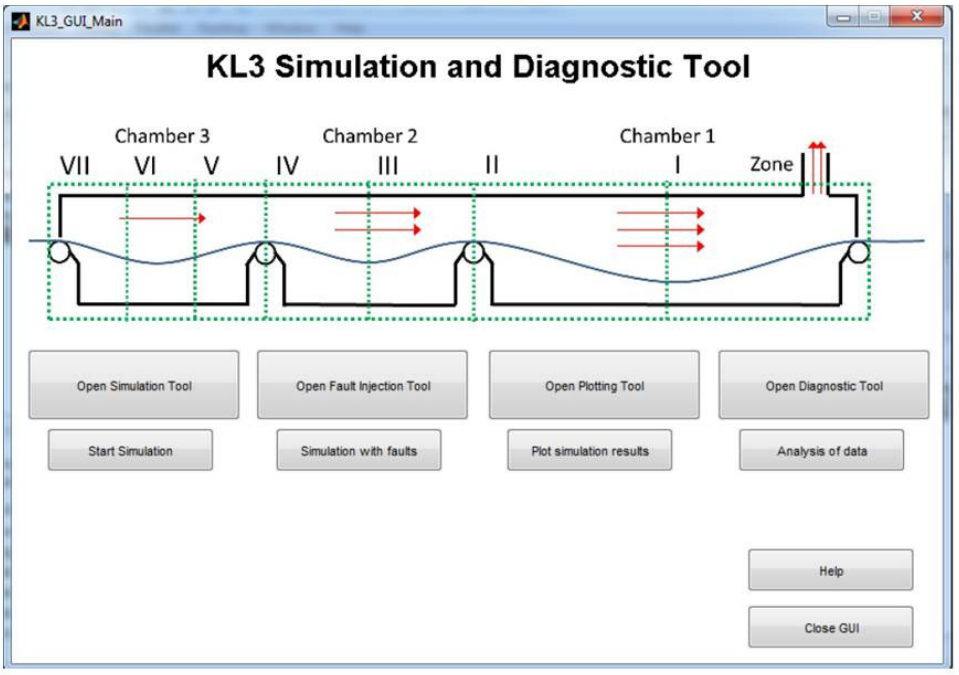

Figure 3.97: Software for performance assessment and root cause diagnosis

The tool has the following features:

- A simulation tool for simulation of the dynamic behaviour of the furnace and controller.
- Fault injection tool to simulate the reaction of the furnace and the controller on faults in sensor and actuator
- Diagnostics tool to analyse the performance and the root cause of performance degradation.
- Plotting tool to illustrate the results of simulation and diagnoses.

The layout of fault in the fault injection tool is shown in figure 3.98 As seen in the figure the following

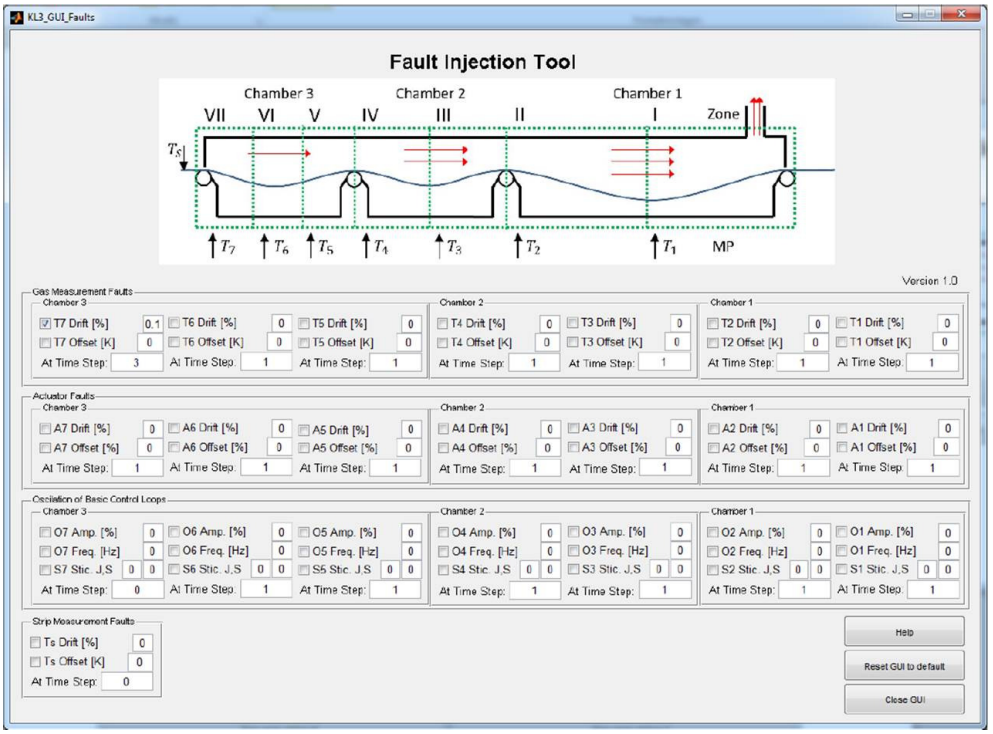

Figure 3.98: Fault injection tool

faults can be specified:

- Senor and actuator drift
- Offset on sensor and actuator

Also the time and the magnitude of faults can be specified. Furthermore for each control loop of the furnace the effect of

- Oscillation
- Stiction in valves (actuator)

can be simulated and analyzed. The results are stored in files and can be analysed by a diagnostic tool shown in figure 3.99. Furthermore also data coming form the plant can be load into the tool. The time

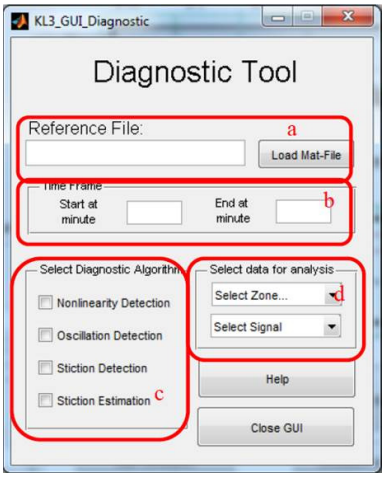

Figure 3.99: Diagnosis of the root cause of performance degradation. a.Selection of the file to be analysed, b.) Time span to be analyses c.) Section of the methods, d:) Selection of the signal to be analysed)

span and the variable can be selected in a menu. The following methods for root cause analyses can be selected:

- Harries index
- Methods for pre-processing the data
- Nonlinearity Index,
- Methods to detect oscillation and stiction

The results are shown by the plotting tool. The results gained with the help of this tool are shown Task 5.2.

Tool for AMEH In figure 3.100 an application of the structure for annealing furnaces is illustrated, being deliverable D4.1, D4.3, D4.4. In this specific case, the performance of the furnace room temperature control at different zones was analysed, and assessment results based on the Harris index and modified variants of it were given. Figure 3.101 shows some more detailed results: the disturbance impulse response and the prediction horizon plot that, indicate the time delay value (i.e. prediction horizon) that should be selected for computing the extended Harris index. How fast disturbances are compensated is depicted in the lower part of figure 3.101. The results gained with this tool were shown in task 5.1.

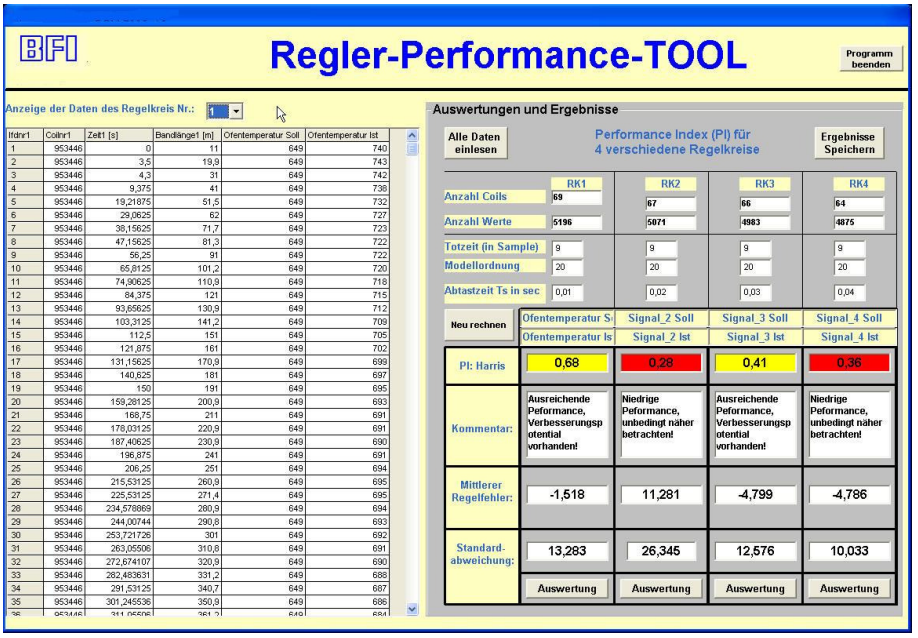

Figure 3.100: Layout of the control performance tool

3.4.2.1 MEFOS monitoring system applied at KBR

This module provided facilities to design and evaluate monitoring engines for improving the detection, identification and diagnosis of faults within complex processes, being deliverable D4.3, D4.4. Each monitor can be exhaustively evaluated by streaming historical process data into the engine. This ensures high robustness and ultimately provides effective and meaningful alarms. Figure 3.102 show the configuration screen of the tool and figure 3.103 the online screen.

3.4.3 Task 4.3: Implementation of continuous monitoring and automatic retuning decision making procedures [BFI, MEFOS, AMEH, TKN]

In the following the implementation of monitoring and automatic retuning decision making procedures is demonstrated.

Figure 3.101: Results of the performance tool

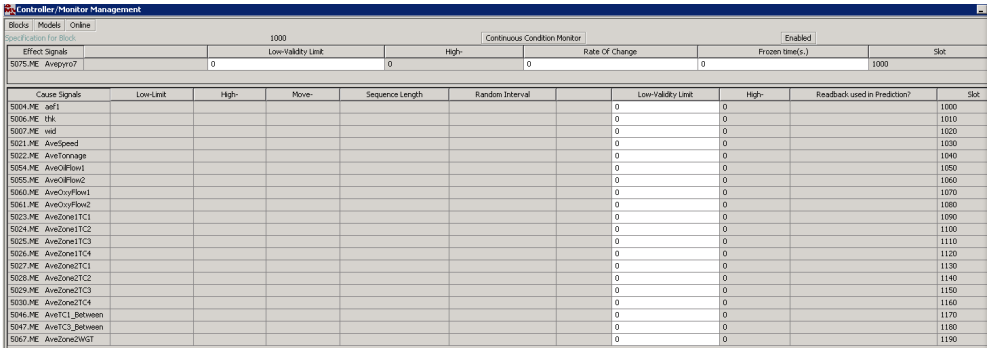

Figure 3.102: Configuration screen of monitoring tool

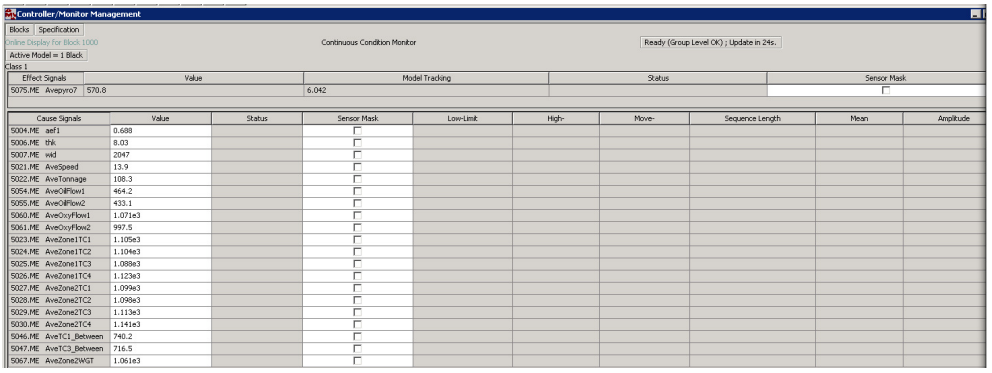

Figure 3.103: On-line screen of the monitoring tool appieled at KBR

3.4.3.1 Retuning tool integrated in the simulation and diagnostic tool for the annealing furnace at TKN

In figure 3.104 the structure of the furnace controller of TKN's annealing furnace is shown. The structure was implemented in the simulation and diagnostic tool described in Task 4.2. The controller consists of seven furnace temperature controllers and one strip temperature controller for the last zone. A set-up system provides the necessary set-points for each temperature controller.

In the tool the parameter of the controller can be edited and optimized as seen in Figure 3.105. Additionally it provides a tool to optimize the set-point-response of the furnace controller. The set-point

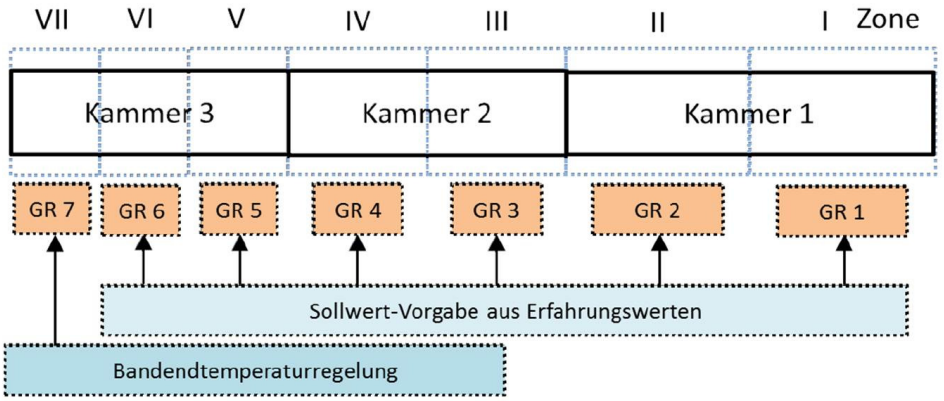

Figure 3.104: Software for performance assessment and root cause diagnosis

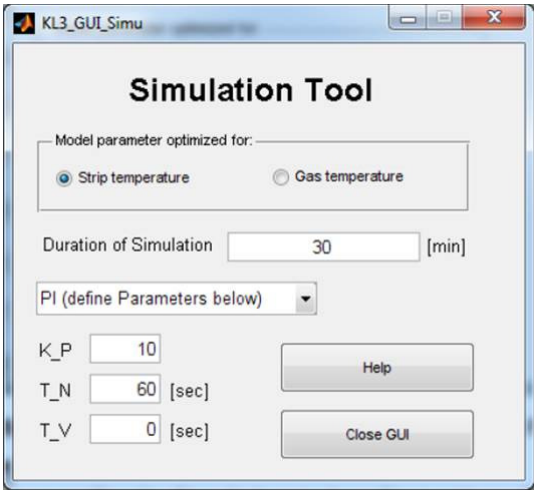

Figure 3.105: Interface for optimization of the control parameter

is optimized in such a way that the deviation from the desired strip temperature caused by thickness changes and strip speed changes is reduced. This would lead to more homogeneous strip quality. The optimized set-point can be simulated with the tool and some results are shown in figure 3.106 - 3.108. Here results are shown for cases where strip thickness does change from 0.9 to 1mm. The set-point is optimized by including an intermediate set-point. The optimisation values are the duration of the intermediate set-point and its height.

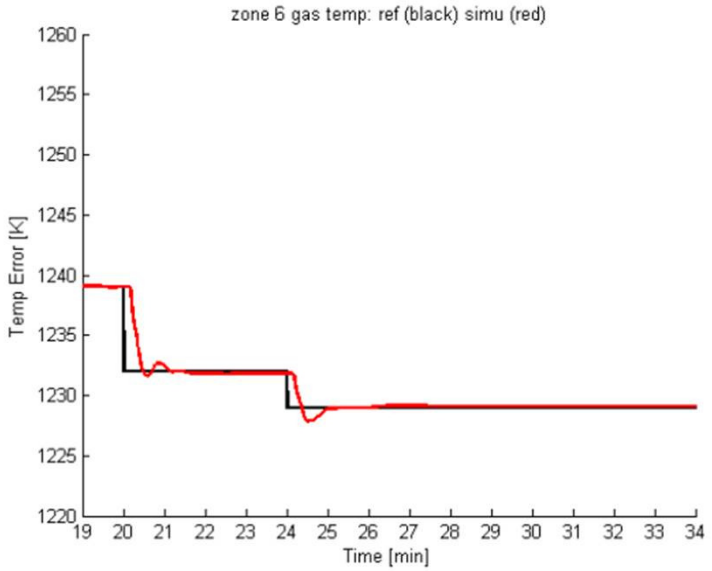

Figure 3.106: Results of the set-point optimization for the first six furnace temperatures

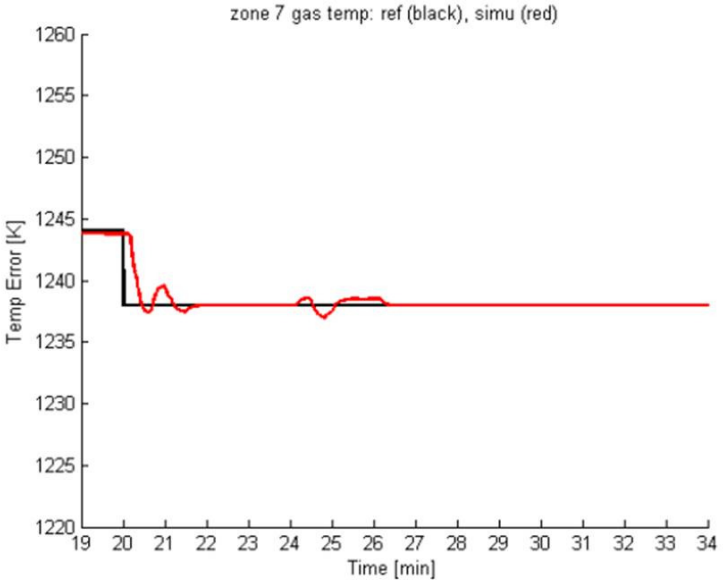

Figure 3.107: Results of the set-point optimization for the zone 7

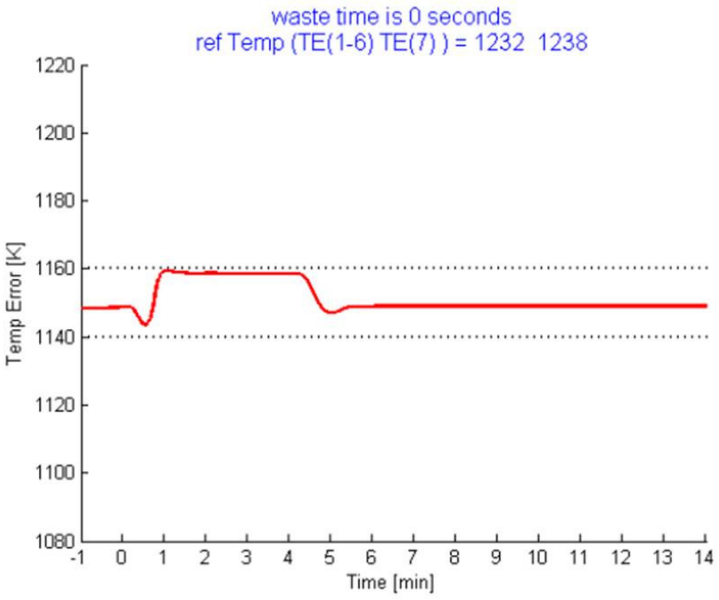

Figure 3.108: Resulting strip temperture

3.4.3.2 Iterative tuning tool used at the galvanizing lines at AMEH

For tuning the controller at the galvanizing line at AMEH the relative damping index was chosen. Figure 3.109 demonstrates the layout of the tool. Data of different coils can be loaded into the tool from a database. The coil data was analyzed and the performance index for each controller and the suggestion if control parameters should be increased or decreased were given.

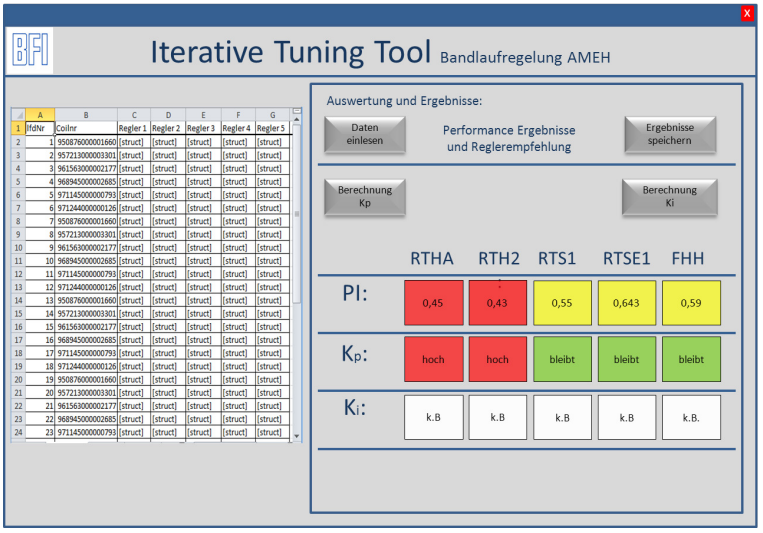

Figure 3.109: Iterative tuining tool

3.4.3.3 System at MEFOS site

The performance and re-tuning tool based on MPC algorithm was applied at KBR. The operators/process developers used this tool for analyzing the system's performance. In figure 3.110 a screen shoot of the specification screen is shown. Here, the parameters of the algorithm can be specified. Figure 3.111 points out the online status of the MPC tuning system.

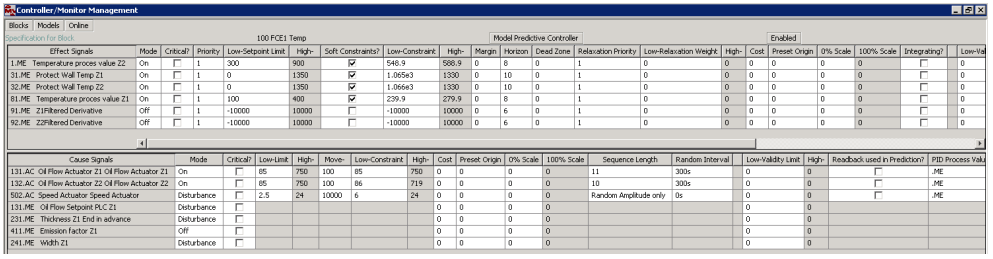

Figure 3.110: Software for performance assessment and root cause diagnosis

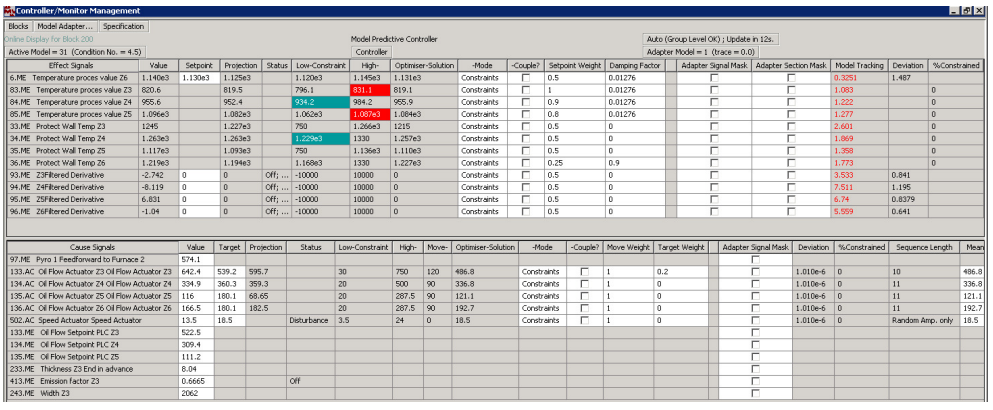

Figure 3.111: Software for performance assessment and root cause diagnosis

3.5 WP 5: Final testing and evaluation of developed tools and systems

The main objectives of this WP were:

- The system developed was integrated into the automation system at different industrial mills .
- The HMIs were tested On/inline.
- The monitoring and automatic re-tuning procedures were tested.
- The complete systems were tested on-/inline.
- The global applications were optimized.
- The results were evaluated and dissemination strategies were worked out.

3.5.1 Task 5.1: Methods and systems for demonstration at the galvanizing lines and linked pickling/cold rolling mill at the ArelorMittal Eissenhüttenstadt [AMEH, BFI]

In this task controller performance analysis, root cause analysis of performance degradation and auto automatic re-tuning using the tools developed in this project were demonstrated at the galvanizing line VZA2 of AMEH, being deliverable D5.2

3.5.1.1 Data set used for the demonstration of the methods and systems at the galvanizing lime VZA2 of AMEH

The following signals of the galvanizing line of AMEH were recorded over a two months production (about 4300 coils):

- furnace temperature for each furnace zone
- strip temperature
- strip speed
- strip width
- strip thickness
- strip position for each furnace zone
- position of the steering for each furnace zone

The data was used for the performance analysis, root cause detection and iterative tuning.

3.5.1.2 Performance analysis and root cause detection

In figure 3.112 the layout of the strip flow controller of the analysed furnace of the VZA2 at AMEH is shown. The strip flow is controlled zone by zone using steering rolls. Here it is done by 5 controller: one at the a preheating section RTHA, the second in heating zone RTH2, the third in the soaking section RTS2, the fourth in the soaking RTSE1 and the fifth controller is placed behind the cooling at the outlet FFH of the furnace. The aim of the strip flow controller was to keep the strip in the centre line of the furnace in order to guarantee the operation of the furnace, e.g. to avoid defect on the strip edges. The following analysis was carried out to investigate the performance of the controller:

- Sorting the coils according to different width, thickness and strength
- Analysing how often hte controller is switched on or off (variance of manipulated variable)
- Performance-analysis (Harris-Index)

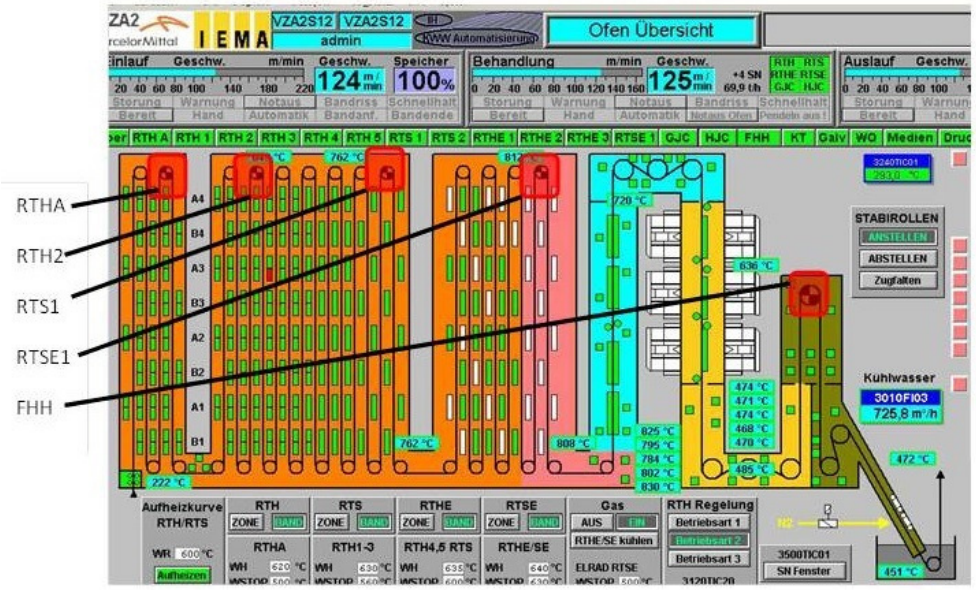

Figure 3.112: Layout of the strip flow controller of the galvanizing line VZA2 at AMEH

- Oscillation (of controls and manipulated variable)
- Linearity (of controls and manipulated variable)
- Possible oscillation cause (e.g. stiction)

The first results are shown in table 3.15. The controller RTH2 has been switched off quite often. If it is switched on, the controller showed no sufficient performance as per controller RTHA. Furthermore the standard deviation of Harries of RTH2 was highly in comparison to the Harries index. This gave also a hint that there was a serious problem with RTH2. Furthermore it was visible that the variance of harries for the other controller were not small. This fact leads to the assumption that process parameter are varying. Therefore it might be beneficial to use adaptive controller to compensate this effect. In the next step the root cause of the performance degradation was investigated. Therefore, the oscillation

Table 3.15: Performance Results

	RTHA	RTH2	RTS1	RTSE1	FHH
Controller switched on ?	100 %	25 %	100 %	100 %	25%
nonlinear	no	no	no	no	no
Harries Index	0.38	0.21	0.61	0.65	0.59
Standard deviation of Harries Index	0.12	0.16	0.20	0.21	0.20

index and an index to detect stiction was calculated for each controller. The results are shown in table 3.16.

Table 3.16: Root cause Analyzes

	RTHA	RTH2	RTS1	RTSE1	FHH
Oscillation	0%	45 %	45 %	45 %	45%
Cause of Oscillation by Stiction ?	no	no	no	no	no

The first controller RTHA did not show any oscillation, but all the other controllers showed oscillations in 45% of the investigated cases. Stiction could be excluded from the list of causes. Figure 3.114 shows an example of controllers with oscillation.

After some further investigation by AMEH it was found out that the strip which reach a temperature of 300°C at end of the RTHA zone did not show any oscillation or just some, but if the strip reached only 180°C in this zone, the strip started to oscillate. Therefore, an additional temperature measurement and controller were installed. The strip temperature at the end of this zone was kept constant to 300°C, since then no oscillations were visible.

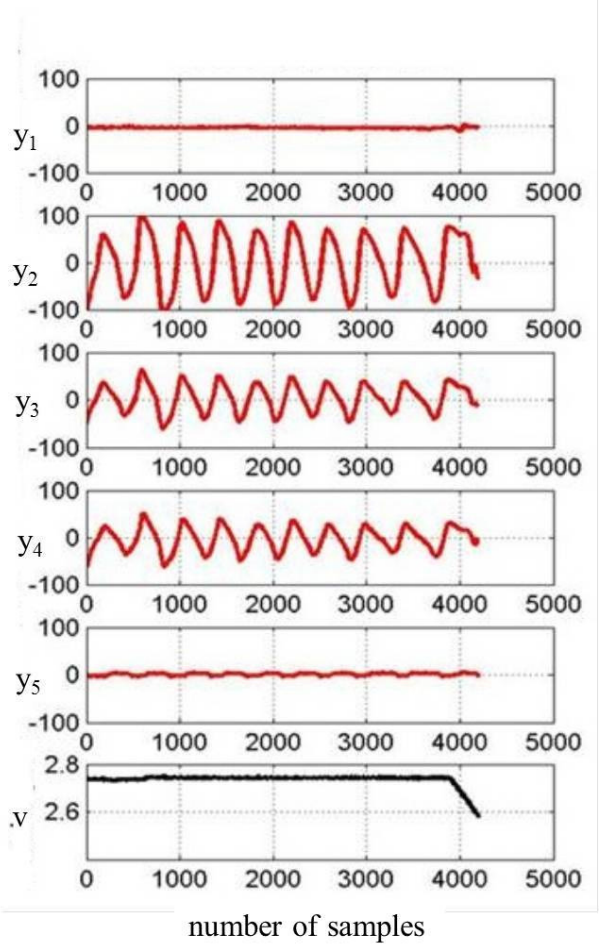

Figure 3.113: Controller with Oscialtion: ($y_i i \in [1,5]$ strip position of the controller, v strip speed)

3.5.1.3 Iterativ tuning of strip guiding controller RTHA

Even if the controller RTHA performed poor/insufficient, no oscillation was visible. Therefore, iterative tuning based on the relative damping index was applied for some iteration. Here, the following strategy was implemented: First, change the proportional gain K_p of the controller by 20% during each iteration until the maximum Harris index is reached. Secondly, change the gain of the integrator K_I by 20 % and see if the Harris index does increase further. Figure 3.114 shows the flow diagram of the iterative tuning method. During the iteration the standard deviation of the Harries index was monitored as well. An increase in the deviation might contain a reference to the fact that the controller was sensitive to process parameter variation. The layout for the software(being deliverable D5.1) used, can be found in 3.109,

In table 3.17 the results for two iterations are shown. The performance was analysed using the Harris index and for the first iteration it was advised to increase K_p by 20%. The new controller parameter were applied over one month. Therefore only 2 iterations were carried out. As one can read from table 3.17 in each iteration the performance index has been increasing and the standard deviation hasn't increased to much.

Table 3.17: Results Of Interative Controller Tuning

Iteration	Harries Index	Standard deviation of Harries Index	Suggestion
1	0.5	0.13	Kp increase by 20 %
2	0.57	0.16	Kp increase by 20 %

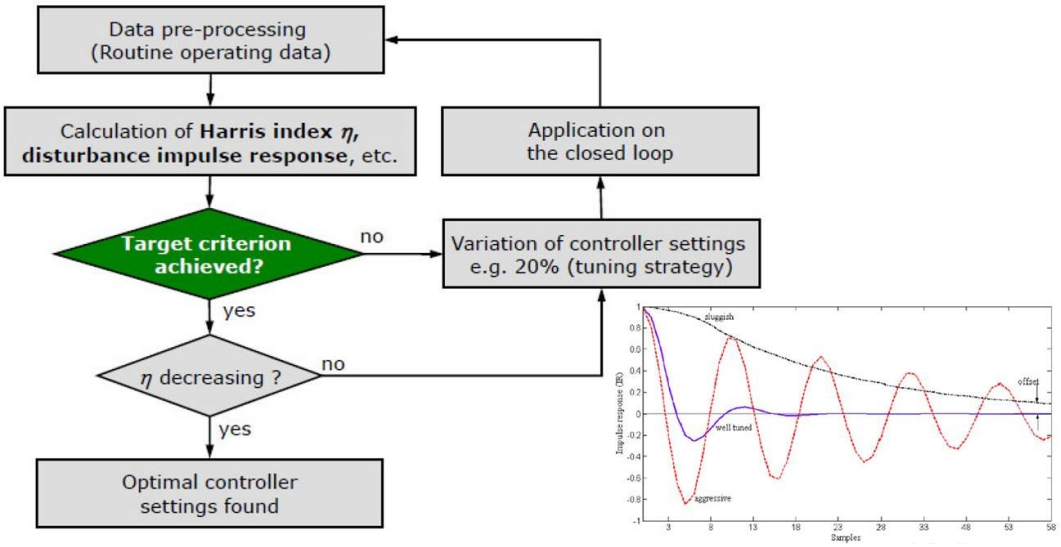

Figure 3.114: Procedure of Iterative Tuning

3.5.2 Task 5.2: Methods and systems for demonstration at (stainless steel) bright annealing lines at ThyssenKrupp Nirosta [TKN, BFI]

In this task the control performance and root cause analysis of performance degradation using the tools developed in this project was demonstrated at the bright annealing line of TKN, being deliverable D5.2. First, the static energy efficiency index was applied. Secondly, the performance of the furnace was analysed using MIMO methods provided by ICC. Afterwards a root cause analysis based on models was applied and suggestions to improve the controller were given, which lead reduced cost and energy consumption.

3.5.2.1 Data set used for demonstration of methods and systems at ThyssenKrupp Nirosta

The following data was recorded over one month period production,

- desired and measured strip temperature
- desired and measured furnace temperature in zone $i \in [1 \cdots 7]$
- mass flow of natural gas in zone $i \in [1 \cdots 7]$
- strip speed
- strip thickness
- strip width

The recorded data was containing approximatly 2100 coils. The data was used for testing the methods and systems.

3.5.2.2 Monitoring of the static energy index and root cause analysis at TKN

In figure 3.115, some results of the energy efficiency index are shown. As expected, the efficienc increased with the production rate. Values above 0.55 had to be interpreted with caution.

In figure 3.116 below the course of the energy index over time is shown (blue curve). An sudden increase of the energy index form 0.4 to 0.8 became visible. In the figure, the course of the flow of natural gas into the furnace zone no.2 showed at the same time a sudden jump to zero. After some investgation it turned out that there was a malfunction in the measurement system of of the gas flow.

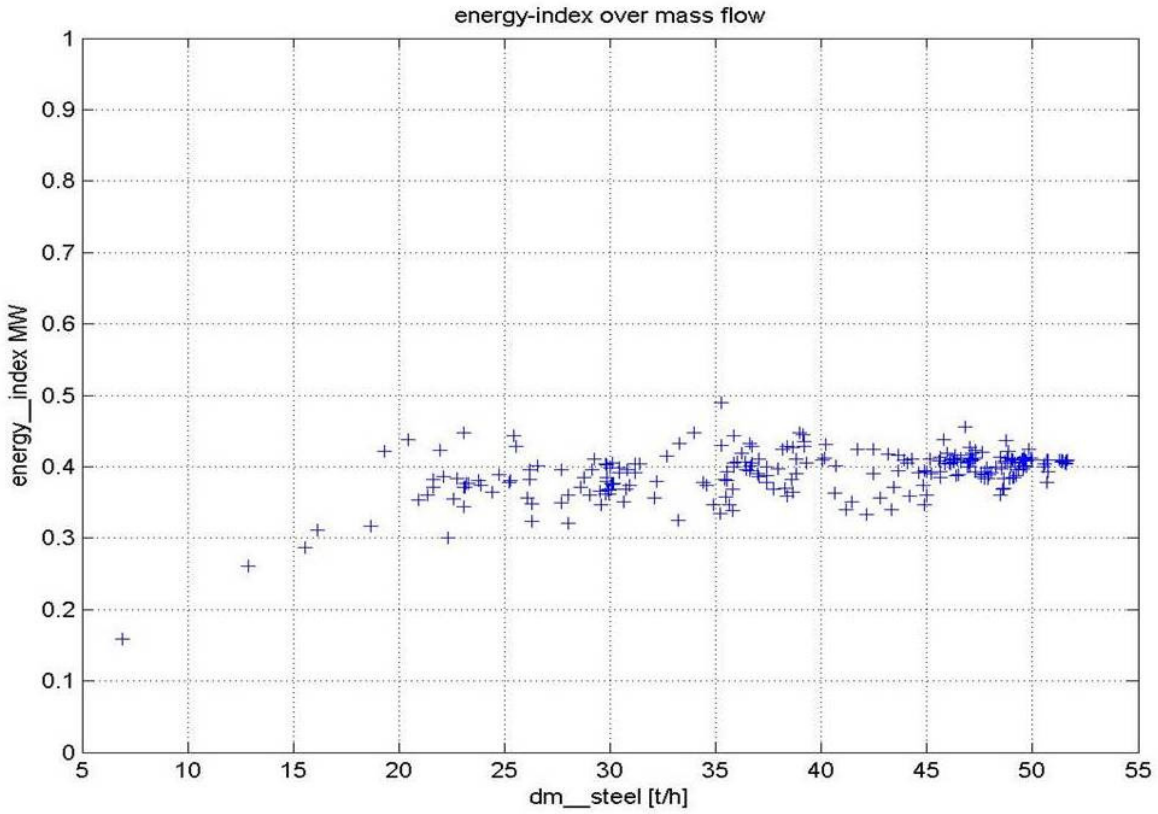

Figure 3.115: Results of the furnace efficiency of the annealing furnace of TKN

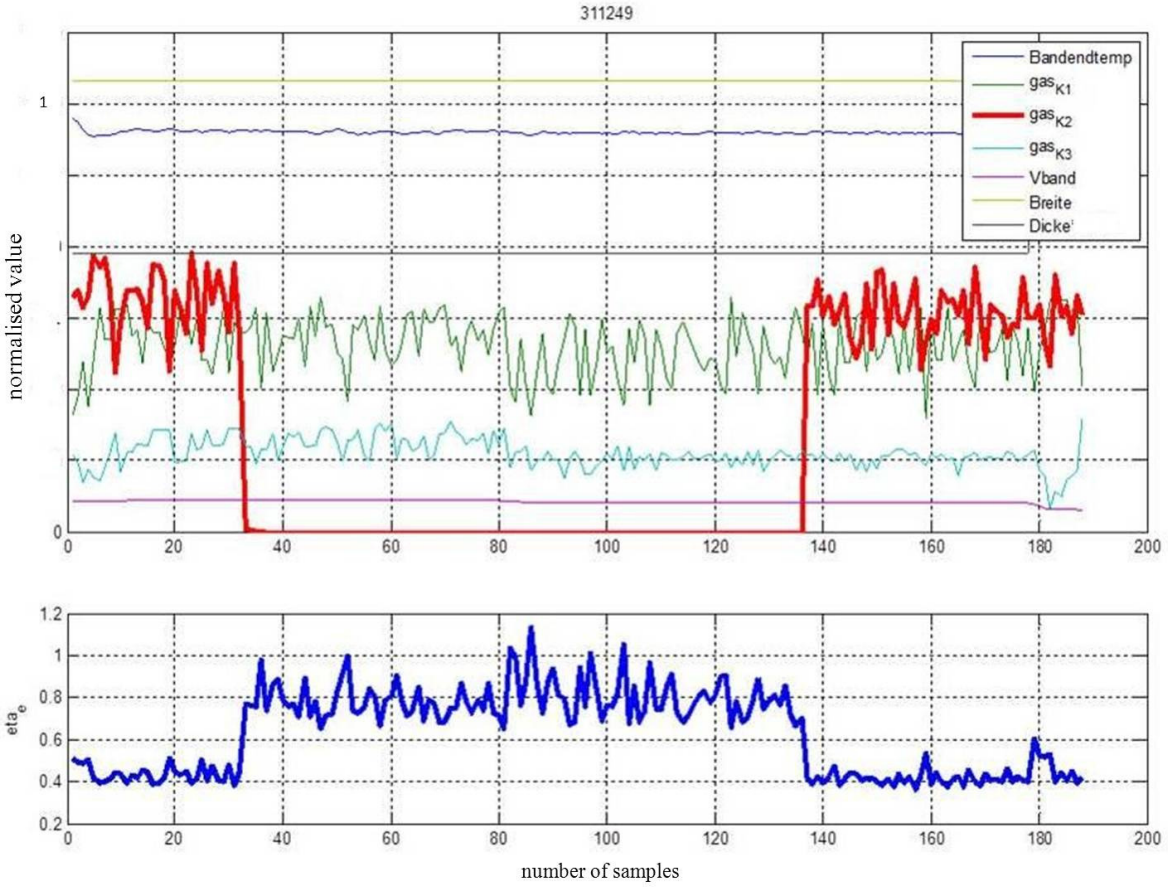

Figure 3.116: Results of the energy Index: energy index over time (blue), natural gas flow in furnace zone 2 (red)

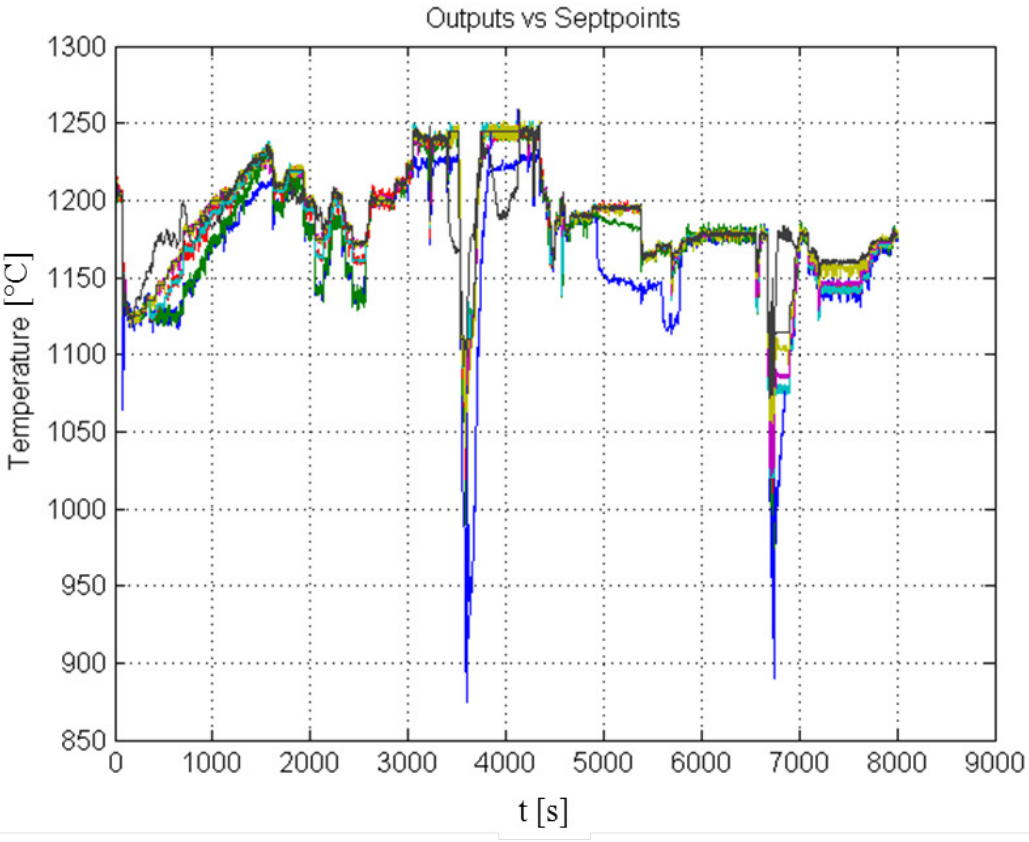

Figure 3.117: KL3 data outputs vs. set-points

3.5.2.3 Analysis of KL3 data with tools provided by ICC

The data showing the course of the set-point and the measured furnace temperature is depicted in Fig. 3.117. The data presented a high output performance index with an average value of $n_y = 0.894$. As seen in Fig. 3.118, the index dropped considerably at several occasions. Significant drops appeared at the beginning of the analysis due to benchmark calibration; before $t = 2000$ due to a high distortion period; between $t = 3000$ and $t = 4000$ due to the huge set-point change; between $t = 4000$ and $t = 5000$ due to an abrupt set-point change; and before $t = 7000$ due to another huge set-point change. For the detection of root causes, four scales were used and the two statistics (T^2 and SPE) were calculated recursively. No threshold violations were found of SPE at any scale; however the data affected repetitively the T^2 statistics. The results of T^2 were the four scales given in Figures 3.119, 3.120 and 3.121. T^2 statistics at scale 1 went out of limits at the beginning of the analysis due to the initial peak of the calibration of the benchmark. T^2 statistics quantified mostly the inflation of the variance. In addition to the analysis carried out on the multivariable case study, **violation of T^2 at high scales is related to oscillatory events which points towards a noisy data or a source of oscillation. This source of oscillation can results from the controller(s) due to the continuous setpoint change**. At scale 1, the threshold violation seemed to be persistent between the ranges $t \in [0, 1000]$ which is where **furnace temperature of zone 7 started to drift from its set-point value**; and $t \in [4000, 5000]$. These ranges also corresponded to zones of fast set-point changes. At scale 2 the ranges of persistent threshold violation are $t \in [2000, 2500]$ and $t \in [6600, 7000]$. The emphasis of the threshold violation in scale 3 appeared at $t \in [500, 1000]$ and $t \in [7300, 7900]$ where the data appeared to be very noisy.

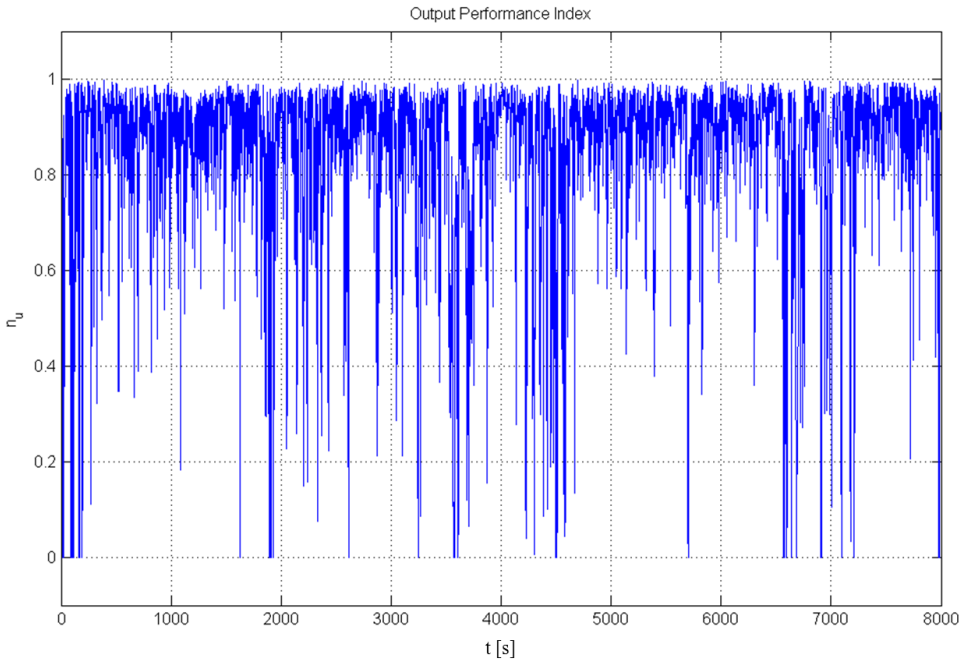

Figure 3.118: KL3 data output performance index

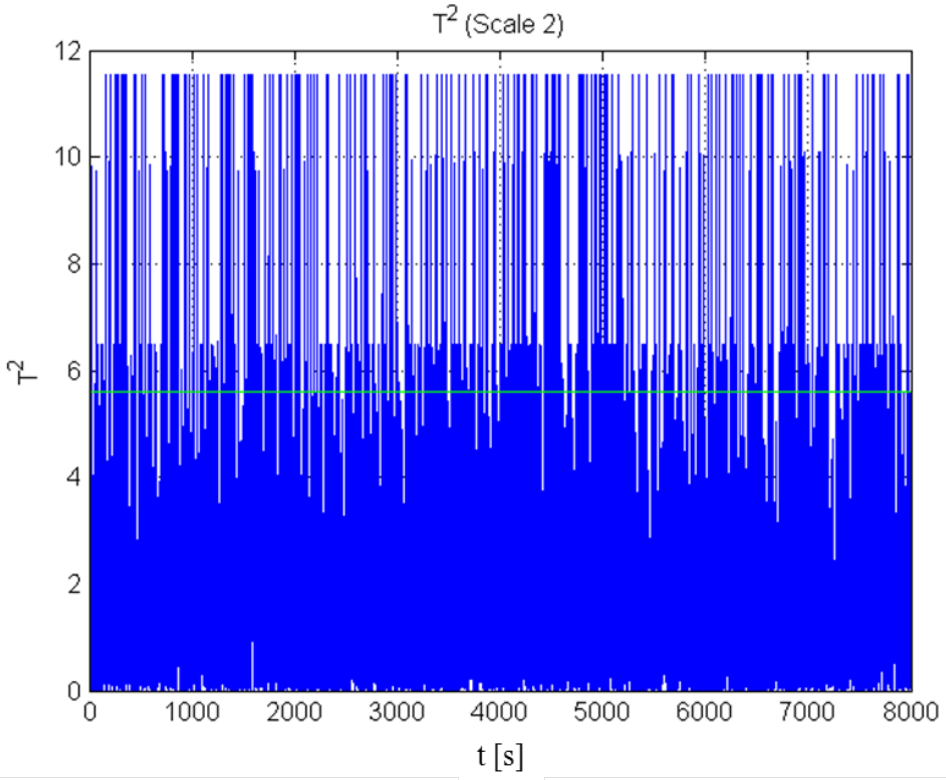

Figure 3.119: T^2 statistics at scale 2 for KL3 data

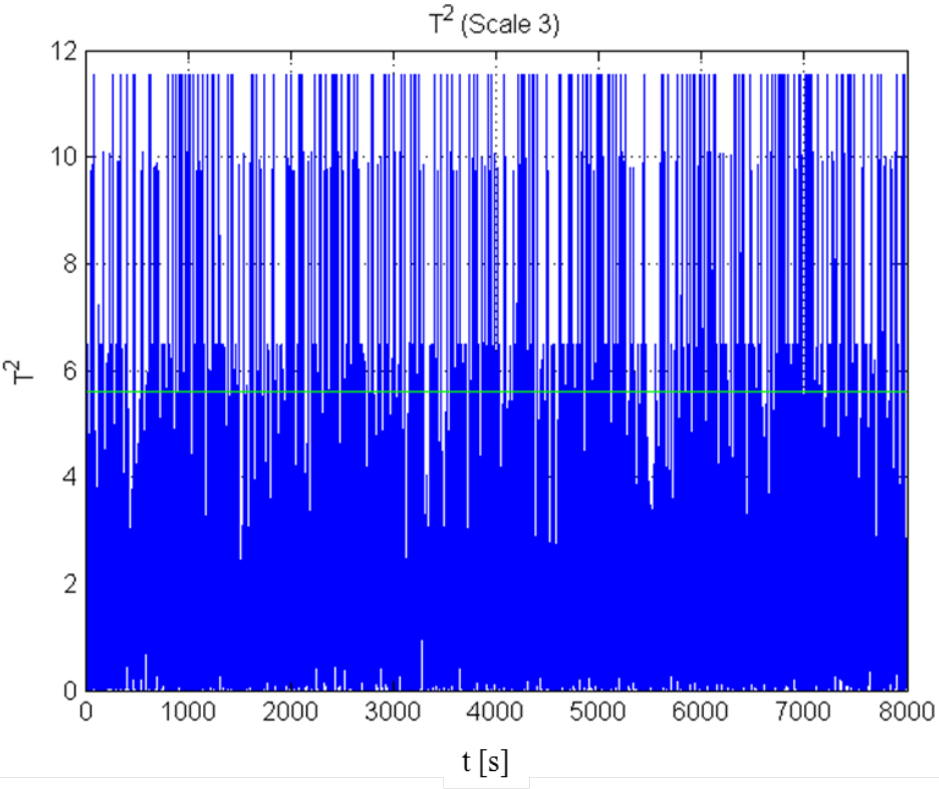

Figure 3.120: T^2 statistics at scale 3 for KL3 data

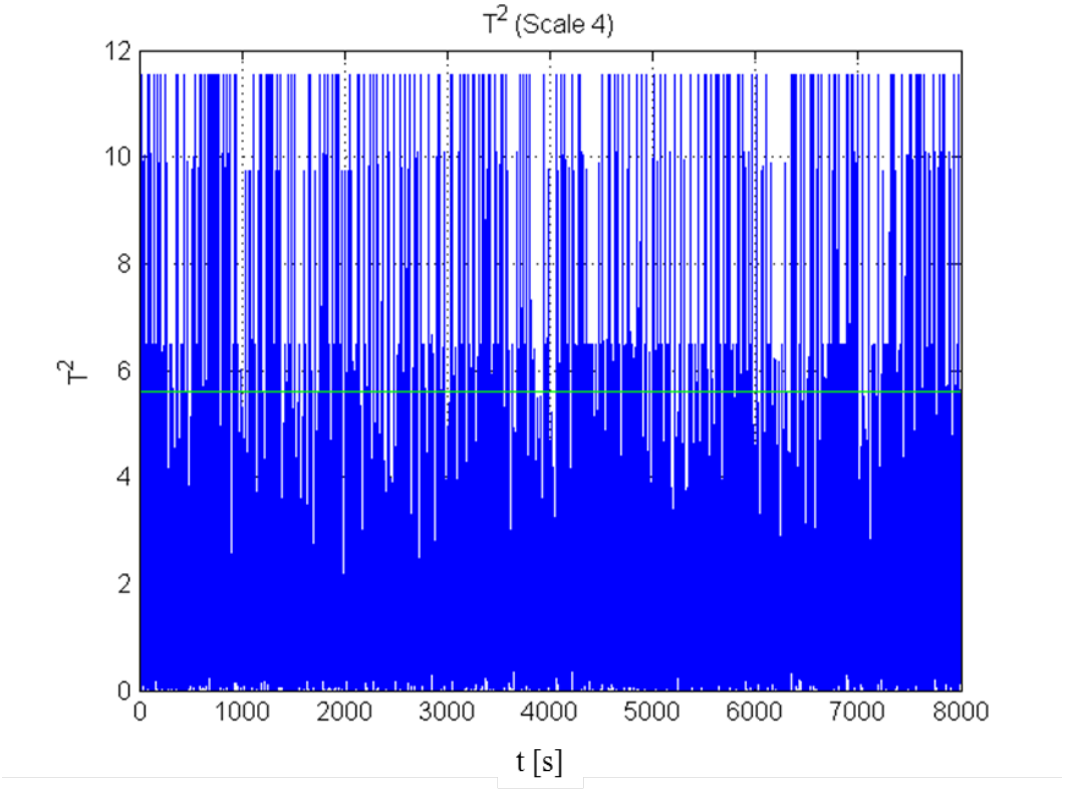

Figure 3.121: T^2 statistics at scale 4 for KL3 data

Non-representative analysis Assessment of the input energy index and the T^2 statistic for scale 1 were also carried out. Fig. 3.122 and 3.123 present the assessment results. Both the input energy index and the T^2 statistic went out of boundaries due to the initial uncertainty of the estimated multivariable model for the design of the MPC benchmark. The input energy index was kept within an amplitude value of $0-1$ and showed rapid variation at periods of high distortion on the KL3 data. During these periods, the MPC benchmark was trying to accommodate the distortions. This result can infer that the controller(s) were not properly tuned for disturbance rejection, but no measure of improvement by re-tuning cannot be given due to the index value which has been out of boundaries. T^2 at scale 1 did not give any useful value. It went out of boundaries at the beginning of the simulation and decreased to a value significantly higher than the scale threshold. Therefore, the analysis could not be used to give any acceptable assessment.

3.5.2.4 Root cause analysis of furnace temperature of zone 7 starts to drift from its set-point value

In this subsection the cause for not reaching the set point was investigated further. The reason could have been that the load in some zones of the furnace reached the limit, while other zones had quite a low load. Therefore, the average load distribution recorded in March 2012 was investigated. In an ideal operation mode it would have been expected that the load is equally distributed. But as seen in Figure 3.124 the load for furnace zone 2 (z2_m) and zone 5 (z5_m) was significantly higher than the average and in zone 4 (z4_m) the load is much lower. To analyze the reasons for this, some simulations with "Furnace Simulation and Diagnoses Tool" were carried out, which have been developed in WP 4. The results are shown in Figure 3.125 and 3.126 and lead to the conclusion that:

- Overall there was a very good agreement between model predictions and temperature measurement data,
- Significant deviations between measurement data and simulation results for gas temperature calculation in zone 2 and 5 were shown,

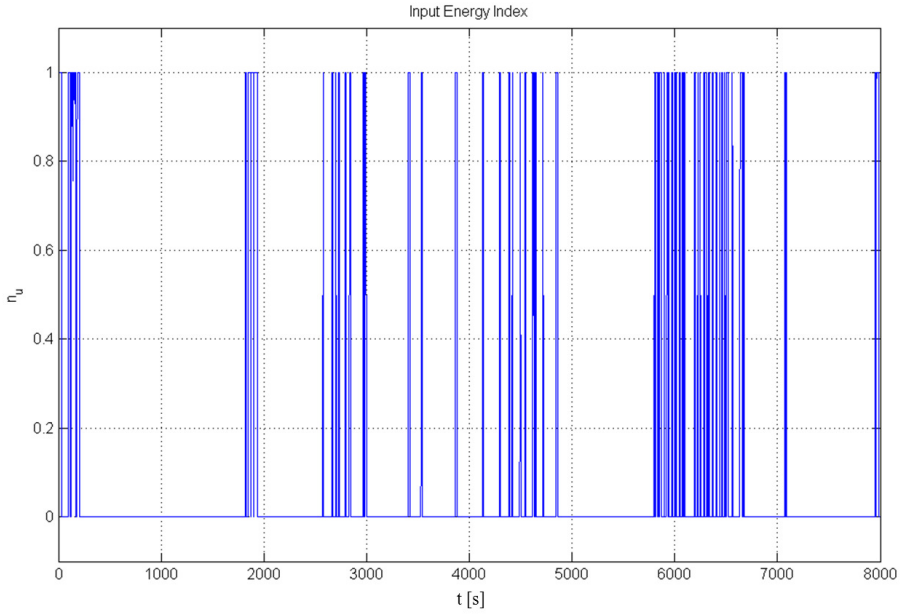

Figure 3.122: KL3 data input energy index

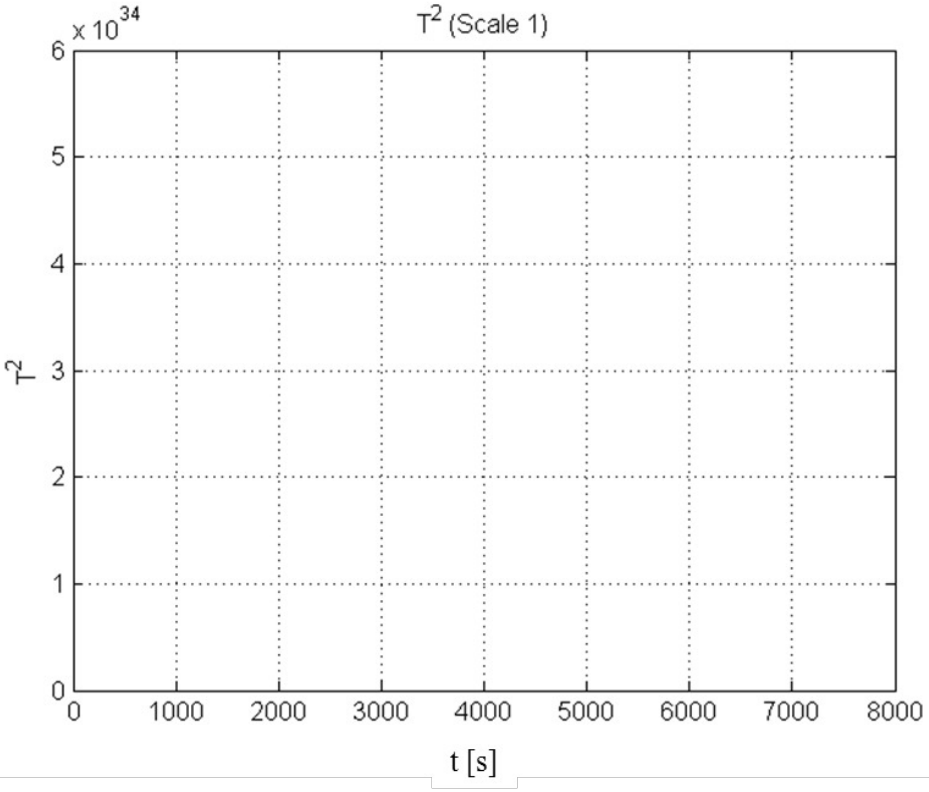

Figure 3.123: T^2 statistics at scale 1 for KL3 data

- Simulation of gas temperature time trends in other zones showed good accordance with measurement data,
- Measurement values were lower than simulated values. Furthermore, there was a change observable in the noise characteristic of the measurements of zone 2 and 5.

This resulted in a strong indication for measurement fault or process change. Further noticeable was that zone 2 and 5 always had a very high load. Therefore the other zones were not fully loaded. This provided an indication of the assumption: the temperature measurement in zone 2 and 5 had an an offset. To verify this assumption simulation with offset in temperature measurement in zone 2 and 5 is

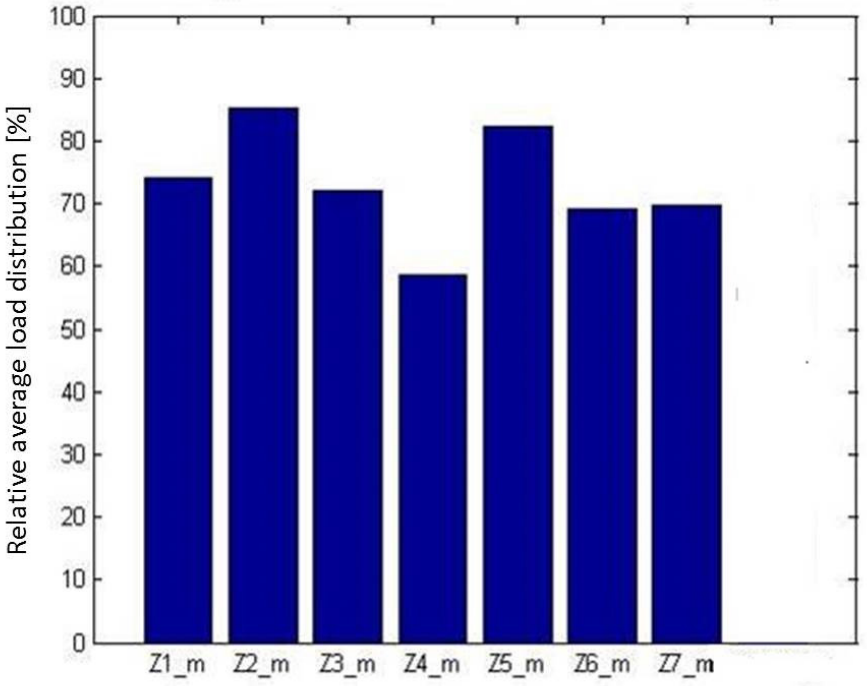

Figure 3.124: Relative average load distribution of annealing furnace KL3 recorded in March 2012

carried out. Two cases will be simulated:

- Temperature offset of - 20 K in zone 2 and 5
- Temperature offset of + 40 K in zone 2 and 5

The results are shown in figure 3.127 and 3.128. The simulation with a + 40 K offset seemed to reduce the load in zone 2 and 4. Therefore, it is assumed that the temperature measured was to low in Zone 2 and 5. Next this assumption was discussed with TKN and it was agreed putting an offset of about 20 K on the temperature measurement of zone 2 and 5. The comparison of the results of the average load before the change (May 2012) and after the change (September 2013) can bee seen in figure 3.129. It showed that the average load is reduced in zone 2 and 5, but not as much as expected. Additionally, the load in zone 1 had increased. Therefore, it could be concluded that this measure lead to a more homogeneous load distribution to improved control performance and higher throughput. This will be verified by TKN in the coming year.

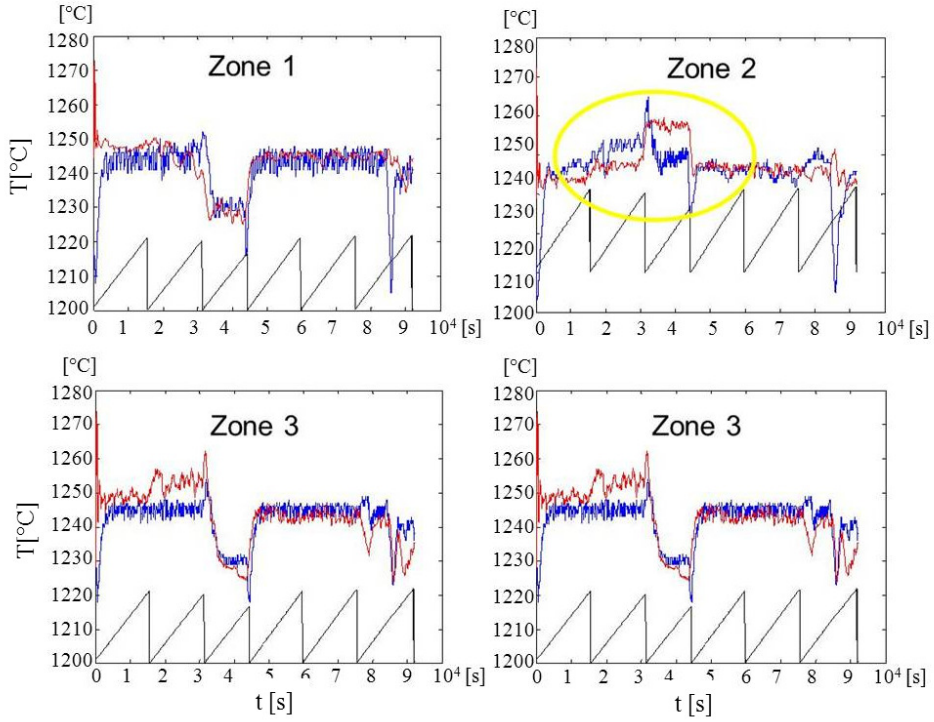

Figure 3.125: Effect on the load distribution in furnace zone 1 (z1_m) to zone 7 (z7_m) if an offset of -20 K is added to the temperature measurement in zone 2 and 5; whereas Simultion (red), Measurment data (blue), normalized strip length (black)

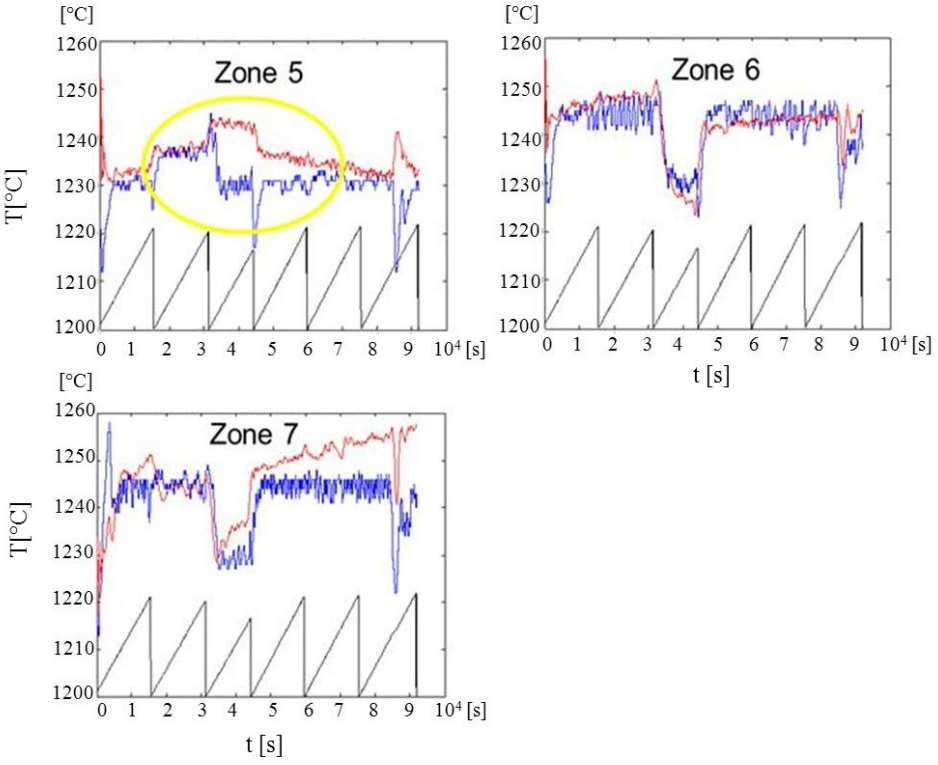

Figure 3.126: Effect on the load distribution in furnace zone 1 (z1_m) to zone 7 (z7_m) if an offset of +40 K is added to the temperature measurement in zone 2 and 5; whereas Simultion (red), Measurment data (blue), normalized strip length (black)

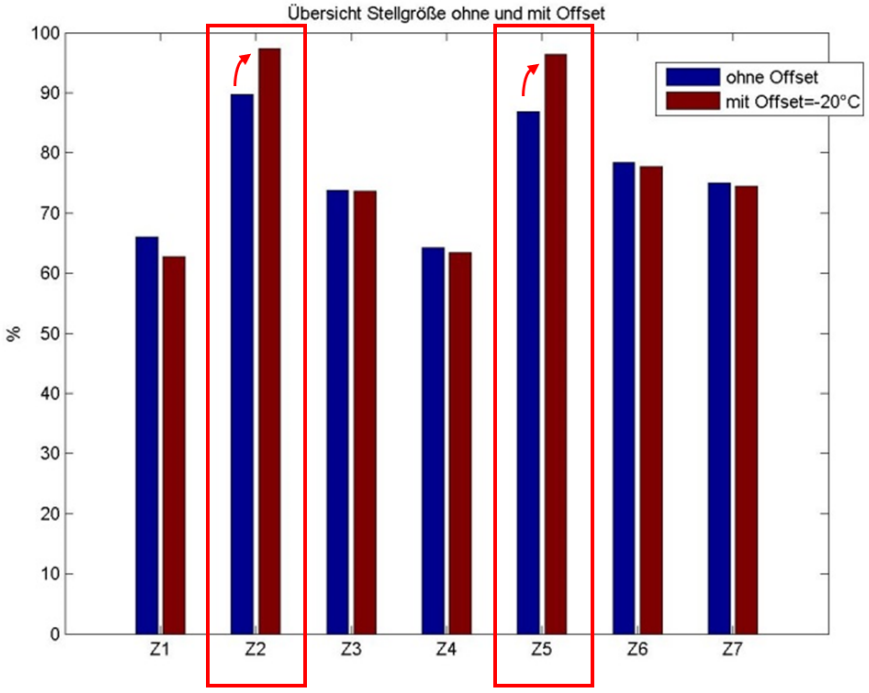

Figure 3.127: Simulation with 20K offset

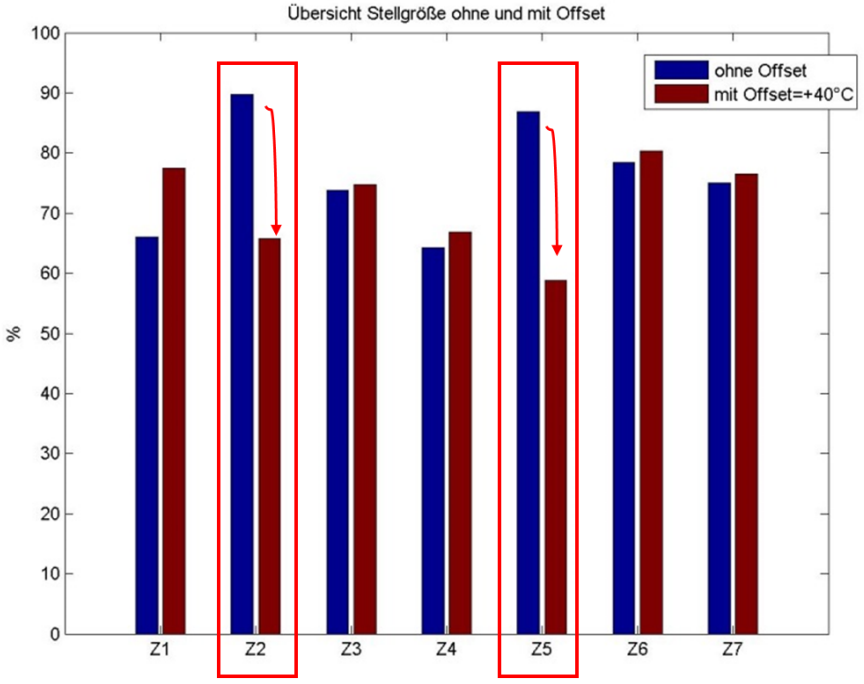

Figure 3.128: Simulation with 40K offset

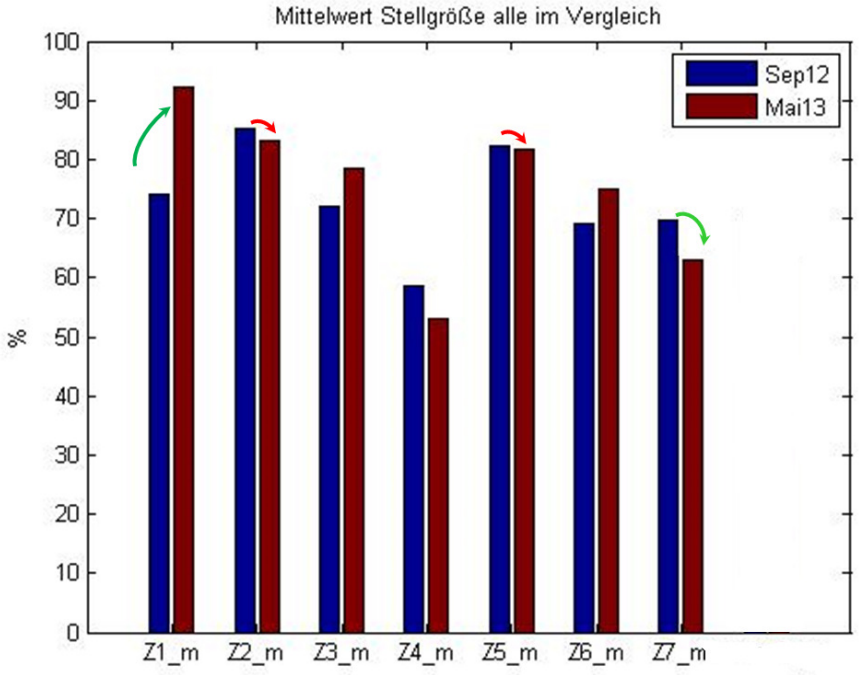

Figure 3.129: Effect on the offset of 20K on the load distribution

3.5.2.5 Root cause analysis of violation of T^2 at high scales of output index and energy index

In the performance analyses it was pointed out that the violation of T^2 at high scales could be related with oscillatory events which indicated noisy data or a source of oscillation. To verify this assumption, the behavior of the temperature control at changes in the thickness was investigated. In Figure 3.130 results are shown for jumps in the strip thickness from $2mm \Rightarrow 1.32mm$ and in figure 3.131 fromm $1.01mm \Rightarrow 1.49mm$. In both figures the upper figures the course of the measured furnace temperature (ist_i $i \in [1,7]$) and the desired furnace temperature (soll_i $i \in [1,7]$ is given. Also the measured strip temperature (IstB, red curve) and the desired strip temperature (SollB, red dotted curve) is shown. Furthermore, the strip thickness (in figure labeled as "Dicke") and line speed (in the figure labeled as "Geschwindigkeit"') is shown in the middle figure. Finally the lower figure shows the variation of the relative natural gas flow for each furnace zone (z_i $i \in [1,7]$).

In the first case , figure 3.130, where the thickness jump goes from the thicker to the thinner strip thickness, the strip was overheated, causing coarser grain of the strip which violated the allowed tolerance. This was not an optimal use of recourses and energy. To reduce this effect, it was advised to decrease the desired furnace temperature about 50 seconds earlier, before the thinner strip enters the furnace, which is, of course dependent on the strip speed.

In the second case , figure 3.131, where the thickness jump goes from the thinner to thicker, the strip is underheated, which caused an insufficient recrystallization and a too small grain size. The course of the strip thickness and speed and furnace temperature gave a hint that there is a conflict between a rule to reduce the furnace temperature when reducing strip speed and the rule to increase furnace temperature when the strip thickness is increasing. A solution could be to block the strip speed rule when at the same time the strip thickness is increased.

Both suggestions have been currently on their way to be implemented by the furnace supplier.

3.5.2.6 Calculated benefit of the above discussed measure

TKN analysed the gained benefit:

- The overall benefit of the measure between 2010 and 2013 lead the reduction out-tolerance of the grains which save about 150.000 € a year

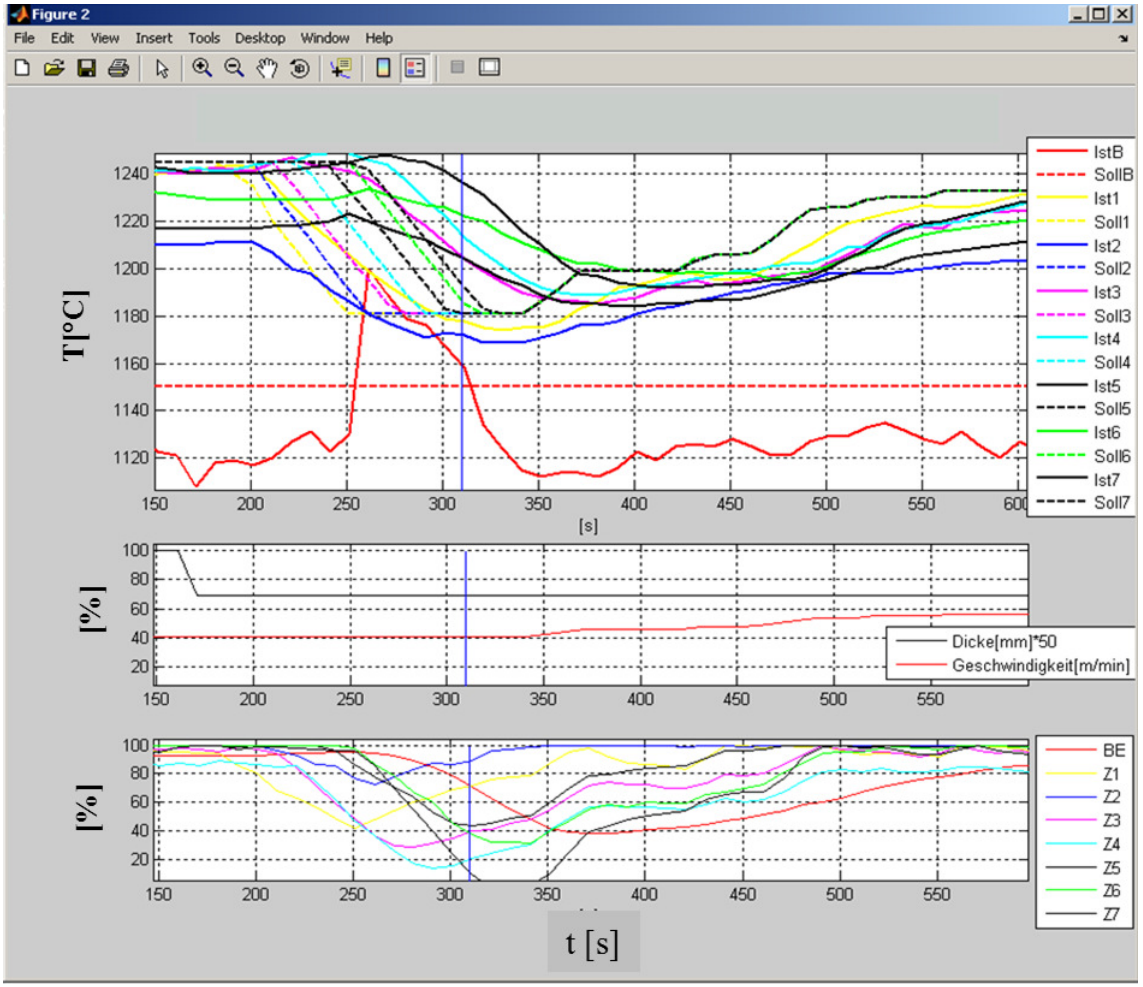

Figure 3.130: Results shown for jump in the strip thickness from $2mm \Rightarrow 1.32mm$the measured furnace temperature (ist_i $i \in [1,7]$),measured strip temperature (IstB, red curve), desired strip temperature (SollB, red dotted curve),strip temperature (SollB, red dotted curve), thickness (Dicke[mm]*50, black curve), strip velocity (Geschwindigkeit[m/min] , red curve), natural gas flow for each furnace zone (z_i $i \in [1,7]$)

- Optimizing of the controller performance on thickness jumps greater 0,2mm has a potential of saving of about 100.000 € a year
- The benefit of the homogenization of the load distribution of the furnace has to be observed over a longer period.

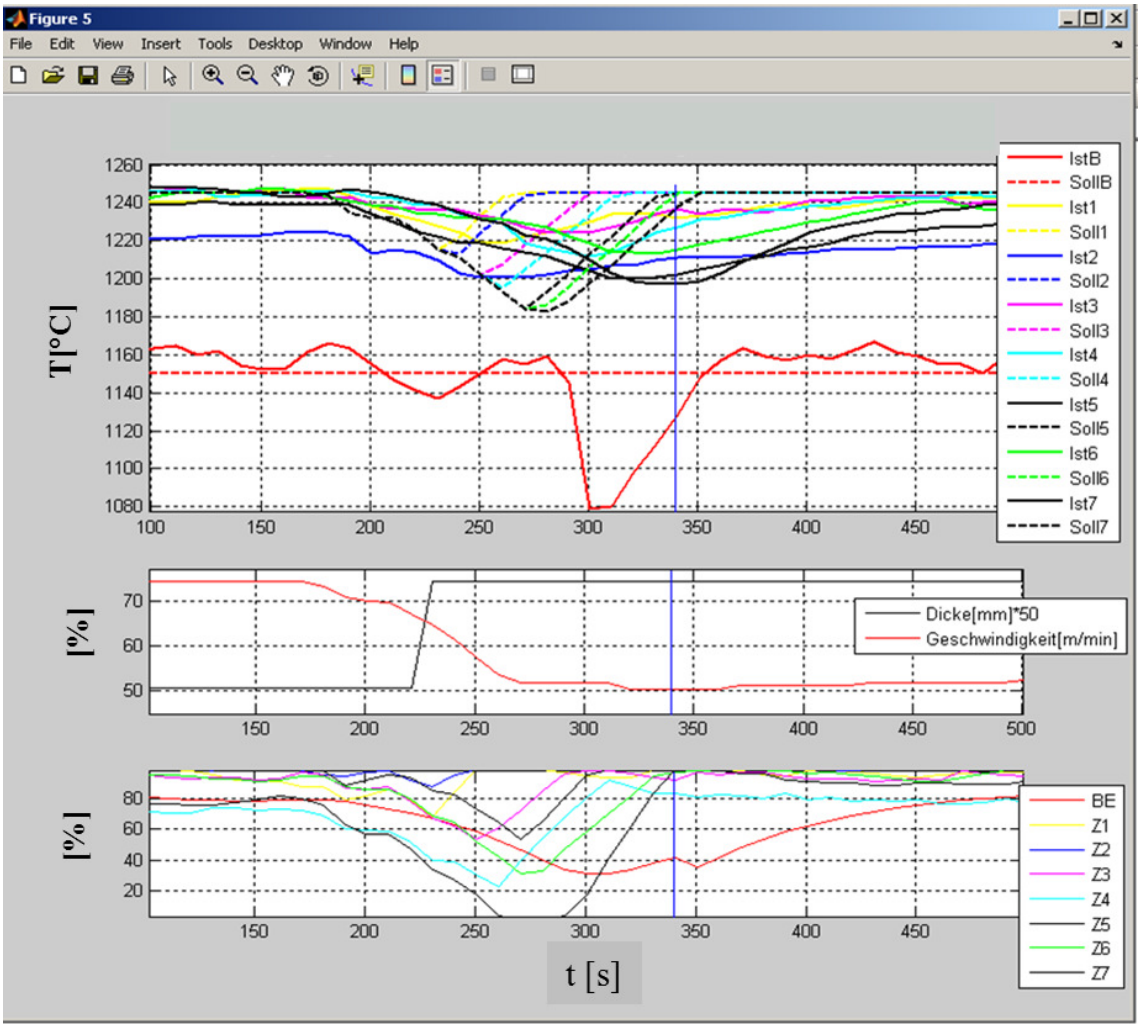

Figure 3.131: Results shown for jump in the strip thickness from $1.01mm \Rightarrow 1.49mm$„the measured furnace temperature (ist_i $i \in [1,7]$),measured strip temperature (IstB, red curve), desired strip temperature (SollB, red dotted curve),strip temperature (SollB, red dotted curve), thickness (Dicke[mm]*50, black curve), strip velocity (Geschwindigkeit[m/min] , red curve), natural gas flow for each furnace zone (z_i $i \in [1,7]$)

3.5.3 Task 5.3: Methods and systems for demonstration at annealing lines of MEFOS [MEFOS]

In this task, based of the performance analysis in Task 1.3 a root cause analysis of performance degradation was carried out using the tools developed in this project, being deliverable D5.2. Suggestions to improve the controller and to save energy were given, which lead to reduced cost and energy consumption.

3.5.3.1 Finding the root cause of the performance degradation

To find out the reasons for the performance degradation of the furnace controller the performance of the model used in the controller was analyzed. Therefore, the temperature calculated by the model was compared to the measurements.

A number temperature measurement using a ”datapaq” and thermocouples attached to strip were carried out in the autumn 2013 up to Jan 2014, with slightly varying results. For each test the calculated temperature of the strip through the furnace was also stored. This made it possible to directly compare the actual strip temperature and the strip temperature in the control system. The strip position in the diagrams is given in "mm". The overall length of the furnace is 39 m. Figures 3.132-3.135 show the measured temperature of the strip through the furnace in the green graph, as well as the calculated temperature from the control system in the red graph. Below are some of the successful measurements. The hump on the temperature curve that can be seen at approx. 14 m is where the strip went from furnace one to furnace two. This was the only place in the process, besides the exit of the furnace, where a satisfying measurement of the strip temperature was accessable.

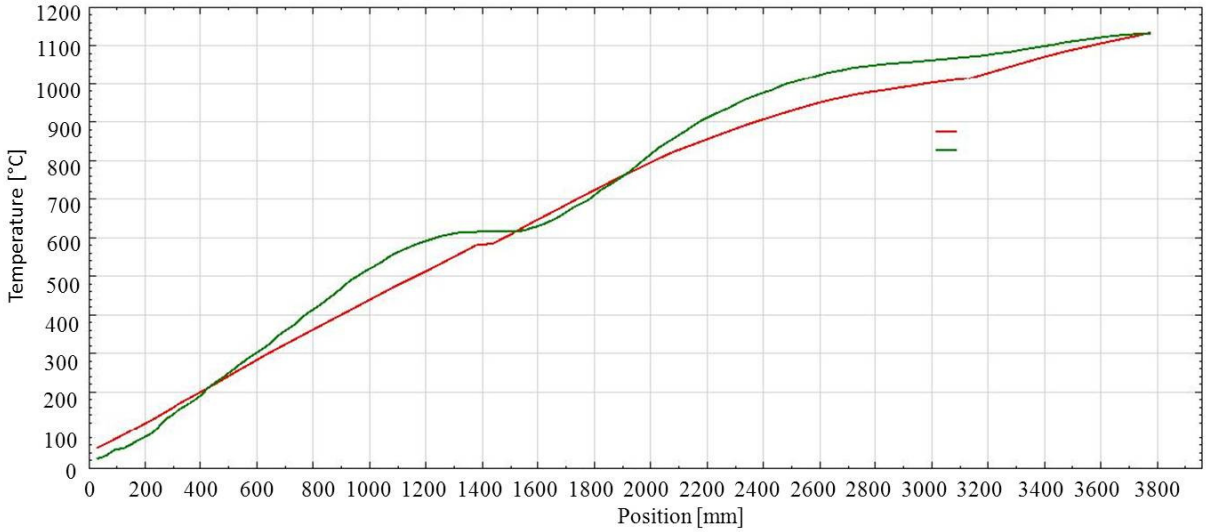

Figure 3.132: Strip ID 63278303 strip temperature through the furnace measured (green) and the calculated (red) [Start time 09:26, width: 2046mm, thickenss: 8.1mm, Speed 9.0m/min. measuring pos:10m (total length 181 m), surface:2B (black)]

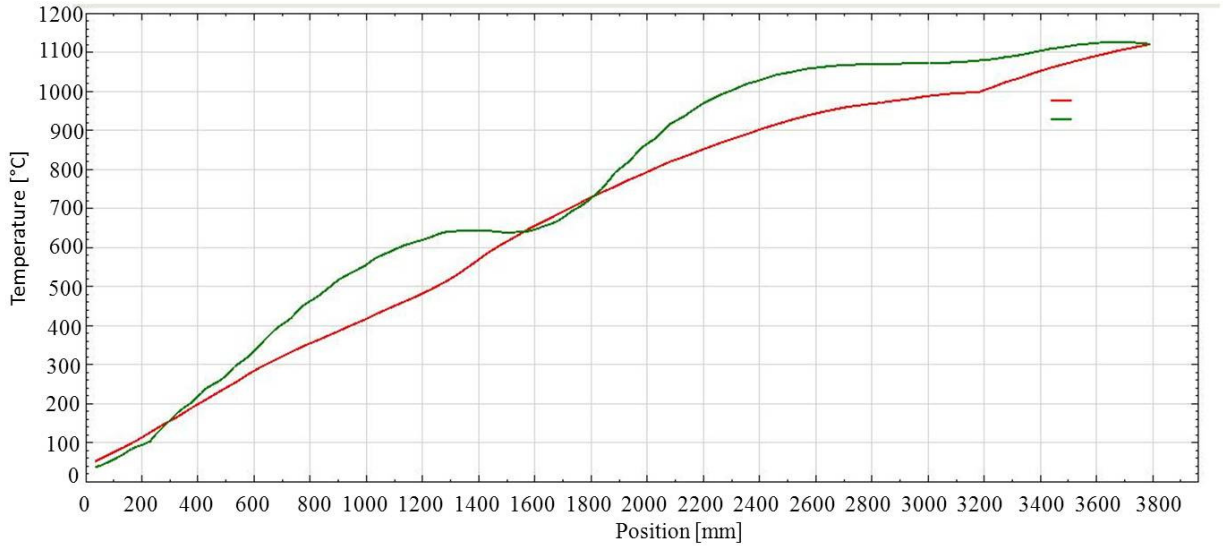

Figure 3.133: Strip ID 63415384 strip temperature through the furnace measured (green) and the calculated (red) [Start time 17:36, width: 2044mm, thickenss: 5.0mm, speed 11.9m/min. measuring pos:4 m (total length 292 m), surface:1D (black)]

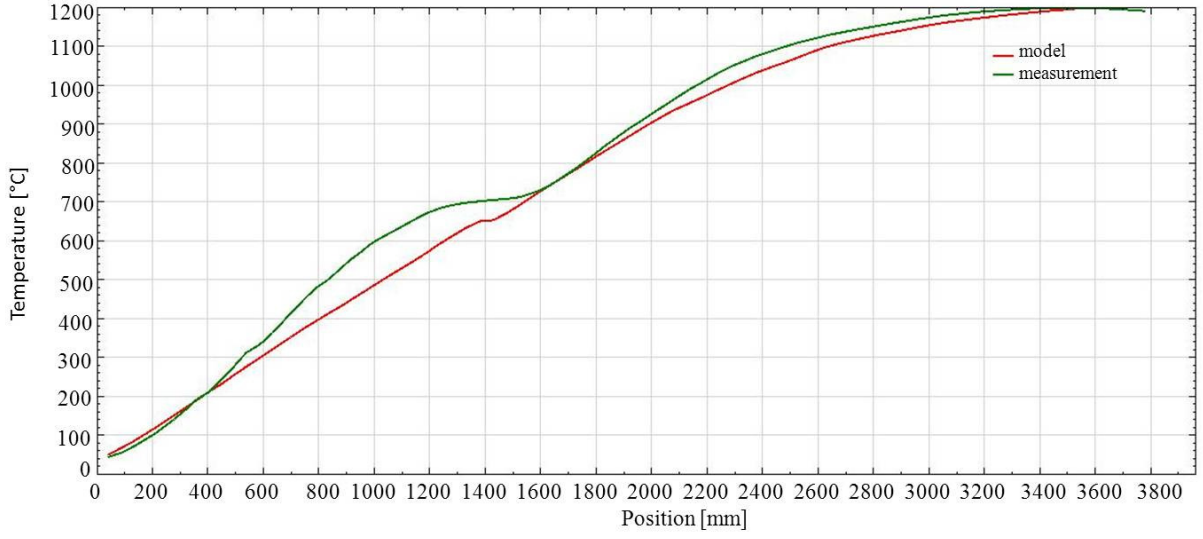

Figure 3.134: Strip ID 63622294 Strip temperature through the furnance measured (green) and the calculated (red) [Start time 09:14, Width: 1574mm, Thickenss: 6.4mm, Speed 10.1m/min. Measuring pos:1 m (total length 273 m), Surface:1D (black)]

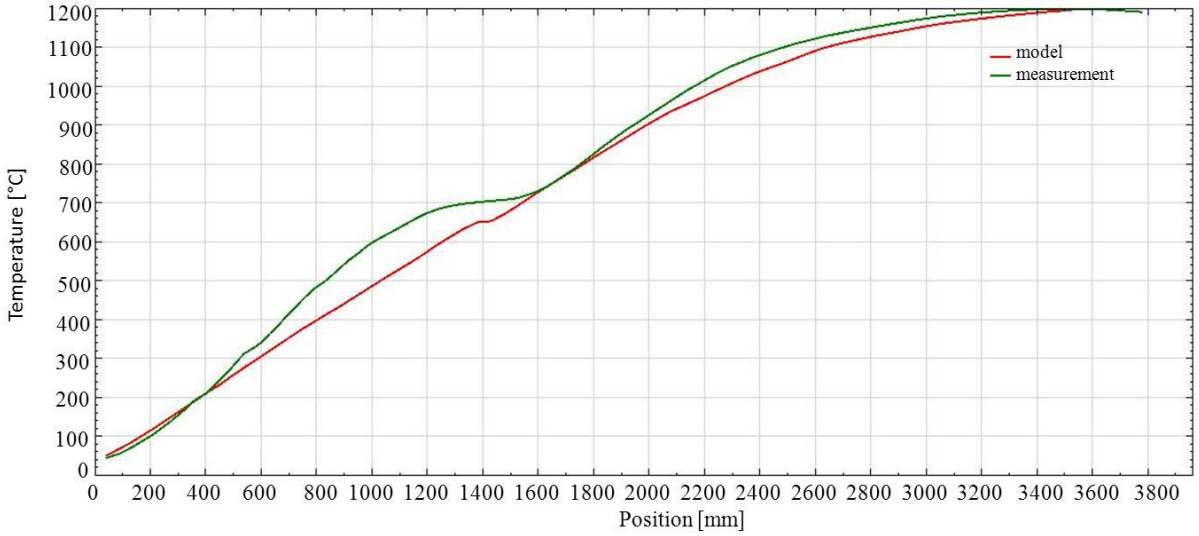

Figure 3.135: Strip ID 63741268 Strip temperature through the furnace measured (green) and the calculated (red) [Start time 12:12, Width: 2058mm, thickness: 8.1mm, Speed 12.2 m/min. measuring pos:120 m (total length 137 m), surface:1D (bright)]

Finding the root cause of divination between measured and calculated temperature It was found out that when decreasing the speed, especially when the furnace already was at a rather low speed, the temperature had a tendency to drop more than calculated. This gave an idea that there could be ”false air” in the furnace. Since the furnace is a regular air-fuel furnace converted to an oxy-fuel furnace it had the larger volume of the conventional furnace. Oxy-fuel combustion produces much less combustion gases compared to the air-fuel and at ”low power” it is advised to control the flue gasses carefully. So the composition of the furnace atmosphere was measured to see if it possible to detect any ”false air”. A high oxygen level indicated that air was leaking into the furnace.

Measuring O_2 and CO_2 levels in annealing furnace During normal, or possibly a little lower than normal, production conditions a gas analyser was attached into the furnace in Zone5. At first an assumption was that there must be a malfunction in the measuring system, because the O2 level was at approximately 15%. After checking and rechecking the equipment it has been realized that the measurement had actually been correct. The exhaust gas valves were closed by making a change in offset. After 5 min the O_2 level decreased and the CO_2 level rose in the furnace. However, both the O_2 level should have been lower and the CO_2 level higher. After adjusting the offset on the fuel gas valves again the O_2 level dropped to about 5 to 8 %. Figure 3.136. The O_2 level could not be decreased

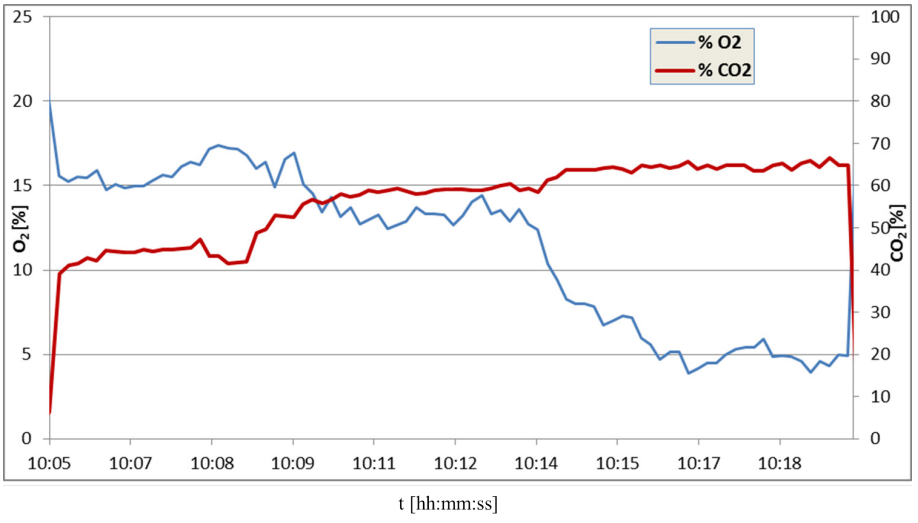

Figure 3.136: The O2 level and CO2 level when adjusting flue gas valves

further by adjusting the fuel gases. Closing the valve further did not change the O_2 level. Therefore the Oxygen quota used in the furnace was investigated. By changing the O_2 quota it was facilitated to decrease the O_2 level to 3 to 5% and increase the CO_2 level to approx. 80 %.

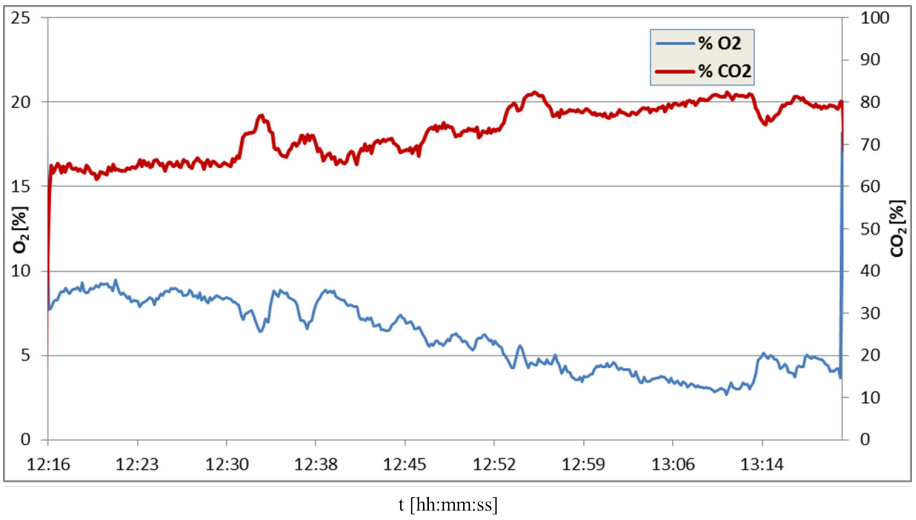

Figure 3.137: The O2 level and CO2 level when adjusting the O2 quota.

Finding the root cause of the errors of the calculated temperature After calculating the energy balance of the furnace, and after looking at the problems at calculating the temperatures through the furnace, it was discussed if there could be a problem that had not been realised. It was soon found that the problem was the difference in atmosphere in oxy-fuel furnaces compared to air-fuel furnaces. Oxy-fuel combustion is the process of burning a fuel using pure oxygen instead of air as the primary oxidant. Therefore, the composition of the combustion gases for oxy-fuel is significantly different from those obtained from typical air-fuel combustion. For air-fuel combustion, the exhaust gases contain approximately 7-11 % CO_2, 10-20 % H_2O and 70- 75 % N_2. For oxy-fuel combustion, there can be as much as 42 % CO_2 and 55 % H_2O. This illustrates how the concentrations of CO_2 and H_2O can be up to about five times greater. This made us research if we could improve the gas radiation model in STEELTEMP especially for oxy-fuel.

3.5.4 Task 5.4: Evaluation of final results and recommendations [ALL PARTNERS]

MEFOS analysed the energy aspects of sensor faults, controller performance, oxygen quota in oxy-fuel furnaces. The economic aspect of the project was analysed by TKN. Furthermore, ICC and BFI together with AMEH provided recommendation on data preparation, assessment, diagnosis and re-tuning.

3.5.4.1 Evaluation of the results

The analyses and tuning methods applied in this project had the following effect on the investigated plants:

Energy aspects of the detection on sensor faults Since it has been very difficult to find slowly drifting thermocouples, so far, it has also been difficult to show a plausible level of improvement. By observing thermocouples in the furnace floor that slowly covered with scale the temperature drift was detected from 0 to 100°C within two to three months. The control system was not adjusted before the deviation in measured temperature was so high that it could be clearly detected. Assuming there is such a case once a year, with the result of the slab getting 20°C too hot, and the error lasting for a month the energy consequences will be approx. 20/1250*30/365*1000GWh = 1.3 GWh per year.

Energy aspects of the controller performance improvement In the case of a thermocouple drifting or deviating temperature values a number of reasons could be the cause as e.g. corrosion. This could lead to thermocouple moves or furnace wall changes or the fastening of the thermocouples is disturbed. Regardless of what happens it is very difficult to detect when such an incident occurs. It is usually detected through secondary effects and there is a long time between the incident and detection of the error. It can be slow drifting of fuel consumption in one zone, bad product quality or just bad fuel efficiency as it was shown in Task 5.2

Economic aspects of the applied measures at TKN TKN analysed a calculation of the benefit the project gained here:

- The overall benefit of the measure between 2010 and 2013 lead the reduction out-tolerance of the grain size which save about 150.000 €a year
- Optimizing of the controller performance on thickness jumps greater 0,2mm has a potential of saving of about 100.000 €each year
- The benefit of the homogenization of the load distribution of the furnace has to be observed over a longer period.

Economic aspects of changing the oxygen quota in oxy-fuel furnaces Besides lowering the actual cost for the oxygen used, there was also a quality aspect. A lowered and more homogeneous oxygen level in the furnace will give greater repeatability of the variation of the emission factor of the strips. This was identified from the beginning as a root cause to variation in temperature and errors in temperature calculations. The industrial partner did not want to comment in detail on the amount of oxygen saved other than it is a significant volume and neither on how the lowered oxygen levels in the furnace has influenced the process.

3.5.4.2 Recommendation

The following recommendation can be given by the partners:

On data preparation

- For any kind of assessment at first the data has to be verified to be consistent, otherwise this could yield to false interpretation of the later analysis steps

Initial analysis step

- The first analysis takes care about whether the signal is “alive” and the second is to check whether the controller to be analysed is really switched on or off. Then the data of interest can be selected. In a third step the basic analyses are recommended like:
  - Steady state detection to select to the relevant part of the signal
  - Detection of nonlinearities
  - Oscillation analysis
  - Estimation of time delay

After this performance and route cause analysis can be carried out.

On assessment

- In order to avoid unnecessary metrics calculations, the controller should be assessed to rule out improper tuning or inadequate control structure first. Improper tuning is considered the main cause of poor performance, however no specific metric only for controller assessment has been developed.

- Model-based metrics are more realistic when it comes to PID-like controllers. Minimum variance metrics are just an easy way to extract the existing disturbances whereas some root-causes show deterministic features.

- In order to develop non invasive performance metrics, identification methods that work with minimum of none external persistent excitation signals should be used. In the literature of systems identification, the excitation of the process in the entire frequency spectrum is essential for accurate results; however most processes cannot be altered or even stopped for identification tests.

On diagnosis

- There is not a database of general root-causes in steel processing lines. Most of the methodologies for diagnosis are based on the identification of new data features against known data features. Even if the accuracy of a given methodology identifies new abnormal data features, they can not be linked to a known or new root-cause. Diagnosis for steel processing lines is at the stage where many destructive tests have to be carried out in order to identify possible root-causes of poor performance.

- It is important to keep in mind that some root-causes have shared effects. The identification of a given root-cause may need several tailored diagnosis methodologies or monitoring at different frequencies.

On re-tuning

- Control re-tuning has to be a task initiated manually. Although diagnosis mechanisms suggest that re-tuning is needed, only the expertise of the plant personnel can dictate if that task is necessary. Iterative controller tuning should be carried out with caution. First it is very important to rule out any other cause for performance degradation like stiction or other causes for oscillation. Otherwise is would lead to inconsistent tuning advice which could lead to instability of the control loop.

3.5.4.3 Dissemination Strategy

The Cognitive Control dissemination strategy (being deliverable 5.3) covered both internal and external communication and dissemination, each of which are discussed in turn below.

For internal purposes, this dissemination strategy provided members of the Cognitive Control consortium with an effective and efficient blueprint to follow in disseminating the project's work and results. Internal communication itself had been conducted via email, monthly teleconferences, periodic face-to-face meetings. Shared documents (including administrative project documents, case study data and reports and publications) are stored in "a Cloud", giving all partners access at all times.

The external objectives of the Cognitive Control dissemination strategy were:

- Dissemination of Methods and Results:
  - Publication of the results in conference paper
  - Publication of the results in journal paper
  - Publishing of a technical monograph
  - Giving workshops about control performance monitoring and re-tuning
- Dissemination of Software:
  - Providing Services to analyze control loops and re-tuning control loops in the steel industry.

A list of already submitted and published papers can be found in the section "Exploitation and impact of the research results".

4 Conclusions

The aim of the proposal was to create cognitive automation systems with the capabilities automatic monitoring of control performance, self-detection and automatic diagnosis of faults (sensors, actuators, and controllers) and self-adaptation in control system environments to optimise the product quality and minimise energy consumption in steel lines.

Based on the methods and analysis developed by BFI, in close cooperation with the industrial partners, it can be concluded that: (1) in practical applications, such as for analysing thickness control systems in hot strip mills, periods of steady and non-steady states should be detected, before the performance assessment takes place; two methods were proposed for this purpose; (2) control performance has an effect on the energy efficiency of annealing processes that should be assessed by static and quality-based furnace efficiency indices.
Root-causes of poor performance, such as the presence of oscillations, nonlinearity or valve stiction were detected reliably by the methods proposed by BFI. Furthermore, model-based procedures were developed and tested at TKN. However, the challenge in diagnosis tasks is still to detect multiple faults that can occur in control loops. For this purpose, a comprehensive procedure was created. This yielded in a "Simulation and Diagnosis Tool" for TKN's annealing furnace and performance and re-tuning tool for AMEH.
Two innovative approaches for automatic retuning of control systems (iterative controller retuning based on CPM and controller retuning based on routine and set-point response data) were proposed by BFI. Open questions concern the selection of the controller parameter variation for the iterative tuning, so that tuning operation was completed in a small number of iterations under strict avoidance of control-system stability problems. For this purpose, a model-free strategy that did not need experimentation with the process was developed and tested at the galvanizing line of AMEH. The set-point-response-based re-tuning method has been applied for performance improvement of TKN's annealing line temperature control. These measures lead to significant cost reduction at TKN's annealing furnace.

The University of Strathclyde has combined all the methodologies used and developed by the ICC into a MATLAB software tool. "Supervisory Control And Data Acquisition" (SCADA) functionality was added to the software tool through the Object linking and embedding Process Control (OPC) toolbox.

Furthermore, the following conclusions on its contribution can be derived:

On assessment

- Controller benchmarks require process and noise models. Identification is a crucial part in CPA and adequate identification methods have to be used to provide a non invasive assessment.

- Linear methodologies on processes with nonlinearities provide inaccurate performance index values. Although a linear metric can be used for CPA, when re-tuning is diagnosed, a further tuning of the existing controller is not sufficient. Instead a change in control structure might be needed to tackle the existing nonlinearities.

- Model-based methodologies can account for energy consumption constraints. Sometimes faults in actuators are due to equipment wear and therefore high performance index values do not mean healthy processes. The use of an energy index or controlled input performance index is needed to verify if performance improvement is beneficial for the process on the long term.

On diagnosis

- Different sources of poor performance have shared effects. In the literature of CPA the use of several tailored diagnosis methods are suggested in order to provide a thorough diagnosis. However, the use of monitoring of root-causes at several frequencies is also useful since root-causes can appear at different frequencies.

- Diagnosis requires detection, reconstruction, identification and if possible isolation of the root-causes. Although this statement comes from fault detection and isolation theory, it applies to CPA, since most root-causes should go through this stages in order to provide an accurate diagnosis.

- Statistical methodologies such as PCA lack identification and isolation capabilities. They have to be used in combination with other methodologies to provide a comprehensive diagnosis.

On re-tuning

- All methodologies require either a priori knowledge of the existing controller or input of external excitation signals.

Swerea MEFOS work revealed the importance of sensors, i.e. thermocouples, supervision in annealing furnaces at Avesta Works, and two types of deterioration, slow drift or breaking, which were analysed. Further analyses and tuning of temperature controller utilising analysis models in cooperation with project partners were carried out. The performance results lead to further investigation. Data analyses showed that root-causes for bad performance were often existent due to basic measuring problems and usually not caused by faulty devices. Sometimes bad material planning and occasionally manual intervention was to blame for bad performance. During these investigations and discussions it became obvious that the process control of the line needs improvement. Therefore, a study was undertaken to investigate the alternatives there are if changing/upgrading the process control in the annealing line. On these grounds the decision was taken to upgrade the process software.
Finally, MEFOS concentrated on analysing the energy consumption of the furnace at different loads to find when it was most efficient. Measuring the actual temperatures of the strips as they passed through the furnace and comparing them to the calculated temperatures to see the calculations' results. This included trying to find a way of improving calculations and understanding what the difference between the heat transfer in an oxy-fuel furnace compared to a conventional air-fuel furnace was.

5 Exploitation and impact of the research results

The benefits and transferability of the developed systems can be summarised as follows. The University of Strathclyde and BFI have condensed its resulting methodologies into several conference, journal papers. The list of papers are the following:

Conference papers:

1. PID based Control Performance Assessment for Rolling Mills: A Multiscale PCA approach. L.F. Recalde, R. Katebi, H. Tauro, IEEE Multi-Conference on Systems and Control (MSC), Hyderabad, India, Aug 2013.

2. Pre-Assessment of Controller Performance via Disturbance Filtering. L.F. Recalde, R. Katebi, H. Yue, Industrial Control System Report, ICC 100-2013, UK.

3. Sequential Control Performance Diagnosis of Steel Processes. L.F. Recalde, R. Katebi, H. Yue, IFAC World Congress, Cape town, South Africa, Aug. 2014.

4. Control Performance Monitoring of nonlinear processes. L.F. Recalde, R. Katebi, H. Yue, To be submitted for publication, June 2014.

5. Continuous performance evaluation of control systems for reducing energy consumption in annealing lines. A. Wolff, M. Jelali, , JSI,Paris, 2012.

6. Kontinuierliche Performanzüberwachung, Diagnose und Tuning für Stahlverarbeitungsprozess, "Duisburger Arbeitskreis für Mathematik in Forschung und Praxis", Duisburg, Mai , 2014

Journal paper drafts:

7. Assessment and Monitoring of Multivariable Processes. L.F. Recalde, R. Katebi, H. Yue, To be submitted for publication, October 2014.

8. Control Re-tuning methodologies for Control Performance Monitoring. L.F. Recalde, R. Katebi, H. Yue, To be submitted for publication, Oct 2014.

The results obtained during the project were quite novel in the field of steel processing lines. Further attention should be paid on the identification of specific sources of poor performance.

Additional tests on more real data can provide a thorough database of root-causes that combined with a complete mathematical framework of the methodologies developed can be the fundamentals of an essentially required technical monograph in the field.

Out of this project several software tools have emerged: the "Supervisory Control And Data Acquisition Tool" (SACDA) by University of Strathclyde, "Simulation and Diagnose Tool"' for annealing furnaces by BFI and TKN, and the performance and re-tuning tool by AMEH and BFI. This tools have been suggestfully applied at the plant off the industrial partner could gain a significant cost savings.

6 Acronyms and Nomenclature

Acronyms

AGC	Automatic gauge control
AI	Area index
ARMAX	Autoregressive-moving-average model with exogenous inputs model
ACF	Autocorrelation function
AMEH	ArcelorMittal Eisenhüttenstadt GmbH
ANOVA	Analysis of variance
BFI	VDEh-Betriebsforschungsinstitut GmbH
cov	Covariance
CPA	Control performance assessment
CPM	Control performance monitoring
CPAMD	Control performance software tool
CUMSUM	Cumulative sum
D	Diagnosis
DA	Data Access
DATAPAQ	Furnace temperature tracker system
F	Feature space
FCOR	Filtering and correlation analysis
FDI	Fault detection and isolation
G	High pass filter
GUI	Graphical user interface
H	Low pass filter
HDA	Historical Data Access
ICC	Industrial Control Center
IFT	Iterative feedback tuning
IMC	Internal model control
IR	Impulse response
IRAI	Impulse-response area index
KL3	annealing furnace at TKN
KBR	annealing furnace at Outouumpu Avesta
LQG	Linear-quadratic regulator
LS	Least-squares
MEFOS	Swerea MEFOS
MPC	Model predictive control
MSE_{sin}	Mean squared error for sinusoidal fitting
MSE_{tri}	Mean squared error for triangular fitting
MSRE	Mean square reconstruction error
MsPCA	Multiscale Principal Component Analysis
MV	Manipulated variable
MV-CPA	Minimum Variance Control Performance Monitoring
NGI	Non Gaussianity Index
NL	Nonlinearity
NLI	Non-Linearity Index
NPI	Nonpredictability index
OP	Controller output
OPC	Object linking and embedding process control
QR	Orthogonal-triangular decomposition

PE	Prediction error
PCA	Principal component analysis
PC's	Principal components
PI	Proportional, Integral Controller
PID	Proportional, Integral and Differential Controller
PV	Process variable
SCADA	Supervisory Control And Data Acquisition
SISO	Single Input and Output System
SP	Setpoint
SPC	Statistical process control
SPE	Square prediction error
SVD	Singular-value decomposition
TKN	ThyssenKrupp Nirosta

fb	feed back
ff	feed forward

Nomenclature

A_i	Area index
A_C	System matrix of a linear controller
A_p	System matrix of a linear process
A_m	gain margian
$B(f_1, f_2)$	bispectrum at frequencies (f_1, f_2)
B_C	Input matrix of a linear controller
B_p	Input matrix of a linear process
C_C	Output matrix od a linear controller
C_p	Output matrix of a linear process
$\{C_i\}_{i=1}^{g}$	Set of classifiers with $i = 1, 2, \ldots, g$, possible causes
D_c	Throughput matrix od a linear controller
$D_{IR,(\ldots)}$	damping factor
D_p	Throughput matrix of a linear process
$E\{\cdots\}$	Expectation function
$F(u_k, e)$	Comprehensive staeady state process modell
F_t	System matrix of a linear state space system
$G_{\ldots}(s)$	Transfere function
H_k	Gain mratrix to represent the forced trajectory
H_L	Scalling-function low pass filter coefficients
H_t	Output matrix a linear state space system
I_a	Area index
I_{ai}	Impulse-response area index
I_i	Idle index
I_o	Output index
I_U^{fb}	Percentage of the input improvement by feedback control
I_y^{fb}	Percentage of the output improvement by feedback control
J_L	Wavelet high pass filter coefficients
$J_{\ldots}$	Cost function
K	Kalman gain
$K_{(\ldots)}(s)$	Transfer function of a controller
$K(X, Y)$	Radial basis function kernel
K_D	Differential gain
K_I	Integral gain
K_p	Proportional gain
K_k, K_t	Kalman filter gain
P_{steel}	Thermal power in the steel strip
P_{fuel}	Theraml power in the fuel
$\hat{P}$	Principle scores
R	steady state index
R_{acf}	Decay ratio
$R_{x_1,x_2}(\tau)$	Cross-correlation of the signal x_1 and x_2
R_f	Filtered steady-state index
R_Y	Covariances of output data sequences
R_Y^{fb}	Covariances of output data sequences by feed back
R_U	Covariances of input data sequences
R_Y^{fb}	Covariances of input data sequences by feed back
RDI	Impulse response relative damping index
$P_{t+1\|t}$	Covarinace matrix of the Kalman filter
T	Temperature
T^2	Hotteling's statistic
$\hat{T}$	Principle Components loadings
T_p	Period of the oscillation
T_s	Sampling time

V	Eigenvector
V_i	Supspace of the classifier C_i
W	Transformation / Decomposition matrix formed by low pass filters and high pass filters
$X(t)$	Data set of multiple signals
$Y(f_i)$	Fourier tranformantion of the output data y at f_i
$Z_{...}^{...}$	Matrix of PCA decomposed data

e_k	Innovation of a time disrecte linear system
r	Regularity factor
t	Time
$x_k^{(...)}$	State of a time discrete linear system
$u_k^{(...)}$	Input of a time discrete linear system
u^{ss}	Steady state input set-point
Δu increments of the input signal	
$y_k^{(...)}$	Output of a time disrecte linear system
y^{ss}	Steady state output set-point
Δy increments of the output signal	
$\vec{y}$	process data vetor
$z_{k,l}$	Data set corresponding to a given scale $l = 2,3,...,L$

$\beta_j(t)$	Estimated certainty
η_{stic}	Stiction index
η	Harries index
η_{energy}	Static energy index
η_y	linear output index
η_y^{nonl}	nonlinear output index
η_y^F	Filtered output variability index
η_u^F	Filtered input energy index
κ_{energy}	Energy monitoring index
λ	Eigenvector
phi_m	Phase margin
$\mu(X)$	Energy of the observation X
$\sigma_{(...)}$	Variance
$\varphi_{mk}(t)$	Orthonormal scale function
$\psi_{mk}(t)$	Orthonormal wavelet function
$\phi(z_i)$	Data mapped in space F
φ_{act}	Feature eigenvector of the most likely possible classifier C
φ_i	Feature eigenvector of the classfier C_i
Σ_a	Covariance matrix of the measurement noise
Σ_e	Covariance matrix of the process noise
$\hat{\theta}_t$	State vector of the Kalman filter
$\theta_{i,j}$	Angle between the classifier C_i and C_j
θ_t	State vector of model used for nonlinear processes

$bic(f_1, f_2)$	Bispectrum at frequencies (f_1, f_2)
$det\{A\}$	Determinant of matrix A
$var\{x\}$	Varinace of the signal x

List of Figures

List of Tables

Bibliography

[And08] Andrews G., et. al. *SMARTFIRE: Real-time intelligent diagnostics and optimisation of reheating furnace performance*. RFSR-CT-2005-00009, Belgium, 2008.

[Bak97] Bakshi B. Multiscale pca with application to multivariate statistical process monitoring. *AIChE Journal*, 44, 1997.

[Bau07] Bauer M., Cox J.W., Caveness M.H., Downs J.J., Thornhill N.F. Nearest neighbors methods for root cause analysis of plantwide disturbances. *Ind. Eng. Chem. Res.*, 46, 2007.

[Bau08] Bauer M., Thornhill N.F. A practical method for identifying the propagation path of plantwide disturbances. *Journal of Process Control*, 18, 2008.

[Bjo03] Bjorklund S. A survey and comparisson of time delay estimation methods in linear systems. *PhD thesis, Lund Institute of Technology, Sweeden*, 2003.

[Bon06] Bonavita N., Bovero J., Martini R. Control performance monitoring: a data-driven approach. *Process and Control System Performance Monitoring ANIPLA Workshop*, 2006.

[Cao95] Cao S., Rhinehart R.R. An efficient method for on-line identification of steady state. *Journal of Process Control 5*, 5:363–374, 1995.

[Che05] Chen J., Yea Y. Assessment and diagnosis of feedforward/feedback control system. *American Control Conference*, 2005.

[Cho04] Choudhury M.S., Shah S.L., Thornhill N.F. Diagnosis of poor control-loop performance using higher-order statistics. *Automatica*, 40, 2004.

[Cho05a] Cho J., Lee J., Choi S., Lee D., Lee I. Fault identification for process monitoring uisng kernel principal component analysis. *Chemical Engineering Science*, 60, 2005.

[Cho05b] Choi S., Lee C., Lee J., Park J., Lee I. Fault detection and identification of nonlinear processes based on kernel pca. *Chemometrics and Intelligent Laboratory Systems*, 75, 2005.

[Cho05c] Choudhurry M.A.A.S., Thornhill N.F., Shah S.L. Modelling valve stiction. *Journal of Process Control*, 13:641–658, 2005.

[Cho08] Choudhurry M.A.A.S., Jain., M., Shah., S.L. Stiction definition, modeling, detection and quantification. *Journal of Process Control*, 18, 2008.

[Cho09] Choudhurry M.A.A.S., Alleyne I. Stabilizing the operation of industrial processes using data driven techniques. *Chemical Engineering Research Bulletin*, 13, 2009.

[Des93] Desborough L., Harris T. Performance assessment measures for univariate feedforward/feedback control. *Canadian Journal of Chemical Engineering*, 71, 1993.

[Dun96] Dunia R., Qin J., Edgar T., McAvoy T. Identification of faulty sensors using principal component analysis. *AIChE Journal*, 42, 1996.

[Dun98] Dunia R., Qin J. Subspace approach to multidimensional fault identification and reconstruction. *AIChE Journal*, 44, 1998.

[Eck10] Eckhard D., Bazanella A. Data-based controller tuning: improving the convergence rate. *IEEE Conference on Decision and Control*, 49, 2010.

[Ger01] Gerry J., Ruel M. How to measure and combat valve stiction online. *Instrumentation, Systems and Automation Society. Houston, TX, USA*, 2001.

[Gor05] Goradia DB., Lakshiminarayanan S., Rangaiash G.P. Attainment of pi achievable performance for linear siso process with deadtime by iterative tuning. *Can. J. Chem. Eng.*, pages 723–736, 2005.

[Hag95] Hagglund T. A control performance monitor. *Control Eng. Practice*, 3(11), 1995.

[Har89] Harris T.J. Assessment of closed loop performance. *Canadian Journal of Chemical Engineering*, 67, 1989.

[He 07] He Q.P., Wang J., Pottmannn M., Qin S.J. A curve fitting method for detecting valve stiction in oscillating control loops. *Ind. Eng. Chem. Res.*, 46:4549–4560, 2007.

[Hja98] Hjalmarsson H., Gevers M., Gunnarsson S., Lequin, O. Iterative feedback tuning: Theory and applications. *IEEE Control Systems*, 1998.

[Hor00] Horch A. Condition monitoring of control loops. *PhD thesis, Royal Institute of Tehcnology, Sweden*, 2000.

[How08] Howard R.,Cooper D.J. Performance assessment of non-self-regulating controllers in a cogeneration power plant. *Appl. Energy*, 86:212–219, 2008.

[How10] Howard R., Cooper D.J. A novel pattern-based approach for diagnostic controller performance monitoring. *Control Eng Pract*, 18:279–288, 2010.

[Hua03] Huang B. A pragmatic approach towards assessment of control loop performance. *International Journal of Adaptive Control and Signal processing*, 17, 2003.

[Hub11] Huba M., Skogestad S., Fikar M., Hovd T.A., Johansen B., Rohal'-Ilkiv. *Selected Topics on Constrained and Nonlinear Control*. Miloslav Roubal ROSA, Slovakia, 2011.

[Hug99] Hugo AJ. Process controller performance monitoring and assessment. 1999.

[iCO] iCONICS. Opc connectivity. `http://www.iconics.com/Home/Products/OPC-Connectivity/Free-OPC-Tools.aspx`.

[Jel06a] Jelali M. An overview of control performance assessment technology and industrial application. *Control Engineering Practice*, 14, 2006.

[Jel06b] Jelali M. An overview of control performance assessment technology and industrial applications. *Control Engineering Practice*, 14, 2006.

[Jel07] Jelali M. Automatisches reglertuning basierend auf methoden des control performance monitoring. *at–Automatisierungstechnik*, 55:10–19, 2007.

[Jel08] Jelali M. Estimation of valve stiction in control loops using separable least-squares and global search algorithms. *Journal Process Control*, 18:632–642, 2008.

[Jel09a] Jelali M., Huang B. *State of the Art and Advanced Methods*, chapter Detection and Diagnosis of Stiction in Control Loops. Springer, 2009.

[Jel09b] Jelali M., Huang B. (eds.). *Detection and Diagnosis of Stiction in Control Loops: State of the Art and Advanced Methods*. Springer, 2009.

[Jel10] Jelali M., Karra S. Automatische diagnose oszillierender regelkreise in komplexen industriellen anlagen. *at–Automatisierungstechnik*, 57:206–216, 2010.

[Jel13] Jelali M. *Control Performance Management in Industrial Automation: Assessment, Diagnosis and Improvement of Control Loop Performance*. Springer-Verlag, London, 2013.

[Joh] Johannesson L. Mäting av värmningskurva pa genom 1760. Intern,Dep of Teknik Band Outikumpu, Avesta Sweden.

[Kad02a] Kadali R., Huang B. Controller performance analysis with lqg benchmark obtained under closed loop conditions. *ISA Transactions*, 41, 2002.

[Kad02b] Kadali R., Huang B. Estimation of the dynamic matrix and noise model for model predictive control using closed-loop data. *Ind. Eng. Chem. Res.*, 41, 2002.

[Kan04] Kano M., Maruta H., Kugemoto H., Shimizu K. Practical model and detection algorithm for valve stinction. *IFAC Symposium on Dynamics and Control of Process Systems*, 2004.

[Kna76] Knapp C., Carter G. The generalized correlation method for estimation of time delay. *IEEE Transactions on Acustics, Speech and Signal processing*, 24, 1976.

[Li 00] Li W., Yue H., Valle-Cervantes S., Qin J. Recursive pca for adaptive process monitoring. *Journal of Process Control*, 10, 2000.

[Lyn96] Lynch C.B., Dumont G.A. Control loop performance monitoring. *IEEE Transactions in Control Systems Technology*, 4, 1996.

[Mat] Matrikon. Matrikon^{TM} control performance monitor. `https://www.matrikon.com`.

[Mat11] MathWorks. *OPC Toolbox User's Guide*, r2011b edition, September 2011.

[McN03] McNabb C.A., Qin S.J. Projection based mimo control performance monitoring: I-covariance monitoring in state space. *Journal of Process Control*, 17, 2003.

[Mia99] Miao T., Seborg D.E. Automatic detection of excessively oscillatory feedback control loops. *Proc. IEEE Conference on Control Applications, Kohala Coast-Island, USA*, 1999.

[Mik99] Mika S., Schülkopf B., Smola A., Müller K., Scholz M., Rätsch G. Kernel pca and de-noising in feature spaces. *Advances in Neural Information Processing Systems*, 11, 1999.

[Pit11] Pittner J., Simaan M.A. *Tandem Metal Cold Rolling Mill Control*. Advances in Industrial Control. Springer, New York, 2011.

[Qin07] Qin J.S., Yu J. Recent developments in multivariable controller performance monitoring. *Journal of Process Control*, 17, 2007.

[Rhi95] Rhinehart R.R. A watchdog for controller performance monitoring. *Proceedings of the American Control Conference Seatle, Washington*, 1995.

[Ros07] Rossi M., Scali C. A comparison of techniques for automatic detection of stiction: simulation and application to industrial data. *Journal of Process Contol*, 1:505–514, 2007.

[Sch96] Schölkopf B., Smola A., Müller K. Nonlinear component analysis as a kernel eigenvalue problem. *Max-Planck-Institut*, 38, 1996.

[Ske98] Skelton R.E., Iwasaki T., Grigoriadis K. *A Unified Algebraic Aprroach to Linear Control Design*. Taylor & Francis, Great Britain, 1998.

[Swa99] Swanda A.P., Seeborg D.E. Controller performance assessment based on setpoint response data. *Proceedings of the American Control Conference, San Diego*, 1999.

[Tak02] Takahashi T., Kurita T. Robust de-noising by kernel pca. *ICANN*, 2002.

[Tat10] Tatjewski P. Supervisory predictive control and on-line set-point optimization. *Int. J. Appl. Math. Comput. Sci.*, 20:483–495, 2010.

[Tho03] Thornhill N.F., Zhang H. Detection of multiple oscillations in control loops. *Control Engineering Practice*, 13:93–100, 2003.

[Tho05] Thornhill N.F. Finding the source of nonlinearity in a process with plant-wide oscillation. *IEEE Trans. Contr. Syst. Technol.*, 13:434–443, 2005.

[Tho07] Thornhill N.F., Horch A. Advances and new directions in plant-wide disturbance detection and diagnosis. *Control Engineering Practice*, 15, 2007.

[Tia11] Tian X., Chen G., Chen S. A data-based approach for multivariable model predictive control performance monitoring. *Neurocomputing*, 74, 2011.

[Vis05] Visioli A. Assessment of tuning of pi controllers for self-regulating processes. In *Proc. IFAC World Congress*, volume Chapter 4, pages 83–96, Prag, 2005.

[Yu,08] Yu, J., Qin, J. Statistical mimo controller performance monitoring. part ii: Performance diagnosis. *Journal of Process Control*, 18, 2008.

[Yua08] Yuan Q., Lennox B. The investigation of multivariable control performance assessment techniques. *Proceedings of the American COntrol Conference*, 2008.

HOW TO OBTAIN EU PUBLICATIONS

Free publications:

- one copy:
  via EU Bookshop (http://bookshop.europa.eu);
- more than one copy or posters/maps:
  from the European Union's representations (http://ec.europa.eu/represent_en.htm);
  from the delegations in non-EU countries (http://eeas.europa.eu/delegations/index_en.htm);
  by contacting the Europe Direct service (http://europa.eu/europedirect/index_en.htm) or calling 00 800 6 7 8 9 10 11 (freephone number from anywhere in the EU) (*).

  (*) The information given is free, as are most calls (though some operators, phone boxes or hotels may charge you).

Priced publications:

- via EU Bookshop (http://bookshop.europa.eu).

KI-NA-27-317-EN-N

The aim of COGNITVE CONTROL was to create cognitive automation systems with the capabilities automatic control performance monitoring (CPM), self-detection and automatic diagnosis of faults (sensors, actuators, controller) and self-adaptation in control system environments to optimise the product quality and minimise energy consumption in steel during the whole life cycle.

In this project several software tools for online Control Performance Monitoring (CPM), monitoring energy efficiency, diagnosis of poor performance root-causes and control re-tuning for univariable and multivariable, linear and nonlinear processes were developed. The software tools were Graphical User Interface (GUI) that provided interface to access process data. The implemented methodologies were subsequently published as conference and journal papers. The methods were tested at hot strip mills, annealing furnaces and galvanizing lines

.

Studies and reports

Publications Office

ISBN 978-92-79-49074-3
doi:10.2777/90680